EFFICIENT PROGRESSIVE COLLAPSE ANALYSIS FOR ROBUSTNESS EVALUATION AND ENHANCEMENT OF STEEL-CONCRETE COMPOSITE BUILDINGS

TAY CHOON GUAN

M.Sc., DIC, Imperial

B.Eng. (Hons.), UTHM

A THESIS SUBMITTED

FOR THE DEGREE OF DOCTOR OF PHILOSOPHY

DEPARTMENT OF CIVIL ENGINEERING
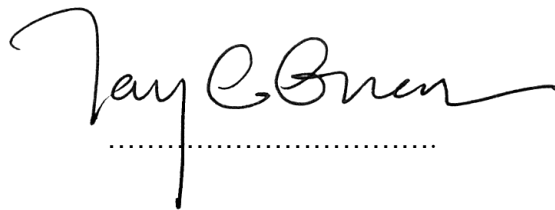
NATIONAL UNIVERSITY OF SINGAPORE

2013

This page intentionally left blank

Declaration

I hereby declare that the thesis is my original work and it has been written by me in its entirety. I have duly acknowledged all the sources of information which have been used in the thesis.

This thesis has also not been submitted for any degree in any university previously.

....

Tay Choon Guan

26 September 2013

This page intentionally left blank

This thesis is dedicated to the memory of my grandmother (1921-2010), for showing me the path of knowledge

This page intentionally left blank

Acknowledgement

This page intentionally left blank

Contents

List of Figures

This page intentionally left blank

List of Tables

List of Symbols

For ease of reference, the definition of commonly used symbols and notations are listed below.

Acronyms

AISC	American Institute of Steel Construction
ALP	Alternate load path
DAC	Double angle cleat
DL	Dead load
DoD	Department of Defense, USA
EC3	Eurocode 3 (BSI, 2005a)
FEA	Finite element analysis
FEMA	Federal Emergency Management Agency, USA
FP	Fin plate
GSA	General Services Administration, USA
LL	Live load
MHA	Ministry of Home Affairs, Singapore
NIST	National Institute of Science and Technology, USA
BT	Belt truss system
OS	Open System for Earthquake Engineering Simulation (OPENSEES)
SAP	Structural Analysis Program (SAP2000) (CSI, 2009)
SDL	Superimposed dead load
SCI	Steel Construction Institute, UK
SDOF	Single degree of freedom
SL	Snow load

UDL	Uniformly distributed load
WL	Wind load
WTC	World Trade Centre, New York City
IStructE	Institution of Structural Engineers, UK

Roman Symbols

A_i	area of the ith fiber of a fiber section
B_1	spacing of grillage in direction of steel deck
B_2	spacing of grillage in direction perpendicular to steel deck
C_1	web thickness of the equivalent T-section grillage member
d	nominal bolt diameter
d_1	distance from top of slab to center of reinforcement mesh
d_{bg}	vertical depth of the bolt-group of a connection
d_i	distance of the ith fiber to centroid
e_0	magnitude of initial crookedness of a frame
E_i	elastic modulus of the ith fiber
EA	axial rigidity of a frame section
EI	flexural rigidity of a frame section
E_s	elastic modulus of steel material
E_c	elastic modulus of concrete material
f_c	concrete crushing strength
f_y	steel yielding strength
$F_{y,j}$	yield capacity of spring representing j[th] bolt-row of connection

$F_{u,j}$	ultimate capacity of spring representing j^{th} bolt-row of connection
h_c	height of concrete above the steel deck of composite slab
h_d	height of steel deck of composite slab
R_n	tear-out resistance of bolt-row on connection
t	thickness of connected material of fin plate connection
k	initial rotational stiffness of connection without contribution of floor slab
$k_{b,j}$	initial axial stiffness of spring representing j^{th} bolt-row of connection
L	length of a frame member
L_c	clear distance between edge of bolt and edge of material
L_p	total length of plastic zone along a frame member
m	total number of fiber throughout a section
n	total number of bolt in the bolt-group of a connection
n_1	number of layer along flange or web plate of a steel section
n_2	number of layer across thickness of web or flange plate of a steel section
r	radius of gyration for calculation of member slenderness
s_j	distance from center of bolt group to the jth bolt-row
s_{max}	distance from center of the bolt group to the most distant bolt
t_d	thickness of steel deck
w	uniformly distributed load on frame member

Greek Symbols

δ	displacement along a frame in second-order analysis
Δ	end displacement of a frame in second-order analysis

$\Delta_{f,j}$ fracture displacement of spring representing j[th] bolt-row of connection

$\Delta_{u,j}$ ultimate displacement of spring representing j[th] bolt-row of connection

α_s strain hardening modulus of steel

χ buckling reduction factor

$\theta_{p,\max}$ total rotational capacity of shear connection

Chapter 1:   Introduction and Literature Review

1.1   Introduction

Recent earthquakes (e.g. Aceh 2004, Sichuan 2008, Christchurch 2010-2011 and Tohoku 2011) and other natural hazards (e.g. tsunami, flood and typhoon) have constantly reminded us of the importance of preparing for unforeseen events which may be low in probability but high in consequence. While Singapore is fortunate in being not near any major fault, occasional tremors felt in Singapore due to Sumatra earthquakes have raised concerns on the potential disastrous effects on our infrastructure and economy. In addition, like many metropolitan cities, Singapore is faced with man-made hazards such as terrorist attacks. In the context of preparedness for multi-hazards, it is therefore essential to design our infrastructure so as to reduce life and economic loss.

One key aspect is the evaluation and enhancement of structural robustness to avoid disproportionate collapse or, more accurately, disproportionate progressive collapse against unexpected events. Progressive collapse defines a chain of collapse reactions that commence with the failure of one or several structural components. Following the initial damage, the structure redistributes internal forces and seeks for alternate load path to share load from the damaged member. If the collapse area is substantial due to a minor triggering event, the phenomenon is defined as disproportionate collapse and the structure is deemed not robust. In accordance with current building codes, e.g. DoD

(2009), GSA (2003) and ODPM (2004), avoidance of disproportionate collapse is considered as a performance objective while progressive collapse refers to a collapse mechanism. According to the codes, structures need to be designed and constructed to avoid disproportionate collapse under the event of sudden removal of any of the columns.

Continuous, well-integrated and redundant framed structures usually can sustain a substantial amount of local damage. This is true for reinforced concrete building frames with relatively small structural bays. Other systems in which it is more difficult to provide continuity and ductility, such as precast concrete construction and long-span composite construction are inherently more vulnerable to disproportionate collapse. In modern construction, the use of high-performance materials and construction technologies aimed at minimizing erection cost has led to steel-concrete composite structures with limited continuity and little energy-absorbing capacity or resistance to disproportionate collapse (Ellingwood, 2006).

Progressive collapse can be triggered by a variety of causes, including man-made and natural hazards. Recommended best practice issued by the National Institute of Science and Technology (NIST) of United States indicates that *"Initial local damage can result from intentional explosions, accidental explosions, vehicle impacts, earthquakes, fire, or other abnormal load events"* (NIST, 2006). These unforeseen events typically stress the structural system into the inelastic response. Therefore, material and geometry nonlinear analysis is prerequisite if robustness performance of a building needs to be evaluated. However, robustness design has been traditionally considered by using prescriptive approaches in the building codes. These prescriptive approaches are easy to implement and do not require nonlinear analysis in the process, but the effectiveness of these approaches has been doubted following the recent collapse events of the Alfred P. Murrah building in 1995 (Hinman and Hammond, 1997) and the World Trade Center Towers in 2001 (NIST, 2005). In the aftermath of these events, a more realistic performance-based approach for robustness evaluation has been developed in the United States (GSA, 2003; DoD, 2009). According to these approaches, one needs to quantitatively analyze the response of a damaged structure caused by a postulated accidental event, and then

2

provides sufficient robustness such that damage is contained within a limit proportionate to its cause. In Singapore, these performance-based approaches have been adopted by the Ministry of Home Affair for the design of building structures against disproportionate collapse (MHA, 2010). Currently research on performance-based robustness design remains relatively immature, and there are significant research gaps that need to be addressed especially on the methodology of progressive collapse analysis and the strategy for robustness enhancement.

1.2   Research gaps

Currently many methods for evaluating robustness performance with regards to disproportionate collapse tend to be too sophisticated for practical application. These methods commonly involve progressive collapse analysis by detailed finite element analysis (FEA) of large numerical model using commercial software such as ABAQUS (ABAQUS, 2005) and LS-DYNA (Hallquist, 2006). Some notable studies adopting detailed FEA include the work by Alashker et al. (2010), Kwasniewski (2010), Yu et al. (2010), Fu (2009) and Sadek et al. (2008) etc. Detailed FEA is not only computationally demanding, but also requires intensive pre/post processing effort. Furthermore, precise information of material and geometry of a structure is rarely available in the real practice. Therefore, it may not be worthwhile to use highly sophisticated and computation-demanding method for robustness design and evaluation in practice. At the other end of the spectrum, simplified FEA involving frame models are used which, however, do not simulate the ultimate and post-ultimate strength well. Some notable studies adopting simplified FEA include the work by Kim and Kim (2009b), Marjanishvili and Agnew (2006) and Kaewkulchai and Williamson (2004) etc. These simplified methods typically ignore the influence of floor slabs in resisting progressive collapse, thereby not providing realistic evaluation of structural system robustness. Furthermore, buckling behavior and connection behavior are often not modeled realistically in these simplified methods.

Apart from efficient and realistic methodology for robustness evaluation, structural engineers are equally interested in effective robustness enhancement and design. Many studies in the past, e.g. the works by Kim and Kim (2009b), Kim et al. (2009c), Liu

(2010a) and Sadek et al. (2008) have proposed the use of full-strength moment connections that are similar to those used for seismic-resistant buildings. Nevertheless, this proposal not only increases the fabrication and erection cost, but also substantially prolongs the construction process. To maintain the competitiveness of the construction industry, it is worthwhile to explore the potential of shear connection in resisting disproportionate collapse.

In addition, there is also a pressing need for innovation of building systems that excel in robustness performance. Forensic study reveals that the exceptional robustness performance of the World Trade Center towers in surviving initial plane impact is attributed to the hat-truss system installed on the top of the towers (NIST, 2005). If not for the failing fire protection and the following multiple-floor fire attack, the towers could have possibly survived the plane impact. To the best knowledge of the candidate, robustness study involving building system and the potential of truss system as robustness enhancement remains quite limited.

1.3   Objectives and scope of research

In view of the research gaps mentioned above, the objective of this thesis is to develop a methodology for progressive collapse analysis that is computationally efficient yet capable of producing reasonably accurate results. The efficient methodology is instrumental for subsequent study on robustness enhancement of structural systems. To achieve the thesis objective, the study covers the following scope.

1. To propose an efficient methodology for progressive collapse analysis of steel-concrete composite building. As the name implies, the methodology needs to be computationally efficient, while its implementation should be derived from technical concepts comprehensible among practicing engineers. Equally important, the method should be capable of simulating damage behaviors key components, i.e. (a) member and global buckling of steel structure, (b) semi-rigid and partial-strength behaviors of shear connection, and (c) flexural and membrane behaviors of composite slab.

2. To identify key factors influencing the robustness performance of realistic composite floor system, and to draw recommendations for robustness design. In particular, the potential of belt truss system as robustness enhancement of multi-storey composite building will be explored for new and existing buildings.

3. To evaluate the effectiveness of equivalent static analysis for robustness evaluation of realistic composite building with belt truss system. Comparison between the results from equivalent static analysis, codified static analysis and the nonlinear dynamic analysis will be performed.

1.4   Research significance

As mentioned earlier, many methodologies for evaluating building robustness are either too sophisticated or too simplified in capturing the nonlinear dynamic behavior. The main significance of this study lies in bridging this gap by means of a realistic yet efficient progressive collapse analysis method for robustness evaluation of buildings. The contribution of this thesis can be summarized in the following two aspects:

1. Effective modeling of key elements (slabs, steel frames and connections) in the progressive collapse analysis. A slab model based on the modified-grillage method is proposed in chapter 2 for realistic yet efficient progressive collapse analysis of composite and reinforced concrete slab. The slab model offers the following desired features:

   • **Accuracy**: The proposed slab model can simulate the ultimate and post-ultimate capacities of floor slab with good accuracy. A numerical example studied in chapter 4 shows that omission of floor slab can greatly underestimate the ultimate capacity of composite floor system by as much as 5 times, whereas the use of conventional grillage method to model the floor slab can underestimate the ultimate capacity by as much as 2 times.

   • **Efficiency**: The proposed slab model maintains the computation-efficiency of the grillage method. A numerical example studied in chapter 4 shows that the

proposed model can save computational time by as much as 22,000 times when compared with detailed finite element analysis using shell and brick elements.

- **Consistency**: The proposed slab model utilizes the plastic zone method to model material damage of the grillage member. The same plastic zone method is also being used to model material damage of steel frames and connections. Therefore, the distinct behaviors of various main structural components of composite building are modeled consistently using the same method. This consistent nature not only makes it easier for users to use only a single failure model but also avoids the use of sophisticated constitutive model for material damage.

2. New findings in structural robustness based on ePCA:

- The study in chapter 5 shows that belt truss system is a superior robustness enhancement for existing and new multi-storey composite building. Nevertheless it also points to a counter-intuitive finding, i.e. strong belt truss system is not necessarily beneficial as it tends to induce large force demand. The position of belt truss system is found to be one of the key factors influencing the force demand in the supporting columns. Therefore, special care should be given to the selection of the strength and position of the belt truss system when using it as robustness enhancement. To the best knowledge of the candidate, little discussion regarding the above-mentioned factors has been reported in the open literature.

- The study in chapter 6 provides a new evidence of the effectiveness of equivalent static analysis for large and realistic building structures. By taking nonlinear time-history analysis as the reference, the comparison study shows that the results of equivalent static analysis are more consistent and more accurate than the results of codified static analysis although both methods require practically the same computational effort. Therefore, it is recommended that the codified static analysis be replaced by equivalent static analysis as a design tool in the practice.

1.5   Research methodology and thesis outline

An overview of the research methodology is shown in Figure 1.1. In general, the research work presented in this thesis can be categorized in two stages. The first stage includes the development and verification of the proposed efficient progressive collapse analysis (ePCA) method. In the second stage, the efficiency of ePCA is utilized to perform dynamic and static progressive collapse analysis of large building systems. The first application of ePCA involves the study of key factors influencing the robustness performance of composite floor system under column removal event. Then, it is applied to study the potential of belt truss system as robustness enhancement of multi-storey composite building. Finally, ePCA is used to study the effectiveness of equivalent static analysis for robustness evaluation of building. In the study, comparison between the results of equivalent static analysis, codified static analysis and nonlinear time-history analysis are to be performed.

The thesis comprises seven chapters as follows:

Chapter 1: Introduction and literature review. This chapter provides an introduction to structural robustness and outlines the objectives, scope of work and the methodology of the research study carried out in this thesis. The final part of the chapter provides literature review of landmark events of structural collapse and current state-of-the-art research on structural robustness.

Chapter 2: Efficient progressive collapse analysis (ePCA): Methodology. This chapter presents an efficient methodology to model progressive failure behaviors of main structural components of a composite building, i.e. steel members, floor slabs and steel connections. One of the main features of ePCA is that the distinct failure behaviors of various main structural components are modeled using a consistent approach (i.e. the plastic zone method). The first component of ePCA is a general beam-column model for analysis of steel structures that exhibit member yielding, member buckling and global buckling behaviors when subjected to extreme loading conditions. Parametric studies are performed to investigate the influence of modeling parameters on the progressive collapse

behaviors and to draw recommendation for numerical studies in the subsequent chapters. The beam-column model is critical for robustness study of belt truss system, which performance is governed by the nonlinear post-buckling response of the brace members. The second component of ePCA is a slab model for analysis of composite slab when subjected to extreme loading conditions. The proposed slab model is based on a modified grillage approach that also uses the same plastic zone method to model the damage behaviors. The third component of ePCA is a connection model for fin plate shear connection. The same plastic zone method is used to simulate the semi-rigid and partial-strength behaviors of the connection.

Chapter 3: Efficient progressive collapse analysis: Verification. This chapter presents the verification study of ePCA. The first part of the verification study involves progressive collapse behaviors of building frames and truss structures under static and dynamic loadings. The second part of the verification study involves progressive collapse behaviors of reinforced concrete and composite slab, and the last part involves the progressive collapse behaviors of fin plate shear connection. In all of the verification studies, numerical solutions and experimental findings from published literature are used for comparison.

Chapter 4: Robustness design of composite floor system. This chapter applies the proposed ePCA to investigate the robustness performance of composite floor system, and subsequently to propose recommendations for robustness design of new composite building. Two critical cases of column removal are considered, namely the internal column removal and perimeter column removal cases. To verify the accuracy of the numerical models used in the studies, published numerical solutions and experimental findings are used for comparison. Subsequently, parametric studies are carried out to identify key design parameters that contribute to robustness of composite floor system, and to draw recommendations for effective robustness design.

Chapter 5: Robustness enhancement of composite building using belt truss system. This chapter applies the proposed ePCA to investigate the potential of belt truss system as robustness enhancement of multi-storey composite building. Parametric study involving

series of nonlinear time-history analyzes are carried out to investigate the influence of brace strength, slenderness ratio, truss configuration and position of the belt truss on robustness performance of the building. Subsequently, recommendations for robustness enhancement of new and existing multi-storey composite building using belt truss system are proposed.

Chapter 6: Equivalent static analysis for robustness evaluation of composite building. This chapter applies the proposed ePCA to investigate the accuracy of equivalent static analysis for robustness evaluation. The study focuses on the dynamic displacement and force demands incurred during sudden removal of column. Comparisons are made between the results produced by equivalent static analysis, codified static analysis and nonlinear time-history analysis for the composite floor systems and belt truss building studied in chapter 5 and 6.

Chapter 7: Conclusion and recommendation. This chapter summarizes the conclusions drawn from the research study, and provides recommendation for future research in structural robustness and progressive collapse analysis.

1.6   Literature review

As mentioned previously, performance-based method is a more realistic but also more computationally demanding method for robustness design of building structure. This method is also called the direct method in current building codes developed in the US (GSA, 2003; DoD, 2009). With the increased computational capacity of personal computers and the advent of advanced analysis software, performance-based method is increasingly popular among researchers and practitioners. In this section the current state-of-the-art research and practice of this method for robustness design will be discussed. In the first place, it is important to appreciate the lessons learned from past collapse events, which lead to the development and evolution of robustness criteria in building codes.

1.6.1   Landmark events of structural collapse

Collapse events in the past have contributed significantly to the evolution of modern structural design, especially on the aspect of safety and robustness. In this section three landmark events of structural collapse are described with emphasis on the lessons learned from these unfortunate failures.

1.6.1.1   Ronan Point Apartment (in 1968)

Partial collapse of the 22-storey Ronan Point Apartment occurred in the early hours of May 16, 1968 as a result of internal gas explosion on the 18th floor. The explosion blew out precast load-bearing wall on the 18th floor, causing a chain collapse in the gravity direction way down to the ground. Four residents were killed in the incident. Official report of the investigation quickly identified substandard brass nut used to connect the gas hose to the stove as the cause of the gas leak (Griffiths et al., 1968). The gas explosion was considered small and is expected to be lesser than 70 kN/m^2 given that the resident's hearing was not damaged and findings of tests conducted on items in the kitchen (Bignell et al., 1977). Lack of structural redundancy was identified as the ultimate cause of the Ronan Point collapse. The initial failure of the load bearing wall on the 18th floor removes the sole support for the floors directly above and created a chain reaction of collapse propagating upwards. Second phase of progressive collapse was initiated by the impact of falling floor debris that caused 18th floor to give way, smashing 17th floor, accumulating momentum while progressing downward until it hits the ground (Delatte, 2009). Deficiency of the structural system was identified at the wall-floor and wall-wall connection. Results from the extensive tests by the Building Research Station and Imperial College indicated that the walls could have been displaced by a pressure of only 19.3 kN/m^2 (Levy and Salvadori, 1992). Official investigation on the collapse estimated that the kitchen and living room walls can be moved at a pressure of as little as 1.7 kN/m^2, and exterior wall at 21 kN/m^2 (Griffiths et al., 1968). Building codes at that time contained no mention of redundancy or progressive collapse (Bignell et al., 1977). The lessons from Ronan Point incident changed building regulations throughout the world, most notably the development of amendment to the U.K. building regulations

in 1970. Under these regulations, all buildings of more than five storeys were to resist progressive collapse by designing for notional removal of a critical element, one at a time, to ensure alternate load paths. For any element that can withstand a specified static pressure in any direction, notional removal scenario can be omitted. For both alternatives, partial safety factor of 1.05 for dead loads plus one-third of live load should be used (Allen and Schriever, 1972). These provisions remain unchanged and are known as the "direct method" in present British code for steelwork design. Guidelines for tying of elements together to increase catenary action in case of local failure were proposed by the Portland Cement Association and the Prestressed Concrete Institute (Ross, 1984). This tying requirement coexists in present building codes and is better known as the "indirect method" in the literature.

1.6.1.2   Alfred P. Murrah Building (in 1995)

Partial collapse of Alfred P. Murrah office building in Oklahoma City occurred on 19 April 1995 due to blast loading. The structural system comprises of RC ordinary moment resisting frame with dimensions of 67 by 30.5 m on plan. The building is stabilized by shear walls in north-south directions and frame action in the rest. Peripheral columns spaced at 6.1m were discontinued on 3rd storey, where transfer girders were used at every 2 columns to increase ground column spacing to 12.2m. Details of the structural system can be found in the literature (Hinman and Hammond, 1997). A truck carrying approximately 1.8 tons of TNT charges detonated at approximately 4.9 m from the north face of the building. The blast action badly damaged three of the peripheral columns and initiated collapse of large area on the north side of the structure. The collapse of Alfred P. Murrah building exhibits an example of progressive collapse i.e. large collapse area caused by initial failure of a few columns in a relatively smaller area. Progression of collapse in both the vertical and horizontal directions were observed, in which the latter was caused by failure of column due to removal of stabilizing element by blast loading. Post collapse study included that modification of structural design using special moment frames and more recently developed detailing rules could reduce collapse area by 50 to 80% (Corley et al., 1998; FEMA, 1996; Hinman and Hammond, 1997). However, a recent study

warned that strengthening for seismic action alone may be insufficient for mitigating progressive collapse (Hayes et al., 2005) because the internal forces exerted on the structural frames are different during seismic excitation and column removal events.

1.6.1.3 World Trade Centre Tower 1 and 2 (in 2001)

The total collapse of WTC on 11 September 2001 is among the deadliest structural disasters ever occurred in modern civilization. Out of about 17,400 occupants of the towers, 2749 lost their lives (NIST, 2005). The collapse event was initiated by the impact of hijacked 767-200ER series airplanes. The WTC1 (north tower) was impacted at estimated velocity of 210 m/s between 94th and 98th storey from the centre of north face. Second collision happened right after the first collision at a velocity of about 254 m/s between 78th and 84th storey of the WTC2 (south tower), from the east face of the tower. Despite suffering great damage to the peripheral frame where great number of peripheral columns was lost, the tower did not collapse immediately. WTC1 stood for 1 hour and 43 minutes and WTC2 stood for 56 minutes after the collision. The fire attack due to flowing of jet fuel and dislodged fire protection weakened the structure over time. Sagging of floor structures due to fire action pulls the peripheral columns inward, which then buckled and initiated global collapse (FEMA, 2002; NIST, 2005). Collaborated study between government agencies and technical experts from the industry has been established to conduct detailed performance investigation (FEMA, 2002; NIST, 2005). The study concluded that both WTC towers should survive the impact was it not for the failing fire protection and multiple floor fire attack. The inherent robustness provided by the structural system, specifically the hat trusses was remarkable, and it is the redundancy and ductility provided by the combined hat-truss and peripheral vierendeel frame that sustain the towers until its global collapse. The tower collapsed in a progressive manner, but the collapse cannot be definitely labeled as disproportionate collapse seeing the cause of the initial damage, being combination of two extreme actions from aircraft impact and fire. It is deemed impossible to prevent collapse of this kind by imposing simple changes to the structural design, except the fire protection that might prolong the time to global collapse.

1.6.2   Robustness criteria in building codes

1.6.2.1   British Standards

The first robustness provision was developed by the British in the aftermath of Ronan Point collapse in 1968, and further motivated by the Irish Republican Army bombing campaign in the eighties. According to robustness provisions in Building Regulations, all buildings not exceeding 15 storeys or 5000 m^2 floor area on each storey and hospitals not exceeding 3 storeys and car parks not exceeding 6 storeys are deemed robust, provided the structural components are effectively tied together (ODPM, 2004). Provision of effective tying is similar to the ones in material-dependant structural design code (BSI, 1997; BSI, 2000). If effective tying cannot be provided, notional removal should be adopted for main load-bearing member, one at a time in each storey, and the remaining structure is to be checked for bridging capability. Performance is deemed satisfactory if collapse within the storey is limited to 15% of floor area of that storey or 70m^2, whichever lesser. A third of wind and imposed load is recommended for stability check, alongside other permanent loads. Partial load factor of 1.05 and 0.90 should be used for permanent loading adding to adverse and beneficial effect (BSI, 2000). For members that fail to satisfy notional removal requirement, key element design applies. These members need to withstand a static 34 kN/m^2 static pressure along with one-third of characteristic live and wind intensity.

1.6.2.2   European Standards

The European practice recognizes the essence of structural robustness in a multiple hazards context. The Eurocode 1 (BSI, 2006), in Clause 1.5.14 defines structural robustness as the ability to withstand accidental events like fire, explosion, flood, impact, earthquake or consequences of human error, without being damaged to an extent disproportionate to the original cause. As a general guide, the code recommends that the probabilities and effects of all accidental and extreme actions to be considered for a set of possible hazard scenarios. The consequences should then be estimated in terms of number of casualties and economic losses. The above-mentioned probabilistic approach is less suitable for implementation in general design office. On the other hand, the code also

recommends provisions of ductility and continuity similar to tying force requirements in British practice (BSI, 1997; BSI, 2000) and notional removal method. Details on evaluation method, however, are not given. The general strategies for robustness design are (a) identifying accidental actions and eliminating or reducing the hazard by designing the structure to sustain them and (b) limiting the extent of localized failure by using prescriptive rules, enhanced redundancy measures, and key element design. Recommendations for limiting damage to localized area documented in Annex A of the code are similar to British practice except minor differences in admissible collapsed area and tensile design forces for ties.

1.6.2.3   US Standards

GSA (2003) is intended as the reference for designing federal building against progressive collapse. The document provides more comprehensive and detailed guidelines than British and European codes. Unlike the British and European codes that do not explicitly require dynamic analysis for robustness evaluation, GSA (2003) recognizes the dynamic nature of progressive collapse events and recommends simplified or rigorous dynamic analysis to evaluate building robustness due to sudden column removal event. The sudden column removal approach is also called alternate load path approach in the literature and the DoD (2009) discussed below. The GSA (2003) suggests four types of analysis methods, i.e. linear static, nonlinear static, linear dynamic and nonlinear dynamic methods. When static analysis is used, the recommended accidental load combination for robustness evaluation is:

$$2.0\left(DL + 0.25LL\right) \tag{1.1}$$

where DL and LL is the dead load and live load respectively. The factor of 2.0 is the constant dynamic increase factor prescribed by the guide if dynamic analysis is not used. In other words, dynamic increase factor equals to unity should be adopted if dynamic analysis is used for robustness evaluation (i.e. linear dynamic or nonlinear dynamic methods).

14

To account for material damage and force redistribution in linear analyses, demand/capacity ratio greater than unity is prescribed in the guide for common structural systems. Nonlinear analysis is recommended by the guide, provided it is used by competent engineers. The linear methods (i.e. linear static and linear dynamic methods) are easier to apply compared to their nonlinear counterparts (i.e. nonlinear static and nonlinear dynamic methods), but do not necessary provide realistic information regarding structural damage. Therefore, the linear methods are not suitable for making design decision. Due to this reason, linear methods are not considered in the work presented in this thesis.

The dynamic deformation and force demands under sudden column removal event should be limited in order to mitigate the risk of disproportionate collapse. For steel-framed structure, excessive deformation demand could cause fracturing of steel connection and subsequently lead to a chain reaction of collapse propagating in vertical direction of the building. For common types of steel connection, the GSA (2003) provides recommendations for rotational capacities to be used in conjunction with nonlinear static or nonlinear dynamic analyses. These recommendations are summarized in Table 1.1. If deformation is exceeded, the structure is deemed to be susceptible to progressive collapse. As a result, the damage area due to the progressive collapse event needs to be evaluated. The guide has higher tolerance for the limitation of damage area as compared to the British code. For removal of interior support, the guide limits damage to 334 m^2 while exterior support damage is to be limited to 167 m^2. The building is categorized as deficient in robustness if the damage area is greater than the prescribed limit. For medium to high-rise buildings in general, any accidental event causing chain reaction of collapse propagating in the vertical direction is most likely to cause damage larger than the prescribed limit. Therefore for robustness design of multi-storey buildings, the vertical progressive collapse phenomenon needs to be mitigated. In addition, the guide also requires that the force demands generated by dynamic excitation during progressive collapse event be lesser than the force capacity of the columns. If this requirement is violated, another type of progressive collapse involving chain reaction of collapse in the horizontal direction may be triggered.

In addition to GSA (2003), the US Department of Defense also produced a guide for design of military facilities. Similarly, the DoD (2009) also suggests four types of analysis methods comprise of linear static, nonlinear static, linear dynamic and nonlinear dynamic for robustness evaluation. Three levels of protection against progressive collapse are defined i.e. very low, low, and medium/high level. A combination of horizontal and vertical tying force requirements, the alternate load path approach, and ductility requirements are recommended for each of protection level. For multi-storey buildings with high occupancy rate and of high importance, the alternate load path approach is a prerequisite. In the 2005 edition of the guide, the following accidental load combination is recommended for static analysis:

$$2.0\left[\left(0.9 \text{ or } 1.2\right)DL + \left(0.5LL \text{ or } 0.2SL\right)\right] + 0.2WL \tag{1.2}$$

where SL and WL is the snow load and wind load respectively. Similarly, the factor of 2.0 is the constant dynamic increase factor prescribed by the guide if dynamic analysis is not used. Elements that fails during a nonlinear dynamic analysis should be removed from the structural model and their loads should be doubled and applied to member directly below before analysis is continued. In the latest 2009 edition, the dynamic increase factor for steel framed structure is related to the ductility of the connection as in equation (1.3),

$$1.08 + 0.76/(\theta_{pra}/\theta_y + 0.83) \tag{1.3}$$

where θ_{pra} and θ_y are the plastic rotation and yield rotation capacities of the connection. Although the design loading is higher in DoD guide (DoD 2009), the underlying principles of both GSA (2003) and DoD (2009) guides are similar. For common steel connections with depth of bolt-group d_{bg}, DoD (2000) proposes the maximum plastic rotation (in radians) $\theta_{p,\max} = 0.0502 - 0.0015d_{bg}$ to be used in conjunction with nonlinear static or nonlinear dynamic methods. In addition, the force demand in supporting column needs also be checked to mitigate horizontal progressive collapse phenomenon.

1.6.3   Robustness evaluation

According to the criteria discussed above, robustness design necessitates progressive collapse analysis to obtain the deformation and force demands under sudden column removal event. Material damage and geometry nonlinearity need to be considered in progressive collapse analysis for realistic performance evaluation. This often leads to complex interaction between different structural components and construction materials. Therefore, robust numerical scheme and comprehensive library of material constitutive model are necessary to model the complex interaction and integrated responses of components and material of a composite building system. Due to these challenges, the use of state-of-art commercial software is common in the literature, e.g. the work by Fu (2009), Kwasniewski (2010), Yu et al., (2010), Sadek et al. (2008), among others.

1.6.3.1   Detailed finite element analysis

Fu (2009) studies the structural behavior of a three-dimensional 20-storey composite steel-framed building under sudden column removal event using finite element software ABAQUS (ABAQUS, 2005). The alternate load path approach as recommended by GSA (2003) (also discussed in section 1.6.2.3) is adopted in the study. The building has a typical column grid of 7.5 m and typical storey height of 3 m. The study considers two types of lateral systems, i.e. central RC core or steel bracing at perimeter frames. All beams and columns are simulated using beam elements in ABAQUS element library (ABAQUS, 2005), while slabs and walls are modeled as 4-node shell elements. The reinforcement in slab is assumed to act as a smeared layer. The material properties of all structural steel components are modeled using an elastic-plastic material model from ABAQUS library (ABAQUS, 2005). For concrete components, the material properties are modeled based on concrete damage plasticity model from ABAQUS library (ABAQUS, 2005). All beams are modeled close to the centerline of the main beam elements and the composite slab is modeled at the centerline of the slab. Rigid link constraint equations are used to couple beam and shell elements together to give composite action between them. Nine integration points for each shell element are used to capture the concrete cracking behavior. Steel beam to column connections are assumed to be fully pinned, and

no damage behavior is modeled for the connections. Therefore, important influences of the connections are not considered in the study. Five cases of column removals are studied, including a case involving removal of two columns. The study finds that the type of lateral-resisting system has insignificant influence on the structural response under column removal. The study also suggests that the axial force in columns, beams and braces are more or less doubled due to dynamic excitation during column removal. Therefore, the study suggests that the design force of connection should be at least twice of the static force under load combination of $1.0DL+0.25LL$.

Kwasniewski (2009) presents a case study of progressive collapse analysis of a multi-storey building using finite element software LS-DYNA (Hallquist, 2006). The building is an existing 8-storey composite steel-framed building built for fire tests in the Cardington Large Building Test Facilities, UK (British Steel, 1998). Similarly, the alternate load path approach recommended by GSA (2003) is adopted in the study. The study utilizes the advantage of parallel processing on multiprocessor computers to analyze detailed three-dimensional model with large number of finite elements. All beams and columns including the flush and fin plate connections are modeled using shell elements. Such detailed model allows for capturing local effects such as inelastic ending of end plates or local buckling of compressed flange. The bolts are represented by 1D beam elements. In the finite element model, component disintegration is represented by deletion (erosion) of a finite element from further calculation. General model for structural steel with hardening behavior is used to model the material behaviors all structural steel components. Von Mises criterion is used to represent the yielding surface of the steel components. The 130 mm composite slab is modeled using 4-node shell elements. Two types of shell element (of different thicknesses) are positioned side by side to model the orthotropic behaviors of composite slab. The first strip has a total thickness of 130 mm and the second 70 mm. Each strip is modeled as a multilayer composite using a sophisticated isotropic elastic-plastic model with different responses for tension and compression (MAT124) (Hallquist, 2006). The rigorous modeling adopted by the study leads to a huge model with 1.08 million number of shell and beam finite elements. Three cases of sudden column removal are considered in the analysis, i.e. removal of a corner

column, removal of a perimeter column or removal of an internal column. The study finds that the most critical case is removal of ground segment of the corner column which sustain less loading but is also less restrained. However, the author concludes that the study shows low potential for progressive collapse of the structure. The author recognizes that the proposed detailed finite element analysis is still not applicable in the practice due to the enormous computational demand. For example, one case of column removal would require 19 days of computational time using 60 parallel processors (Kwasniewski, 2009).

Yu et al (2010) studies the progressive collapse behaviors of composite floor system due to push-down experiment of the perimeter column using finite element software LS-DYNA (Hallquist, 2006). The focus of the study is the influence of connection and concrete slab on the effective tying of steel beams. The composite floor system studied is a single-storey composite steel-framed specimen tested by Tan and Astaneh-Asl (2003) at University of California, Berkeley. The floor slabs are made of concrete over metal deck that is supported by longitudinal and transverse beams. Fin plate shear connection is used for all beam-to-column and beam-to-beam connections. In the numerical model, the beams and columns are modeled as beam elements, while the metal decks are modeled as shell elements. Concrete slabs are modeled as constant stress 8-node solid elements. The slip between the metal deck and concrete is ignored. A simplified approach is adopted to model the connection behaviors, in which three basic types of connection are considered, i.e. pin connection, semi-rigid connection and hinged connection. Tensile deformation is simply accounted for by assuming a degradation of the elastic and tangent modulus of the elements in the vicinity of the connection. Findings of the study show that the rotation stiffness of the connection has significant effect of effective tying and has an important role to play in preventing progressive collapse of buildings. Therefore, more rigid connection is recommended for structural design. For retrofitting of existing building, Yu et al. (2010) also studies the potential of applying prestressed cables to improve the effective tying of the beams. The study shows that the prestressed cables can effectively improve the progressive collapse resistance, and its effectiveness increases with increase of number of attachments to the beam.

Sadek et al. (2008) studies the robustness of composite floor system with simple shear connection under internal column removal event using finite element software LS-DYNA (Hallquist, 2006). The floor system used in the study is a 2x2 bay subassembly of a prototype steel framed building designed by NIST (Liang et al., 2008) for robustness study. It has typical column grid of 6.1 m by 9.14 m. The beams, columns and metal decks are modeled using shell elements. Bilinear stress-strain relationship is used to model the material properties of the steel components. The concrete slabs are modeled as solid elements. A sophisticated concrete damage model (Material model 72 in LS-DYNA) (Hallquist, 2006) is used to model the concrete material properties. The concrete model uses a three-invariant, damage-based, non-associated plasticity formulation to model the inelastic behavior of concrete along multiple radial paths, including uniaxial, biaxial, and triaxial tension and compression. The formulation also employs a damage index that accumulates as a function of both the effective plastic and volumetric strains. Slab reinforcement is modeled using truss element which has a bilinear stress-strain relationship like other steel components. Shear studs are explicitly modeled as beam elements that are embedded in the concrete slab. Multiple contact constraints are defined between the concrete slab and metal deck, and the metal deck and top flanges of steel beams. The study shows that the membrane action of slab plays an important role in the collapse resistance. It contributes to the tensile catenary action to enhance floor capacity, at the same time providing the in-plan restraint to prevent column from being pull inward. The study also shows that the floor will be vulnerable to collapse when using GSA (2003) criteria for partially-restrained shear connection. As a result, the study proposes the use of stronger shear connection, thicker metal deck, higher density of slab reinforcement, and the use of moment connections instead of shear connections at every or intermittent floor.

Alashker et al. (2010) extends the study by Sadek et al. (2008) to investigate the key parameters influencing the robustness of composite floor subjected to internal column removal event. The numerical model is the same as the one used by Sadek et al. (2008) except some minor modifications, and it comprises of 295,000 shell and solid finite elements in total. The study shows that the steel deck contributes significantly to overall

collapse resistance of the composite floor system. Therefore, the study recommends that continuity of the steel deck should be ensured. The DIF derived from the composite floor system is 1.29, which is significantly smaller than the DIF = 2.0 specified by design codes.

1.6.3.2   Simplified finite element analysis

Marjanishvili and Agnew (2004) compare the effectiveness of linear static, nonlinear static, linear dynamic and nonlinear dynamic analyses for sudden column events. The author reviews respective advantages and disadvantages of each method and suggests that each analysis should be checked and selected for a target in a progressive way from linear static to nonlinear dynamic analysis. In a subsequent study (Marjanishvili and Agnew, 2006), the authors compare the effectiveness of the 4 methods suggested by GSA (2003) for progressive collapse analysis of a three-dimensional 9-storey moment resistant framed building. The study employs increasingly complex analytical procedures: linear static, nonlinear static, linear dynamic and nonlinear dynamic analyses for sudden column removal event. Numerical analyses are performed using finite element software SAP2000 (CSI, 2009). In the study, material damage is considered using simplified plastic hinge approach while geometry nonlinearity is ignored. This assumption prevents the development of catenary action which usually prevails when floor system is loaded to large deformation. On the other hand, the influence of floor slabs and beam-to-column connections are also ignored in the study. The findings show that dynamic analysis not only yields more accurate results, but is also easy to perform. In addition, the study also shows that the linear analysis method prescribed by GSA (2003) can sometimes be not conservative.

Kaewkulchai and Williamson (2004) developed a beam-column element for nonlinear dynamic progressive collapse analysis. The formulation assumes multi-linear, lumped plasticity hinge model with axial-bending interaction. Damage index is used to predict damage state at onset of failure. Stiffness and strength degradation are accounted for by a damage-dependant constitutive relationship. The influence of floor slabs and beam-to-column connections are ignored in the study. Application study on a planar frame shows that nonlinear dynamic analysis is more superior to nonlinear static method as some

failure modes and deformation demands are not correctly predicted by nonlinear static method. In a subsequent study, the authors extended the capability of the analysis to consider impact of failed members (Kaewkulchai and Williamson, 2006). Underlying assumptions on simulating impact are that the falling beam is assumed as point mass, and impacted beam is initially at stationary state, and full plastic impact where both beams move together after the impact and local deformation are insignificant. A 3-node beam element is used, where the 3rd node which is located at the mid-span is used to simulate the point of impact. An externally applied force is used to represent the gravity load carried by the falling beam. By using condensation process, degree-of-freedom of the third node is eliminated. The proposed numerical method is only sufficient for planar frame structure as it is unable to capture the behaviors of floor slab, connection and also three-dimensional frame action.

Izzuddin et al. (2008) proposes a simplified multi-level framework for progressive collapse assessment under sudden column-loss scenario in steel-frame structure. The method based on virtual work principle facilitates multi-level idealization to be implemented in daily design calculation. Simplified dynamic assessment based on energy equivalency concept is proposed as an alternative to rigorous nonlinear dynamic analysis. Mechanical models based on Eurocode 3 (BSI, 2005a) are used to represent the semi-rigid partial-strength behavior of the beam-to-column steel connections. On the other hand, simplified modeling of the floor slab is carried out using the equivalent width concept of Eurocode 3 (BSI, 2005). Numerical studies in the companion paper shows that common fin plate connection is more vulnerable although being more ductile compared to end-plate and angle-cleat shear connection (Vlassis et al., 2008). Moreover, provision of reinforcement bar continuous over the support greatly improves the connection performance. Recent study by Vlassis et al. (2009) extends the multi-level framework and simplified dynamic assessment to address floor impact scenario. Perfectly rigid and plastic impact scenarios are studied in analytical and numerical approach using nonlinear analysis program ADAPTIC.

Powell (2009) reviews the alternate load path method for progressive collapse analysis using nonlinear dynamic analysis on simple single-storey frame. In the study, material

damage is considered using simplified plastic hinge approach while geometry nonlinearity is ignored. The influence of floor slabs and beam-to-column connections are also ignored in the study. The author discusses the differences and efficiency associated with linear static, nonlinear static and dynamic analyses in predicting displacement demand. The study shows that nonlinear model is feasible for collapse assessment and model typically associated with earthquake analysis should be extended to consider for catenary action. A simplified dynamic analysis similar to Izzuddin et al. (2008) is proposed to account for dynamic effects associated with sudden removal of load-bearing component. The author, although recognizes the importance of nonlinear analysis in predicting key behavior during collapse, advocates that linear analysis should possibly be more practical in designing robust structure. The underlying principle of this recommendation is the complexity and uncertainty in predicting component behavior in accurate nonlinear analysis. The author concluded that nonlinear analysis provides better insight into structural behavior and should only be used for special and important structures, where else static linear analysis is adequate for common structures. Moreover, ductility and continuity e.g. horizontal and vertical ties should be provided throughout the structure.

Khandelwal and El-Tawil (2005) studies the vulnerability of moment resisting frames to sudden removal of internal column using macro-model numerical analysis. In the study, mechanical models are used to represent the semi-rigid partial-strength behavior of the beam-to-column steel connections. On the other hand, the influence of floor slabs is ignored in the study. The analysis shows behavior of inward pulling of exterior frame by internal column loss, which in turn forces out-of-plane deformation of the exterior frame. Significant P-Delta effects resulting from the unbalanced gravity force created additional demands, which ended with catastrophic failure of the entire structure. The study by Sadek et al. (2008) using detailed FEA shows that the floor slab can prevent column from being pull inward. Therefore, simplified FEA which ignores the floor slab may lead to unrealistic robustness evaluation. Nonetheless, Khandelwal and El-Tawil (2005) recognize that the accuracy of the presented results depends greatly on various modeling assumptions, which include frame idealization, use of roller for the boundary conditions,

modeling of gravity system using pin ended elastic members, the adoption of arbitrary failure criterion and consideration of rigid ground.

1.6.4   Robustness enhancement

For robustness design of new composite building, many researchers in the past, e.g. the works by Kim and Kim (2009b), Kim et al. (2009c), Liu (2010a), Sadek et al. (2008) have proposed the use of full-strength moment connections instead of shear connections. Their studies show that moment connections can improve the energy-absorbing capacity and survivability rate of a building when sudden column removal is considered. For buildings in low seismicity region that do not need ductile moment connection in the lateral resisting systems, their proposals can have significant impact on the economics of construction.

Liu (2010a) proposes novel retrofitting scheme for simple connection by converting conventional partial strength shear connection to full-strength moment connection. By using the proposed strengthening, progressive collapse resistance of floor structure under column removal event can be improved by catenary action. In the first paper (Liu, 2010a), catenary action of beam structure is being evaluated theoretically using a truss model. In the companion paper (Liu, 2010b), finite element analysis using commercial program ABAQUS (ABAQUS, 2005) is presented. In the numerical study, nonlinear responses of the original and strengthened connection under sudden column removal are compared. The study shows that the strengthened connection exhibits greater load carrying capacity compared with the original connection due to more effective catenary action.

Tan and Astaneh (2003) conducted experiment on a steel composite floor structure measuring 20 x 6m on plan. Fin plate shear connection is used at beam-to-beam and beam-to-column connections. First part of the experiment involves placing a series of four steel cables in floor deck and anchored to stiff core. Second part of the experiment involves retrofitting facade beams with series of two retrofit cables installed on the web of facade beams, one at each corner of the web-flange intersection. Experimental findings

show that the cables acting in catenary mode added to the strength of the system and prevented progressive collapse of the floor after removal of a middle column. The same floor system is also studied by Yu et al (2010) using finite element software LS-DYNA (Hallquist, 2006). The findings from Yu et al. (2010) also show that the prestressed cables can effectively improve the progressive collapse resistance. Furthermore, the effectiveness of the cable retrofit can be improved by increasing the number of attachment to the steel beam.

1.6.5 Concluding remarks

Literature review shows that most state-of-the-art robustness studies utilized detailed finite element analysis method using commercial program such as ABAQUS (ABAQUS, 2005) and LS-DYNA (Hallquist, 2006). This method is not only computationally demanding, but also very sophisticated for practical application. On the other hand, the use of simplified finite element analysis may lead to unrealistic evaluation of structural robustness due to omission of floor slab and simplified treatment of material failure in the analysis. Therefore, there is a pressing need to develop a realistic yet efficient method to bridge the gap between detailed finite element analysis and simplified finite element analysis. The realistic yet efficient method will be instrumental for innovation of robustness enhancement strategy, e.g. the development of innovative building system that performs well in structural robustness.

Table 1.1: Rotational capacities of partially-restrained steel connections (GSA, 2003)

Failure mode governed by	Plastic rotation (deg)	Plastic rotation (% rad)
Rivet in shear, flexural yielding of plates, angle or T-section	1.5	2.5
Bolt in shear, tension failure of plate, angle or T-section	1.0	1.5
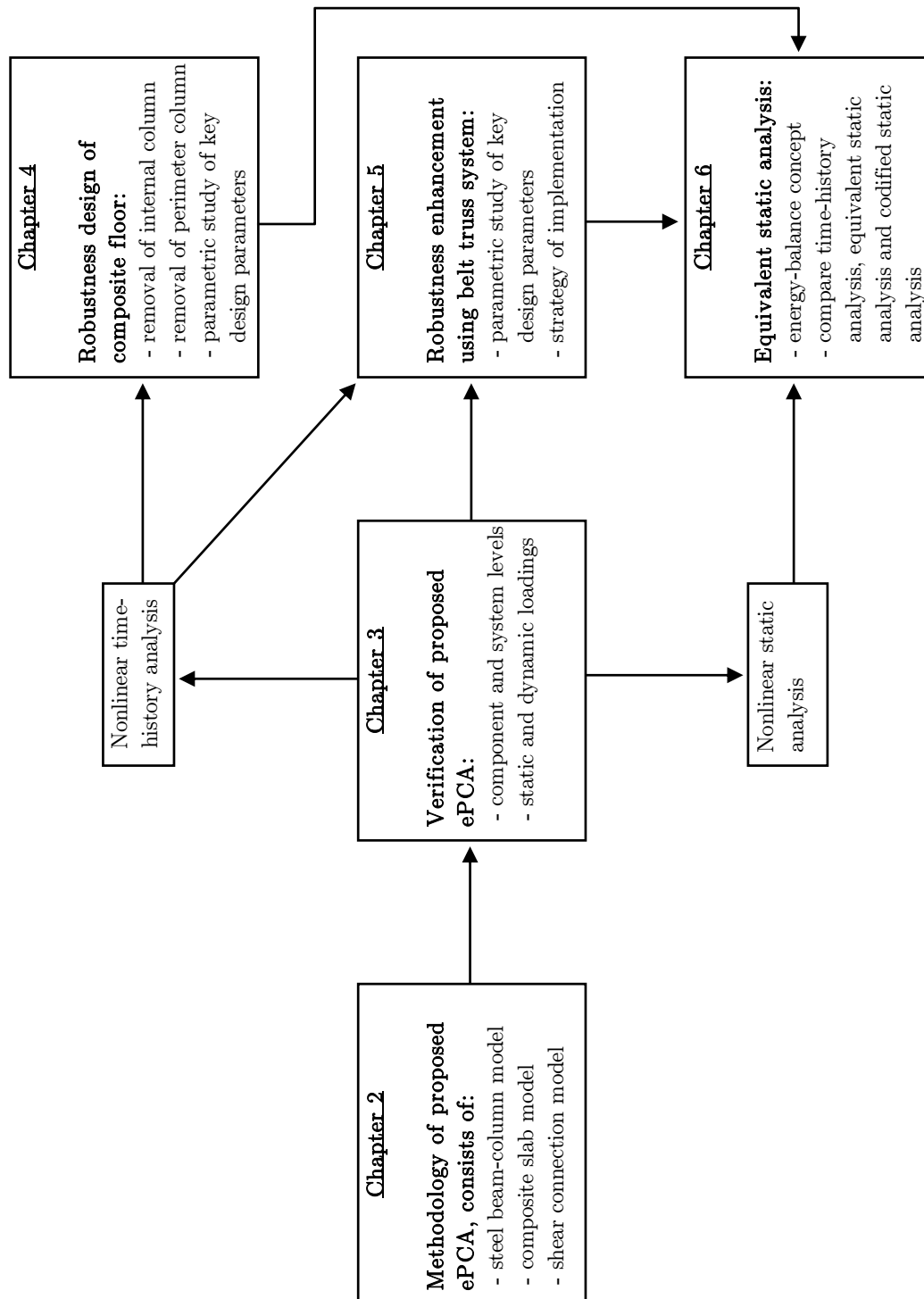
Figure 1.1: Overview of research methodology

Figure 1.2: Partial collapse of Ronan Point Apartment (Griffiths et al., 1968)

Figure 1.3: Partial collapse of Alfred P. Murrah Building (Hinman and Hammond, 1997)

Figure 1.4: Aircraft entry hole on the north side of WTC1, 30s after impact (NIST, 2005)

This page intentionally left blank

Chapter 2:   Efficient Progressive Collapse Analysis: Methodology

2.1 Introduction

Currently many methodologies for evaluating building robustness with regards to disproportionate collapse tend to be too sophisticated for practical application. These methods commonly involve progressive collapse analysis by detailed finite element analysis of large numerical model using commercial software such as ABAQUS (ABAQUS, 2005) and LS-DYNA (Hallquist, 2006). Some notable studies include the work by Alashker et al. (2010), Kwasniewski (2010), Yu et al. (2010), Fu (2009) and Sadek et al. (2008) etc. Detailed finite element analysis is not only computationally demanding, but also requires intensive pre/post processing effort. Furthermore, precise information of material and geometry of a structure is rarely available in the design stage. Therefore, it is often not justifiable to use highly sophisticated and computation-demanding method for robustness evaluation. At the other end of the spectrum, simplified finite element analysis involving macro-models, e.g. Kim and Kim (2009a), Marjanishvili and Agnew (2006), and Kaewkulchai and Williamson (2004) etc., are used which, nevertheless, do not simulate the ultimate and post-ultimate strength well. These simplified methods ignore the influence of floor slabs in resisting progressive collapse, thereby not providing realistic evaluation of structural system robustness. Motivated by the need for fast and reasonably accurate analysis, an efficient methodology for progressive collapse analysis of building due to column removal is proposed here.

The main purpose of efficient progressive collapse analysis (ePCA) is to provide practicing engineers with a fast and reasonably accurate method for design, involving efficient ways to model damage behaviors of main structural components of a composite building, i.e. steel members, floor slabs and connections. One of the main benefits of ePCA is that the distinct failure behaviors of various main structural components are modeled consistently using the same plastic zone method. This consistent nature not only makes it easier for users to use only a single failure model but also avoids the use of sophisticated constitutive model to account for material failure.

2.2 Modeling of slender steel member

Frames are likely the most common forms of man-made engineering structures. With the advent of strong material like steel, the influence of buckling in compression member becomes more pronounced due to its relatively slender dimensions. Therefore, the numerical model for steel member e.g. steel column and beam member of multi-storey building, brace member of truss system etc. should capture member and global buckling behavior in the progressive collapse analysis.

2.2.1 Review of column buckling capacity

Slender structural member fails in buckling under compression load. The basis of this failure mode is the Euler column theory, a perfectly straight and centrally loaded column supported by pin ends. One of the principal assumptions of Euler column theory is such that column remains elastic at onset of buckling. This assumption is only valid for very slender column. Many practical columns fall in the range of slenderness in which buckling response is governed by yielding of material. On the other hand, material and geometry imperfections exist in all practical columns. The imperfections are unavoidable products of fabrication and construction process, and have significant influence on the buckling capacity of steel columns.

2.2.1.1   Material and geometry imperfection

Residual stress is observed in all structural sections, which arises primarily from uneven cooling from rolling process and cooling of weld metal during fabrication of built-up section. The magnitude and distribution of residual stress in hot-rolled sections depend on the shape, rolling temperature, cooling conditions, straightening procedures and metal properties (Beedle and Tall, 1960). In welded sections, maximum tensile residual stress is found at a weld or in a narrow zone adjacent to a flame-cut edge.

Initial out-of-straightness due to fabrication process exists in all real columns and is often invisible to naked eyes. This is an unavoidable product of fabrication and construction process but it can be limited to a tolerable magnitude, often 1/1000 of the length. Laboratory measurements show that most hot-rolled wide flange sections tend to have out-of-straightness magnitude towards the maximum tolerable, with mean value of 1/1500 (Bjorhovde, 1972). Tubular sections exhibit smaller out-of-straightness value in the order of 1/3000 to 1/8000, with a mean of 1/6300 (Bjorhovde and Birkemoe, 1979). In the development of column strength criteria e.g. the Structural Stability Research Council curves (SSRC) (Bjorhovde, 1972) and the European Convention for Constructional Steelwork (ECCS) curves (Beer and Schultz, 1970), maximum tolerable value of initial out-of-straightness of 1/1000 is used. ECCS curves form the basis of current EC3 column curves (BSI, 2005a).

2.2.1.2   Buckling capacity according to Eurocode 3

A proper column strength model is one that incorporates both residual stress and initial out-of-straightness. In a major study that covers a spectrum of practical sections, steel grades and manufacturing methods, an extensive database of column strength has been developed (Bjorhovde, 1972). Key problem in developing rational column strength criteria is the strength variability through a collection of 112 maximum strength column curves. Distinct grouping of column curves in the database has been observed. This leads to the introduction of multiple column curves concept (Bjorhovde and Tall, 1971). The resulting average curves from the sub-groups were identified and known as SSRC column strength curve 1, 2 and 3. Subsequent work on multiple column curve concept in Europe

(Beer and Schultz, 1970) serves as the basis for column curves in current European practice, Eurocode 3 (BSI, 2005a). According to Eurocode 3 (BSI, 2005a), buckling reduction factor χ defines the ratio of buckling to yielding capacity of a column, and is expressed in equation (2.1) as,

$$\chi = \frac{1}{\varphi + \sqrt{\varphi^2 - \bar{\lambda}^2}} \leq 1.0 \qquad (2.1)$$

where,

$$\varphi = 0.5\left[1 + \alpha\left(\bar{\lambda} - 0.20\right) + \bar{\lambda}^2\right]$$

and,

$$\bar{\lambda} = \frac{1}{\pi}\sqrt{\frac{f_y}{E}}\frac{L}{r} \qquad \alpha = \begin{cases} 0.13 \text{ ... for curve } a_0 \\ 0.21 \text{ ... for curve } a \\ 0.34 \text{ ... for curve } b \\ 0.49 \text{ ... for curve } c \\ 0.76 \text{ ... for curve } d \end{cases}$$

where f_y, E_s, L and r are the yield strength, elastic modulus, buckling length and radius of gyration about axis of buckling. The influence of imperfections is considered by imperfection factor, α. EC3 (BSI, 2005a) provides guidelines on selection of α based on the structural shape, fabrication method and buckling axis of a column.

2.2.2 Review of column post-buckling capacity

In conventional inelastic analysis, response of truss member is represented by simplified axial force-displacement or axial stress-strain relationship. Elastic response is assumed in the compression response up to the buckling capacity, magnitude of which is determined by theory of Euler column. Effective length factor needs to be assumed based on the boundary conditions of the truss member. Beyond the elastic response, the post-buckling capacity is assumed as a fraction of its buckling capacity.

2.2.2.1   Strut Model by Hill et al. (1989)

Hill et al. (1989) presents a simplified model to simulate the post-buckling response of pin-end truss structure. Response of the truss model in compression and tension is idealized as shown in Figure 2.1a. When subjected to tension force, the truss behaves in an elastic-perfectly-plastic manner. Therefore, the stress-strain relationship in tension is as,

$$\sigma = \begin{cases} E\varepsilon \ \dots \ \varepsilon < \varepsilon_y \\ \sigma_y \ \dots \ \varepsilon \geq \varepsilon_y \end{cases} \qquad (2.2)$$

where ε_y and σ_y is the yield strain and corresponding stress. In compression, the stress-strain relationship is linear up to a critical stress, σ_{cr}. The critical stress is derived directly from Euler buckling load, which is described as,

$$\sigma_{cr} = \frac{\pi^2 EI}{AL^2} \qquad (2.3)$$

$$\varepsilon_{cr} = \frac{\sigma_{cr}}{E}$$

For stocky member, response dominated by material yielding is represented by the yield plateau (constant critical stress between $\boldsymbol{\varepsilon}_{cr}$ and $\boldsymbol{\varepsilon}_0$ in Figure 2.1a). However, for slender member, unloading occurs almost immediately after critical stress is achieved; therefore ε_{cr} is equal to ε_0. The unloading phase is described by,

$$\sigma = \sigma_1 + (\sigma_{cr} - \sigma_1)\exp\left[-\left(\chi_1 + \chi_2\sqrt{\varepsilon'}\right)\varepsilon'\right] \qquad (2.4)$$

where χ_1 and χ_2 are the parameters calculated using nonlinear regression analysis techniques to fit the experimental data. The initial slope of the inelastic post-buckling curve is a function of χ_1. Parameter χ_2 influences the rate of change of the inelastic post-buckling modulus (Hill et al., 1989).

2.2.2.2   Strut model by the Canadian standard (CSA, 1984)

The Canadian standard recommends a simplified tri-linear truss model as shown in Figure 2.1b. In compression, the force-shortening relationship is linear up to the buckling capacity C_r. Beyond that, the capacity reduces linearly to the post-buckling capacity, C_r'. Constant post-buckling capacity is assumed beyond a displacement equals to five times of the yielding displacement. For a truss with cross-sectional area (A) and yield strength (F_y), the response of the model can be described as,

$$C_r = \phi A F_y \left(1 + \lambda^{2n}\right)^{-1/n} \tag{2.5}$$

$$C_r' = \frac{C_r}{1 + 0.35\lambda}$$

$$\lambda = \frac{kL}{r\pi}\sqrt{\frac{f_y}{E}}$$

where,

$$\phi = \text{resistance factor} = 0.9$$

$$k = \text{effective length factor}$$

$$n = 2.24 \text{ for wide-flange and hollow section}$$

2.2.3 Beam-column model including effects of imperfection

The simplified models are unable to explicitly address the influence of imperfections, boundary conditions and interaction between global second-order effect (P-Δ) and member second-order effect (P-δ). As a result, the simplified models are only applicable for conventional and regularly-shaped structures, e.g. pin-end trusses and braced frames etc. An advanced analysis will be required for realistic performance evaluation of complex structure such as the composite building with belt truss system discussed in Chapter 5.

Advanced analysis refers to numerical method that captures the strength and stability of a structural system in such a way that separate member capacity checks are not required (Chen, 2008). In general, there are three categories of advanced analysis, i.e. elastic-plastic hinge, refined plastic hinge and plastic zone method, in ascending order of accuracy and complexity. The elastic-plastic hinge method is the simplest approximation of material inelasticity by assuming that all inelastic effects concentrate at zero-length plastic-hinge location. For second-order analysis, geometric nonlinearity can be included using stability function. This method is sufficiently accurate for slender member, but can overestimate the strength of stocky column under combined axial force and bending moment due to distributed plasticity effect (Chan, 2001). The refined plastic hinge method is an improved version of elastic-plastic hinge method by incorporating effects of residual stress, member imperfection and distributed plasticity. The plastic zone method is the most accurate method among all (Chan, 2001; Chen, 2008), and is commonly used as the reference for calibration of other methods. The plastic zone method is also the most computational demanding method among the advanced analysis methods. However, with the advent of cheap and powerful personal computer, this method is gaining popularity among researchers and practicing engineers in recent years.

2.2.3.1   Plastic zone method

A beam-column model capable of capturing buckling and post-buckling behaviors of steel member is shown in Figure 2.2. The model is based on plastic zone method that requires discretization of a section into fibers and a member into many beam-column elements. The stiffness of the section is obtained by integrating the stiffness of those fibers across the section by assuming plane section remains plane. This way, gradual spreading of plasticity across section and along member can be accurately analyzed. The beam-column model can also consider the influence of material and geometry imperfection. Residual stress can be included into stress-strain relationship of individual fiber according to measured profile or simplified profile as recommended by European Convention for Constructional Steel (ECCS, 1983). To consider for geometry imperfection, explicit modeling of the initial out-of-straightness e_0 is adopted according to principal buckling mode shape (Chen, 2008). The main assumptions of the method are (1) plane sections

remain plane after deformation, (2) lateral torsional buckling is prevented, (3) local buckling of cross-section is prevented, (4) effect of shear on yielding of the material and deformation is negligible, and (5) residual stress is uniformly distributed over the entire length of a member.

The beam-column model is implemented in a commercial finite element analysis program SAP2000 (CSI, 2009). For ease of illustration, the steel member shown in Figure 2.2 is discretized into 14 elements, in which eight of them are inelastic (hatched region) and the remaining are elastic elements. For inelastic element, distributed plasticity along the element is simulated by using a fiber hinge (monitored locations shown in Figure 2.2) located at the centre of element. In each inelastic element, distribution of plastic moment and curvature are constant. Therefore, small element length is required within the inelastic region for accurate simulation of distributed plasticity along the steel member. The inelastic element requires significantly greater computational resources than elastic element. Therefore, a good engineering practice is to use inelastic elements only at critical locations where inelasticity is expected. For a beam-column subjected to axial and bending forces, these critical locations are most likely at the mid-span and member ends.

The plastic zone length L_p represents the region where inelasticity can take place. Therefore it should cover critical locations where inelasticity is most likely to occur, e.g. member ends and mid-span. The length of L_p is governed by two requirements. First, the plastic zone should extend sufficiently to simulate spread of plasticity of the steel member in the post-buckling response. Second, the plastic zone should extend sufficiently to capture yielding which occur away from the mid-span. This phenomenon is possible for fixed-pinned column in a non-sway frame and continuous column in a sway frame as shown in Figure 2.3.

At the monitored location, the column cross-section is discretized into fibers as shown in Figure 2.4. The fibers are assumed to follow standard bilinear hardening model as shown in Figure 2.2a. The stress (σ) and strain (ε) relationship can be expressed as,

$$\sigma = \begin{cases} E_s \varepsilon & \dots \ \varepsilon < \varepsilon_y \\ f_y + \alpha E_s \left(\varepsilon - \varepsilon_y \right) & \dots \ \varepsilon \geq \varepsilon_y \end{cases} \qquad (2.6)$$

where f_y, E_s and α is the yield stress, elastic modulus and strain-hardening ratio respectively.

The geometric characteristics of the fiber are its location in the local axis system and the fiber area. Section constitutive relations are obtained by integrating uniaxial stress of the fibers across the section. Assuming plane section remains plane, the axial and bending rigidities can be defined as,

$$EA = \sum_{i=1}^{m} E_i A_i \qquad \text{and} \qquad EI = \sum_{i=1}^{m} E_i A_i d_i^2 \qquad (2.7)$$

The axial resistance (N) and bending resistance (M) can be defined as,

$$N = \sum_{i=1}^{m} \sigma_i A_i \qquad \text{and} \qquad M = \sum_{i=1}^{m} \sigma_i A_i d_i \qquad (2.8)$$

where,

E_i = material tangent modulus

A_i = area of the i$^{\text{th}}$ fiber

σ_i = normal stress of the i$^{\text{th}}$ fiber

d_i = level arm of the i$^{\text{th}}$ fiber

and m is the total number of fibers in the cross section. The use of fiber cross-section has eliminated the need for axial-moment interaction relationship.

Geometric nonlinearity effects are captured by updating the geometry at each incremental displacement step. The concept of the method in tracing equilibrium path of a static problem can be written in the incremental equilibrium equation as follows (Chan, 2001),

$$\left[K_p + K_G + K_0 \right]\left[\Delta\lambda\Delta F \right] = \left[\Delta u \right] \tag{2.9}$$

where, $\Delta\lambda$, ΔF and Δu are the incremental load factor, incremental force vector and incremental displacement vectors respectively. K_p and K_G are the elastic-plastic stiffness matrix considering material inelasticity and geometric stiffness matrix considering effects of initial stress. The effect of large displacement is included in the large deflection matrix K_0. The nonlinear equation can be solved based on incremental-iterative scheme using displacement-based Newton-Raphson algorithm.

2.2.3.2   Parametric study of key modeling parameters

Finite element method is an approximate approach, which relies on shape function in estimating structural response. Accuracy of this method generally increases with degree of discretization and computational demand. Therefore, parametric study is necessary to determine the proper degree of discretization for best compromise between efficiency and accuracy. In this section, buckling response of column under incremental compression load is studied for varying modeling parameters. These parameters comprise plastic zone length L_p, element length along member, number of fiber across section, geometry and material imperfections. The column specimens considered in the numerical study consist of a wide-flange section (UC305x406x634) and a box section (SHS150x150x8). In addition, two boundary conditions are considered for each column specimen, i.e. pinned-pinned and fixed-pinned conditions. In the parametric study, all steel materials are assumed to have consistent yield strength, elastic modulus and strain hardening ratio of 355 N/mm^2, 210 kN/mm^2 and 0.3% respectively.

2.2.3.2.1   Plastic zone length, L_p

L_p equal to L, $L/2$, $L/4$ and $L/8$ are used in the parametric study, where L denotes the member length. L_p is proportioned in such a way that plastic zone at the mid-span is twice of the one at member ends as larger plastic rotation is expected at the mid-span. All specimens are modeled using consistent member and cross-section discretization, in which element length of $L/72$ and $L/24$ are used in the plastic zone and elastic zone, respectively. Parametric study in the next section (i.e. section 2.2.3.2.2) shows that the selected element length is sufficient to ensure convergence of results. All specimens are modeled using consistent out-of-straightness of $L/1000$ whilst residual stress is ignored. The first specimen is a fully plastic member and is deemed as the most accurate among all. Therefore, this specimen is treated as the control specimen.

Influence of L_p for different cross sections and boundary conditions is shown in Figure 2.5. For comparison purpose, column capacities for various L_p are normalized to the control specimen (i.e. $L_p = L$) as summarized in Table 2.1. For both types of boundary conditions, the buckling strengths are found to be about 26.6×10^3 kN and 1.45×10^3 kN for wide-flange and box column, respectively. In this study, post-buckling strength is taken as the residual capacity at ten times the buckling displacement, i.e. about 10 mm for wide-flange and 6.5 mm for box column. The findings shows that shorter plastic zone tend to produce stiffer response, especially in the post-buckling strength. Maximum overestimation of buckling strength and post-buckling strength is found to be about 4% and 15% for wide-flange column modeled with shortest L_p, i.e. $L/8$. This overestimation is more pronounced in specimens with wide-flange section and fixed-pinned boundary condition than others. The larger difference in wide-flange specimens is due to the significant spread of plasticity in these stocky columns. On the other hand, the larger difference in fixed-pinned boundary condition is due to the inability of short L_p to capture yielding located away from the mid-span. This study recommends that L_p should be at least $L/2$ such that overestimation of post-buckling response is kept within 3%.

2.2.3.2.2 Element length within plastic zone

In this section, influence of element length within plastic zone is studied. Four element lengths, i.e. $L/72$, $L/36$, $L/24$ and $L/12$ are studied. Accuracy of adopting L_p of $L/2$ is verified in the previous section, therefore is adopted in current study. Influence of element length for different cross-sections and boundary conditions is shown in Figure 2.6, while the normalized buckling and post-buckling capacities are summarized in Table 2.2. Comparing to L_p, element length has significantly lesser influence on both buckling and post-buckling responses. Maximum difference of 6% is observed in specimen with the largest element length. This study recommends that the element length within the plastic zone should be lesser than $L/24$ such that overestimation of post-buckling response is kept within 3% range.

2.2.3.2.3 Number of fibers across section

Section fiber subdivision can be done according to rectangular grid of lines for wide-flange and rectangular hollow section, or radial grid of lines for pipe section as shown in Figure 2.4. Each plate component of a cross section can be subdivided into n_1 layers along the plate and n_2 layers through the plate thickness. For parametric study, six modeling techniques shown in Figure 2.7 are used. The study shows that subdivision based on $n_1 = 5$ and $n_2 = 1$ can be used without compromising its accuracy in predicting the buckling and post-buckling response. Refined subdivision is not required for steel member as most of its material is concentrated at the extreme fibers of the cross section.

2.2.3.2.4 Material imperfection (residual stress)

Residual stress exists in all practical columns and can reduce buckling capacity of a column. In this section, influence of the residual stress on the buckling and post-buckling responses is studied. Based on the residual stress profile recommended by the European Convention for Constructional Steelwork (ECCS, 1983), maximum residual stress of 0%, 25%, 50%, 75% and 90% of the yield strength (i.e. 355 N/mm^2) is considered in the study. According to ECCS (1983), the residual stress profiles for beam (H/B > 1.2) and column (H/B ≤ 1.2) are shown in Figure 2.8. Previously recommended values for plastic zone

length, element length and fiber section discretization are used in this study. As shown in Figure 2.9, residual stress can significantly reduce the buckling capacity of wide-flange (UC356x406x634) specimens, and highest reduction is observed in specimen with pinned-pinned boundary condition. However, the residual stress has negligible effect on the post-buckling response in both specimens. Therefore, the softening effect of residual stress on the buckling capacity can either be omitted or considered using simplified method (i.e. enhanced out-of-straightness discussed in section 3.2.1 of chapter 3) in progressive collapse analysis.

2.2.3.2.5   Geometry imperfection (initial out-of-straightness)

In addition to material imperfection, geometry imperfection or out-of-straightness also exists in all practical columns. In this section, influence of the out-of-straightness is studied. Based on sinusoidal profile, maximum out-of-straightness of 4%, 2%, 1%, 0.1% and 0.01% of the column length is introduced at the mid-span. Previously recommended values for plastic zone length, element length and fiber section discretization are used in this study. As shown in Figure 2.10, geometry imperfection can significantly reduce the buckling capacities of both box and wide-flange specimens. Similar to the influence of residual stress, the initial out-of-straightness has negligible influence on the post-buckling response of the column specimens. Modeling of initial out-of-straightness for large and complex building system is more convenient as compared with modeling of material imperfection. Therefore, it is possible to increase the magnitude of initial out-of-straightness to account for the softening effect of material imperfection without compromising the accuracy for progressive collapse analysis. Based on this concept, enhanced out-of-straightness will be calibrated in chapter 3 to produce buckling capacity that is consistent with Eurocode 3 (BSI, 2005a).

2.3 Modeling of concrete and composite slab

In most of framed building, the floor consists of reinforced concrete slab that spans between grids of supporting beams. Despite the thin and lightly-reinforced nature, the slab can still contribute significantly to the overall progressive collapse resistance of a

building in the event of sudden column loss. Under normal loading condition, the out-of-plane deformation of the slab is relatively small compared to the span length. Therefore the slab behaves predominantly in flexural mode. Membrane action is negligible at this stage of response, except the strip of slab along the supporting beam where the slab acts as the top flange of composite beam system. When a slab is subjected to extreme loading, e.g. sudden column removal, very large out-of-plane deformation is expected. Under such condition, the slab is no longer behaving in flexural mode, but more toward membrane mode in maintaining force equilibrium in the vertical direction.

For a uniformly-loaded simply-supported slab as shown in Figure 2.11, tensile membrane action (i.e. catenary action) prevails when the maximum displacement exceeds the depth of the slab (Elghazouli and Izzuddin, 2004). Force equilibrium is achieved in the form of membrane forces and improves the load carrying capacity of the slab. Compression membrane action in the form of a "ring" is generated to resist the out-of-balance tensile force in maintaining force equilibrium of the highly-deformed slab. The progressive collapse behavior of floor slab is highly complex and most numerical tools used in design office are incapable to simulate these behaviors with reasonable accuracy. In this section, an efficient slab model based on modified-grillage approach is proposed. Due to the numerical efficiency and simple pre/post-processing, the proposed model can potentially be used by practicing engineers to perform robustness evaluation for building design. The proposed slab model is mainly developed for analysis of composite slab comprises of profiled deck with reinforced concrete topping as shown in Figure 2.12. However, the model is also applicable for conventional reinforced concrete slab as shown in the numerical examples discussed in chapter 3.

2.3.1 Proposed slab model based on modified grillage approach

The use of grillage method for progressive collapse analysis of slab is not new. In the past, some studies (e.g. Elghazouli and Izzuddin, 2001; Izzuddin et al., 2002) have adopted grillage method to investigate fire performance of composite floor. In the studies, steel deck is ignored because it loses stiffness and strength very quickly once exposed to fire

action. However, this assumption is not valid when sudden column removal is considered as the steel deck contributes significantly to the ultimate and post-ultimate strength of composite floor system (as will be shown in chapter 4). Therefore, the grillage method needs to be modified to include the contribution of the steel deck to the progressive collapse resistance.

2.3.1.1 Grillage member

For a plate element under transverse loading q, governing equation for vertical equilibrium can be expressed as,

$$\frac{\partial^2 m_x}{\partial x^2} + \frac{\partial^2 m_y}{\partial y^2} + 2\frac{\partial^2 m_{xy}}{\partial x \partial y} = -q \tag{2.10}$$

where m_x and m_y are moments per unit length about x axis and y axis, and m_{xy} is the torsional moment per unit length. The flexural responses of the plate can be decoupled by ignoring the torsional response (the third term from left hand side of equation (2.10)). As a result, the plate can be simplified as a series of torsion-free frame elements consist of the geometry equivalent to the slab strip it represents. This simplification leads to lower-bound estimation of the flexural capacity. However, the magnitude of underestimation is negligible as progressive collapse resistance is predominantly governed by the membrane action at large deformation.

Figure 2.13 shows the main components of the proposed slab model based on modified-grillage method. In direction transverse to the steel deck, the grillage member can be taken as a rectangular section with height h_c, which is the same as the height of reinforced concrete topping above the steel deck. The concrete within the steel deck height h_d is ignored. In direction parallel to the steel deck, the smeared behaviors of profiled composite slab can be represented by series of grillage members with equivalent T-section. The geometries of the equivalent T-section can be derived as,

$$C_1 = \left(\frac{B_1}{s}\right)\left\{0.5\left(b_2 - b_1\right) + b_1\right\} \tag{2.11}$$

where B_1 and C_1 is the width of the flange and web of the equivalent T-section. b_1, b_2 and s are the geometries of the rib as shown in Figure 2.13c. Unlike the physical deck that consists of uniform thickness t_d, deck thickness of the equivalent T-section varies according to the grillage and deck geometries as,

$$t_1 = \left(\frac{b_1 t_d}{s}\right)\left(\frac{B_1}{C_1}\right) \tag{2.12}$$

$$t_2 = \left(\frac{B_1}{s}\right)\left(\frac{t_d}{h_d}\right)\sqrt{\left\{0.5\left(b_2 - b_1\right)\right\}^2 + h_d^{\,2}} \tag{2.13}$$

$$t_3 = \left(\frac{b_1 t_d}{s}\right)\left(\frac{B_1}{B_1 - C_1}\right) \tag{2.14}$$

The same plastic zone method presented in section 2.2.3 can be used to model the damage behavior of the grillage member. Sectional response of the grillage member is accounted for by the fiber section approach. Internal forces are determined by integrating the uniaxial response of each fiber across the section assuming plane section remains plane. Axial-bending interaction relationship is accounted for implicitly by the fiber section approach therefore no assumption of this relationship is necessary. For each of the concrete fiber, the uniaxial stress-strain behavior is assumed to follow Eurocode 2 unconfined concrete model (BSI, 2004a). The compressive stress-strain relationship is shown in Figure 2.14 and expressed in the following equation,

$$\sigma_c = f_c\left(\frac{k\eta - \eta^2}{1 + \left(k - 2\right)\eta}\right) \tag{2.15}$$

where,

$$\eta = \varepsilon_c \,/\, \varepsilon_{c1}$$

$$\varepsilon_{c1} = \text{strain at peak stress} = 0.7 f_c^{0.31} < 2.8$$

$$k = 1.05 E_c \times \varepsilon_{c1} \times \frac{1}{f_c}$$

$$E_c = 22,000 \times \left(\frac{f_c}{10}\right)^{0.3}$$

Meanwhile, the materials of steel deck and reinforcement mesh are assumed to follow the same stress-strain relationship of the structural steel as shown in Figure 2.2a and also expressed in equation (2.6).

2.3.1.2   Truss analogy

The slab is likely to undergo large deformation when subjected to extreme loading event, such as sudden column removal. Membrane action in the form of tensile catenary and compressive ring become the main load resisting mechanism of floor slab in the large out-of-plane deformation state. Conventional grillage method cannot capture these membrane behaviors due to deficiency in modeling the in-plane shear response. To overcome this, a truss analogy is adopted in the proposed slab model to realistically model the in-plane shear behavior.

The pin-ended truss system shown in Figure 2.15 can be used to demonstrate the concept of truss analogy adopted in the proposed slab model. At small deformation, the truss system has negligible stiffness when subjected to out-of-plane load. The truss system gains higher stiffness due to tension catenary action as it deflects downward. To maintain vertical force-equilibrium, the out-of-balance force at member-end of tension truss is resisted by the diagonal truss in compression (dashed line in Figure 2.15). This self-equilibrium load-resisting system resembles the tensile catenary and "compressive ring" action of a floor slab when loaded to large deformation. To represent the in-plane shear behavior of a concrete panel using the truss analogy, an equivalent axial stiffness for the diagonal truss member needs to be derived.

Assuming classical shear stress-stain rule of $\tau = G\gamma$ and uniform distribution of shear stress across the shear area, the shear deformation Δ of a concrete panel with width B and depth D as shown in Figure 2.16a can be derived as,

$$\Delta = \left(\frac{B}{D}\right) \times \left(\frac{V}{Gh_c}\right) \qquad (2.16)$$

where V, G and t is the acting shear force, material shear modulus and thickness of the shear panel respectively. Meanwhile, the shear deformation Δ of an equivalent truss system of similar geometry as shown in Figure 2.16b can derived as,

$$\Delta = \left(\frac{V}{k_s}\right) \times \left[1 + \left(\frac{D}{B}\right)^2\right] \qquad (2.17)$$

where k_s is the spring stiffness. By combining equation (2.16) and (2.17), the equivalent spring stiffness that gives the same shear deformation can be derived as,

$$K_s = Gh_c\left(\frac{D}{B}\right)\left[1 + \left(\frac{D}{B}\right)^2\right] \qquad (2.18)$$

For modeling purpose, the spacing of grillage in orthogonal direction should be made similar (i.e. $B \approx D$), because the direction of shear force is unknown for complex problem. Therefore, the spring stiffness can be simplified to,

$$K_s = 2 \times G \times h_c \qquad (2.19)$$

When using equation (2.18) and (2.19), the material shear modulus needs to be specified. For concrete material, the shear modulus is described in equation (2.20) as the function of the elastic modulus E_c and Poisson ratio υ.

$$G = \frac{E_c}{2(1+\upsilon)} \qquad (2.20)$$

According to Eurocode 2 (BSI, 2004a), the Poisson ratio can be taken as 0.2 for uncracked concrete, and the elastic modulus is related by the concrete compressive strength f_c as,

$$E_c = 22,000 \times \left(\frac{f_c}{10}\right)^{0.3} \qquad (2.21)$$

2.4 Modeling of steel connection

The collapse resistance of a composite floor system is not only governed by the floor slab, but also the steel connection. In the event of column removal, floor structure is forced to span longer in search of alternate load path. As a result, the connections being the weakest segments of the structural frame are subjected to significant increase of stresses. In most circumstances, the connections are the first to suffer damage and fracture among all other failure modes.

Many studies in the past (e.g. Kim and Kim, 2009b; Liu, 2010; Kim et al., 2009c; Sadek et al., 2008) have proposed the use of full-strength moment connections for robustness design of new composite building. The studies show that moment connections can improve the energy-absorbing capacity and survivability rate of a building when sudden column removal is considered. For buildings in low-seismic region that do not use ductile moment connection in the lateral resisting systems, their proposals can have significant impact on the economics of construction. On the other hand, it is common in low-seismic practice (e.g. Singapore) to adopt nominally pinned connection, i.e. shear connection in multi-storey composite buildings. It is invariably cheaper to fabricate than moment connection, because it provides significant degree of simplicity and standardization (Davison and Owens, 2003).

The shear connection has relatively low bending stiffness and strength as compared to the connected steel members. It is only designed for nominal moment and axial force according to current prescriptive code (BSI, 2000). Therefore the connection may not be able to sustain the significant increase in stress in the event of sudden column removal. Currently research on the survivability of building adopting shear connections has not come to a consensus. Some studies (e.g. Sadek et al., 2008; Vlassis et al., 2009) suggest that shear connection designed to the minimum tie force requirement of the prescriptive code does not necessarily protect against disproportionate collapse in the event of sudden column loss, while the opposite is claimed by others (e.g. Tan and Asl Astaneh, 2003; Kwasniewski, 2010). In respect to this, it is likely that the survivability of a building depends on the structural configuration on a case by case basis, and the use of shear connection cannot be totally disregarded based on findings of a few specific cases. Therefore, it is important to develop a computationally-efficient methodology for progressive collapse analysis, such that building robustness can be evaluated on a case by case basis.

There are three common types of shear connection, i.e. (1) flexible end plate, (2) double angle cleat and (3) fin plate. Among all, fin plate is the most popular type of shear connection in local construction practice because it offers advantages such as flexibility to allow for non-orthogonal framing, rapid erection, simple fabrication and it is more tolerable to lack-of-fit problem during the construction (BCSA, 2002). Therefore, the work presented here will focus primarily on the influence of fin plate shear connection on progressive collapse resistance of composite floor system. In the following section, a numerical model will be presented to capture the semi-rigid and partial-strength behaviors for this type of connection.

2.4.1 Component model for fin plate shear connection

Component-based connection model can be used to model semi-rigid and partial-strength behavior of shear connection. In general, component-based model idealizes a connection into a series and parallel springs, each behaving in a nonlinear manner according to the

failure mode it represents. The behavior of each spring is derived from experimental study and is presented analytically in codes of practice such as Eurocode 3 Part 1-8 (BSI, 2005b). The application of such model for progressive collapse analysis has been observed in the past, mainly for performance evaluation during fire hazards. The most notable component-based models for shear connection are proposed by Yu et al. (2009), Ramli-Sulong et al. (2007) and Al-Jabri et al. (2005) for fin plate, double angle cleat and flexible end plate, respectively.

In this section, a component-based model for fin plate shear connection shown in Figure 2.17 is adapted. This model is previously proposed by Sadek et al. (2008). In the model, each bolt-row of the connection is represented by an equivalent axial spring that behaves in a tri-linear relationship. The compressive and tensile behaviors of the spring are shown in Figure 2.18a. According to Sadek et al. (2008), the connection rotational stiffness k, without the contribution of floor slab is taken from FEMA 355D (FEMA, 2000) as,

$$k = 124,550\left(d_{bg} - 142.2\right) \text{ kNmm/rad} \tag{2.22}$$

where d_{bg} is the vertical depth of the bolt group (in mm). Therefore, the initial stiffness of an axial spring representing the j$^{\text{th}}$ bolt-row, $k_{b,j}$, can be estimated as,

$$k_{b,j} = \frac{k}{\sum_{j}^{n} s_{j}^{2}} \tag{2.23}$$

where s_{j} and n is the distance of the j$^{\text{th}}$ bolt to center of the bolt group and total number of bolt in the bolt group. The yield resistance $F_{y,j}$ and ultimate resistance $F_{u,j}$ of the spring are determined from the governing failure mode of the bolt-row under pure axial force. The critical failure modes to consider are (1) yield and ultimate resistance of the bolt in single shear with threads excluded, (2) ultimate resistance of the transversely loaded fillet weld along the side of the fin plate, (3) yield and ultimate block shear failure resistance of the beam web or fin-plate whichever is lesser, and (4) yield and ultimate

tear-out (bearing at bolt holes) resistance through the beam web or fin plate whichever is lesser. The resistance of each failure mode is determined in accordance to AISC 360-05 (AISC, 2005) with resistance factor of 1.0. According to recommendation from British practice (BCSA, 2002), the brittle failure modes (i.e. mode 1 to 3 mentioned above) should be avoided when possible for the design of shear connection. For the numerical studies considered in chapter 4, ductile tear-out failure of the beam web and fin plate (mode 4 mentioned above) is found to be the governing failure modes. The resistance of bolt-row governed by tear-out failure is,

$$R_n = 1.5 \ L_c \ t \ F_u \quad \leq \quad 3.0 \ d \ t \ F_u \qquad (2.24)$$

where L_c, t, F_u and d is the clear distance between edge of hole and edge of material, thickness of the connection material, tensile strength of the connection material and nominal bolt diameter.

According to FEMA355D (FEMA, 2000), the ultimate rotational capacity of shear connection in radian is related to the depth of the bolt-group as $\theta_{p,\max} = 0.15 - 0.00014 d_{bg}$. Sadek et al. (2008) proposes an additional elastic rotation capacity of 0.02 rads for the shear connection. Therefore, the total rotational capacity $\theta_{p,\max}$ of the connection is,

$$\theta_{p,\max} = 0.17 - 0.00014 d_{bg} \qquad (2.25)$$

Subsequently, deformation of the jth bolt-row corresponds to the ultimate resistance can be calculated as,

$$\Delta_{u,j} = s_{\max} \theta_{t,\max} \qquad (2.26)$$

where $s_{\max}$ is the distance from center of the bolt group to the most distant bolt. Beyond the ultimate tension resistance of $F_{u,j}$, the bolt-row gradually loses its resistance to zero when failure displacement of $\Delta_{f,j}$ is reached. The failure displacement is taken as the

distance between center of bolt and edge of the plate. In small rotation response, the connection is not in contact with the column face therefore its bending resistance and stiffness are contributed by the bolt-rows alone. When the connection rotates large enough for the top and bottom flanges of the beam to be in contact with the column, significant increase of bending stiffness and resistance occur. The increase is due to the greater level arm in resisting bending forces caused by the shift of rotational center from center of bolt group to the beam's flange. To represent the contact behavior, gap element is positioned at the level of the beam flanges as shown in Figure 2.17. The gap element is essentially a compression-only spring with properties shown in Figure 2.18. The compression stiffness of the gap element occurs only when compressive displacement reaches the gap distance.

2.4.2 Plastic-zone element representing fin-plate connection

The series of spring-bar system shown in Figure 2.17 can be converted into an equivalent plastic zone to simplify modeling and to facilitate analysis of large building system. Based on the plastic zone method described previously (i.e. section 2.2), a plastic zone with length L_p can be used to represent the integrated responses of a connection (i.e. axial and moment responses). The fiber strain is constant along the plastic zone length. Therefore the equivalent stress-strain relationship for the ith fiber representing the jth bolt-row as shown in Figure 2.18 can be derived as,

$$\sigma_i = F_j \, / \, A_i \tag{2.27}$$

$$\varepsilon_i = \Delta_j \, / \, L_p \tag{2.28}$$

where L_p and A_i are the plastic zone length and area of the ith fiber. The axial-moment interaction response of the connection is accounted for directly by the fiber section. Therefore no assumption of this relationship is required.

The model proposed by Sadek et al. (2008) is relatively simple, but is realistic enough to resemble the behavior of fin plate shear connection predicted by detailed finite element

analysis (as will be shown in section 3.5 of chapter 3) and progressive failure response of a composite floor system tested in the laboratory (as will be shown in section 4.3 of chapter 4). For specific application where localized behavior, e.g. friction and slip between the bolt and bolt hole, is sought, more comprehensive model like one proposed by Yu et al. (2009) should be adopted. The same approach to convert the spring-bar model into an equivalent plastic zone is still applicable regardless of the properties adopted for the spring.

2.5 Concluding remarks

1. This chapter presents the concept and formulation of an efficient progressive collapse analysis (ePCA) method for evaluation of building robustness.

2. ePCA consists of efficient numerical models for main structural components of a composite building, i.e. steel frames, composite floor slabs and steel connections.

3. For progressive collapse analysis of steel frames, a general beam-column model based on the plastic zone method is proposed. The method can realistically model the spread-of-plasticity across-section and along-member of steel frame. Parametric study on member with length L recommends that the plastic zone length should be greater than $L/2$, while the element length within the plastic zone should be lesser than $L/24$. The degree of fiber section discretization is less influential, but a minimum of 5 divisions is recommended for steel section. Parametric study also shows that the rigorous modeling of material imperfection can be represented easily by enhanced geometry imperfection.

4. For progressive collapse analysis of composite floor slab, a slab model based on the modified grillage method is proposed. Equivalent grillage member including the effect of steel deck is introduced to simulate the lower-bound flexural capacity of composite floor slab. When the slab is loaded to large out-of-plane deformation, membrane actions in the form of tensile catenary and compressive ring mechanism dominate the response. Truss analogy is proposed to model these membrane actions with

reasonable accuracy. For consistency, material damage behavior of the grillage member is also modeled using the same plastic zone method.

5. For progressive collapse analysis of steel shear connection, a component-based model for fin plate shear connection is adapted from Sadek et al (2008). Modification is proposed to convert the spring-bar model to an equivalent plastic zone to simplify modeling for large building system, at the same time to promote consistency in the modeling.

6. Verification examples are presented in the next chapter to investigate the accuracy of the proposed models for steel frame, slab and connection mentioned above.

Table 2.1: Influence of plastic zone length (L_p) on buckling and post-buckling responses of column

(a) box section (SHS 150x150x8)

Plastic zone length, L_p	Element length in zone		Normalized strength (F-F / F-P)	
	Inelastic	Elastic	Buckle	Post-buckle
L	L/72	L/24	1.000 / 1.000	1.000 / 1.000
L/2	L/72	L/24	1.002 / 1.010	1.000 / 1.012
L/4	L/72	L/24	1.004 / 1.007	1.008 / 1.063
L/8	L/72	L/24	1.005 / 1.013	1.016 / 1.103

(b) wide flange section (UC 305x406x634)

Plastic zone length, L_p	Element length in zone		Normalized strength (F-F / F-P)	
	Inelastic	Elastic	Buckle	Post-buckle
L	L/72	L/24	1.000 / 1.000	1.000 / 1.000
L/2	L/72	L/24	1.002 / 1.003	1.000 / 1.025
L/4	L/72	L/24	1.020 / 1.011	1.022 / 1.094
L/8	L/72	L/24	1.015 / 1.018	1.042 / 1.152

Note: F-F and F-P denotes fixed-fixed and fixed-pinned boundary condition

Table 2.2: Influence of element length on buckling and post-buckling responses of column

a) box section (SHS 150x150x8)

Plastic zone length, L_p	Element length in zone		Normalized strength (F-F / F-P)	
	Inelastic	Elastic	Buckle	Post-buckle
L/2	L/72	L/24	1.002 / 1.010	1.000 / 1.012
L/2	L/36	L/12	1.003 / 1.010	1.004 / 1.015
L/2	L/24	L/12	1.003 / 1.010	1.014 / 1.020
L/2	L/12	L/12	1.005 / 1.011	1.040 / 1.046

b) wide flange section (UC 305x406x634)

Plastic zone length, L_p	Element length in zone		Normalized strength (F-F / F-P)	
	Inelastic	Elastic	Buckle	Post-buckle
L/2	L/72	L/24	1.002 / 1.003	1.000 / 1.025
L/2	L/36	L/12	1.002 / 1.003	1.005 / 1.025
L/2	L/24	L/12	1.003 / 1.003	1.012 / 1.030
L/2	L/12	L/12	1.003 / 1.004	1.040 / 1.057

Note: F-F and F-P denotes fixed-fixed and fixed-pinned boundary condition

(a) Truss model by Hill et al. (1989)   (b) Truss model by CSA (1984)
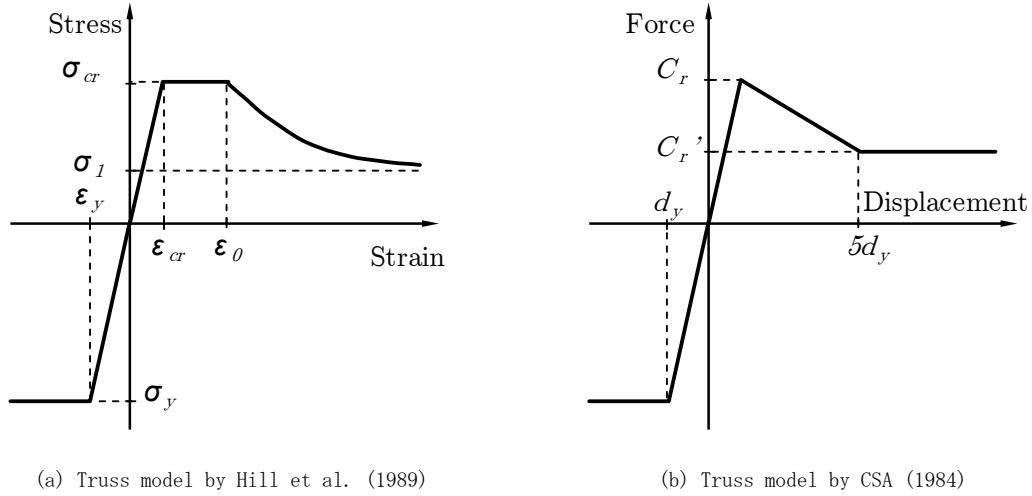
Figure 2.1: Simplified truss models by Hill et al. (1989) and CSA (1984)

(a) fiber section at monitored locations and uniaxial stress-strain relationship of steel material

(b) modeling along beam-column member
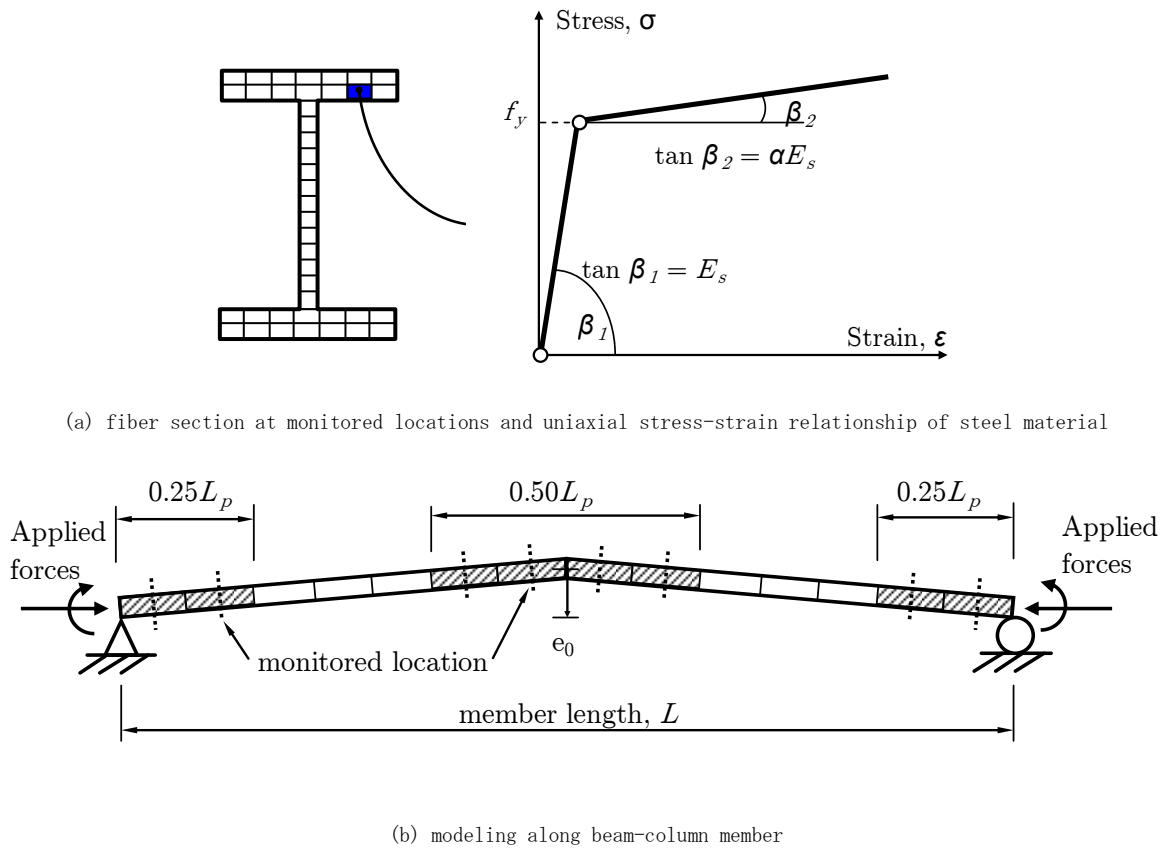
Figure 2.2: Proposed beam-column model for progressive collapse analysis of steel frames

57

(a) sway mode   (b) non-sway mode
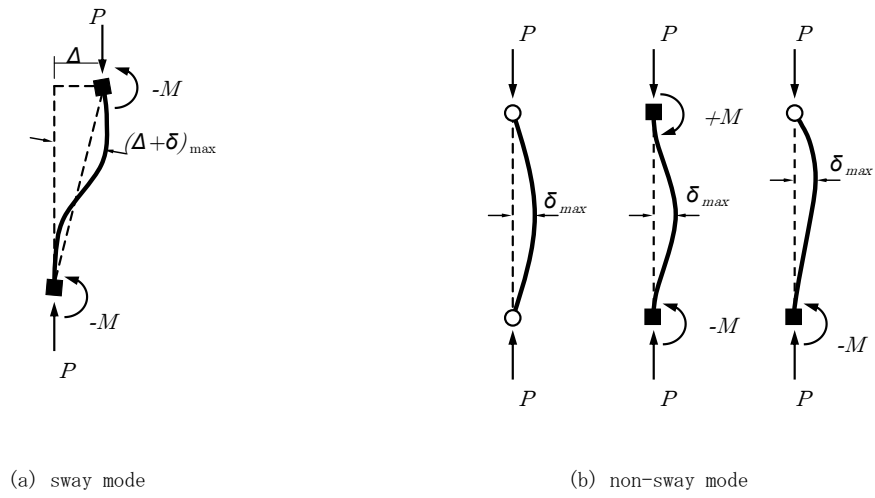
Figure 2.3: Second-order effects in sway and non-sway columns
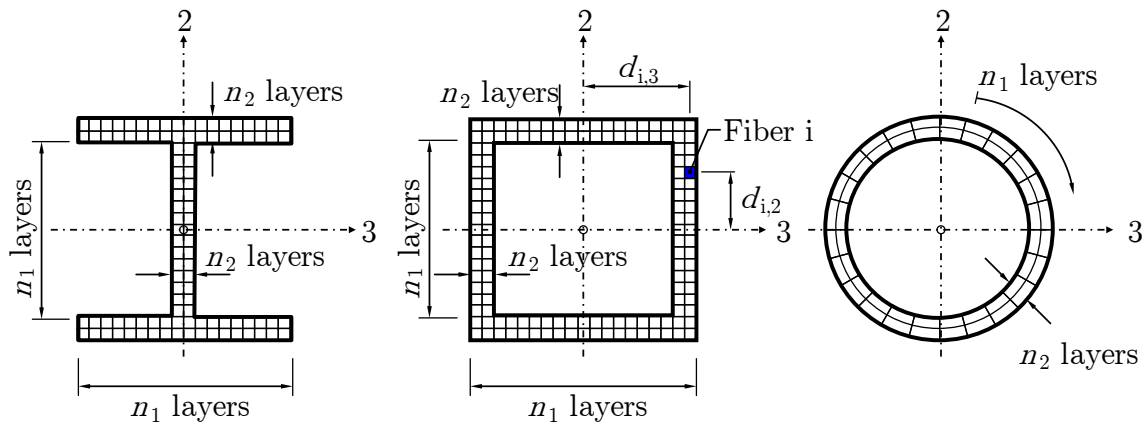
Figure 2.4: Fiber sections for common steel shapes
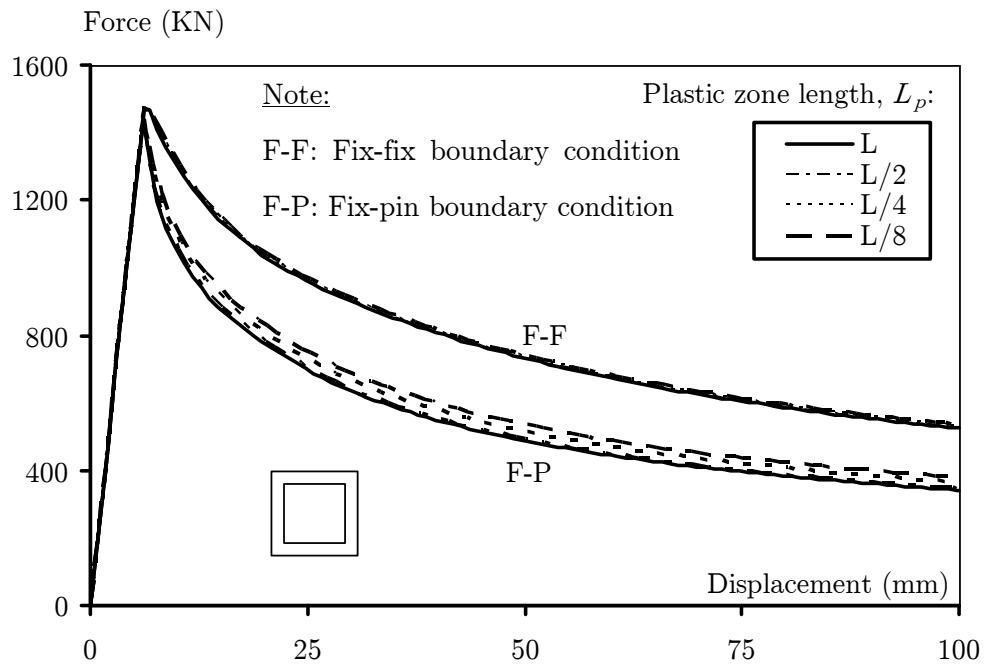
(a) box section (SHS150x150x8)
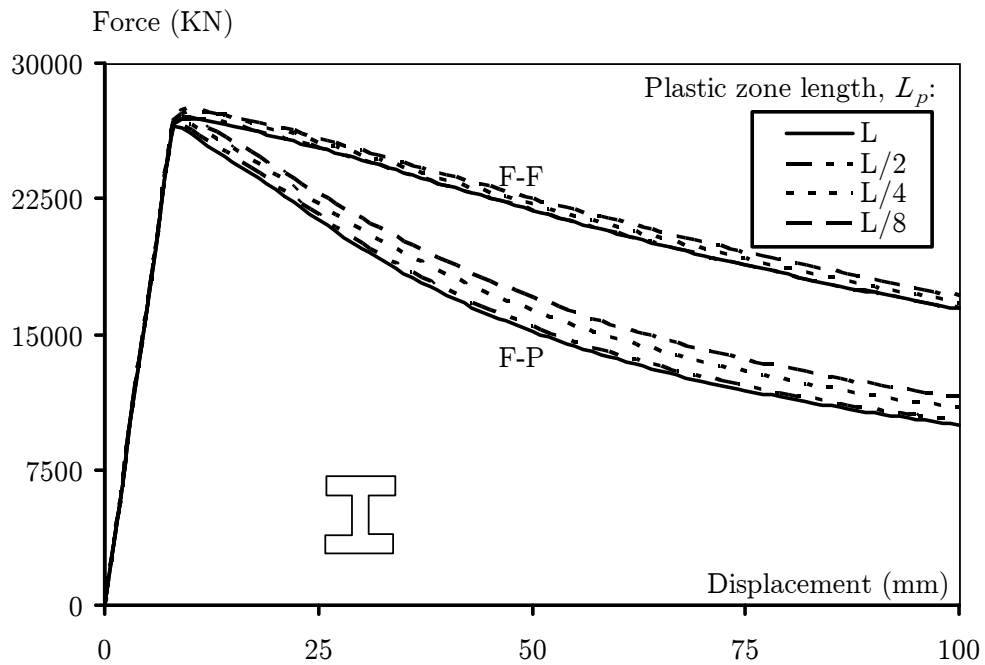
(b) wide-flange section (UC356x406x634)

Figure 2.5: Influence of plastic zone length (L_p) on buckling response

59

(a) box section (SHS150x150x8)

(b) wide-flange section (UC356x406x634)
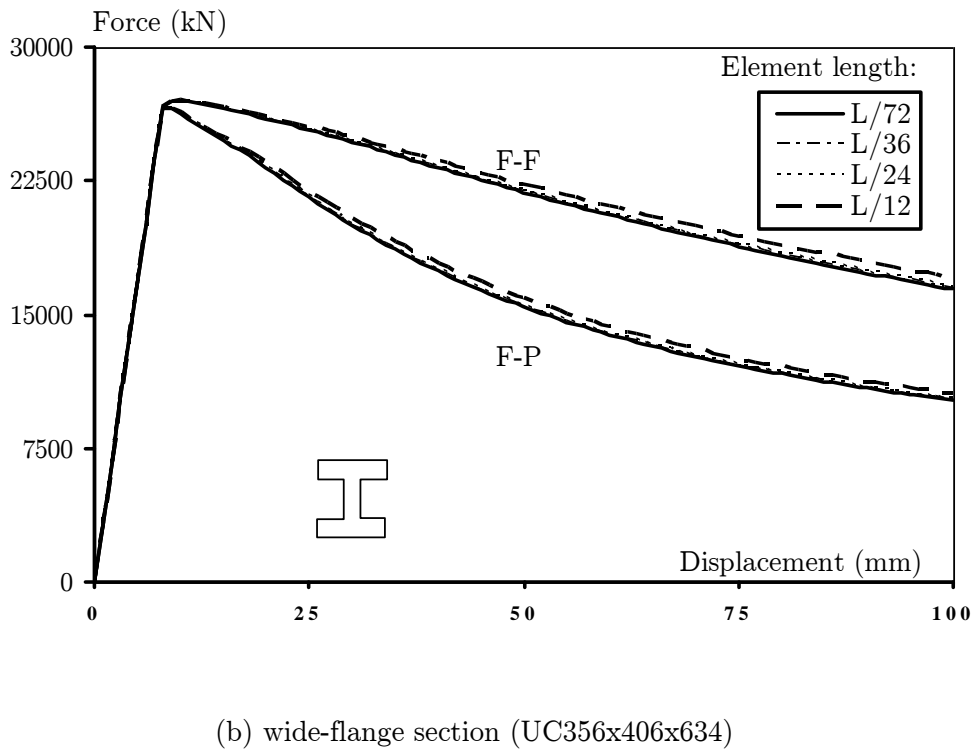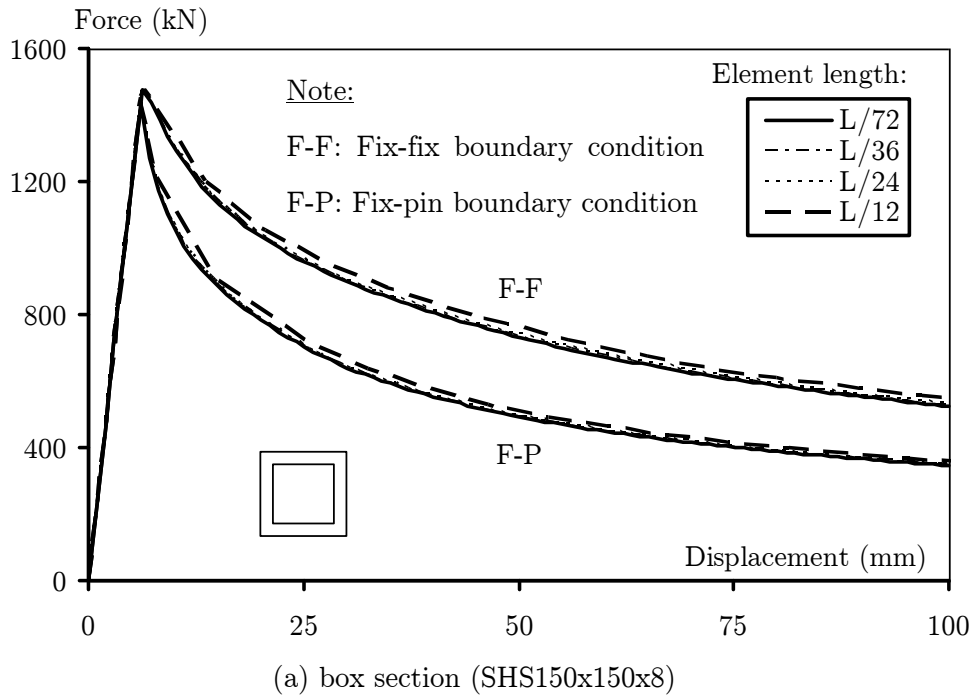
Figure 2.6: Influence of element length within plastic zone on buckling response
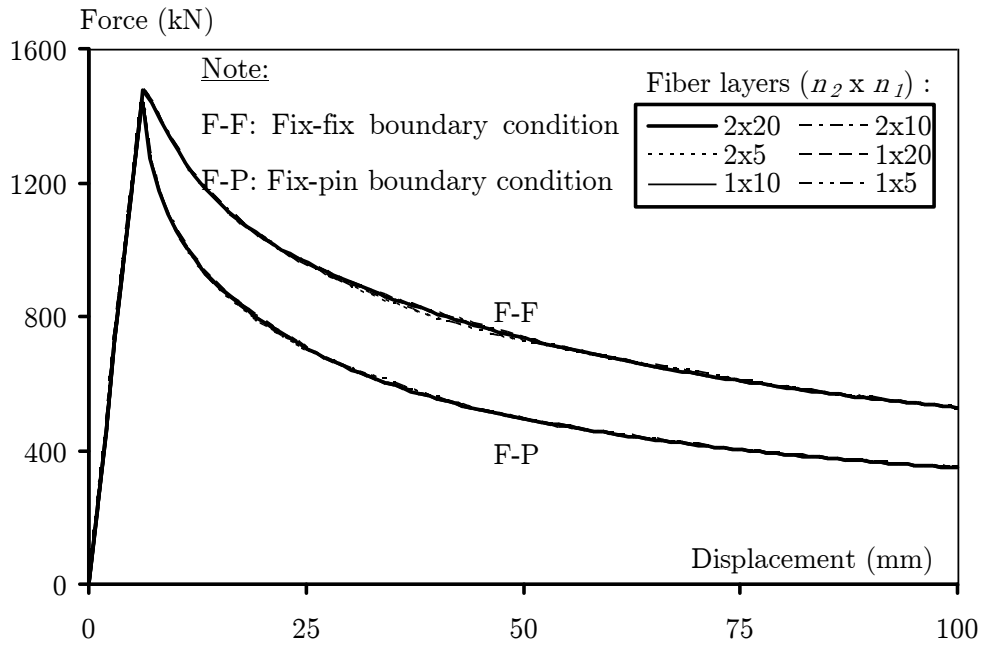
(a) box section (SHS150x150x8)
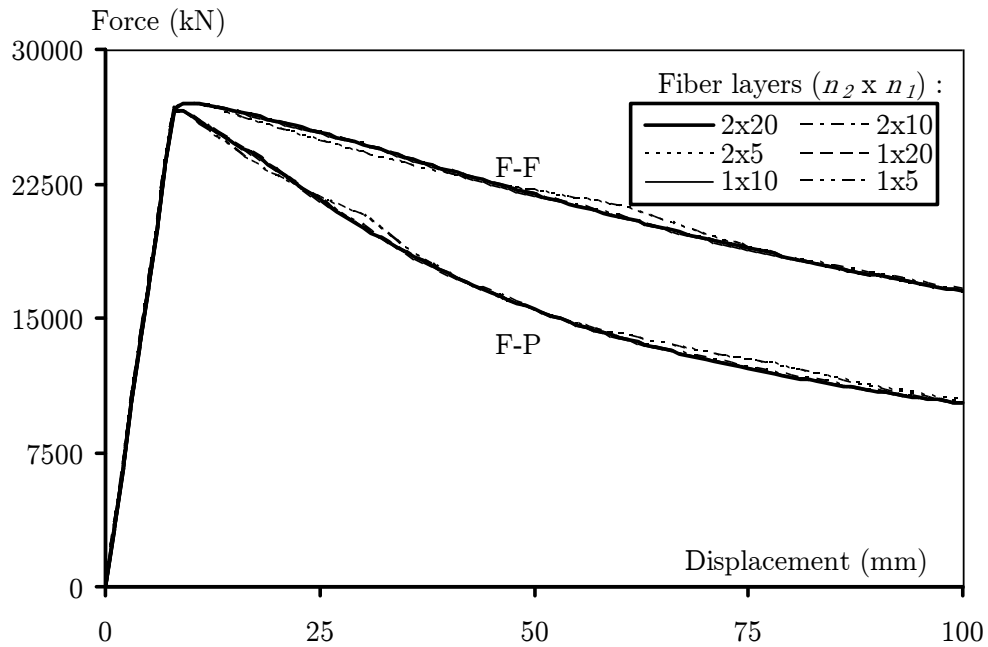
(b) wide-flange section (UC356x406x634)

Figure 2.7: Influence of number of fibers at monitored locations on buckling response
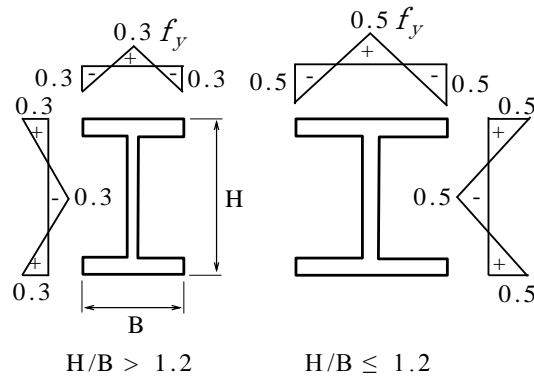
Figure 2.8: Residual stress profile recommended by European Convention for
Constructional Steelwork (ECCS, 1983)
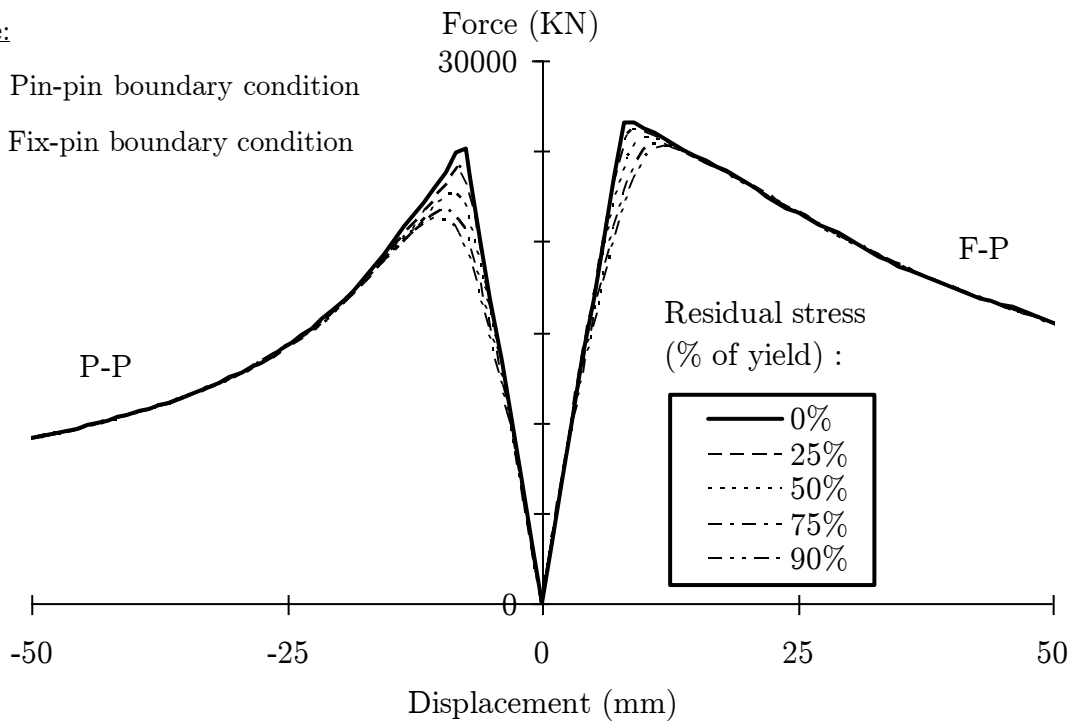
Figure 2.9: Influence of residual stress on column buckling response
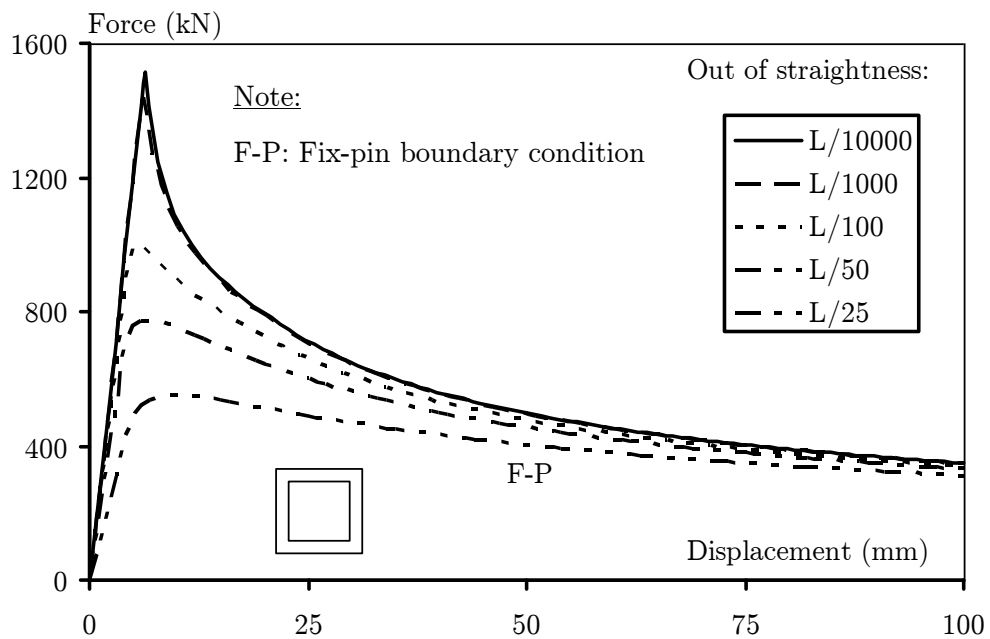
(a) box section (SHS150x150x8)
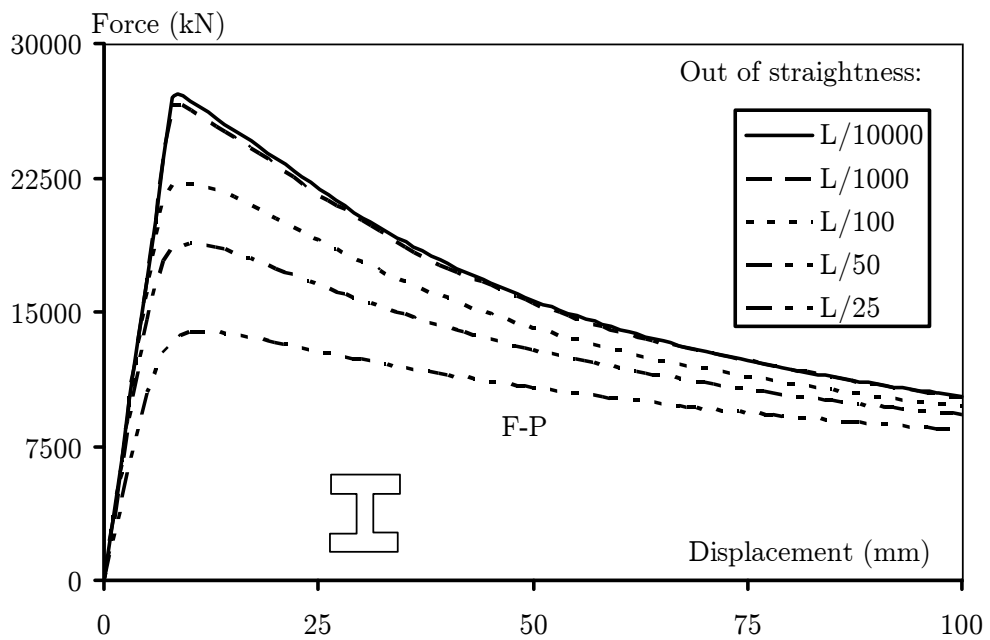
(b) wide-flange section (UC356x406x634)

Figure 2.10: Influence of out-of-straightness (e_0) on buckling response

63
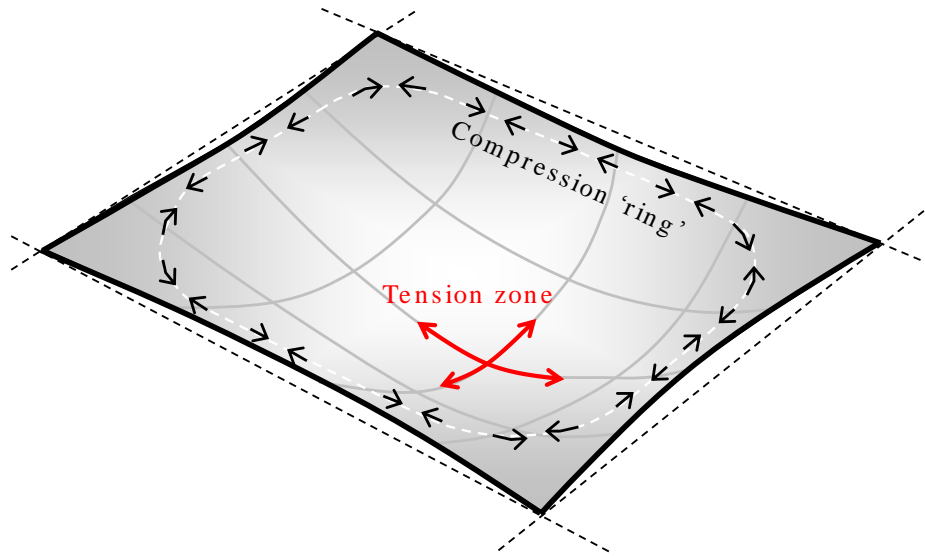
Figure 2.11: Membrane action of unrestrained slab at large out-of-plane deformation
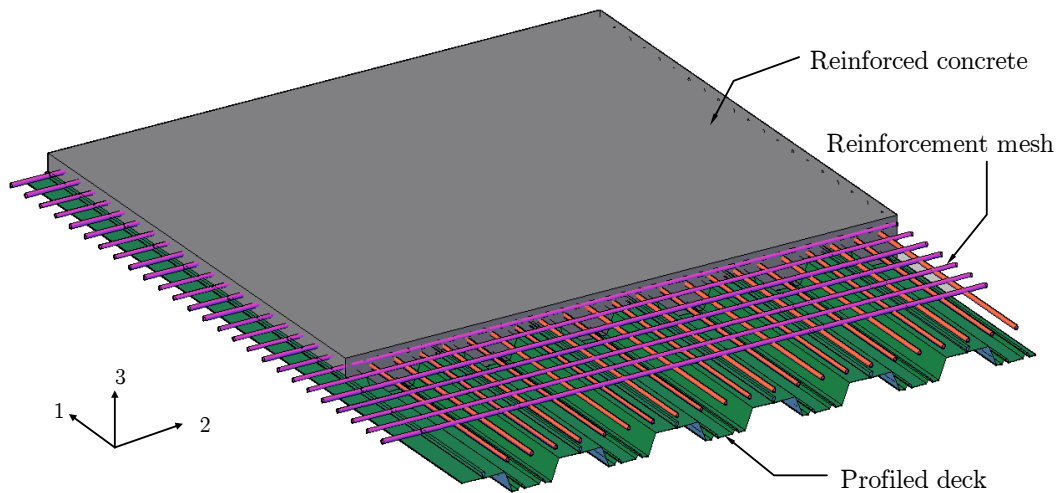
Figure 2.12: Composite slab comprises of profiled deck and reinforced concrete slab

(a) Grillage transverse to ribs

(b) Grillage in direction of ribs

(c) combined grillage and truss system
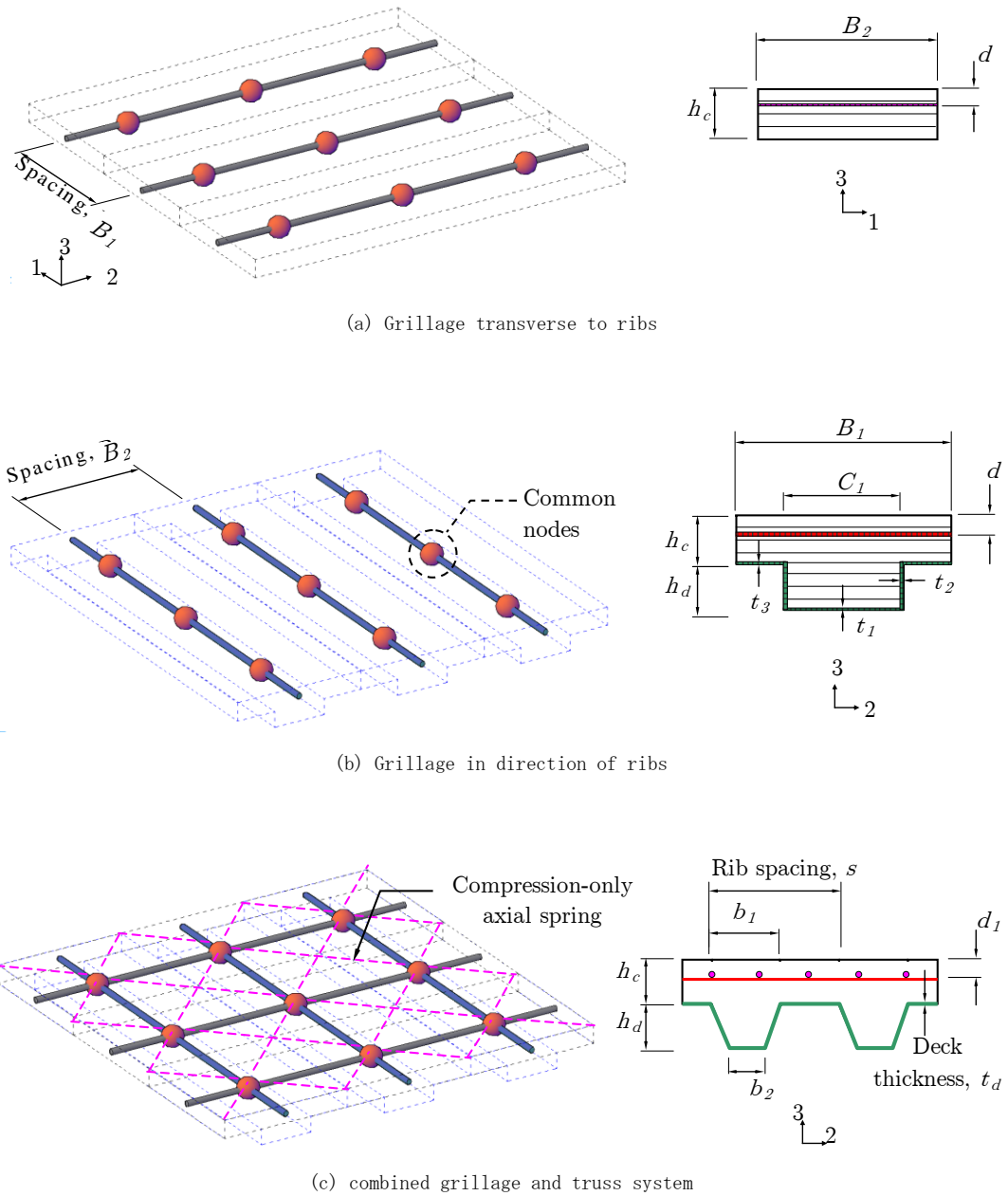
Figure 2.13: Proposed composite slab model based on modified grillage method
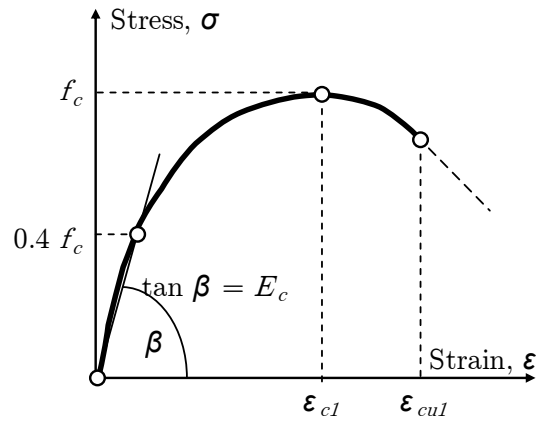
Figure 2.14: Uniaxial stress-strain relationship of concrete material according to Eurocode 2 (BSI, 2004a)
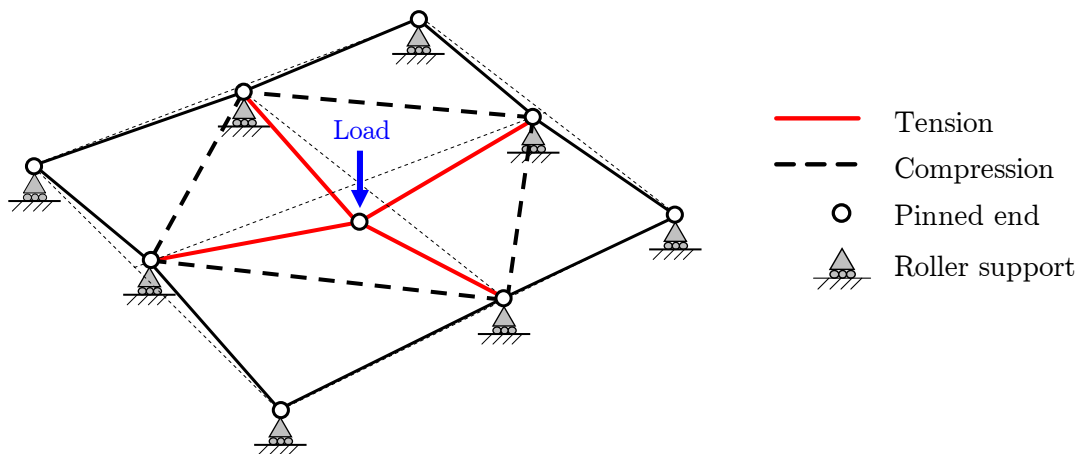
Figure 2.15: Membrane action of unrestrained pin-ended truss system at large out-of-plane deformation
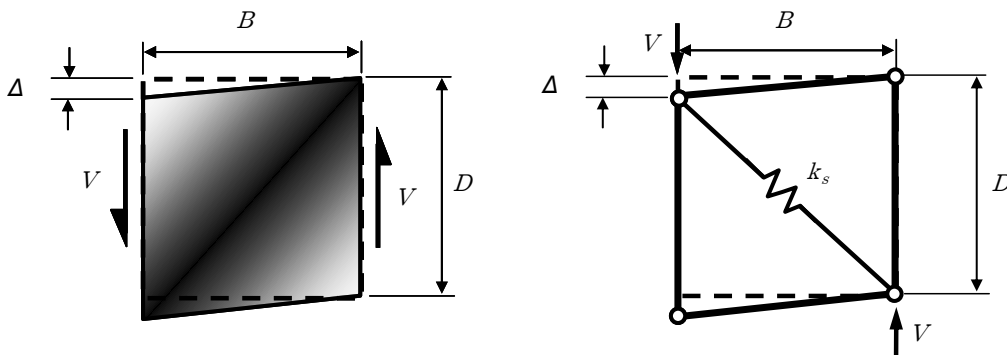
Figure 2.16: In-plane shear deformation of concrete panel and the equivalent truss system

66

(a) physical fin-plate (FP) connection

(b) numerical model for FP connection
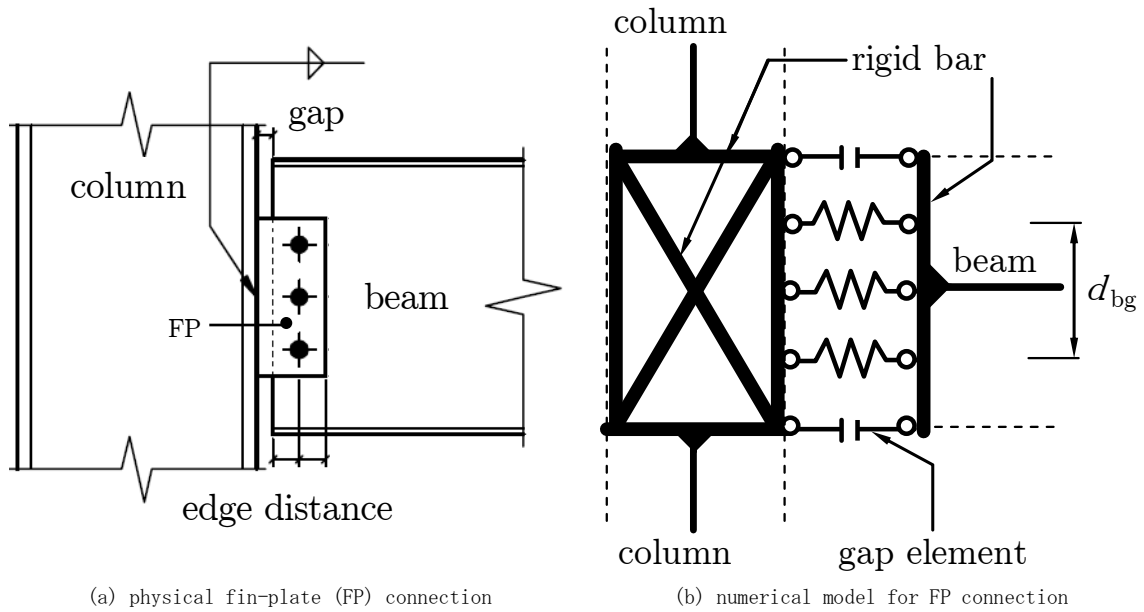
Figure 2.17: Component model for fin plate shear connection proposed by Sadek et al. (2008)

(a) properties spring representing bolt-row

(b) properties of gap element
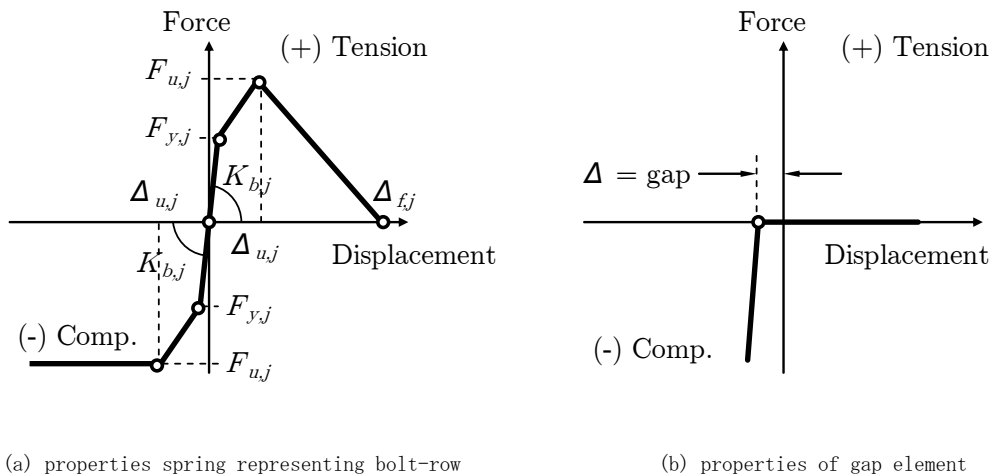
Figure 2.18: Spring properties of component model proposed by Sadek et al. (2008)

Chapter 3:   Efficient Progressive Collapse Analysis: Verification

3.1   Introduction

This chapter presents the verification study of the efficient progressive collapse analysis (ePCA) method presented in chapter 2 of this thesis. The study aims to investigate the effectiveness and also the limitation of ePCA on simulating the progressive failure behaviors of steel and composite structures when subjected to extreme loadings. Findings of the studies are critical to demonstrate that realistic robustness evaluation can be performed using ePCA in the subsequent chapters. In all the verification examples, numerical solutions and experimental findings from published literature are used for comparison. The scope includes progressive collapse behavior of steel members, steel frames, composite slabs, reinforced concrete slabs and steel connections.

3.2 Buckling and post-buckling of slender steel member

The first part of the verification study focuses on the buckling and post-buckling responses of steel members. Specimens consist of various shapes, slenderness ratios and boundary conditions are considered. In the study, the beam-column model proposed in the previous chapter is used consistently for all numerical examples discussed herein.

3.2.1 Buckling capacity

As discussed in section 2.2.1, residual stress exists in all columns and is influenced by fabrication process, structural shape and plate thickness. Eurocode 3 (BSI, 2005a) recognizes the influence of residual stress on column buckling capacity, and recommends different imperfection factors to address the above-mentioned factors. Buckling reduction factors calculated from Equation (2.1) using different imperfection factors are plotted in Figure 3.1 as column curve "a_0" to "d". For hot-finished wide-flange sections with steel grade below S460 and flange plate thinner than 40 mm, the major-axis and minor-axis buckling capacities should be determined from column curve "b" and "c", respectively. For hot-finished tubular sections with steel grade below S460, column curve "a" should be used to calculate buckling capacities for tubular sections (i.e. pipe and box sections) in any axis.

72 numerical specimens as tabulated in Table 3.1 are used to verify the accuracy of the proposed beam-column model on simulating column buckling capacities. The specimens comprise different section shapes, slenderness ratios and boundary conditions. All of the specimens are categorized as compact sections according to Eurocode 3 (BSI, 2005a). Therefore, local buckling effects can be ignored in calculation of column buckling capacity. The steel material is assumed to have elastic modulus, yield strength and strain-hardening ratio of 210 kN/mm^2, 355 N/mm^2 and 0.3% respectively for all specimens. Imperfection in the form of initial out-of-straightness e_0 is considered, while residual stress is ignored in the study.

Firstly, the code recommended initial out-of-straightness of $L/1000$ is adopted. Buckling capacities derived from numerical studies using the beam-column model proposed in the previous chapter are tabulated in Table 3.1. For ease of comparison, the buckling capacities obtained from numerical studies are converted to buckling reduction factors using Equation (2.1) of the previous chapter. These buckling reduction factors are plotted against the slenderness ratio and are compared with Eurocode 3 (BSI, 2005a) buckling curves in Figure 3.1a. The envelope of 112 column capacities tested by Bjorhovde and Tall (1971) is also plotted on the same figure. From the figure, it is obvious that the

change of buckling capacity with slenderness ratio follows the same trend as Eurocode 3 (BSI, 2005a) buckling curves. However, it is found that the numerical results tend to follow curve a_0 closely. Therefore, buckling capacities are overestimated in the numerical study for most of specimens with intermediate slenderness. Maximum overestimation of the buckling capacity is found to be about +33% for wide-flange specimen with slenderness ratio close to 1.0. The overestimation of capacity is due to the omission of residual stress in the numerical studies. For specimens with high slenderness, little difference between the numerical results and Eurocode 3 (BSI, 2005a) is observed. This is because very slender member is governed by elastic buckling; therefore material strength has no effect on the buckling capacity.

Residual stress needs to be considered in the numerical study to produce buckling capacity that is consistent with Eurocode 3 recommendations (BSI, 2005a). Although residual stress can be modeled explicitly using the plastic zone method as discussed in section 2.2.3, the approach can be difficult to implement for large structural systems due to large amount of structural members. Previous parametric studies (i.e. section 2.2.3.2.4 and 2.2.3.2.5) have shown that both initial out-of-straightness and residual stress have similar influence on column capacity; both of them reduce the column buckling capacity but have negligible influence of post-buckling response. Therefore, the effect of residual stress can be resembled by using larger initial out-of-straightness without affecting post-buckling capacity of column. From calibration study, it is found that larger out-of-straightness of $e_0 = L/600$ and $L/250$ are appropriate for tubular and wide-flange sections to comply with curve "a" and curve "c" of Eurocode 3. (BSI, 2005a). The capacities obtained from numerical studies using enhanced initial out-of-straightness are shown in Figure 3.1b. It is evident that the enhanced out-of-straightness method can produce buckling capacity consistent with the code.

3.2.2 Post-buckling capacity

Energy-absorbing capacity is one of the key factors that govern the robustness performance of a structural system. For a slender steel member, e.g. brace member of a

70

truss system, the energy-absorbing capacity is measured as the area under the force-displacement curve. Therefore, the post-buckling response of steel structures needs to be simulated realistically for robustness evaluation. In this section, accuracy of post-buckling response predicted by the beam-column model is verified against published experimental results (Black et al., 1980; Jain et al., 1978). Three wide-flange columns, three box columns and a pipe column are selected for the study. These specimens comprise different slenderness ratios and boundary conditions as summarized in Table 3.2. No local buckling of cross-section is observed during the experiment as all the specimens are compact sections. In modeling the material response, average properties of coupon test from the flanges are adopted. In addition, another beam-column model proposed by Spacone et al. (1996) is used to verify the consistency of the proposed beam-column model. The beam-column model was originally developed for nonlinear analysis of reinforced concrete frame, but can be used to analyze steel frame with some modifications. This model is implemented in Opensees software (Mckenna et al., 2006) based on the methodology recommended by Uriz et al. (2008).

Firstly, wide-flange and pipe specimens tested by Black et al. (1980) are studied. Two wide-flange specimens (i.e. strut 19, 5 and 1 in the reference report) and a pipe specimen (i.e. strut 15 in the reference report) are selected for the verification study. Slenderness ratio of these specimens ranges from 40 to 120. All of the struts are pinned-ended except strut 19 which is fixed at one end and pinned at the other. The response of these specimens due to more than 20 cycles of load reversal is shown in Figure 3.2a and Figure 3.2b, while the compression envelopes are summarized in Figure 3.3. Based on initial out-of-straightness $e_0 = L/1000$, buckling capacity is well captured in all specimens except strut 5, in which over-estimation up to 40% is observed in the present study. The over-estimation is caused by the inability of the adopted simplified steel model to capture cyclic strength-loss (or "*Bauschinger*" effect). On the other hand, the use of more sophisticated steel model i.e. Giuffre-Menegotto-Pinto (Pinto and Giuffre, 1970) in Opensees leads to more accurate prediction of the buckling load. Strut 5 is the only specimen that is tensioned in the first cyclic. Therefore *Bauschinger* effect has less influence on other struts. The weakness of the steel material model is not critical for

progressive collapse analysis due to column removal because maximum displacement and internal forces usually occur in the first deformation cycle (Kim and Kim, 2009a; Powell, 2009). Therefore, it is not wise to use sophisticated steel material model for progressive collapse analysis at the expense of higher computational demand and pre/post-processing efforts. In post-buckling response, the present study compares well with Opensees (Mckenna et al., 2006) and experimental results (Black et al., 1980). The area under the force-displacement envelope represents the energy-absorbing capacity of the system. Therefore, accurate post-buckling response is of utmost importance for performance evaluation of structure under extreme loading conditions.

In addition to the wide-flange and pipe specimens, box specimens tested by Jain et al. (1978) are also studied here. Three box specimens (specimen 4, 5 and 11 in the reference report) are selected for the verification study. Slenderness ratio of these specimens ranges from 30 to 140. All of the struts are fixed-ended except specimen 11 which is pinned. The cyclic response of these specimens is shown in Figure 3.2c, while the compression envelopes are summarized in Figure 3.4. Based on $e_0 = L/250$, buckling load is well captured in all specimens except specimen 15, where over-estimation of up to 30% is observed in both the present study and Opensees (Mckenna et al., 2006). The enhanced out-of-straightness ($L/250$ instead of codified $L/1000$) is used to replicate the effect of pre-tensioning that was done prior to compression test as documented in the test report (Jain et al., 1978). As shown in chapter 2, the discrepancy is not critical for progressive collapse analysis as the energy-absorbing capacity is mainly governed by the post-buckling response. In post-buckling response, the present study compare very well with Opensees (Mckenna et al., 2006) and experimental results (Jain et al., 1978).

3.3 Buckling and post-buckling of steel frames

Steel frames exhibit progressive yielding and softening under extreme loading conditions. Experimental study on full-scale structure is expensive and hard to perform, therefore most of the experiment tests involving inelastic response of steel structure is limited to single members. In the previous section, a beam-column model proposed in chapter 2 has been verified using experimental studies published on literature. Although good

agreement between the experimental study and the proposed beam-column model is observed, application of the model on large three-dimensional structural system still requires further study. In this section, ten verification examples comprise of three-dimensional truss systems and multi-storey building systems are studied. The structures are subjected to different loading conditions as summarized in Table 3.5.

Firstly, the effectiveness of the proposed beam-column model on progressive collapse analysis of space truss and sway frame is studied. Static analysis is carried out so as to better understand the collapse characteristics of these structures, and the accuracy of the column model can be better verified by comparing to published solutions. Distinct collapse behavior is observed for both types of structure. The first is governed by member buckling and the latter by global buckling. The interaction of these behaviors is expected for building incorporating truss system. One example of such a building system is the belt truss building studied in chapter 5 of this thesis. Therefore, accurate simulation of these behaviors is critical for realistic evaluation of the robustness performance of belt truss building.

Then, dynamic collapse analysis of moment-resisting frames involving sudden column removal is studied. The study is intended to verify the accuracy of the beam-column model in prediction of ductility and force demands in the event of structural collapse, which is dynamic in nature. Inertia effects due to excitation of the building self-weight in an accidental event, e.g. column loss due to blast loading, have significant influence on survivability of the damaged structure. To address this, current robustness practice recommends sudden removal of column for robustness evaluation (GSA, 2003; DoD, 2009). This approach is more rational compared with the static approach of the British and European practice (BSI, 2000; BSI, 2006) which ignores dynamic excitation of building self-weight in an accidental event.

3.3.1 Response of space truss under gravity load

Nonlinear response of space trusses is studied in this section. These structures are subjected to increasing gravity load up to the ultimate strength. Due to pinned ends,

truss members are subjected to only axial forces upon loading. Therefore, their ultimate strengths are governed by buckling of respective truss member. Beyond the ultimate strength, displacement control method is used to track the force-displacement relationship. Due to the shallow geometry, these structures exhibit complex snap-in and snap-through behavior in the post-buckling response. These complex behaviors provide an excellent insight into accuracy of the column model in capturing second order $P - \delta$ effects associated with member buckling. This failure mode is common to brace member of truss system in the event of extreme loading.

For all analyses of space truss, plastic zone length and mesh size of $L/4$ and $L/24$ is adopted. No moment is generated at member ends, therefore only plastic zone at mid-span is considered. On cross-section level, bilinear steel material with strain hardening parameter of 0.3% is assumed for the fibers. Magnitude of initial out-of-straightness influences the prediction of buckling capacity, therefore is calibrated to match response obtained by published solution. In practical application, recommended magnitude of initial out-of-straightness (section 3.2.1) should be used for consistency with design code.

3.3.1.1 Plane Truss

Figure 3.5a shows a 2-member plane truss subjected to a point load at the crown node. Each member of the truss consists of 254 mm square section with slenderness ratio L/r of 150. The elastic modulus and yield stress of the material are $E_s = 206$ kN/mm^2 and $f_y = 235$ N/mm^2 respectively. The structure was previously analyzed by Thai and Kim (2009) and Liew et al. (1997), among others, both using generalized displacement control method respectively. To represent post-buckling behavior of truss member, Liew et al. (1997) adopts a column model with initial-out-of-straightness, magnitude of which is calibrated to match buckling curve "b" of BS 5950 for design consistency (BSI, 2000). Influence of residual stress is accounted for by the enhanced out-of-straight approach, therefore is not modeled explicitly in the numerical study. Computed based on second-order analysis, an elastic-perfect-plastic hinge is inserted at mid-span of the strut when cross-sectional forces reach the section plastic strength.

In this chapter, the beam-column model proposed in chapter 2 is adopted. Elastic and inelastic analyses are performed for the truss system using the same beam-column model with exception in material properties. Enhanced out-of-straightness of $e_0 = L/250$ is adopted to be consistent with Liew et al. (1997). The results of force versus vertical displacement at the crown node as predicted by the present study and Liew et al. (1997) are compared in Figure 3.5a. Initial stiffness of the truss system is derived from arching effect alone, because the pinned truss member cannot resist load in flexural action. However, gradual softening caused by second-order effects is observed as the deformation increases. Eventually, the system achieves ultimate load capacity at displacement of about 300 mm and 115 mm for elastic and inelastic analysis respectively. The deformation shape at this state of response is shown as mode (i) in Figure 3.5b. After the ultimate capacity, the system unloads drastically and eventually loses all its capacity at a displacement of about 700 mm. This displacement is the same as the height of the dome structure. At this state of response, the truss system is similar to a 2-beam system with pinned-ends spanning horizontally between the pin supports.

Beyond the displacement of 700 mm, the truss system switches from arching mode to catenary mode, in which stiffness is gained from cable action shown as mode (ii) in Figure 3.5b. At this state of response, the truss system snap-through from positive load-carrying capacity to negative capacity. Beyond this displacement, internal force of the truss member reverses direction from compression towards tension as catenary action develops. The truss system gradually regains stiffness through catenary action and eventually snap-back to positive load-carrying capacity when displacement is about twice the height of the truss system. In general, the present study has shown good consistency in simulating the energy-absorbing capacity (i.e. area under the force-displacement curve) of the truss system. Furthermore, prediction of the limit load capacity also agrees well with the findings of Liew et al. (1997). The limit load obtained from the elastic analysis is 1293 kN (-1.5%) compared to 1313 kN, while the limit load obtained from inelastic analysis is 487 kN (+9%) compared to 445 kN given by Liew et al. (1997)

3.3.1.2   Star Dome

Figure 3.6b shows a 24-member star dome subjected to point load at the internal node. Two load cases are considered here. All internal nodes are subjected to point load in load case 1, while only the crown node is subjected to point load in load case 2. Each member of the truss has an area of 0.1 cm^2 and inertia moment of 4.170 x 10^{-3} cm^4. The elastic modulus and yield stress of the material are E_s = 2.034 x 10^7 N/cm^2 and f_y = 4 x 10^4 N/cm^2 respectively. The structure was analyzed previously by Blandford (1996) and Liew et al. (1997), among others, using arc-length and generalized displacement control method respectively. To represent post-buckling behavior of truss member, Blandford (1996) adopts a truss model based on simplified equations of stress-strain relationship proposed by Hill et al. (1989), while Liew et al. (1997) adopts a column model based on the same methodology used for study of plane truss. In the present study, the beam-column model proposed in the previous chapter is adopted. Elastic and inelastic analyses are performed for the truss system using the same beam-column model with exception in material properties.

In load case 1, all internal nodes are subjected to point load as shown in Figure 3.6. Enhanced out-of-straightness of e_0 = L/250 is adopted to be consistent with the assumption of Liew et al. (1997). The relationships between the force and vertical displacement at crown node as predicted by the present study and Liew et al. (1997) are compared in Figure 3.6a. It can be seen that the response of both methods agrees well. The limit load obtained from the elastic analysis is 10.930 kN (+1.2%) compared to 10.801 kN given by Liew et al. (1997), while the limit load obtained from inelastic analysis is 1.677 kN (+1.1%) compared to 1.659 kN given by Liew et al (1997).

In load case 2, only the crown node is subjected to point load as shown in Figure 3.7a. Initial out-of-straightness of $e_0 = L/250$ is adopted to be consistent with Blandford (1996) prediction of buckling capacity. The relationships between the force and vertical displacement at crown node (i.e. node 1) as predicted by the present study and Blandford (1996) study are compared in Figure 3.7a. Similar to the plane truss system, initial stiffness of the star dome is also derived from arching effect alone. As displacement

increases, the gradual softening due to second-order effect is also observed. Eventually, the system achieves ultimate load capacity at displacement of about 7.7 mm and 3.8 mm for elastic and inelastic analysis respectively. The ultimate load corresponds to buckling of the 6 central truss members as shown as mode (i) in Figure 3.8b. After the ultimate capacity, the system unloads drastically and eventually loses all its capacity at a displacement of about 20 mm. This displacement is the same as the height of the dome structure. At this state of response, 6 central truss members behave like a 6-beam system with pinned ends spanning horizontally.

Beyond the displacement of 20mm, the star dome system switches from arching mode to catenary mode, in which stiffness is gained from cable action of the 6 central members shown as mode (ii) in Figure 3.8b. At this state of response, the dome structure snap-through from positive load-carrying capacity to negative capacity. Beyond this displacement, internal force of the truss member reverses direction from compression towards tension as catenary action develops. The system gradually regains stiffness through catenary action and eventually snap-back to positive load-carrying capacity when displacement is about twice the height of the dome structure. The load-carrying capacity increases with displacement up to about 43 mm. At this state, secondary buckling of the truss member occurs as shown in mode (iii) in Figure 3.8b. Unloading occurs after the displacement of 43 mm and followed with the stiffening effect by catenary action. The relationship between the imposed load and horizontal displacement at node 2 is also plotted in Figure 3.7b. The limit load capacities have been shown to agree well with the findings of Blandford (1996). The limit load obtained from the elastic analysis is 1293 kN (-1.5%) compared to 1313 kN, while the limit load obtained from inelastic analysis is 487 kN (+9%) compared to 445 kN given by Blandford (1996).

Although there is marginal difference between both methods in predicting the inelastic snap-through and snap-back behaviors, generally the present study has shown good consistency in simulating the energy-absorbing capacity of the system before snap-through response. The difference can be caused by the inability of the adopted simplified steel material to capture material behaviors during load-reversal. However, the weakness of the adopted steel material is not critical for progressive collapse analysis due to column

removal because maximum displacement and internal forces usually occur in the first deformation cycle (Kim and Kim, 2009a; Powell, 2009)

3.3.1.3   Circular Dome

Figure 3.9a shows a 168-member circular dome subjected to a point load at the crown node. Each member of the truss has an area of 50.431 cm^2 and inertia moment of 52.942 cm^4. The elastic modulus and yield stress of the material are E_s = 2.04 x 10^7 N/cm^2 and f_y = 2.5 x 10^4 N/cm^2 respectively. The structure was first analyzed by Yang et al. (1997) and then by Thai and Kim (2009), among others, using incremental-iterative and generalized displacement control method respectively. To represent post-buckling behavior of truss member, Thai and Kim (2009) adopted a truss model based on simplified equations of stress-strain relationship proposed by Hill et al. (1989). In the present study, the beam-column model proposed in previous chapter is adopted. Elastic and inelastic analyses are performed for the truss system using the same beam-column model with exception in material properties.

To be consistent with Thai and Kim (2009) prediction of buckling capacity, initial out-of-straightness of $L/2000$ is adopted in the present study. The force-displacement relationship at crown node predicted by the present study and Thai and Kim (2009) for elastic and inelastic analyses is compared in Figure 3.10. The circular dome exhibits similar snap-through and snap-back behaviors as the star dome system. It can be seen that the response of both methods agrees well. The limit load obtained from the elastic analysis is 838 kN (-1%) compared to 846 N given by Thai and Kim (2009), while the limit load obtained from inelastic analysis is 448 N (-10.4%) compared to 500 N given by Thai and Kim (2009).

Similar to the findings of star dome, there is also a marginal difference between both methods in predicting the inelastic snap-through and snap-back behaviors. As explained earlier, this difference is caused by inability of simplified steel material to capture material behaviors during load-reversal, which is not critical for progressive collapse analysis due to column removal (Kim and Kim, 2009a; Powell, 2009).

3.3.1.4   Geodesic Dome

Figure 3.9b shows a 156-member geodesic dome subjected to a point load at the crown node. Each member of the truss has an area of 650 mm^2 and inertia moment of 1 x 10^4 mm^4. The elastic modulus and yield stress of the material are E_s = 6.895 x 10^4 N/mm^2 and f_y = 400 N/mm^2 respectively. The dome geometry is described by the following equation,

$$x^2 + y^2 + (z + 7.2)^2 = 60.84 \qquad\qquad (3.1)$$

This structure was first analyzed by Ramesh and Krishnamoorthy (1994) and then by Thai and Kim (2009), among others, using dynamic relaxation method and generalized displacement control method respectively. To represent post-buckling behavior of truss member, both studies adopt a truss model based on simplified of stress-strain relationship proposed by Hill et al. (1989). In the present study, the beam-column model proposed in the previous chapter is adopted. Elastic and inelastic analyses are performed for the truss system using the same beam-column model with exception in material properties.

To be consistent with Thai and Kim (2009) prediction of buckling capacity, initial out-of-straightness of L/2000 is adopted in the present study. The force-displacement relationship at crown node predicted by the present study and Thai et al. (2009) for elastic and inelastic analyses is compared in Figure 3.11. It can be seen that the response of both methods agrees well. The limit load obtained from the elastic analysis is 3.169 kN (-0.1%) compared to 3.172 kN given by Thai and Kim (2009), while the limit load obtained from inelastic analysis is 2.048 kN (-20%) compared to 2.580 N given by Thai and Kim (2009). In overall, the energy-absorbing capacity is well estimated in the present study. Similarly, marginal difference is also observed in the snap-through and snap-back responses. However, this difference is considered insignificant for robustness evaluation in view of the reasons mentioned above (i.e. section 3.3.1.3).

3.3.2 Response of building frames under gravity and lateral loads

Nonlinear response of sway frames sensitive to global second order effects i.e. P-Δ is studied in this section. The frames are subjected to increasing gravity and lateral load up to the ultimate strength. At initial stage of loading, the frames behave almost linearly. The frames gradually lose the lateral stiffness as lateral deformation increases. The softening behavior is caused by destabilizing effect of gravity loads. Global sway and torsional rigidity of the frames are provided by bending action of the continuous frames. Therefore, beams are predominantly subjected to bending effects, whereas columns are subjected to combined axial and bending effects. Ultimate strength of the frames is governed by yielding at member ends, location of which maximum bending effects are most likely to occur. From the numerical studies, accuracy of the beam-column model can be validated in capturing (1) global buckling due to $P - \Delta$ effects, (2) distributed plasticity along member and across section, and (3) interaction of axial loading and biaxial bending.

For all analyses of sway frames, plastic zone length and element length of $L/2$ and $L/24$ is adopted. All members are continuous and therefore significant end moments are expected. Plastic zone is equally distributed at mid-span and member ends. At the cross-sectional level, bilinear steel material with strain hardening parameter of 0.3% is assumed for the fibers. Initial out-of-straightness, although present in all structures, is ignored in the reference solutions and the present study.

3.3.2.1 One-storey 2D Building Frame

The one-storey 2D frame shown in Figure 3.12b is subjected to vertical and horizontal loads at top of the frame. The horizontal load produces a side-sway and induces significant second-order $P - \Delta$ moment on the members. The load magnitude shown in the Figure 3.12b corresponds to load factor of 1.0. In the collapse analysis, the vertical and horizontal loads will be multiplied by this load factor simultaneously. To include material imperfection in the analysis, residual stress profile recommended by the European Convention for Constructional Steelwork (ECCS, 1983) (as discussed in

80

Chapter 2) is used. The analysis also includes geometry imperfection (initial inclination of 1/400) recommended by ECCS (1983) as,

$$\psi_0 = \frac{1}{300} r_1 r_2 \tag{3.2}$$

where,

$$\psi_0 = \text{ initial angle of inclination}$$

$$r_1 = \begin{cases} \sqrt{5/L} & \dots L > 5 \text{ m} \\ 1 & \dots L \leq 5 \text{ m} \end{cases}$$

$$r_2 = \frac{1}{2}\left(1 + \frac{1}{n}\right)$$

$$L = \text{ height of frame (m)}$$

$$n = \text{ number of columns in plane of frame}$$

The frame was first introduced in Europe for calibration of second-order analysis (Vogel, 1985). The force-displacement relationship at top of the frame predicted by the present study and Vogel (1985) is compared in Figure 3.12a. The effect of residual stress is also shown in the figure. It can be seen that both methods compare well. The predicted ultimate load factor is 0.990 (-3%) compared to 1.022 given by Vogel (1985). Residual stress is shown to have little effect on the ultimate load, but tends to induce gradual yielding in the transition from elastic to plastic response. The residual stress causes softer sway stiffness and greater second-order effects as a result.

3.3.2.2   Six-storey 2D Building Frame

The six-storey 2D frame shown in Figure 3.13b is subjected to vertical and horizontal loads at storey level of the frame. The horizontal load at top of the frame is half that of intermediate storeys because the projected area for the top storeys is half. Similarly, the load magnitude shown in Figure 3.13b corresponds to load factor of 1.0. The analysis also includes material and geometry imperfection recommended by ECCS (initial inclination

of 1/300 according to equation (3.2)). The frame was another structure introduced in Europe for calibration of second-order analysis (Vogel, 1985). The force-displacement results at the sixth and fourth storey predicted by the present study and Vogel (1985) are compared in Figure 3.13a. The comparisons with the effect of residual stress are also shown in the same figure. It can be seen that both methods compare well. The predicted ultimate load factor is 1.079 (-3%) compared to 1.111 given by Vogel (1985). Similar to the previous structure, residual stress is shown to have little effect on the ultimate load. Softening of the sway stiffness in the transition from elastic to plastic response is still observed, but its magnitude is small compared to the single-storey frame.

3.3.2.3   Six-storey 3D Building Frame

Figure 3.14 shows a 63-member six-storey space frame subjected to uniform floor load of 9.6 kN/m^2 and wind load of 53.376 kN in the Y-direction at every beam-column joint. The floor load is converted into equivalent loads imposed on top of the columns. The load magnitude shown in Figure 3.14 corresponds to load factor of 1.0. In the collapse analysis, the vertical and horizontal loads will be multiplied by this load factor simultaneously. Beam sections are typical for every storey while column sections are different for the top and bottom three storeys. The elastic modulus and yield stress of the material are E_s = 206.85 kN/mm^2 and f_y = 250 N/mm^2 respectively. The structure was first analyzed by Orbison et al. (1982) and then by Jiang et al. (2002) using modified arc-length method. Member inelasticity is considered based on plastic hinge approach in the former and mixed element approach in the latter.

Material and geometry imperfection are not considered in the works by Orbinson et al. (1982) and Jiang et al. (2002), and therefore are also ignored in the present study for comparison purpose. As a result, second order effect in the frame members are contributed only by lateral sway caused by wind loads. The force-displacement relationship at point A predicted by the present study and Jiang et al. (2002) is compared in Figure 3.14a. It can be seen that the response of both methods agrees well. The limit load factor is 1.018 (-1.1%) compared to 1.029 given by Jiang et al. (2002). Deformed shape of the frame under gravity load and wind loads in Y-direction is shown

Figure 3.14d. Torsional deformation is observed due to the eccentricity between wind load resultant and center of rigidity of the frame. One way to reduce this torsional deformation is by increasing the sizes of beams and columns of the structural frame along Y-axis (i.e. x=0).

3.3.2.4 Twenty-storey 3D Building Frame

Figure 3.15 shows a 460-member twenty-storey space frame subjected to uniform floor load of 4.8 kN/m^2 and wind load of 0.96 kN/m^2 acting in the Y-direction. These loads are converted into point loads applied at the beam-column joints. The load magnitude shown in Figure 3.15 corresponds to load factor of 1.0. In the progressive collapse analysis, the vertical and horizontal loads will be multiplied by this load factor simultaneously. Beam sections are typical for every storey while distribution of column sections is shown in Figure 3.15a. The elastic modulus and yield stress of the material are $E_s = 200$ kN/mm^2 and $f_y = 344.8$ N/mm^2 respectively. The structure was previously analyzed by Liew et al. (2001), among others, using generalized displacement method and refined plastic hinge approach to consider material inelasticity.

Material and geometry imperfection are not considered in the published and present solutions. Therefore, second-order effects in the frame members are contributed only by lateral sway caused by wind loads. Rigid floor diaphragm is assumed in analysis. Significant twisting effect is observed in the inelastic response, because the frame is asymmetrical and eccentricity exists between frame rigidity center and the wind load resultant. The force-displacement results at point A and B predicted by the present study and Liew et al. (2001) are compared in Figure 3.15c. It can be seen that the response of both methods agrees well. The limit load factor is 1.025 (-0.6%) compared to 1.031 given by Liew et al. (2001). Twisting deformation due to eccentricity between load resultant and rigidity center of the frame is also shown in Figure 3.15d. The computational time of the present study is only 20 minutes using Intel Core 2 Quad CPU with 3.00 GHz and 3 GB of RAM. This structure can be considered as large system, and is therefore a good illustration on the accuracy and efficiency of the present study for collapse analysis of large and practical structure.

3.3.3 Response of moment frames under sudden column removal

Static collapse behaviors of space truss and building frames have been studied in the previous sections. In this section, the dynamic collapse behavior of moment frames is studied under sudden column removal events. The study focuses on a two-storey and three-storey moment frames proposed and studied by Kaewkulchai and Williamson (2004) previously for development of an analysis program to simulate dynamic behaviors of plane frames up to, and through, collapse. The geometries of these moment frames are shown in Figure 3.16 and Figure 3.18.

3.3.3.1   Structural configurations

The frames have typical bay width and storey height of 240 in (6.096 m) and 144 in (3.658 m), and are subjected to gravity load of 0.4 kips/in (70.051 kN/m) distributed along the beam length. Adopting lumped mass approach, discrete mass of 0.124 kips-s^2/in (21.713 tons) is considered at each beam end. Steel members are assumed to have properties summarized in Table 3.3.

In Kaewkulchai and Williamson (2004), structural damping is ignored as material yielding is deemed to dominate energy absorption of inelastic response. Material nonlinearity is assumed to occur only at member ends using lumped plasticity model (discrete plastic hinge). An implicit direct-integration scheme, the Newmark-Beta method is employed to solve the governing equations of motion coupled with Newton-Raphson iterations for solving nonlinear equations. To address the effects of strength and stiffness degradation of structural member, a damage index is employed in the analysis. This factor has shown some insignificant influence on prediction of dynamic demands.

3.3.3.2   Modeling and assumptions

In the present study, physical steel sections with equivalent stiffness and strength are used. This results in 806 mm square box with thickness of 2.41 mm for the beam member, and 489 mm square box with thickness of 6.7 mm for the column member. Yield strength of $f_y = 314$ N/mm^2 is used throughout the analysis. Instead of using plastic hinge method as Kaewkulchai and Williamson (2004), the beam-column model based on plastic zone

method is used. The plastic zone beam-column model is the same model proposed in the previous chapter. Plastic zone length and element length of $L/2$ and $L/24$ is adopted, and the plastic zone is equally distributed at mid-span and member ends. On cross-section level, bilinear steel material with strain hardening parameter of 0.3% is assumed for the fibers. Initial out-of-straightness is ignored in Kaewkulchai and Williamson (2004). Therefore, this factor is also not considered in the present study.

As shown in Figure 3.16 and Figure 3.18, equivalent reaction forces (i.e. axial P, moment M and shear force V) are used to represent the columns that need to be removed for robustness evaluation. These forces are equivalent to the internal forces of the columns before removal, and are tabulated in Table 3.4. In Kaewkulchai and Williamson (2004), the sudden column removal event is simulated in three phases as shown in Figure 3.16c. In the first phase, gravity load and reaction forces are applied slowly to full magnitude following a linear ramp function. Then, the loads are kept constant over a period of time to damp out the inertia force effects. In the final phase, reaction forces are removed by reducing the magnitude to zero over a short period of time. The first and second phases of the simulation are time-consuming and can lead to inconsistent results if insufficient time-step is used. A better way to simulate sudden column removal is to use nonlinear static approach to simulate steady state condition of the structure prior to column removal (DoD, 2009; Marjanishvili and Agnew, 2006). This way, simulation of sudden column removal is reduced to only two phases.

Significant saving in computation time is achieved by adopting the two-phase approach in the present study. In the implementation, the first and second phases (shown as dotted lines in Figure 3.16c) of the time-history is performed using static analysis. Information of the deformation and internal force of the structure is used as the initial conditions for subsequent time-history analysis (i.e. the third phase). In the third phase, removal of reaction forces is carried out over a 0.01s period. The adopted removal time is determined from previous convergence study, and is close to the recommendation by DoD (2009) of using 10% of principal natural period. In the nonlinear time-history analysis, very small time-step of 0.001s for a period of 2.0s is adopted in each analysis case.

Structural damping is ignored in Kaewkulchai and Williamson (2004), but small magnitude is used in the present study to avoid numerical instability.

3.3.3.3   Dynamic demands of two-storey moment frame

For the two-storey frame shown on Figure 3.16, two column removal cases are considered in the study. The first case involves the sudden removal of perimeter column as shown in Figure 3.16a while the second case involves the sudden removal of internal column as shown in Figure 3.16b. Large vertical deformation is observed above the position of column removal almost immediately after the removal. The displacement time-histories at the column removal position for case 1 and case 2 are plotted on Figure 3.17a. The displacement time-histories obtained from Kaewkulchai and Williamson (2004) study are also plotted on the same figure for comparison. The general trend of displacement time-history obtained from the present study compares well with the findings from Kaewkulchai and Williamson (2004). For case 1, the maximum displacement is found to be 292 mm (-1%) compared to 295 mm from Kaewkulchai and Williamson (2004). For case 2, the maximum displacement is found to be 176 mm (+5%) compared to 167 mm from Kaewkulchai and Williamson (2004).

Besides deformation, structural components near the removed columns also experience significant increase in internal forces after the column removal. As shown in Figure 3.17b, the column axial force increases by about 204% and 240% for case 1 and case 2 respectively. Likewise, as shown in Figure 3.17c, the bending moments in member 1 and member 2 also increase by about 341% and 362% for case 1 and case 2 respectively. The general trend of force time-history obtained from the present study compares well with the findings from Kaewkulchai and Williamson (2004). For case 1, the maximum axial force is found to be 1861 kN (+0.4%) compared to 1852 kN from the study by Kaewkulchai and Williamson (2004). For case 2, the maximum axial force is found to be 950 kN (-1%) compared to 963 kN from the study by Kaewkulchai and Williamson (2004). For both displacement and force responses, marginal softening is observed in the free vibration phase of the time-histories. The softening effect can be caused by

distributed plasticity behavior of steel frame ignored in the study by Kaewkulchai and Williamson (2004).

3.3.3.4 Dynamic demands of three-storey moment frame

For the three-storey frame shown on Figure 3.18, two column removal cases are considered in the study. The first case involves the sudden removal of perimeter column as shown in Figure 3.18a while the second case involves the sudden removal of internal column as shown in Figure 3.18b. Large vertical deformation is observed above the position of column removal almost immediately after the removal. The displacement time-histories at the column removal position for case 1 and case 2 are plotted on Figure 3.19a. The displacement time-histories obtained from Kaewkulchai and Williamson (2004) are also plotted on the same figure for comparison. The general trend of displacement time-history obtained from the present study compares well with the findings from Kaewkulchai and Williamson (2004). For case 1, the maximum displacement is found to be 236 mm (-2%) compared to 240 mm from Kaewkulchai and Williamson (2004). For case 2, the maximum displacement is found to be 166 mm (+0.6%) compared to 165 mm from Kaewkulchai and Williamson (2004).

Similar to the two-storey frame, structural components near the removed column also experience significant increase in internal forces after the column removal. The general trend of force time-history obtained from the present study compares well with the findings from Kaewkulchai and Williamson (2004). For case 1, the maximum bending moment is found to be 458 kN-m (+12%) compared to 411 kN from Kaewkulchai and Williamson (2004). For case 2, the maximum axial force is found to be 401 kN-m (-3%) compared to 415 kN from Kaewkulchai and Williamson (2004). For both displacement and force responses, marginal softening is also observed in the free vibration phase of the time-histories. The softening effect can be caused by the same explanation for two-storey frame.

3.4 Flexural and membrane behaviors of floor slab

In this section, consistency of the slab model the proposed in previous chapter is studied by comparing with experimental and published numerical results. Three types of floor structures, i.e. reinforced concrete slab, composite slab and ribbed reinforced concrete slab, are studied. Each of the floor structures is subjected to different loading conditions as summarized in Table 3.5.

3.4.1 Reinforced concrete slab under point load

The orthogonally-reinforced square reinforced concrete slab shown in Figure 3.20 is subject to increasing point load at centre of the slab. The slab has a geometry of 914 x 914 x 44.45 mm, and is simply supported at the four corners. It is reinforced in both directions at 70% of its depth. The slab was studied experimentally by Jofriet and McNeice (1971). For the concrete material, the initial stiffness, compressive crushing and tensile strength tested in laboratory are found to be 28.613 kN/mm^2, 38 N/mm^2 and 3.8 N/mm^2, respectively. For the reinforcement steel material, the stiffness and yield strength tested in laboratory are found to be 200 kN/mm^2 and 380 N/mm^2, respectively.

In the present study, a grillage approximation of 12 x 12 grids with total of 650 frame elements is used. The cross section of frame element is discretized into 15 concrete fibers and 2 steel fibers. The degree of discretization is found to be sufficient based on a convergence study. As shown in Figure 3.20, the present study compares well with experiment in terms of overall force-displacement behavior, but underestimates the ultimate strength marginally. The ultimate capacity of slab obtained from the present study is about 18.1 kN (-4%) compared to the experimental result of 18.83 kN. The lower ultimate strength is attributed by ignoring torsional rigidity in slab as described in the previous chapter.

3.4.2 Composite slab strip under two-point loads

The inelastic response of composite slab strip tested by Abdullah and Easterling (2009) is studied in this section. In the event of column removal, floor structure is forced to span longer in search of an alternate load path. Therefore, the specimen with highest slenderness ratio is chosen in the study here (i.e. specimen #9 in the reference paper). The composite slab strip has geometry of 305 x 4270 x 125 mm as shown in Figure 3.21. The total slab thickness of 125 mm includes the 76 mm deep steel deck (1.5mm thickness). 2-point bending test with shear span of 1320 mm was carried out in the experimental study. In the experimental study, two tests (i.e. tests A and B) for the same specimen were carried out to determine the average response. From tests, the yield strength and ultimate strength of the steel deck are found to be 350 N/mm^2 and 410 N/mm^2, respectively, while the concrete crushing strength is found to be 31 N/mm^2.

Material properties tested at laboratory are used for numerical study based on the present study. Due to the narrow width of the specimen, only a single line of beams is used to model the slab. A total of 40 frame elements are used in the analysis. Each cross section is discretized into 15 concrete fibers and 2 steel fibers. The degree of discretization is found to be sufficient based on convergence study. The relationship between the total push down force and the vertical displacement at mid-span is shown in Figure 3.21. It is evident that the present study compares well with the experimental finding up to the ultimate capacity of the slab.

In the experiment conducted by Abdullah and Easterling (2009), ultimate capacity of the specimen is found to be governed by horizontal slip between the steel deck and concrete topping. Horizontal slip behavior is ignored in the present study. Therefore, overestimation of post-ultimate capacity is observed in the present study. Horizontal slip has significant influence on the ultimate strength of floor slab with low span-to-depth ratio. In the event of column removal, floor slab is forced to span significantly longer than its design situation. Experimental studies by Tan and Astaneh-Asl (2003) and detailed finite element analysis by Sadek et al. (2008) on large scale composite floor system show that the damage behavior of floor slab is primarily governed by flexural and

tensile capacities of the composite slab, rather than horizontal shear at interface between concrete topping and steel deck. Therefore, omission of horizontal slip behavior between the concrete topping and steel deck is reasonable for robustness evaluation involving column removal. This assumption is commonly adopted in current state-of-the-art research, e.g. the work by Kwasniewski (2010), Fu (2009), Yu et al. (2010), among others.

3.4.3 Large ribbed reinforced concrete slab under uniform area load

The ribbed slab shown in Figure 3.22 is subjected to increasing uniform load up to total failure. The slab has an effective geometry of 9500 x 6460 x 150 mm measured from the centerline of the supporting beams. It is reinforced with anti-crack A142 cross-wires placed downward as shown in Figure 3.22a. Steel deck is ignored in the study to resemble the situation under fire hazard. The slab is studied experimentally by Bailey et al. (2000) and numerically by Elghazouli and Izzuddin (2004) using detailed finite element analysis in ADAPTIC program. For the concrete material, average density and cube strength tested in laboratory are found to be 1913 kg/m^3 and 52 N/mm^2 respectively. Therefore, the self-weight of the slab can be estimated as 2.33kN/m^2. For the reinforcement steel material, average yield strength, ultimate strength and ultimate strain tested in laboratory are found to be 583 N/mm^2, 641 N/mm^2 and 12.3% respectively.

The present study adopts a grillage approximation of 16 x 12 grids, with a total of 1620 frame elements. Each cross section is discretized into 15 concrete fibers and 2 steel fibers based on convergence study. The present study compares well with experiment (Bailey et al., 2000) and detailed finite element analysis (Elghazouli and Izzuddin, 2004) in terms of overall force-displacement behavior, but underestimates the flexural strength marginally in the small deformation response. The lower flexural strength is attributed by the same reason associated with the omission of torsional rigidity in the slab. However, the underestimation has negligible influence on progressive collapse resistance as its magnitude is significantly lower than the enhanced capacity due to catenary action. Catenary action prevails only when vertical displacement exceeds the depth of slab, i.e. 150 mm (Elghazouli and Izzuddin, 2004). This additional load carrying capacity is

beneficial for robustness design of building, and is captured realistically in the present study as evident in Figure 3.22. If conventional grillage method is used (setting K_s of equation (2.18) to zero), it can be seen that the beneficial catenary action cannot develop. The reason is that the membrane action of floor slab is not correctly modeled when the compression spring is absent. Therefore, it is concluded that the use of conventional grillage method cannot correctly consider the contribution of tensile catenary action of the slab, and can lead to unrealistic prediction in the large-deformation response.

3.5 Catenary response of fin plate shear connection

The half model shown in Figure 3.23 is an idealized model of a double-span beam system studied by Sadek et al. (2008) using detailed finite element analysis. The fin plate shear connection comprises 9.5 mm thick fin plate and 3 numbers of A325 22mm-diameter bolts. ASTM A36 steel ($f_y = 248.2$ N/mm^2) is used for the fin plate. The beam consists of W16x26 wide-flange beam with ASTM A992 steel material ($f_y = 344.8$ N/mm^2). There is a gap of 25 mm between the beam and the column face. The right end of the half model is idealized as pinned (i.e. restrained in the horizontal and vertical directions but free to rotate about all axes).

In the study by Sadek et al. (2008), a state-of-art software LS-DYNA (Hallquist, 2006) is used in the numerical study. The fin plate connection and the connected beam are modeled rigorously using brick and shell elements. Failure behaviors of the connection, e.g. friction-slip mechanism between the bolt and bolt holes, plasticity at bolted plates, the contact between the column and beam, fracture of bolt and plates, among others, can be simulated with reasonable accuracy. Therefore, their numerical results are used as the basis of comparison in this verification study. In the present study, fin plate connection is modeled as a plastic zone element using the method described in section 2.4 of the previous chapter. Failure mode of spring representing the bolt-row is found to be governed by the bearing capacity of beam web. Therefore, yielding and ultimate capacities of the spring can be derived from equation (2.24). In the implementation, the plastic zone length L_p for the plastic zone element is taken as the length of the fin plate,

i.e. 100 mm, while the fiber area A_i is taken as 1000 mm^2 for each fiber representing the bolt-row. Therefore, the equivalent uniaxial stress-strain relationship for fiber can be calculated using equations (2.27) and (2.28) of the previous chapter.

The double-span beam system is subjected to increasing point load at the mid-span. Relationship between the total force and the vertical displacement at mid-span is plotted in Figure 3.24a. Initial stiffness of the system is relatively low due to the rather flexible connection. However, the system gains additional stiffness as the deformation increases. This phenomenon is caused by the tension stiffening effect of catenary action which is evident in Figure 3.24b. The same figure shows that the tension force increases as the mid-span displacement increases in downward direction. This process imposes higher stresses to the connection, and causes gradual plasticity and softening of the connection until the ultimate load capacity is reached. The system achieves ultimate load capacity of about 46.4 kN (+2%) as compared to the capacity of 45.3 kN in detailed finite element analysis by Sadek et al. (2008). The displacement corresponding to the ultimate load capacity is about 498 mm, which is about 10% more than 454 mm obtained from detailed finite element analysis. Unloading takes place immediately after the ultimate load capacity is achieved. The capacity of the connection is reduced to zero at a displacement of about 800 mm. From the beginning of loading until the ultimate load capacity, the energy-absorbing capacity of the system (i.e. area under the force-displacement curve) obtained from the present study agrees well with the results obtained from detailed finite element analysis. The good agreement between both methods shows that the proposed connection model can be used with sufficient accuracy yet efficient in dealing with large building system.

3.6 Concluding remarks

1. The beam-column model, slab model and connection model proposed in chapter 2 as part of efficient progressive collapse analysis methodology have been validated by experimental and numerical studies published in the open literature.

2. The beam-column model shows reasonable accuracy in predicting the buckling and post-buckling capacities of column specimens. Application of the beam-column model in the analysis of complex space trusses and large building frames also yields the same finding. However, the beam-column model is shown to be less suitable for analysis under cyclic loading due to the inability of simplified material model in dealing with load reversal. This limitation is less critical for robustness evaluation involving column removal as maximum deformation and force demands occur in the first deformation cycle.

3. The slab model shows reasonable accuracy in predicting flexural and membrane responses of reinforced concrete and composite slab specimens. In small deformation response, the proposed slab model underestimates flexural capacity of slab marginally. The underestimation is caused by omission of torsional rigidity in the proposed model. In large deformation response, the model shows reasonable accuracy in capturing the enhanced load-carrying capacity contributed by tension catenary action and compressive ring effect by adopting truss analogy in the model.

4. A connection model is developed for fin plate shear connection based on the spring-bar model proposed by Sadek et al. (2008). The model shows reasonable accuracy in predicting the semi-rigid and partial-strength behaviors of the connection under combined flexural and tensile loading. The consistency and efficiency of the model are helpful for progressive collapse analysis of large building system that comprises large number of connections.

Table 3.1: Comparison of column buckling capacities obtained from the present study and Eurocode 3 (BSI, 2005a)

(i) Wide-flange section

no.	Section	L (m)	Section slenderness		Column slenderness, $\bar{\lambda}$			Buckling capacities, EC3			Buckling capacities - Simulation					
											$e_0/L = 1000$			$e_0/L = 600 / 250$ **		
			Web	Flange	P-P[+]	F-F[+]	F-P[+]	P-P[+]	F-F[+]	F-P[+]	P-P[+]	F-F[+]	F-P[+]	P-P[+]	F-F[+]	F-P[+]
W1	UC356x406x634	5	6.735	2.444	0.593	0.296	0.415	22579	27195	25433	25964	27101	26721	22940	25989	25117
W2	UC356x368x177	6	22.264	7.525	0.819	0.410	0.574	5158	7079	6355	6569	7390	7267	5349	6915	6488
W3	UC305x305x97	6	27.990	9.591	1.012	0.506	0.709	2297	3620	3102	2936	3972	3790	2348	3582	3233
W4	UC254x254x107	7	17.633	6.000	1.383	0.691	0.968	1705	3499	2678	2158	4076	3580	1721	3506	2790
W5	UC356x406x634	9	6.735	2.444	1.067	0.534	0.747	14353	23564	19885	18358	26024	24255	14628	23400	20713
W6	UC356x368x177	9	22.264	7.525	1.229	0.615	0.860	3334	6163	4954	4336	7127	6314	3379	6173	5171
W7	UC305x305x97	15	27.990	9.591	2.531	1.266	1.772	559	1741	1038	636	2229	1268	559	1724	1071
W8	UC254x254x107	15	17.633	6.000	2.963	1.481	2.074	466	1537	883	521	1914	1048	467	1526	909

(ii) Box section

no.	Section	L (m)	Section slenderness		Column slenderness, $\bar{\lambda}$			Buckling capacities, EC3			Buckling capacities - Simulation					
											$e_0/L = 1000$			$e_0/L = 600 / 250$ **		
			Web	Flange	P-P[+]	F-F[+]	F-P[+]	P-P[+]	F-F[+]	F-P[+]	P-P[+]	F-F[+]	F-P[+]	P-P[+]	F-F[+]	F-P[+]
B1	Box700x700x22	4		29.818	0.189	0.095	0.132	21181	21181	21181	20341	20766	20629	20264	20626	20540
B2	Box500x500x16	4		29.250	0.265	0.132	0.185	10838	10996	10996	10387	10648	10570	10337	10599	10504
B3	Box250x250x12	4		18.833	0.538	0.269	0.377	3699	3993	3889	3700	3825	3795	3583	3794	3737
B4	Box150x150x8	4		16.750	0.902	0.451	0.631	1182	1515	1416	1281	1487	1443	1181	1456	1397
B5	Box100x100x6	4		14.667	1.361	0.681	0.953	350	686	559	377	704	623	361	671	574
B6	Box80x80x6	4		11.333	1.727	0.864	1.209	184	478	331	196	513	371	189	478	347
B7	Box60x60x5	4		10.000	2.322	1.161	1.625	66	217	127	69	233	138	67	223	132
B8	Box50x50x5	4		8.000	2.832	1.416	1.982	37	131	72	38	140	77	38	132	75

(iii) Pipe section

no.	Section	L (m)	Section slenderness		Column slenderness, $\bar{\lambda}$			Buckling capacities, EC3			Buckling capacities - Simulation					
											$e_0/L = 1000$			$e_0/L = 600 / 250$ **		
			Web	Flange	P-P[+]	F-F[+]	F-P[+]	P-P[+]	F-F[+]	F-P[+]	P-P[+]	F-F[+]	F-P[+]	P-P[+]	F-F[+]	F-P[+]
P1	Pipe900x20	4		43.000	0.168	0.084	0.118	19629	19629	19629	19061	19376	19252	18953	19321	19120
P2	Pipe400x10	4		38.000	0.380	0.190	0.266	4167	4350	4286	4072	4161	4109	4008	4141	4075
P3	Pipe220x10	4		20.000	0.704	0.352	0.493	1981	2260	2170	2051	2193	2147	1955	2162	2110
P4	Pipe150x20	4		5.500	1.126	0.563	0.788	1678	2620	2327	1831	2625	2443	1688	2533	2318
P5	Pipe100x5	4		18.000	1.556	0.778	1.090	185	428	320	199	446	343	191	422	331
P6	Pipe75x3	4		23.000	2.055	1.027	1.438	51	156	96	54	163	105	52	156	100
P7	Pipe70x12	4		3.833	2.500	1.250	1.750	114	388	221	117	412	233	114	383	224
P8	Pipe60x5	4		10.000	2.681	1.341	1.877	39	137	77	41	145	82	40	139	79

* Steel elastic modulus, $E_s = 210$ kN/mm^2, $E_s = 210$ kN/mm^2 ; yield strength, f_y=355N/mm^2 ; imperfection parameter, $\alpha = 0.21$ and 0.49 for box/pipe and wide-flange section

** Enhanced out-of-straightness, $e_0/L = 600$ and 250 for box/pipe and wide-flange section

[+] P-P, F-F and F-P denote for pinned-pinned, fixed-fixed and fixed-pinned boundary conditions

Table 3.2: Column specimens tested by Jain et al (1978) and Black et al. (1980)

Reference	no.	* f_y (MPa)	Section	L/r	kL/r	Support 1	Support 2	Section w/t Web	Section w/t Flange
(Jain et al., 1978)	4	260	1x0.105**	60	30	Fix	Fix	9.5	9.5
	15	260	1x0.105	160	80	Pin*	Pin***	9.5	9.5
	11	260	1x0.105	156	140	Fix	Fix	9.5	9.5
(Black et al., 1980)	19	277	W6x20	57	40	Fix	Pin	21.0	7.9
	5	291	W6x20	80	80	Pin	Pin	21.0	7.9
	1	279	W8x20	120	120	Pin	Pin	29.9	6.3
	15	360	Ø4x0.237	80	80	Pin	Pin	-	16.9

Note: * Yield strength = average value from flange's coupon test ; 0.3% strain-hardening

   ** 1x0.105 = square box with 1 in (25.4 mm) width and 0.105 in (2.667 mm)

   *** Rotational restraint with spring stiffness = 11.65 kip-in/rad (1.317 kN-m/rad)

   -- Elastic modulus = 200 kN/mm^2 ; out-of-straightness = $L/1000$ for Jain et al. (1978) and $L/200$ for Black et al. (1980)

Table 3.3: Member properties of two-storey and three-storey moment frames studied by Kaewkulchai and Williamson (2004)

Property	Beam	Column
Elastic modulus of steel, E_s	200 kN/mm^2	200 kN/mm^2
Cross section area, A	7.774 x 10^{-3} m^4	1.29 x 10^{-2} m^4
Inertia moment, I	8.325 x 10^{-4} m^4	4.995 x 10^{-4} m^4
Plastic moment resistance, M	734 kN-m	734 kN-m

Table 3.4: Reaction forces used for simulating sudden column removal of two-storey and three-storey moment frames studied by Kaewkulchai and Williamson (2004)

Structure	Column removal scenario	P (kN)	M (kN.m)	V (kN)
Two-storey	Case 1 - Perimeter column removal	398.74	39.50	28.07
	Case 2 - Internal column removal	924.40	-	-
Three-storey	Case 1 - Perimeter column removal	616.00	73.96	27.20
	Case 2 - Internal column removal	1305.65	0.79	0.07

Table 3.5: Summary of numerical examples considered in the verification study

| Section	Structure	Loading	Analysis type	References for comparison
3.3.1.1	Plane truss	Gravity	Static	Liew et al. (1997)
3.3.1.2	Star dome	Gravity	Static	Liew et al. (1997)
3.3.1.3	Circular dome	Gravity	Static	Thai and Kim (2009)
3.3.1.4	Geodesic dome	Gravity	Static	Thai and Kim (2009)
3.3.2.1	One-storey 2D building	Gravity and lateral	Static	Vogel (1985)
3.3.2.2	Six-storey 2D building	Gravity and lateral	Static	Vogel (1985)
3.3.2.3	Six-storey 3D building	Gravity and lateral	Static	Jiang et al. (2002)
3.3.2.4	Twenty-storey 3D building	Gravity and lateral	Static	Liew et al. (2001)
3.3.3.3	Two-storey frame	Gravity	Dynamic	Kaewkulchai and Williamson (2004)
3.3.3.4	Three-storey frame	Gravity	Dynamic	Kaewkulchai and Williamson (2004)
3.4.1	Reinforced concrete slab	Gravity point load	Static	Jofriet and McNeice (1971)
3.4.2	Composite slab	Gravity two-point load	Static	Abdullah and Easterling (2009)
3.4.3	Ribbed reinforced concrete slab	Gravity uniform area load	Static	Bailey et al. (2000)
3.5	Fin plate shear connection	Gravity point load	Static	Sadek et al. (2008)
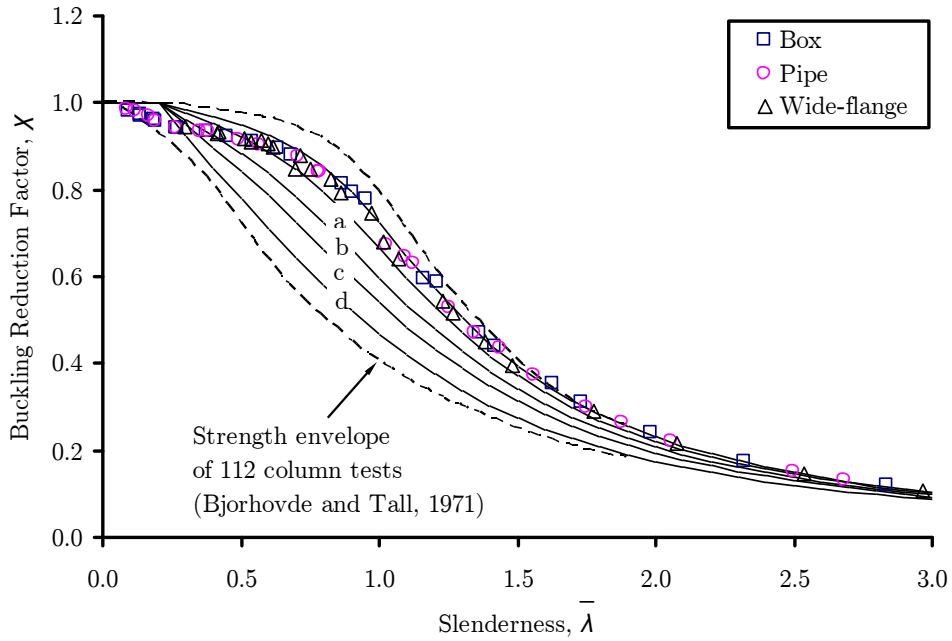
(a) codified out-of-straightness ($e_0 = L/1000$), residual stress ignored
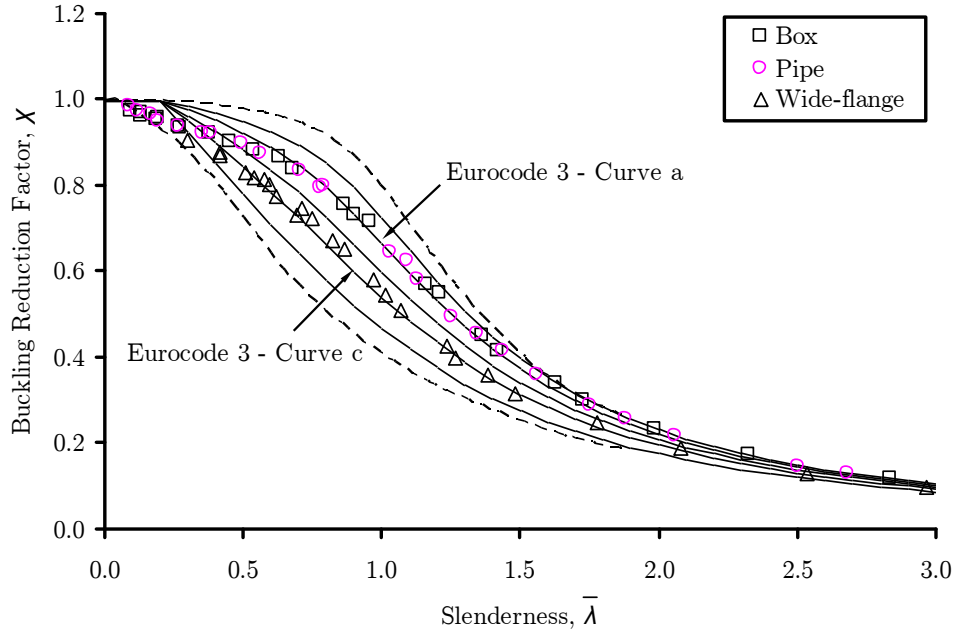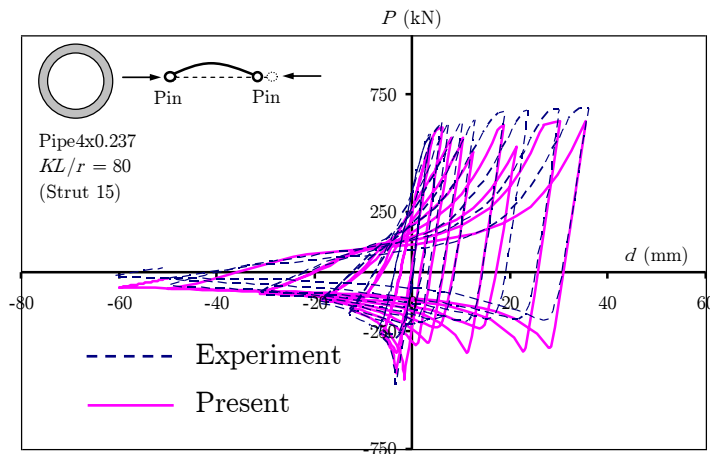

(b) enhanced out-of-straightness as simplified modeling of residual stress
($e_0 = L/600$ for tubular, $L/250$ for wide flange section)

Figure 3.1: Buckling capacities of 72 columns consist of different shapes and boundary conditions: Comparison between Eurocode 3 (BSI, 2005a) and the present study
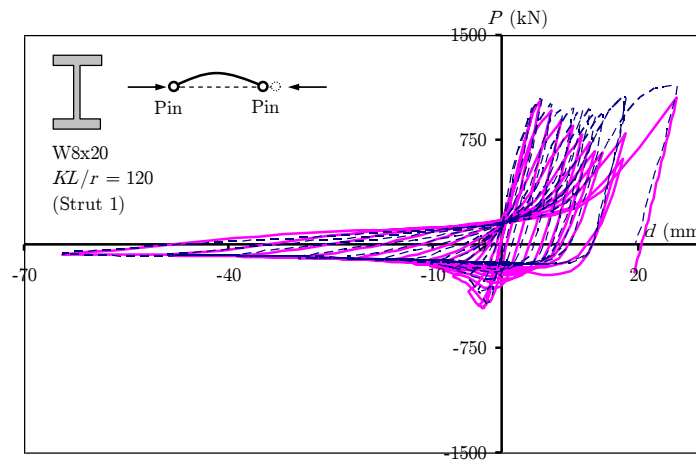
(a) Wide-flange column tested by Black et al. (1980)

(b) Pipe column tested by Black et al. (1980)
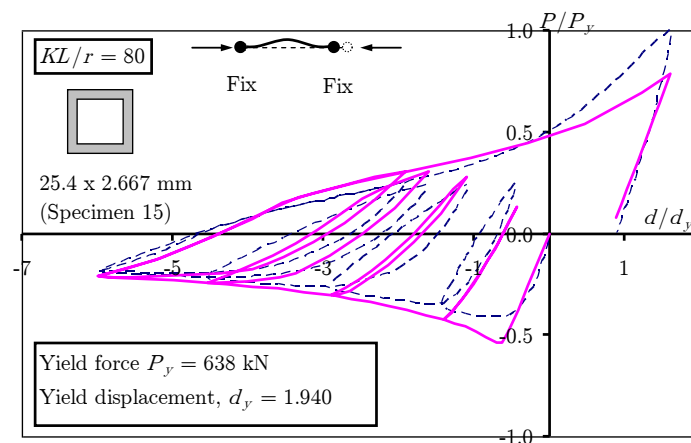
(c)) Box column tested by Jain et al. (1978)

Figure 3.2: Cyclic post-buckling response of column consists of different shapes, slenderness and boundary conditions: Comparison between the present study and experiment by Jain et al. (1978) and Black et al. (1980)

99
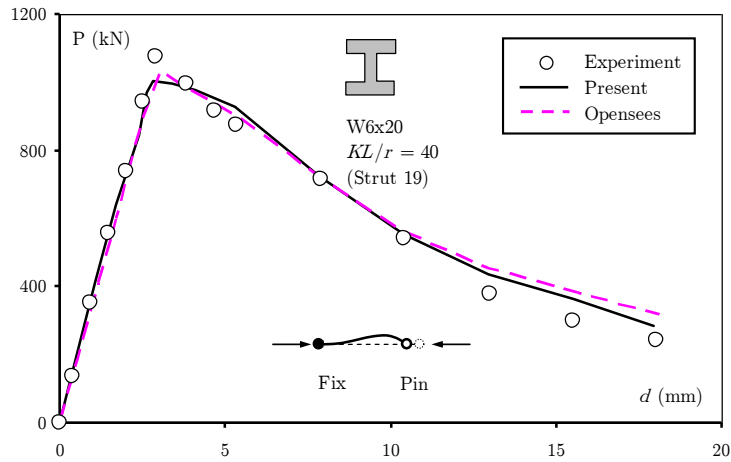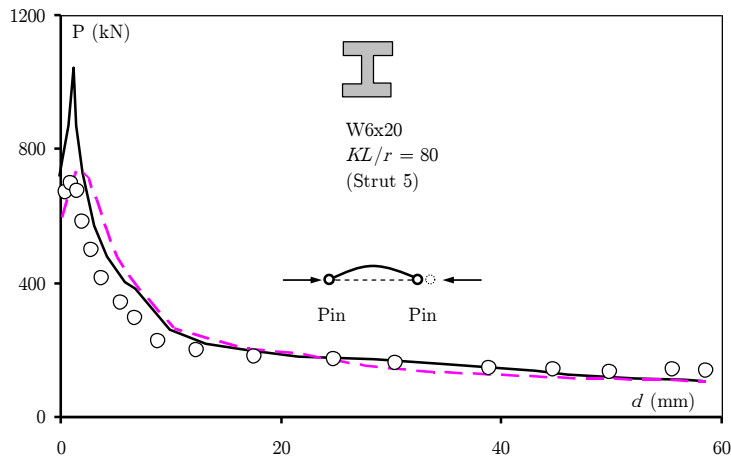
(a) strut 19

(b) strut 5
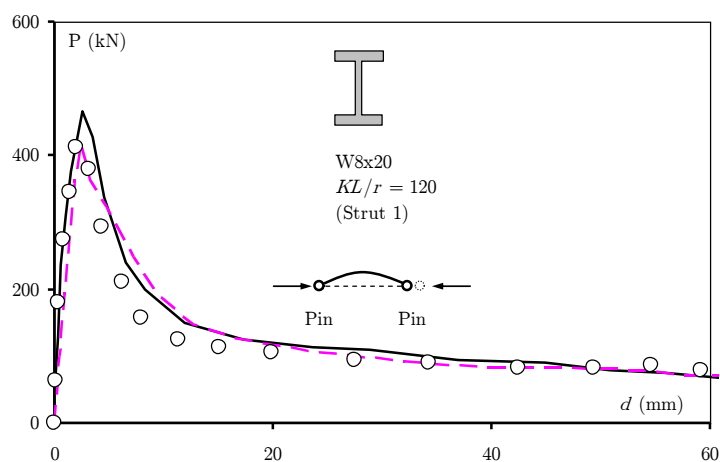
(c) strut 1

Figure 3.3: Compression envelope of post-buckling response of wide-flange column consists of different slenderness and boundary conditions: Comparison between the present study, Opensees (McKenna et al., 2006) and experiment by Black et al. (1980)
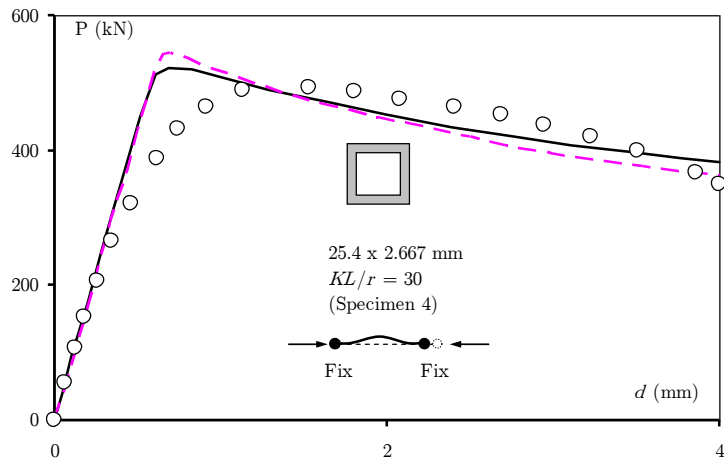
(a) specimen 4
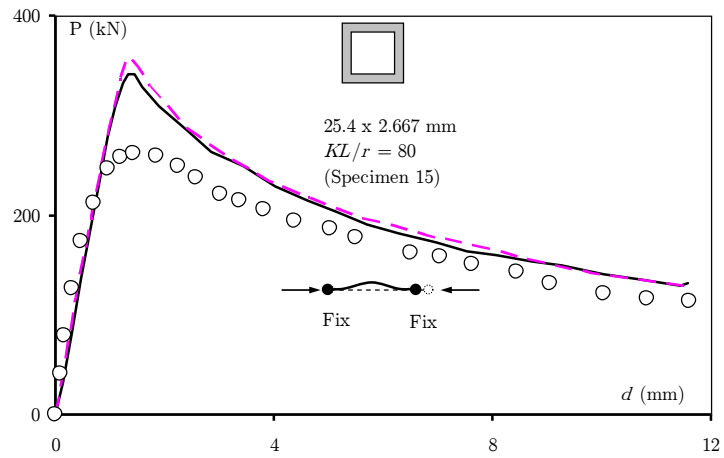
(b) specimen 15
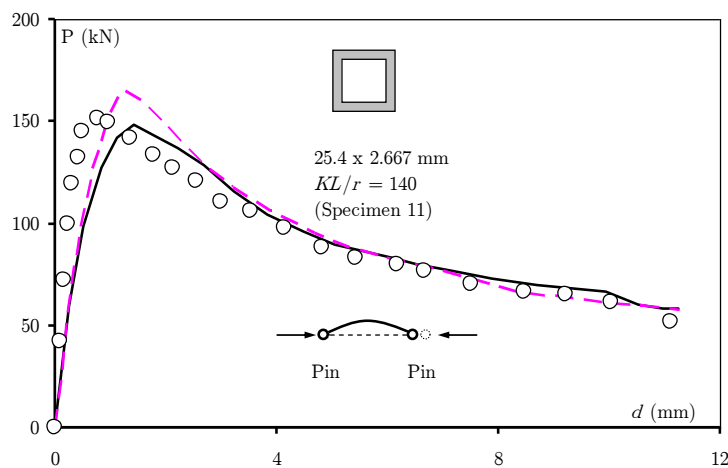
(c) specimen 11

Figure 3.4: Compression envelope of post-buckling response of box column consists of different slenderness and boundary conditions: Comparison between the present study, Opensees (McKenna et al., 2006) and experiment by Jain et al. (1978)

101
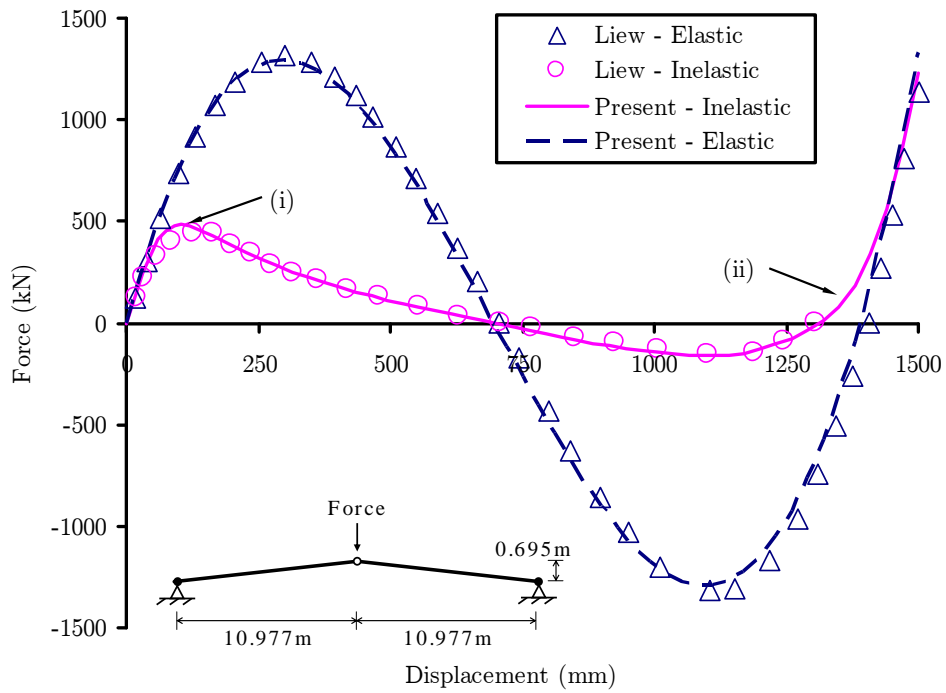
(a) total push-down load versus vertical displacement at crown
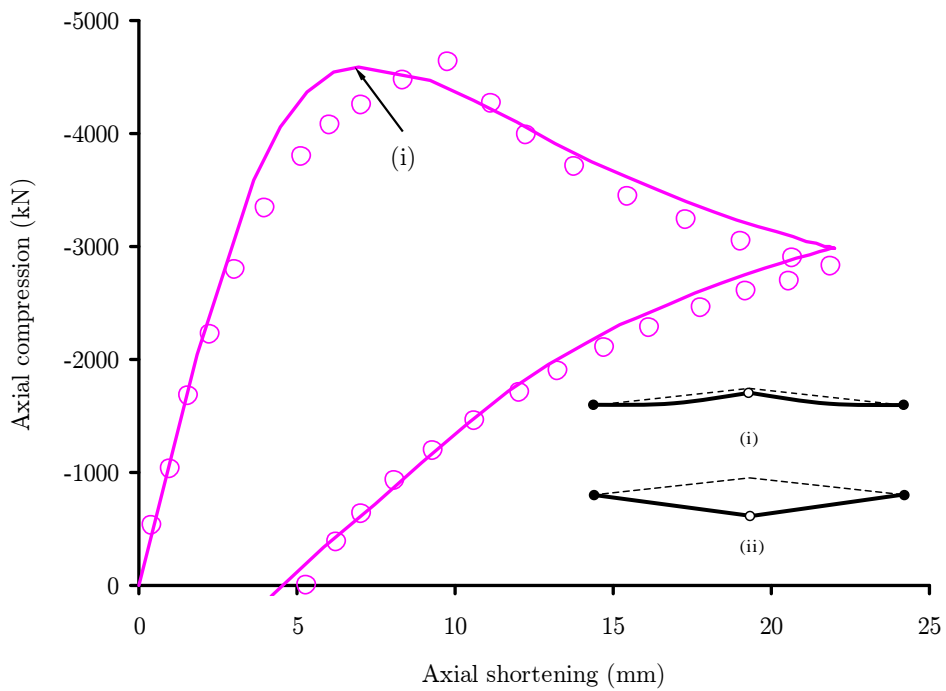
(b) axial force versus shortening of the truss member

Figure 3.5: Static response of two-bar truss under gravity load: Comparison between the present study and numerical study by Liew et al. (1997)
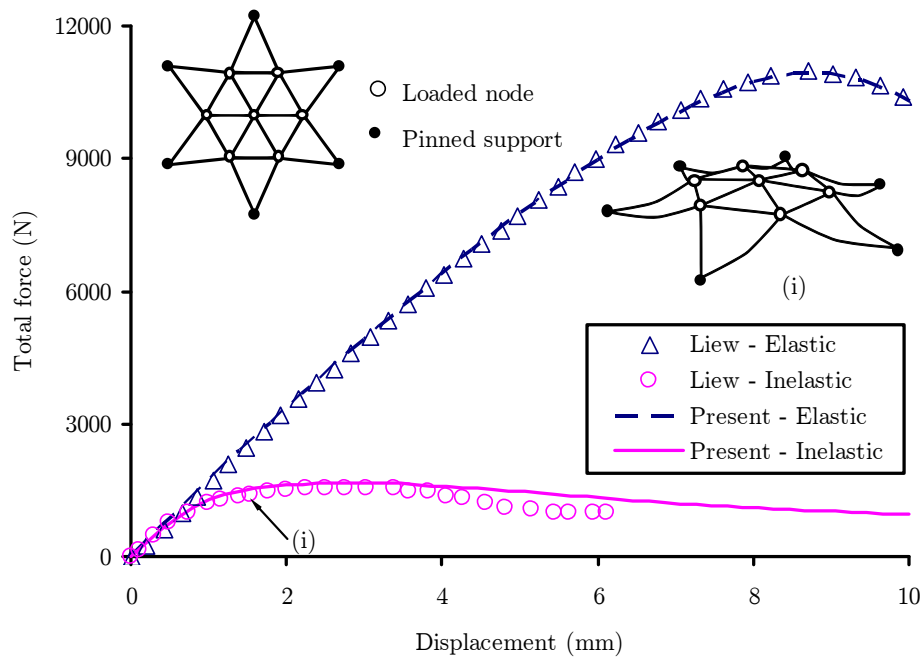
(a) total push-down load versus vertical displacement at crown
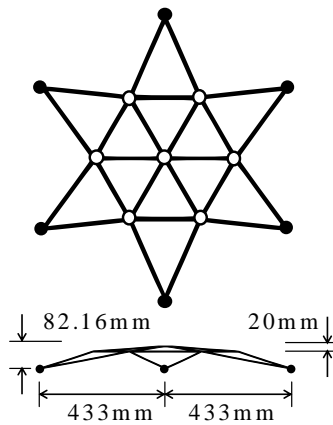
(b) geometry of star dome

Figure 3.6: Static response of star dome under gravity load (case 1): Comparison between the present study and numerical study by Liew et al. (1997)
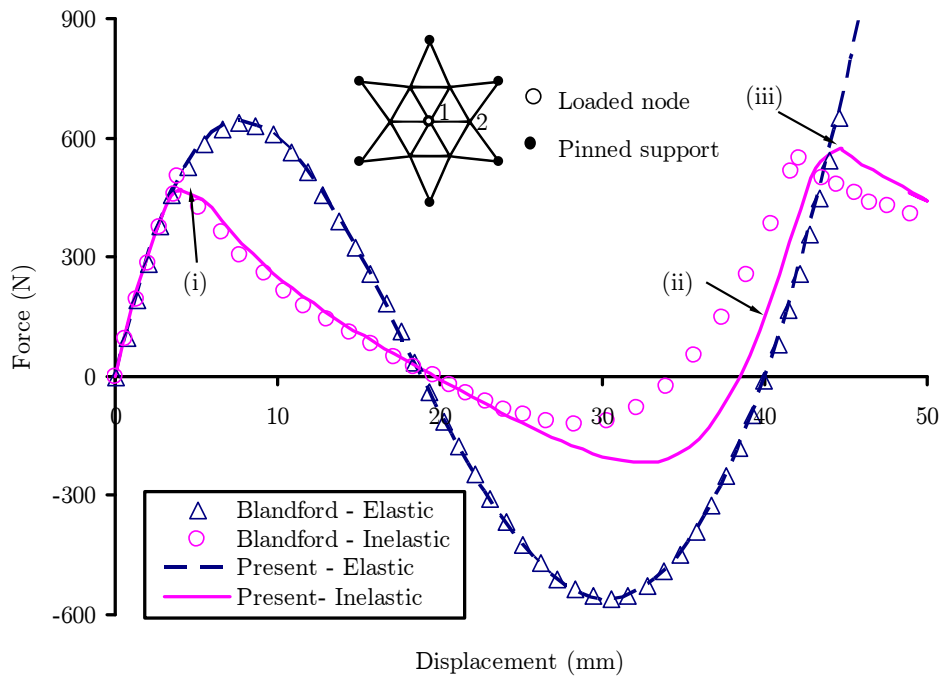
(a) total push-down load versus vertical displacement at node 1
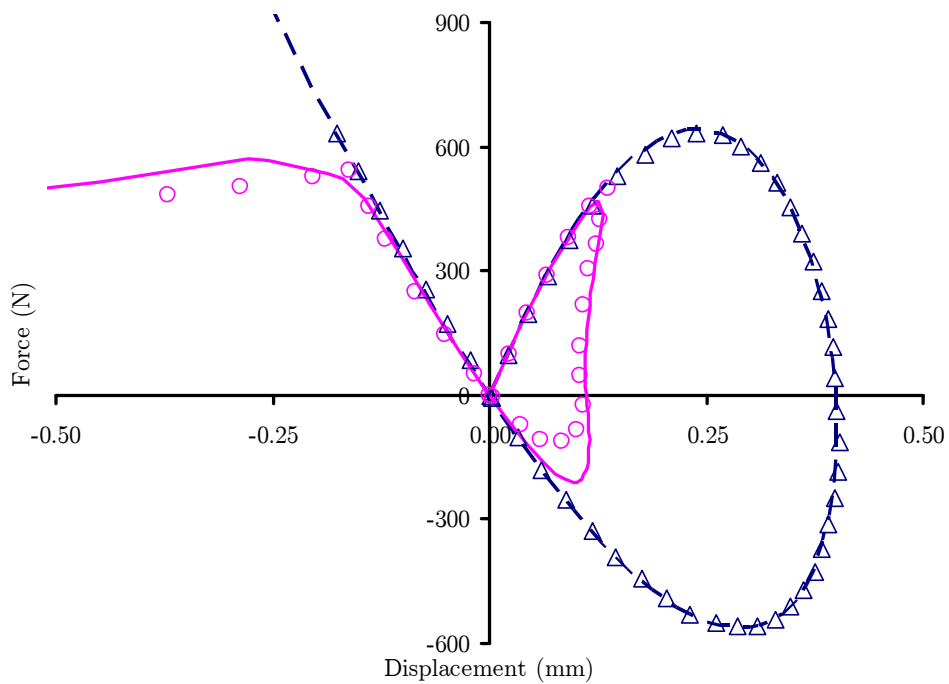
(a) total push-down load versus lateral displacement at node 2

Figure 3.7: Static response of star dome under gravity load (case 2): Comparison between the present study and numerical study by Blandford (1996)

(i)   (ii)   (iii)
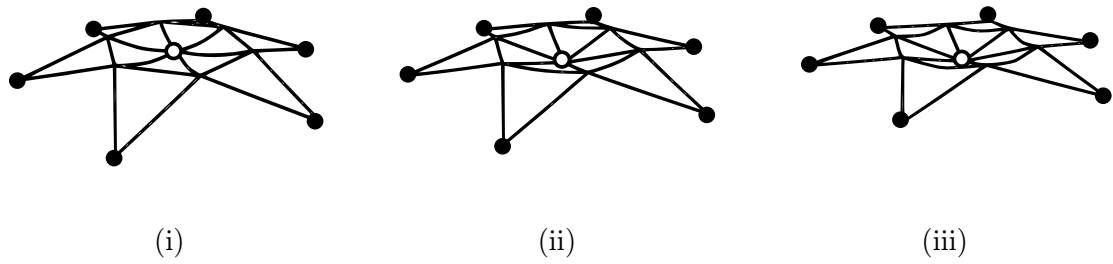
(b) deformation shapes at different loading conditions

Figure 3.8: Progressive collapse sequence of star dome under point load at crown node (case 2)

○ Loaded node	$A = 50.431$ cm^2	○ Loaded node	$A = 650$ mm^2
● Pinned support	$I = 52.942$ cm^4	● Pinned support	$I = 1 \times 10^4$ mm^4
	$E_s = 2.04 \times 10^7$ N/cm^2		$E_s = 6.895 \times 10^4$ N/mm^2
	$f_y = 2.5 \times 10^4$ N/cm^2		$f_y = 4 \times 10^3$ N/mm^2

(a) Circular dome   (b) Geodesic dome
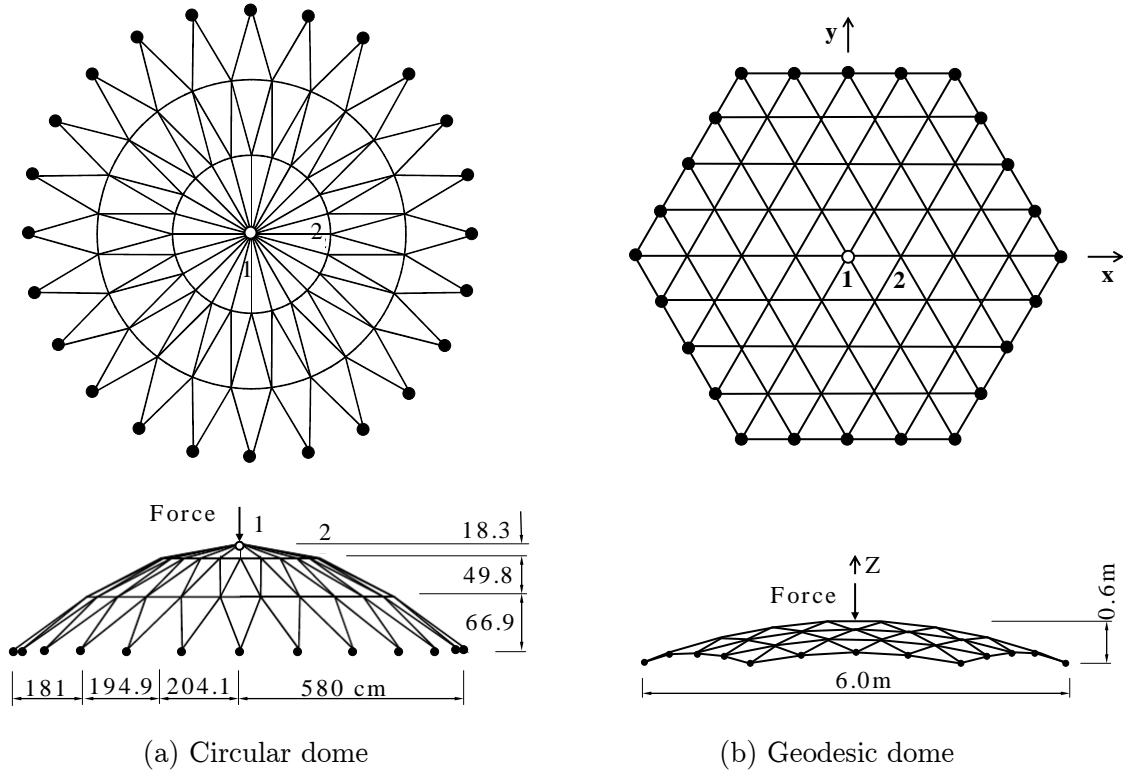
Figure 3.9: Geometries of circular dome and geodesic dome
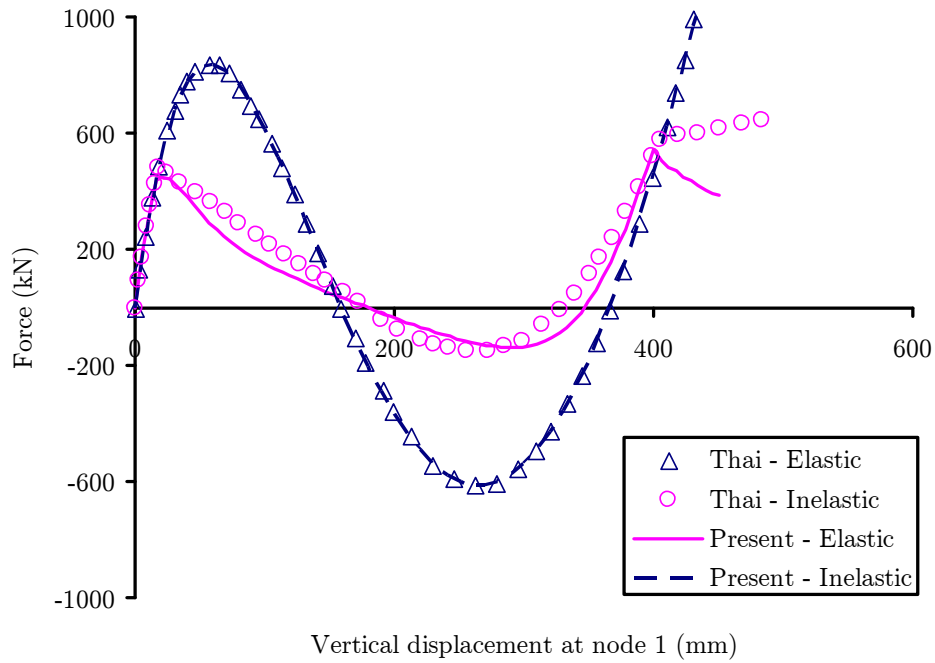
Figure 3.10: Static response of circular dome under gravity load: Comparison between the present study and numerical study by Thai and Kim (2009)
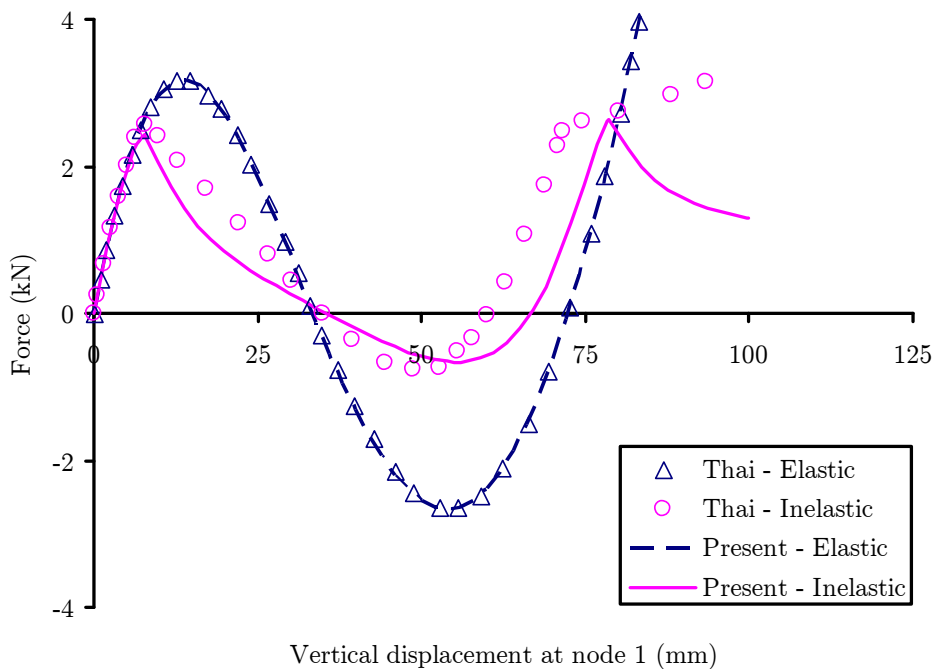
Figure 3.11: Static response of geodesic dome under gravity load: Comparison between the present study and numerical study by Thai and Kim (2009)

(a) load factor versus roof displacement

(b) frame geometry
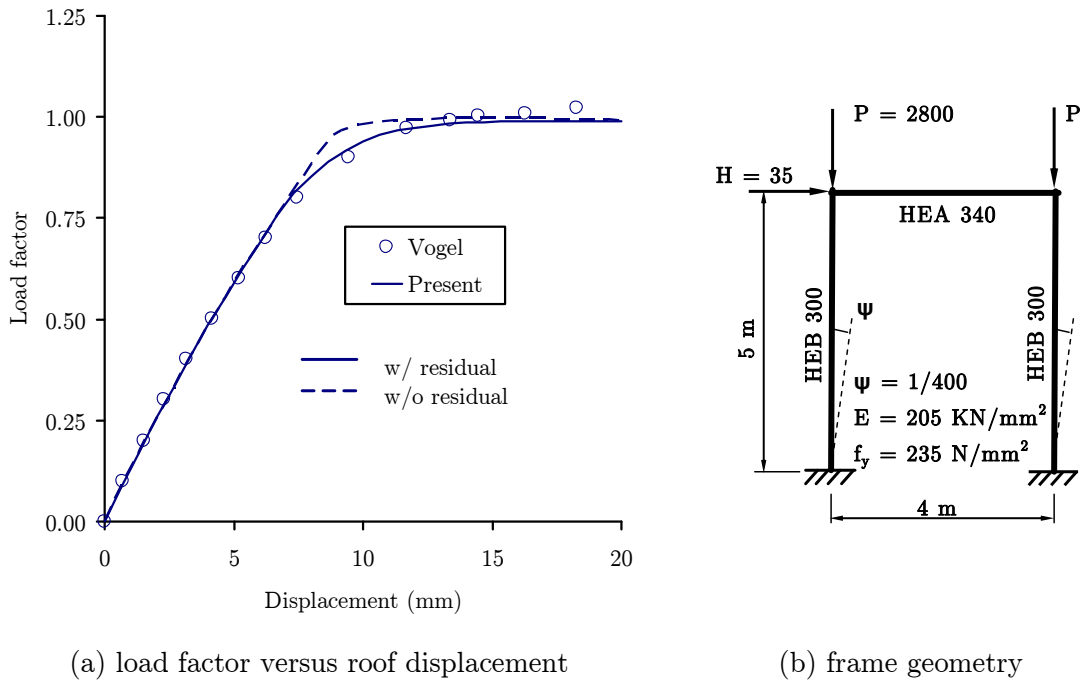
Figure 3.12: Static response of single-storey 2D frame under gravity and lateral loads: Comparison between present study and numerical study by Vogel (1985)

(a) load factor versus displacement on 6th and 4th storey

(b) frame geometry
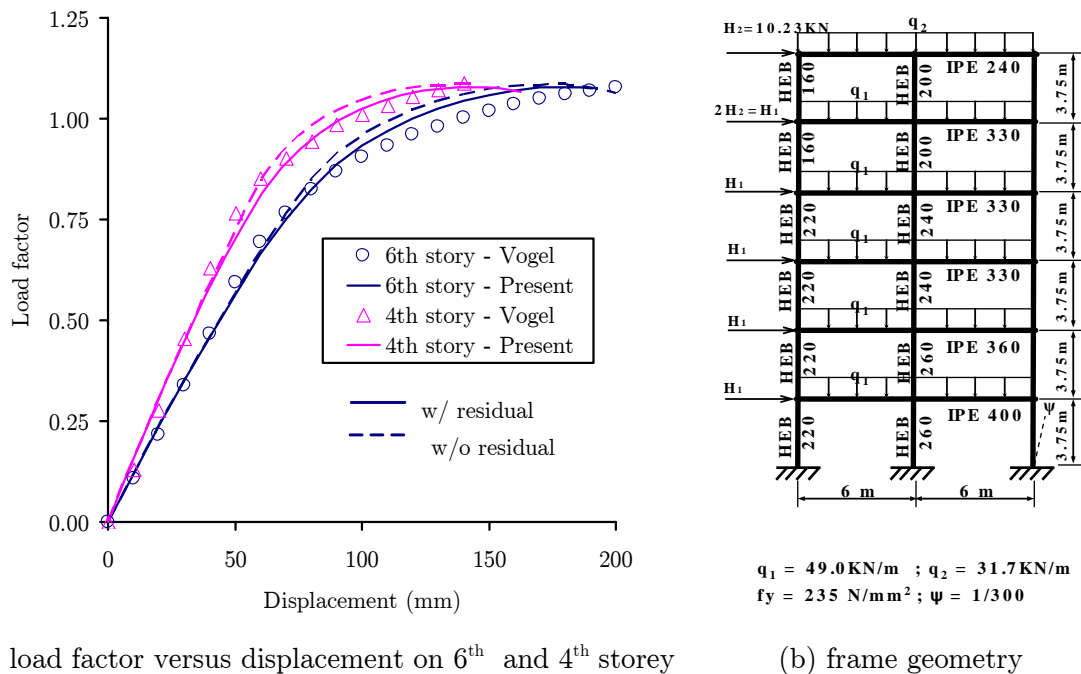
Figure 3.13: Static response of six-storey 2D frame under gravity and lateral loads: Comparison between present study and numerical study by Vogel (1985)

(a) building geometry

(b) floor geometry

(c) load factor versus roof displacement

(d) deformed shape
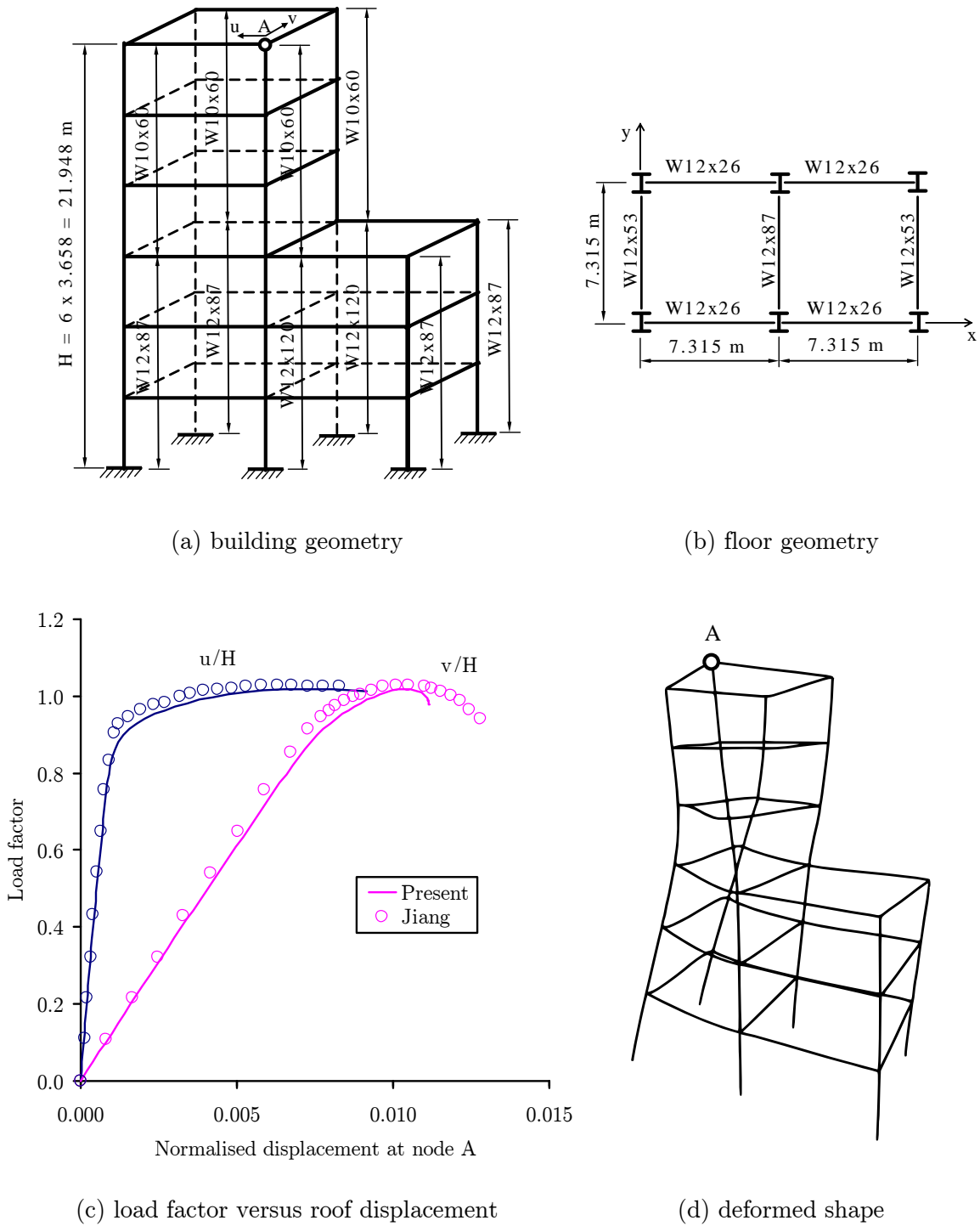
Figure 3.14: Static response of six-storey 3D building under gravity and lateral loads: Comparison between the present study and numerical study by Jiang et al. (2002)

(a) building geometry

(b) floor geometry

(c) load factor versus roof displacement

(d) deformed shape
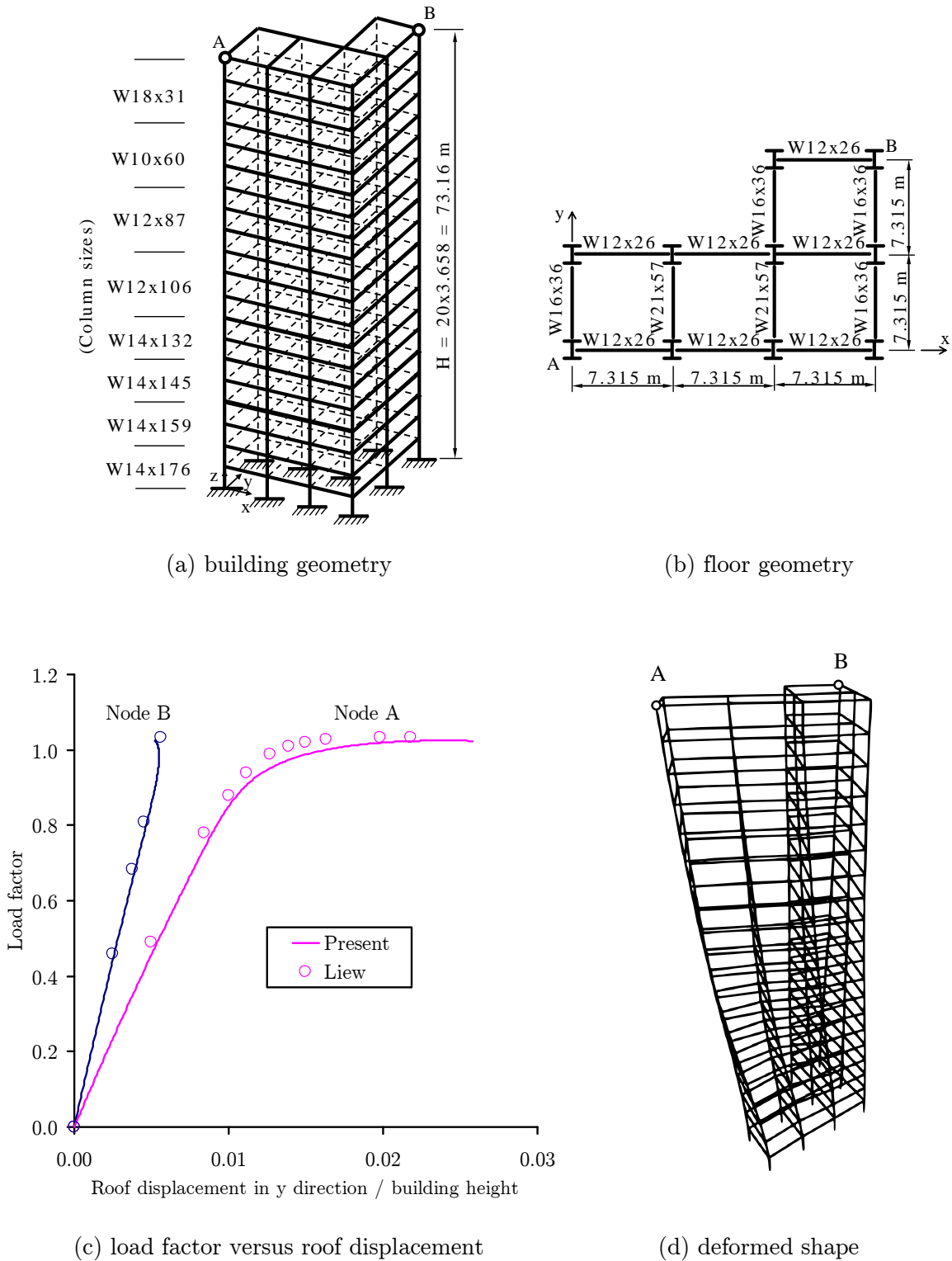
Figure 3.15: Static response of twenty-storey 3D building under gravity and lateral loads: Comparison between the present study and numerical study by Liew et al. (2001)

(a) case 1: removal of perimeter (b) case 2: removal of internal (c) load history for
column   column   column removal
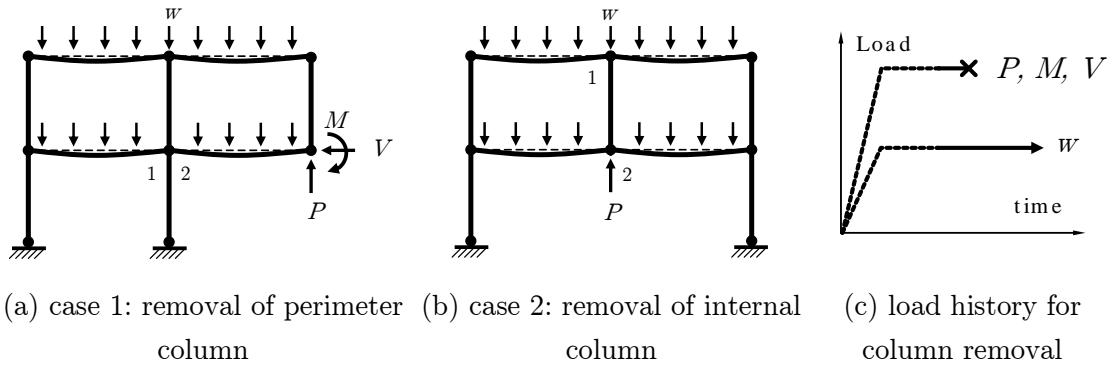
Figure 3.16: Cases of column removal considered for two-storey moment frames studied
by Kaewkulchai and Williamson (2004)

(a) vertical displacement time-history   (b) column axial force time-history

(c) bending moment time-history (case 1)   (d) bending moment time-history (case 2)
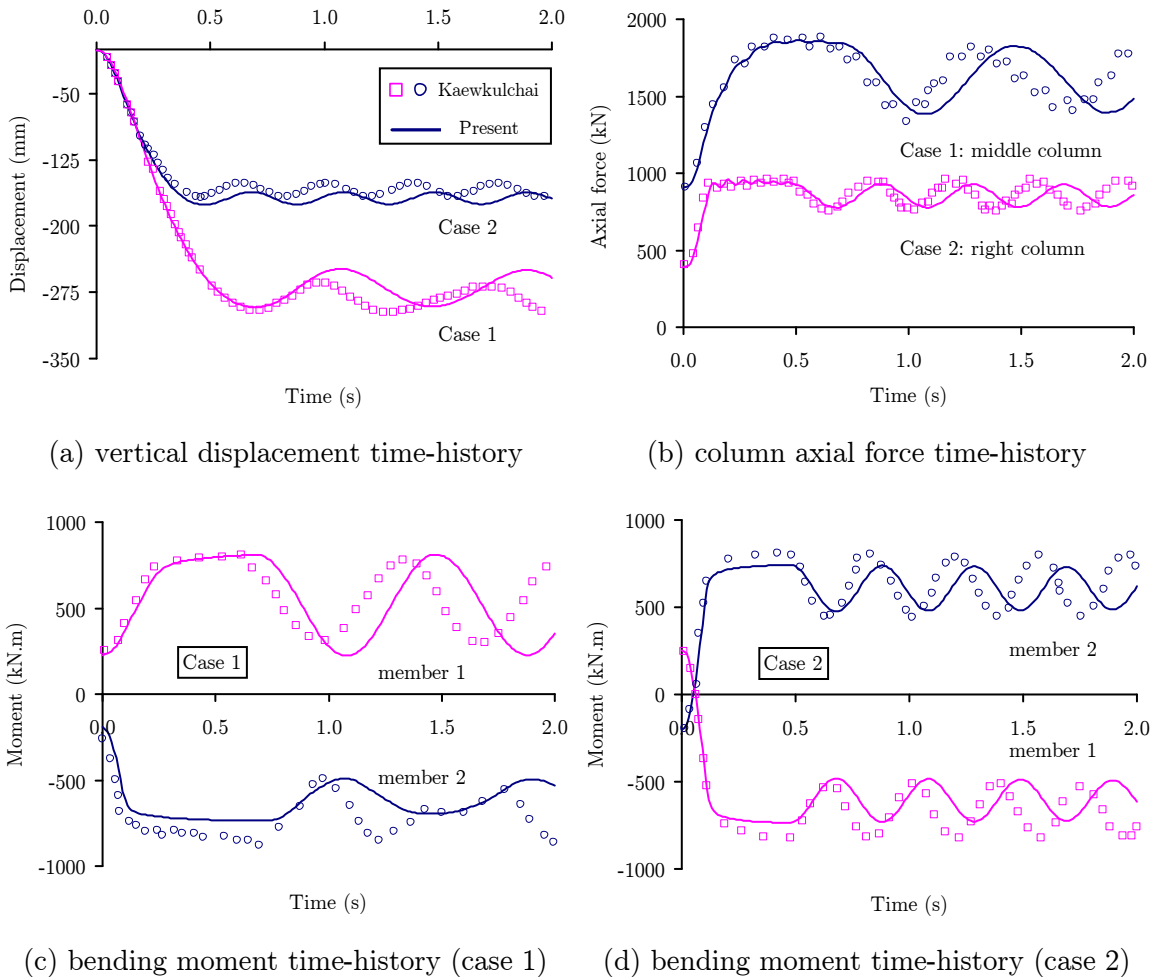
Figure 3.17: Dynamic response of two-storey moment frame due to sudden column
removal: Comparison between the present study and numerical study by Kaewkulchai
and Williamson (2004)

(a) case 1: removal of perimeter column   (b) case 2: removal of internal column
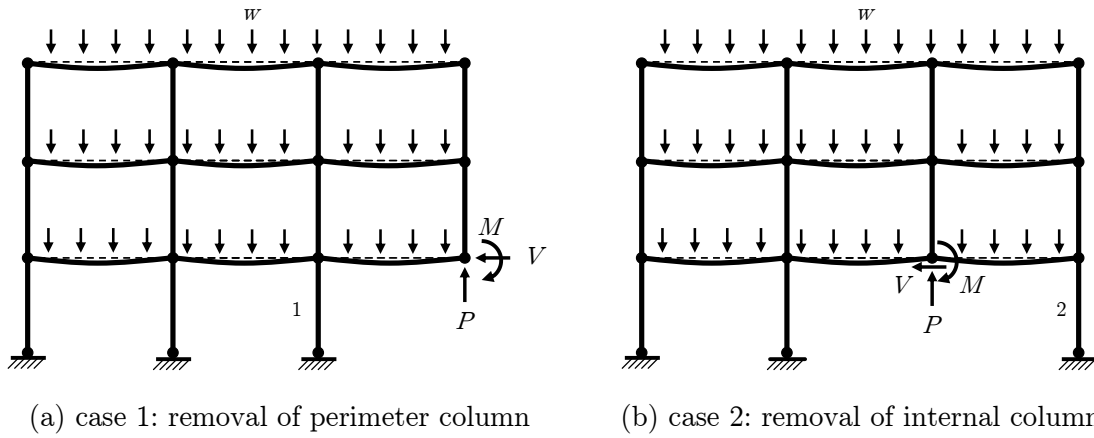
Figure 3.18: Cases of column removal considered for three-storey moment frame studied by Kaewkulchai and Williamson (2004)

(a) vertical displacement time-history   (b) bending moment time-history
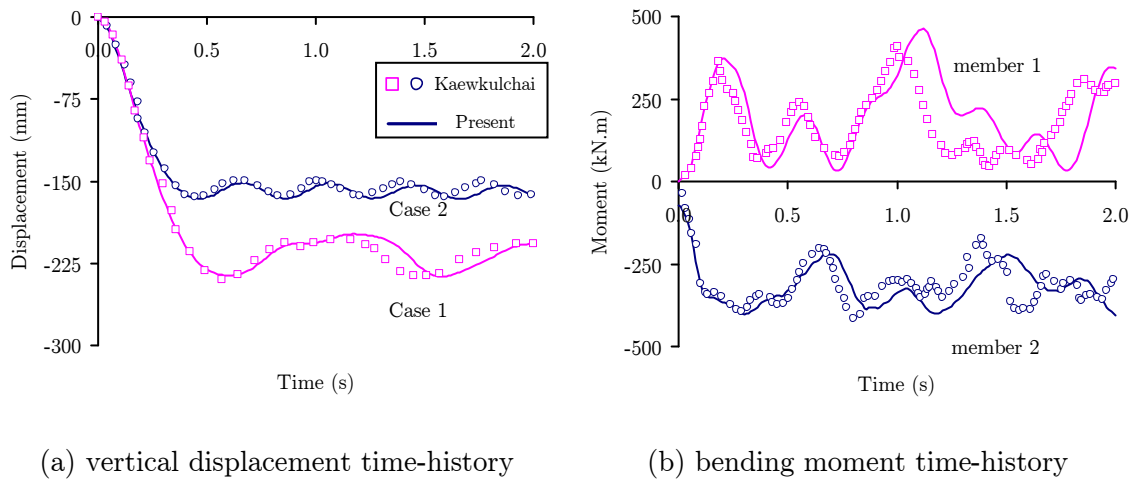
Figure 3.19: Dynamic response of three-storey moment frame due to sudden column removal: Comparison between the present study and numerical study by Kaewkulchai and Williamson (2004)

111
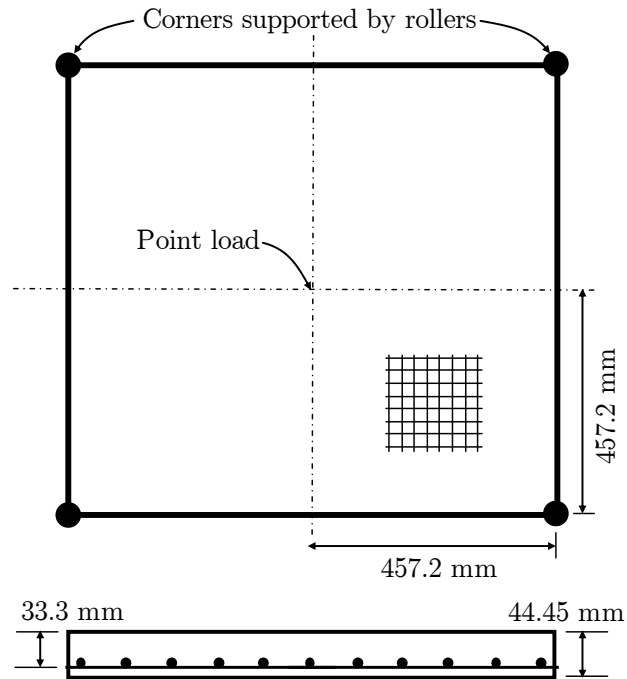
(a) 914 x 914 x 44.5 mm square reinforced concrete slab
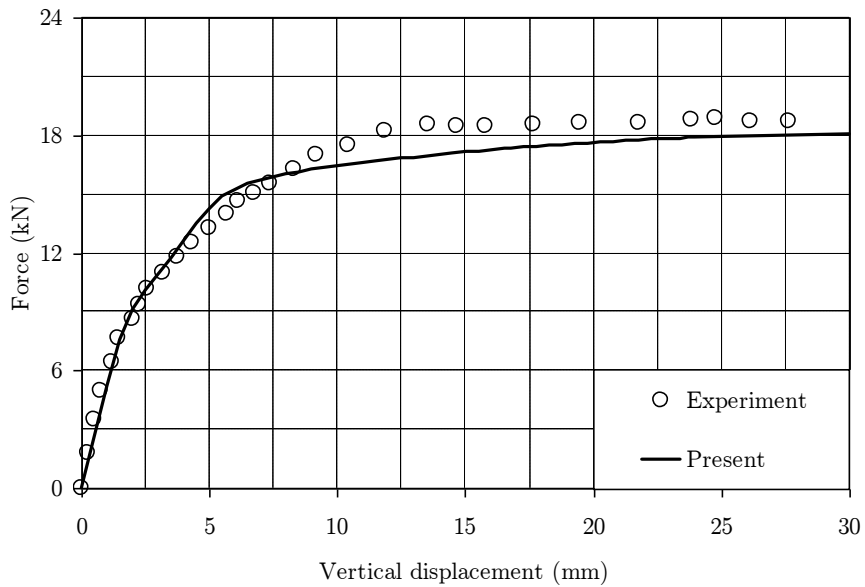
(b) push-down load versus mid-span displacement

Figure 3.20: Static response of a reinforced concrete slab under gravity load: Comparison between the present study and experiment by Jofriet and McNeice (1971)
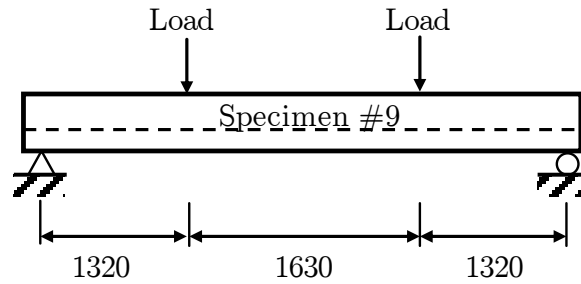
(a) 305 x 4270 x 125 mm composite slab strip (specimen #9 in reference paper)
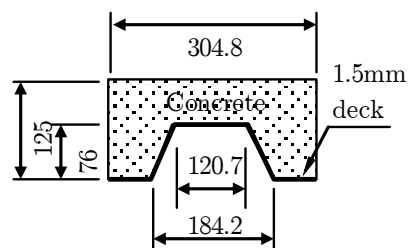
(b) cross section of specimen
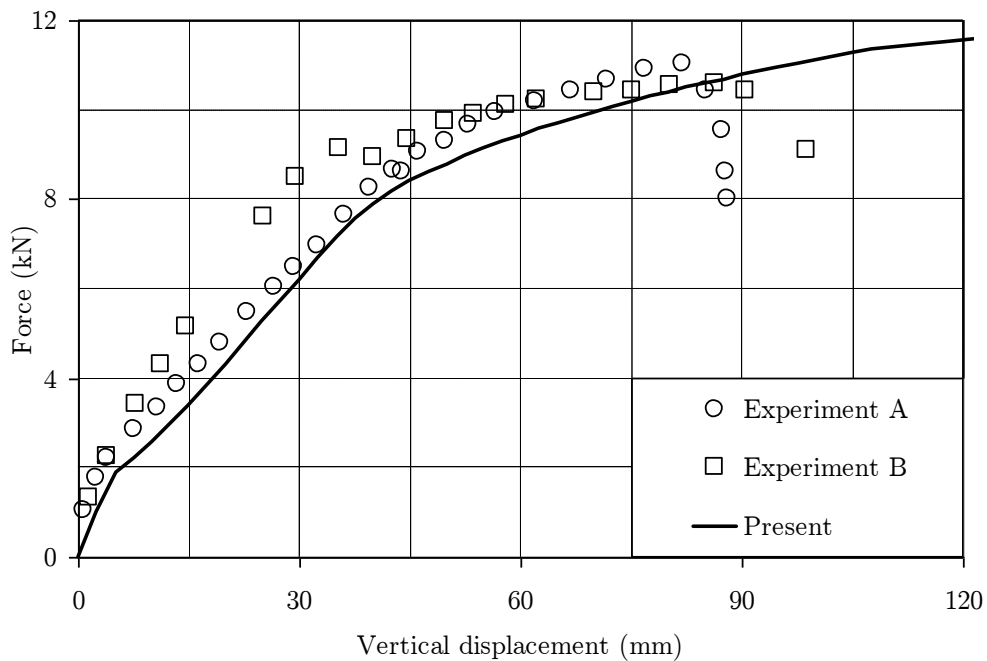
(c) total push-down load versus mid-span displacement

Figure 3.21: Static response of a composite slab strip under 2-point loads in gravity direction: Comparison between the present study and experiment by Abdullah and Easterling (2009)

113
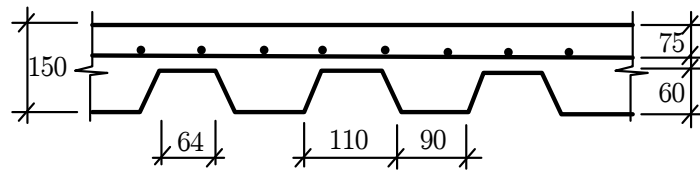
(a) geometry of ribbed slab specimen (without steel deck)
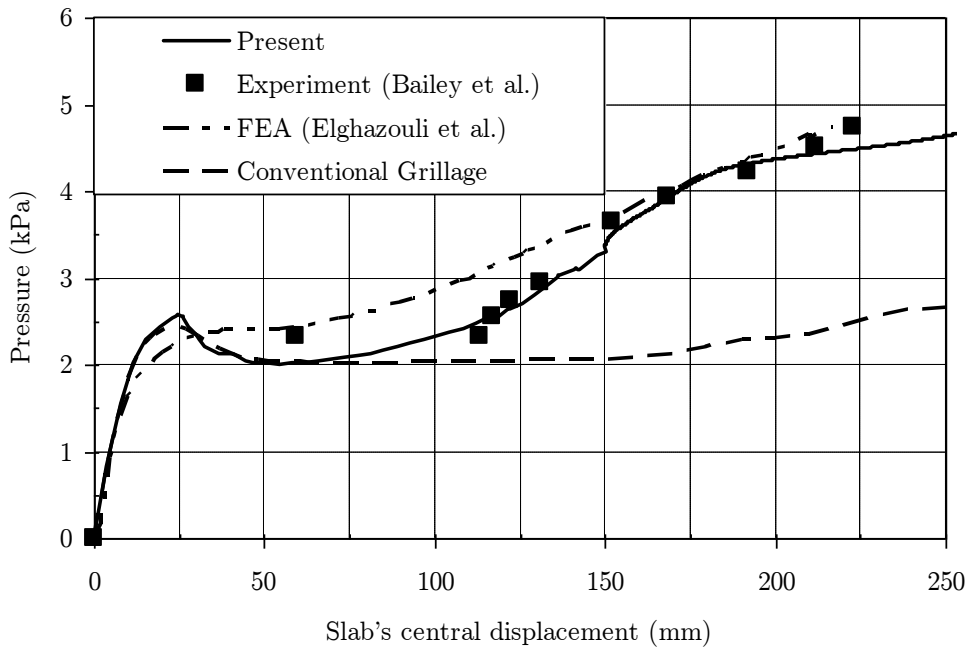
(b) floor pressure versus mid-span displacement

Figure 3.22: Static response of a large ribbed reinforced concrete slab under uniform area load in gravity direction: Comparison between the present study, experiment by Bailey et al. (2000), and detailed finite element analysis by Elghazouli and Izzuddin (2004)
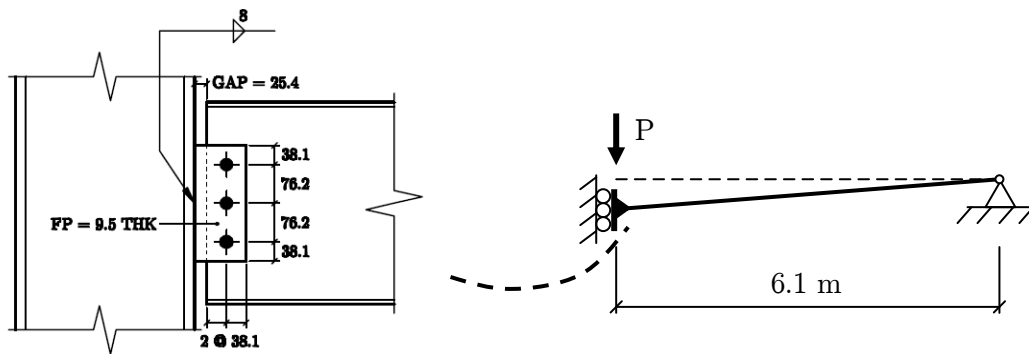
Figure 3.23: Configuration of fin plate shear connection studied by Sadek et al. (2008)
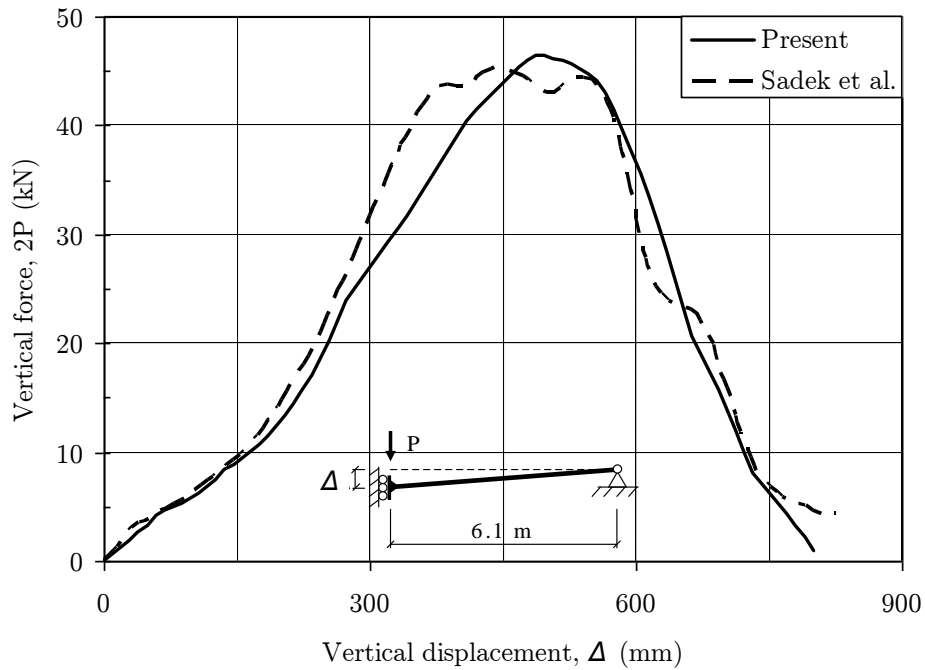
(a) vertical force versus vertical displacement
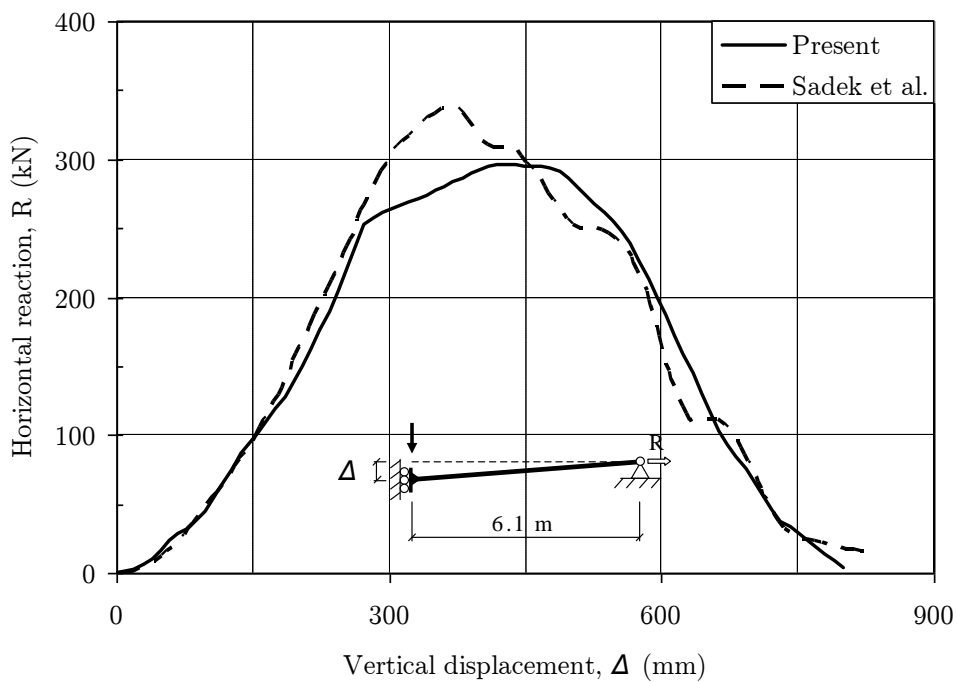
(b) horizontal reaction versus vertical displacement

Figure 3.24: Static response of fin plate shear connection under point load: Comparison between the present study and numerical study by Sadek et al. (2008)

115

Chapter 4: Robustness Design of Composite Floor System

4.1 Introduction

Traditionally, progressive collapse analysis is performed using simplified finite element analysis (FEA) e.g. the work by Kaewkulchai and Williamson (2004), Marjanishvili and Agnew (2006), Lee et al. (2010), Kim and Kim (2009b), among others. In the analysis, the structure is represented by a macro model in which main structural components, i.e. beams and columns, are modeled by one-dimensional frame elements. Floor slab is ignored in the analysis due to enormous computational demand and complexity involved in analyzing its large deformation behaviors. The simplified method is not appropriate for performance-based robustness evaluation as it discounts the important roles floor slab plays in resisting progressive collapse. In small-deformation response, floor slab can contribute significantly to the flexural strength of the composite beam system. In large-deformation response it plays double roles in providing reserved strength through catenary action and at the same time providing diaphragm stiffness for catenary action to develop.

The influence of floor slab was not taken into account until recently using detailed finite element analysis e.g. the work by Fu (2009), Kwasniewski (2010), Yu et al., (2010), Sadek et al. (2008), among others. In their studies, structural components are modeled rigorously using 2D shell elements and 3D solid elements in combination with

sophisticated material constitutive models. The findings of these studies point to the potential of floor slab in arresting progressive collapse in the event of sudden column loss. However, these sophisticated methods are computationally demanding, and hence are less appropriate for behavioral study and application in design practice. Instead, the method for robustness evaluation should be computationally efficient yet capable of simulating key damage behaviors of composite floor system with reasonable accuracy, i.e. the flexural and membrane response of composite slabs, semi-rigid and partial strength response of shear connections, and member and global buckling of steel frames. This philosophy is the main motivation of the development of efficient progressive collapse analysis (ePCA) method as presented in chapter 2 of this thesis.

In this chapter, the proposed ePCA is used to investigate the robustness performance of composite floor system. Two critical cases of column removal are considered, namely internal column removal and perimeter column removal cases. To verify the effectiveness of the numerical models used in the studies, published numerical solutions and experimental findings are used as the reference for comparison. Subsequently, parametric studies are carried out to identify key design parameters that contribute to robustness of composite floor system, and to draw recommendations for effective robustness design. The study focuses on optimizing the potential of shear connection in resisting progressive collapse, such that the use of expensive moment connection can be avoided or minimized in practice.

4.2 Collapse resistance of composite floor due to internal column removal

Sudden removal of internal column is one of the critical cases recommended by current codified methods for robustness design of building structures (GSA, 2003; DoD, 2009). In this section, study is focused on the collapse resistance of a large and realistic composite floor system subjected to this column removal event. The structure used in the study is a prototype building designed by NIST based on the latest building codes of practice (Liang et al., 2008).

4.2.1 Floor subassembly of NIST prototype building

The structure is designed by NIST for robustness study and has realistic material and geometrical properties commonly used in construction practice (Liang et al., 2008). Figure 4.1 shows the floor subassembly (i.e. hatched region) and the location of column removal considered in the study. The building is a ten-storey office building with dimensions of 30.5 m x 45.7 m on plan. The lateral-resisting system of the building consists of perimeter moment-resisting frames designed to withstand seismic excitation. The interior of the building consists of gravity frames in which fin plates are used for all beam-to-beam and beam-to-column connections. The fin plate connection consists of 3 number of A325 high-strength bolts in 22 mm diameter clearance holes and 9.5 mm thick fin plate. The fin plate consists of ASTM A36 steel with yield strength of $f_y = 248.2$ N/mm^2. The geometry of fin plate connection is shown in Figure 4.2a. All primary beams and secondary beams in the gravity frames consist of typical section of W16x26 and W14 x 22 respectively. ASTM A992 structural steel with yield strength of $f_y = 344.8$ N/mm^2 is assumed for the steel frames. The floor system consists of 82.5 mm lightweight concrete topping (compressive strength $f_c = 20.7$ N/mm^2, density = 17.3 kN/m^3) on 76.2 mm steel deck. The steel deck is assumed to be 0.9 mm thick with yield strength of $f_y = 248$ N/mm^2. The slab is reinforced with welded wire mesh W1.4x1.4 at 28 mm below the concrete top surface. The welded wire mesh has yield strength of $f_y = 650$ N/mm^2. Shear studs are welded to the steel beams and are embedded in the concrete to achieve composite action.

The same floor subassembly was previously studied by Sadek et al. (2008) and then by Alashker et al. (2010) using the same detailed FEA with LS-DYNA (Hallquist, 2006). In Sadek et al. (2008) model, solid and shell elements are used to elaborately model the composite slab, shear connection, structural frames and the interaction between the composites. The friction-slip behavior between steel deck and concrete topping and that between the composite slab and steel beam are modeled rigorously using nonlinear contact and gap elements. As a result, a total of 295,000 solid and shell elements are used in the numerical model (Sadek et al., 2008). The numerical model is used to study the influence of slab membrane action to the collapse resistance of the floor system when

subjected to concentrated load at the column removal location. In the subsequent study, Alashker et al. (2010) uses the same numerical model proposed by Sadek et al. (2008) to investigate the influence of deck thickness, slab reinforcement the connection design on global progressive collapse resistance of the floor system when subjected to uniform floor load. The connection design considered in Alashker et al. (2010) study consists of single line bolt-group shown in Figure 4.2a. To validate the numerical model used in the present work, numerical results published by Alashker et al. (2010) are used as the reference for comparison.

4.2.2 Numerical model

In the present work, a numerical model as shown in Figure 4.3 is developed by using the ePCA method proposed in chapter 2. Due to symmetry, only a quarter of the floor system needs to be modeled. The fin plate shear connection is modeled using the plastic zone element as discussed in section 2.4 of chapter 2. The critical failure mode of the bolt-row is governed by ductile tear-out of the beam web (bearing at bolt holes). Therefore, the yield and ultimate resistance of each bolt-row can be determined from AISC360-05 (AISC, 2005) with resistance factor of 1.0. An equivalent plastic zone element is developed for the connection based on the method discussed in section 2.4.2 by taking the plastic zone length L_p equals to the length of fin plate (i.e. 100 mm) and the area A_i of the ith fiber representing the jth bolt-row as 1000 mm^2. The composite slab is modeled using the modified grillage method as discussed in section 2.3 of chapter 3. The spacing of the grillage is about 760 mm in both orthogonal directions. The equivalent T-section grillage in deck direction is determined from equation (2.11) to (2.14) based on the deck geometry of $s = 304.8$ mm , $b_1 = 190.5$ mm, and $b_2 = 114.3$ mm. Stiffness of the compression-only spring k_s is determined as 1.881 x10^6 N/mm by taking h_c equal to the concrete topping, i.e. 82.5 mm in equation (2.19).

The beams, columns and slabs are modeled using frame elements at their respective centroids. Due to the difference in depth, rigid link constraint is used to enforce full composite action between the beam and slab. Therefore, the friction-slip behavior

between the composite slab and steel beam is not considered. The assumption is reasonable for progressive collapse analysis involving column removal because localized behavior has little influence on the global load-displacement response. However, for specific application when the friction-slip behavior needs to be considered, nonlinear link element should be used instead. The numerical model consists of only 996 frame elements, which are significantly less than the 295,000 solid and shell elements used by Sadek et al. (2008) and Alaskher et al. (2010). As a result, each nonlinear static analysis requires only 10 to 15 minutes to be performed on a normal personal computer (i.e. Intel core 2 Quad CPU with 3.00 GHz and 3GB of RAM). For comparison purpose, the computational demand is approximated as N^2, where N is the number of degree of freedom of a numerical model. Therefore, the numerical model used by Sadek et al. (2008) and Alaskher et al. (2010) requires 22,000 times approximately more computational demand than the present model, which is developed based on ePCA method. The approximation assumes that the total number of node in the system is equal to the number of element, which is reasonably accurate for large system. Each node of frame element used in the present model has 6 degrees of freedom, while each node of solid element used in the reference paper has 3 degrees of freedom.

4.2.3 Verification study

The relationship between the floor load and vertical displacement at the location of column removal is plotted in Figure 4.4. When subjected to uniform gravity load, the floor system deforms downward almost linearly in the initial stage. Stress concentration occurs at the connections as the connections are the weakest links in the overall structural system. Gradual softening of the response occurs as the connection goes into the inelastic range. The floor system continues to exhibit increase of load-carrying capacity albeit with increasing damage to the connection due to the contribution of tensile catenary action. Out-of-balance force in the slab due to catenary action is resisted by the slab itself in the form of a "compressive ring".

The global load-displacement relationships predicted by ePCA and detailed FEA by Alaskher et al. (2010) are compared in Figure 4.4. They agree well in terms of initial stiffness and ultimate capacity. The ultimate capacity predicted by ePCA is about 1113 kN (+1%) as compared to 1099 kN by the detailed FEA. The vertical displacement at the removed column location corresponding to the ultimate capacity is found to be about 1.1 m. Beyond this displacement, the floor system begins to lose its strength as many parts of connections, steel decks and slab reinforcements reach the material fracture limit. The energy-absorbing capacity (i.e. area under the load-displacement curve) after displacement of 1.1 m as predicted by ePCA is found to be about 896 kN-m (+1%) as compared to 890 kN-m by the detailed FEA.

Similar to the findings for the ribbed slab system discussed in section 3.4.3 of chapter 3, proper modeling of slab membrane action is important to achieve realistic simulation of its tension catenary action in the large-deformation response. As shown in Figure 4.4, ignoring the floor slabs can underestimate ultimate strength of floor system by almost 5 times! Also, if conventional grillage model is used which neglects the slab membrane action (when $K_s = 0$ in equation 2.18), the ultimate capacity of floor system can be underestimated by almost 2 times. Therefore, a reasonably accurate yet fast analysis method like the present method can be helpful for engineers to account for the contribution of floor slabs for robustness evaluation in the early stage of design process. As a result, it allows slab reinforcement and shear connection to be designed to fulfill robustness requirements

Alashker et al. (2010) also analyzes the same floor system for cases with different deck thicknesses, slab reinforcement densities and connection designs. The different structural properties considered in the parametric study are summarized in Table 4.1. Figure 4.5 to Figure 4.7 show the global load-displacement relationships for these cases predicted by the present method and the detailed FEA by Alashker e al. (2010). It is evident that the general trends of load-displacement relationship for all cases agree well with the prediction by the detailed FEA. The ultimate capacities and energy-absorbing capacities after displacement of 1.1 m predicted by both ePCA and detailed FEA are compared in Table 4.1. The value in the parenthesis denotes the ratio of capacity predicted by ePCA

to capacity predicted by the detailed FEA. Out of the 7 cases studied, only case 2 shows a difference in prediction greater than 7%. The ultimate capacity and energy-absorbing capacity for case 2 are underestimated by 17% and 11% using ePCA, which are on the safe side for robustness evaluation. The maximum overestimation of ultimate capacity and energy-absorbing capacity are only 7% for case 4 and case 3. The good agreement between ePCA and detailed FEA shows that ePCA can be used for robustness evaluation of large and realistic floor systems with reasonable accuracy and efficiency.

4.2.4 Factors influencing collapse resistance

The key design parameters that influence progressive collapse resistance of a composite floor system are discussed in this section. These parameters include the deck thickness, slab reinforcement and connection design. The load-displacement relationships for various deck thicknesses, slab reinforcement densities and connection designs are shown in Figure 4.8 to Figure 4.10.

4.2.4.1 Deck thickness

Load-displacement relationships for cases with different deck thicknesses are shown on Figure 4.8. It is evident that the deck contributes significantly to the ultimate and reserved strengths of the composite floor. The term reserved strength defines the load carrying capacity of a structural system beyond the ultimate strength. The ultimate capacities and energy-absorbing capacities at displacement of 1.1 m for the all the cases are summarized in Table 4.2. The ultimate capacity and energy-absorbing capacity of the floor system that uses the commonly used deck thickness, i.e. 0.9 mm are nearly twice of the floor without steel deck. If thicker deck of 1.8 mm is used, the ultimate capacity and energy-absorbing capacity can be improved by 37% and 33%, respectively. The significant influence of the steel deck is justifiable as it is the main source of tensile resistance in the floor slab for catenary action. Increasing the deck thickness can enhance the robustness performance of floor system, but this practice is less practical as thick steel deck is difficult to work with. For good practice of robustness design, it is advisable to ensure full continuity between steel decks such that the contribution of steel deck can

be fully mobilized. To achieve full continuity, puddle welds and self-drilling screws can be used (Sadek et al., 2008).

4.2.4.2 Slab reinforcement

Steel reinforcement is normally not required for strength design of composite slab, but nominal amount of reinforcement is still required to control crack width due to shrinkage and creep effects of the concrete topping. In most cases, the amount of slab reinforcement is far lesser than the steel deck. The reinforcement density of 0.06 mm^2/mm as shown in Figure 4.9 denotes smeared cross-sectional area of reinforcement of 0.06 mm^2 per millimeter run of slab in each orthogonal direction. In terms of steel tonnage, the orthogonal reinforcement mesh is equivalent to a flat steel plate of 0.12 mm thick. Compared to the 0.9 mm steel deck, the amount of reinforcement is 7.5 times lesser. Despite the small amount, the slab reinforcement has substantial contribution to the collapse resistance. As shown in Figure 4.9 and Table 4.3, a marginal increase of slab reinforcement by 0.06 mm^2/mm can increase the ultimate capacity and energy-absorbing capacity by 13% and 11%, respectively. If reinforcement is ignored in the analysis, the ultimate capacity and energy-absorbing capacity of the floor system can be reduced by 8% and 13%, respectively. The higher density of slab reinforcement improves the catenary action of the floor system at large-deformation response similar to the role of the steel deck. For robustness design, there are a few merits of specifying more reinforcement than specifying thicker deck: (1) thick steel deck is difficult to work with, (2) steel deck is exposed to external loadings e.g. explosion and fire attack, (3) full continuity of reinforcement can be achieved easily by sufficient lapping or mechanical joint.

4.2.4.3 Connection design

In addition to the single line bolt-group studied by Alashker et al. (2010) (see Figure 4.2a), the present study extends the investigation to stronger fin plate configuration that utilizes double line bolt-group (see Figure 4.2b). In order to avoid brittle weld failure at the stronger double line connection, larger fillet weld and thicker plate are specified to enable the connection to fail in ductile mode, i.e. tear-out bearing of the beam. To do this,

greater amount of fitting and bolt material is needed but the material cost is small compared with cost of workmanship (BCSA, 2002). The connection design can have significant influence on the progressive collapse resistance of composite floor system. As shown in Figure 4.10, an increase of bolt number in the connection can significantly improve the ultimate capacity and energy-absorbing capacity of the floor system in the small-deformation response. The contribution of stronger connection to ultimate capacity and energy-absorbing capacity of the floor system is summarized in Table 4.4. It is evident that stronger connection has greater contribution to the energy-absorbing capacity than the ultimate capacity of the floor system. When two additional bolts are used in the connection, the ultimate capacity and energy-absorbing capacity of the floor system are found to increase by 13% and 27%, respectively. If stronger connection with two lines of bolts is used, i.e. 5x2 bolt group, the ultimate capacity and energy-absorbing capacity of the floor system are found to increase by 50% and 63%, respectively.

Comparing the effectiveness of single and double line bolt-group design, significant increase of initial stiffness and ultimate strength in the small deformation response is observed in the latter. This is desirable as it increases the energy-absorbing capacity in small deformation response, and subsequently leads to smaller deformation in the event of sudden column removal. As a result, a lower risk of disproportionate collapse is expected. However, the strength of the shear connection has less contribution to the large-deformation response of the floor system. This behavior is the direct opposite of the contribution of steel deck and slab reinforcement on the collapse resistance of floor system as discussed previously. Therefore, strong and ductile shear connection complemented with sufficient slab reinforcement and effective deck continuity can be an effective strategy for robustness design of composite floor system.

4.3 Collapse resistance of composite floor due to perimeter column removal

This section focuses on the collapse resistance of large and realistic composite floor system subjected to perimeter column removal. The structure used in the study is a

single-storey composite floor system studied experimentally by Tan and Astaneh-Asl (2003) at University of California, Berkeley. The experiment studies the effectiveness of prestressed cable to improve the collapse resistance of composite floor system when subjected to removal of its perimeter column. This column removal case is one of the critical cases recommended by current codified methods for robustness design of building structures (GSA, 2003; DoD, 2009). This structure is also studied numerically by Yu et al. (2010) using detailed FEA by LS-DYNA (Hallquist, 2006) as discussed in literature review of chapter 1.

4.3.1 Single-storey test floor at UC Berkeley

The specimen is a single-storey steel-concrete composite floor system as shown in Figure 4.11. The specimen consists of 20 feet (6.1 m) wide and 60 feet (18.3 m) long dimensions on plan view. The height of the floor is 1.9 m above the laboratory floor level. The floor consists of typical primary beams of W18 x 35, secondary beams of W21 x 44 and columns of W14 x 61. The steel frames consist of ASTM A36 material with yield strength $f_y = 248$ N/mm^2. Fin plate shear connections are used for all beam-beam and beam-column connections. The connections of east and west beams have geometry similar to the 3x1 connection shown in Figure 4.2a. The fin plate thickness is 9 mm, the gap between beam and column face is 12.7 mm, and the bolt edge distance (along the beam direction) is 35 mm. The connections of secondary beams (spanning north-south direction) are similar to the 5x1 connection shown in Figure 4.2b. The fin plate thickness is 8 mm, the gap between beam and column face is 12.7 mm, and the bolt edge distance (along the beam direction) is 50.8 mm to allow for horizontal slotted holes of 24 mm long.

The floor slab consists of 89 mm concrete topping over steel deck with total thickness of 165 mm. The concrete material has cylindrical strength of 27.6 N/mm^2 at the 21st day. The slab is reinforced with ASM A82 6x6 W1.4x1.4 welded wire mesh that rests above the steel deck. The steel deck consists of 0.9 mm thick Verco structural steel decking type W3 Formlok with yield strength of 262 N/mm^2. Composite action between slabs and beams are enforced by shear studs that are embedded in the concrete slab and welded to

the steel beams. The shear studs are 19 mm in diameter and 114 mm in length. In the experimental study, high strength cables are attached to steel beams to improve the progressive collapse resistance through catenary action. The cables consist of 19 mm diameter ASTM A586 zinc-coated helical steel wire structural strands. The strand has an approximate gross cross-sectional area of 218 mm^2, minimum breaking stress of 1520 N/mm^2, allowable stress of 507 N/mm^2, and elastic modulus of 165 kN/mm^2.

The experiment (Tan and Astaneh-Asl, 2003) aims to investigate the resistance of floor system against progressive collapse in the event of column removal due to, for example bomb explosion. For practicality of experiment, no explosives are used to physically destroy the column. Instead, the central column at grid C/2 (referred as the "drop column") is constructed to terminate 914 mm above the laboratory floor. Hydraulic actuators are attached to the drop column to impose downward force, to simulate "sudden" column removal. The displacement-control loading is imposed by the actuators at a rate of 6 mm per second. Displacement is measured as the downward vertical displacement of the drop column with respect to the original horizontal position of the beams. The experimental work is divided into three tests. The first test aims to investigate the progressive collapse resistance of composite floor system with fin plate connection. For the test, new fin plate connections were installed to replace previously tested single-angle seated shear connections. Cable retrofit is not used in test 1. The drop column is displaced to a maximum of 560 mm. Significant damage occurs at the east beam fin plate connection. Visual inspection shows that the weld on the fin plate has fractured prematurely due to welding imperfection. The specimen is propped back to the original position at the end of test 1. For test 2, the damaged connection is replaced and the primary beams along gridline 2 are retrofitted with 2 numbers of 19 mm diameter high-strength steel cables. The similar loading protocol is used to displace the column drop to a maximum of 560 mm. During test 2, the most significant damage observed is the fracture of the edge distance of the fin plate bolt holes at west of column C2. The specimen is propped back to the original position at the end of test 2. For test 3, the specimen is unaltered from the previous test. The objective of test 3 is to displace the drop column to the limit of the specimen set-up, i.e. 810 mm. During the test, significant

damage is also observed at the edge distance fracture of the fin plate bolt holes. At the end of the test, all remaining bolt holes at the connection have fractured.

4.3.2 Numerical model

In the present work, a numerical model as shown in Figure 4.12 is developed by using the ePCA method proposed in chapter 2 of this thesis. Fin plate connection is modeled using plastic zone element as discussed in section 2.4 of chapter 2. The critical failure mode of bolt-row is governed by ductile tear-out of fin plate (bearing at bolt holes). Therefore, the yield and ultimate resistance of each bolt-row can be determined from AISC360-05 with resistance factor of 1.0. An equivalent plastic zone element is developed for the connection based on the method discussed in section 2.4.2 by taking the plastic zone length L_p equal to the length of fin plate (i.e. 100 mm) and the area A_i of the ith fiber representing the jth bolt-row as 1000 mm^2. To model the slotted connection in the secondary beams, the force-displacement relationship for the bolt-row shown in Figure 2.18a needs to be modified. In the present work, the force-displacement curve in both tension and compression is shifted by a distance equal to the length of slotted connection, i.e. 24 mm. As a result, the connection has negligible rotational and axial stiffness when displacement of the bolt-row is less than 24 mm. The composite slab is modeled using the modified grillage method as discussed in section 2.3 of chapter 2. The spacing of grillage is about 680 mm in both orthogonal directions. The equivalent T-section grillage in deck direction is determined from equation (2.11) to (2.14) based on the deck geometry of $s = 304.8$ mm , $b_1 = 190.5$ mm, and $b_2 = 114.3$ mm. Stiffness of the compression-only spring k_s is determined as 2.213 x10^6 N/mm by taking h_c equal to the concrete topping, i.e. 89 mm in equation (2.19).

Beams, columns and slabs are modeled using frame elements at their respective centroid. Due to the difference in depth, rigid link constraint is used to enforce full composite action between the beam and slab. Therefore, the friction-slip behavior between composite slab and steel beam is not considered. The assumption is reasonable for progressive collapse analysis involving column removal because localized behavior has

insignificant influence on the global load-displacement response. However, for specific application when friction-slip behavior needs to be considered, nonlinear link element should be used instead. The cables are modeled as truss elements connected directly at mid-height of the steel beam. The cables contribute to tensile catenary action of the floor system as vertical displacement increases while shear connection gradually loses strength. The numerical model consists of only 1990 frame elements, which is significantly lower than the elements required if detailed FEA is used as shown in previous numerical example (i.e. see section 4.2). As a result, each nonlinear static analysis requires only 15 to 25 minutes to be performed on a normal personal computer (i.e. Intel core 2 Quad CPU with 3.00 GHz and 3GB of RAM).

4.3.3 Verification study

The relationship between column drop load and vertical displacement for test 1 is shown in Figure 4.13a. When subjected to column drop load, the floor system deforms downward almost linearly in the initial stage. Gradual softening occurs as the connection goes into inelastic response. The floor system continues to exhibit increase of load-carrying capacity albeit with increasing damage to connection due to the influence of tensile catenary action. Out-of-balance force in the slab due to catenary action is resisted by the membrane action. From Figure 4.13a, it is evident that the global load-displacement relationships predicted by ePCA, detailed FEA and experimental findings agree well in terms of initial stiffness and energy-absorbing capacity from initial loading up to vertical displacement of 274 mm. At the displacement of 274 mm, premature connection failure is observed in the experiment. This results in sudden drop of load carrying capacity of the floor system. Experimental observation shows the unexpected connection failure is caused by imperfect welding (Tan and Astaneh-Asl, 2003).

For tests 2 and 3, the relationships between the column drop load and vertical displacement are shown in Figure 4.13b. In the experiment, damaged connection has been replaced and steel beams along gridline 2 have been retrofitted with 2 numbers of 19 mm diameter steel cables. It can be seen that the cable retrofit improves large-deformation

capacity of the floor system quite substantially. Based on results from the present method, the drop column load corresponding to displacement of 500mm is about 19% greater in test 2 than test 1. Nevertheless, it is also evident from Figure 4.13b that the inelastic capacity of test 3 is marginally lower than test 2. This is because the specimen used in test 3 has been partially damaged during test 2. The general trend of load-displacement relationship predicted by the present method agrees well with experimental results for both test 2 and test 3. As compared to the experimental finding for test 2, the present method tends to underestimate the inelastic capacity and energy-absorbing capacity of floor system. The energy-absorbing capacity at displacement of 500 mm is 41.5 kN-m (-7%) as compared to 44.5 kN-m based on the experimental finding. The underestimation can be caused by omission of torsional strength of slab, omission of tensile strength of concrete material and difference in material properties used in the numerical study. However, this small underestimation is favorable for design purpose as it tends to produce slightly conservative evaluation of robustness performance.

4.3.4 Influence of shear connection on collapse resistance

Section 4.2 shows that stronger shear connection can improve the progressive collapse resistance of the NIST floor (Liang et al., 2008) in the event of internal column removal. In this section, the influence shear connection on progressive collapse resistance when subjected to removal of perimeter column is studied. Uniform floor loading instead of column drop load is imposed on the numerical model of floor structure (Tan and Astaneh-Asl, 2003) to study the structural response due to static and "sudden" removal of the perimeter column. For the east and west beams, a stronger 5x1 type fin plate connection is considered in addition to the original 3x1 type connection. For static case, the load-displacement relationships of the floor system for two types of connections are shown in Figure 4.14a. It can be seen that the two additional bolts in 5x1 connection improves the initial stiffness, inelastic capacity and energy-absorbing capacity of the floor system substantially. Ultimate capacity of the floor system with the original 3x1 connection has a ultimate load capacity of about 600 kN at a vertical displacement of about 250 mm. When stronger connections are used for the east and west beams, the

load capacity at the same displacement is improved by about 21%. The energy-absorbing capacity at this displacement is also found to be improved by about 24% when stronger connection is used.

The improvement of energy-absorption capacity is beneficial in reducing the dynamic displacement demand when sudden column removal is considered. The procedures adopted in the study to simulate sudden column removal are discussed in section 3.3.3.2 of chapter 3. In the dynamic analysis, floor load equal to 6 kN/m^2 is assumed to represent the mass carried by the floor system during accidental limit state. The displacement time-history at the position of column removal is shown in Figure 4.14b. It can be shown that the floor deforms downward almost immediately after column C2 is suddenly removed. The maximum displacement of the floor adopting original 3x1 connection is found to be about 200 mm. The displacement is reduced by as much as 60% when stronger 5x1 connection is used. This finding shows that vertical progressive collapse resistance can be improved substantially by slightly increasing connection strength.

4.4 Concluding remarks

1. The ePCA method as proposed in chapter 2 is used to study progressive collapse resistance of large and realistic composite floor system. Two critical cases, i.e. internal and perimeter column removal are studied. Comparison with experimental and numerical results from the literature shows reasonable accuracy of ePCA for performance evaluation of large and realistic floor system. The present study shows that membrane action of floor slab plays an important role in collapse resistance in two ways, i.e. (a) it enhances load-carrying capacity of floor system by catenary action, and (b) it resists the out-of-balance force of catenary action in slab and restrains the column from being pulled inward.

2. The use of ePCA instead of detailed FEA can significantly reduce the computation time and pre/post-processing effort. For the study of NIST floor system, the model based on ePCA method consists of only 996 frame elements compared to 295,000

solid and shell elements used in detailed FEA by Sadek et al. (2008) and Alashker et al. (2010). Based on a conservative estimate, the use of ePCA instead of detailed FEA can save computational time by as much as 22,000 times.

3. The use of plastic zone method to model material damage of the grillage member eliminates the need for sophisticated material constitutive model and the assumption of axial load-moment interaction relationship. Therefore a realistic, fast yet simple numerical model is useful to reduce over-conservatism in the design practice.

4. The collapse resistance can be improved by thicker steel deck, more slab reinforcement and stronger connection. When a floor system is subjected to column removal, the study shows that stronger connection improves initial stiffness and inelastic capacity in small-deformation response, while the slab reinforcement and steel deck improves the inelastic capacity in large-deformation response. Therefore, strong and ductile shear connection together with sufficient slab reinforcement and effective deck continuity can be a cost effective strategy for enhancing the robustness of composite floor system. When designing shear connection, brittle failure modes e.g. shear failure of bolts, should be avoided to ensure sufficient ductility and post-ultimate resistance in the inelastic response.

Table 4.1: Collapse resistance of NIST floor due to internal column removal for varying deck thicknesses, slab reinforcement densities and connection designs: Comparison between detailed FEA by Alashker et al. (2010) and the presented method

No.	Deck thickness (mm)	Slab rebar (mm²/m)	Connect -ion	Ultimate capacity (kN)		Absorbed strain energy at d = 1.1m (kN-m)	
				Detailed FEA	Presented ePCA	Detailed FEA	Presented ePCA
*1	0.90	60	3x1	1099	1113 (1.01)	890	896 (1.01)
2	0.45	60	3x1	891	743 (0.83)	748	668 (0.89)
3	1.80	60	3x1	1504	1526 (1.01)	1114	1190 (1.07)
4	0.90	0	3x1	958	1022 (1.07)	822	780 (0.95)
5	0.90	120	3x1	1198	1260 (1.05)	936	995 (1.06)
6	0.90	60	4x1	1205	1151 (0.96)	1039	1001 (0.96)
7	0.90	60	5x1	1282	1260 (0.98)	1111	1134 (1.02)

Note: * control specimen

( ) ratio of capacity predicted by ePCA to capacity predicted by detailed FEA

Table 4.2: Contribution of steel deck to collapse resistance of NIST floor

Deck thickness (mm)	Ultimate capacity (kN)		Absorbed strain energy at d = 1.1m (kN-m)	
0	460	(0.41)	435	(0.49)
0.45	743	(0.67)	668	(0.75)
*0.90	1113	(1.00)	896	(1.00)
1.80	1526	(1.37)	1190	(1.33)

Note: * control specimen

( ) capacity normalized to control specimen

Table 4.3: Contribution of slab reinforcement to collapse resistance of NIST floor

Density (mm^2/m)	Ultimate capacity (kN)		Absorbed strain energy at d = 1.1m (kN-m)	
0	1022	(0.92)	780	(0.87)
*60	1113	(1.00)	896	(1.00)
120	1260	(1.13)	995	(1.11)

Note: * control specimen

( ) capacity normalized to control specimen

Table 4.4: Contribution of connection to collapse resistance of NIST floor

Connection	Ultimate capacity (kN)		Absorbed strain energy at d = 1.1m (kN-m)	
*3x1	1113	(1.00)	896	(1.00)
4x1	1150	(1.03)	1001	(1.12)
5x1	1260	(1.13)	1134	(1.27)
3x2	1306	(1.17)	1106	(1.23)
4x2	1433	(1.29)	1325	(1.48)
5x2	1667	(1.50)	1463	(1.63)

Note: * control specimen

( ) capacity normalized to control specimen
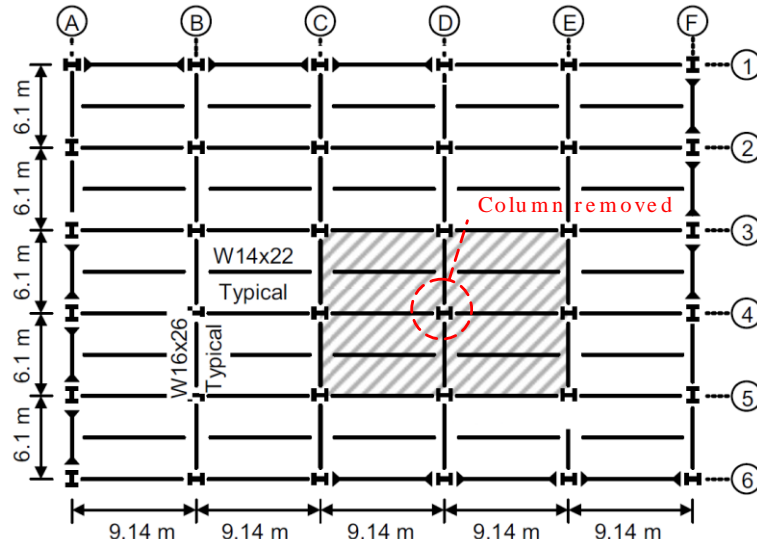
Figure 4.1: Floor layout of the NIST prototype building, area of floor system studied (hatched) and location of internal column removal

3x1 A325 Φ22 bolts   4x1 A325 Φ22 bolts   5x1 A325 Φ22 bolts

(a) Single line of bolted connection (A325 22.2mm diameter bolts in 24mm clearance hole)

3x2 A325 Φ22 bolts   4x2 A325 Φ22 bolts   5x2 A325 Φ22 bolts

(b) Double line of bolted connection (A325 22.2mm diameter bolts in 24mm clearance hole)
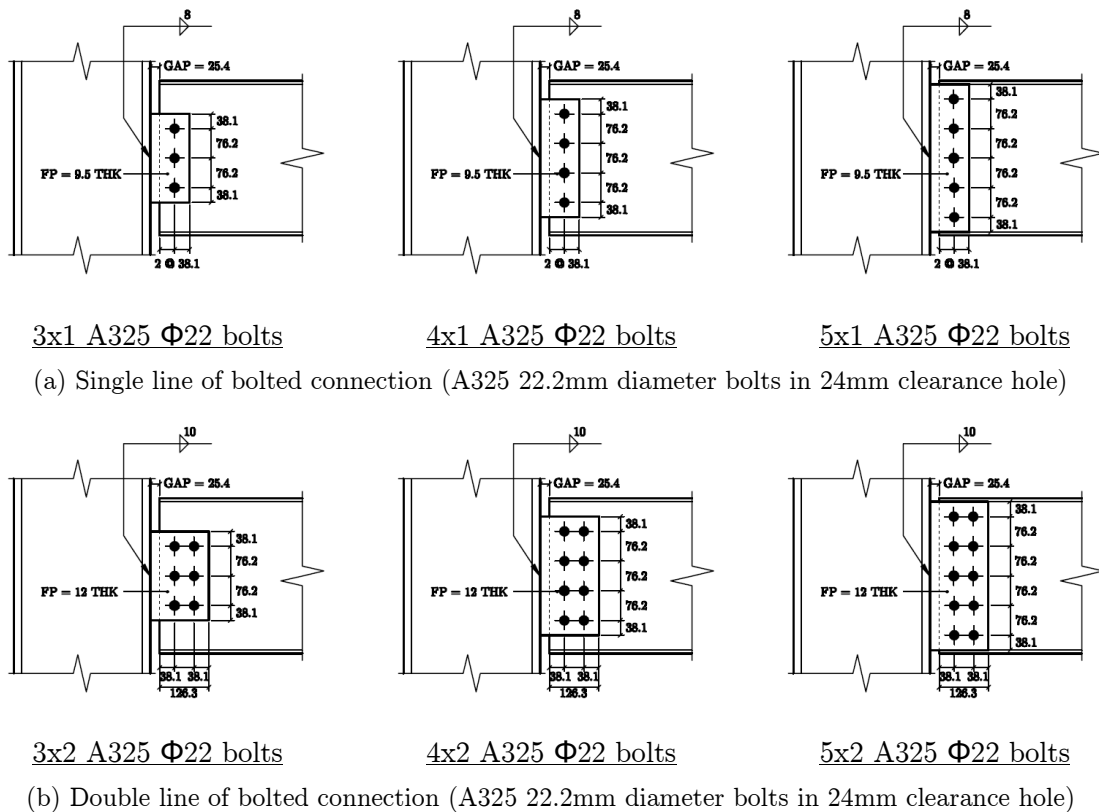
Figure 4.2: Various fin plate connections considered in the study of NIST floor system
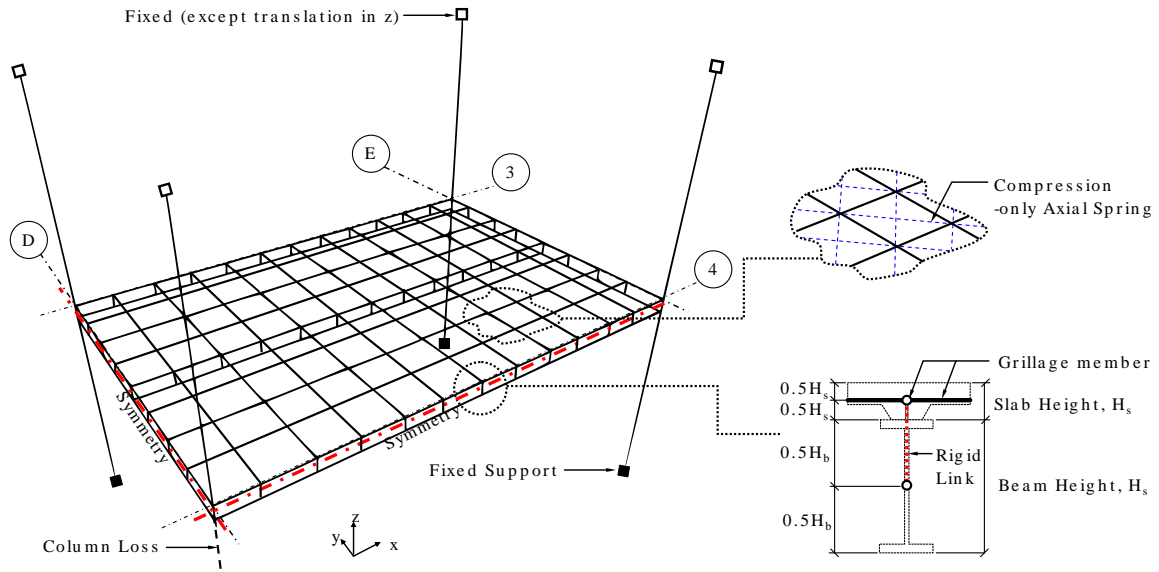
Figure 4.3: Numerical model of NIST floor system used in the study
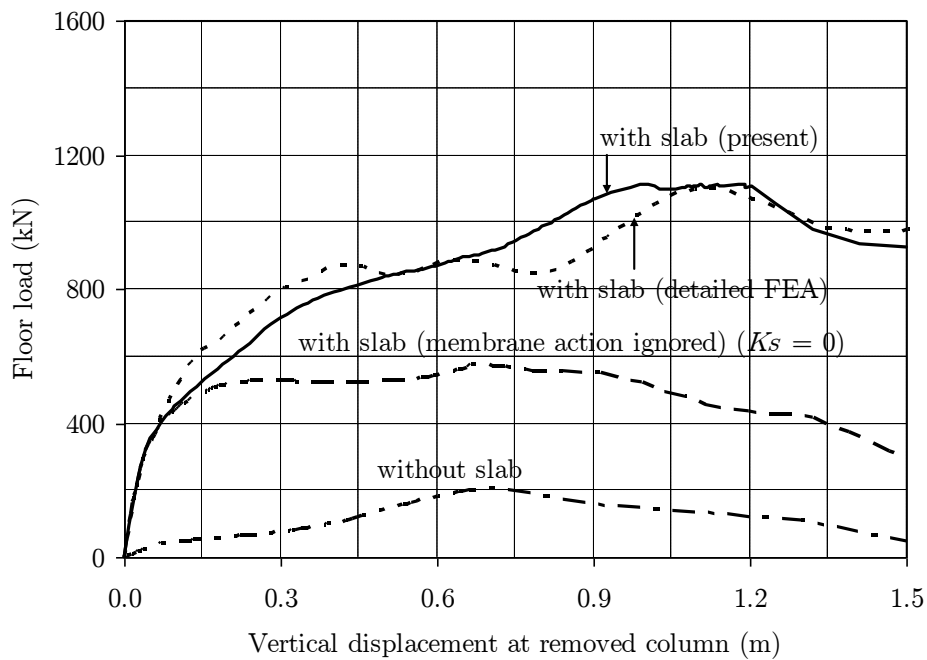
Note: bolt-group = 3x1, slab reinforcement = 60mm^2/m, deck thickness = 0.9 mm

Figure 4.4: Collapse resistance of NIST floor due to internal column removal for various methods of slab modeling: Comparison between the presented method and detailed FEA by Alashker et al. (2010)

135
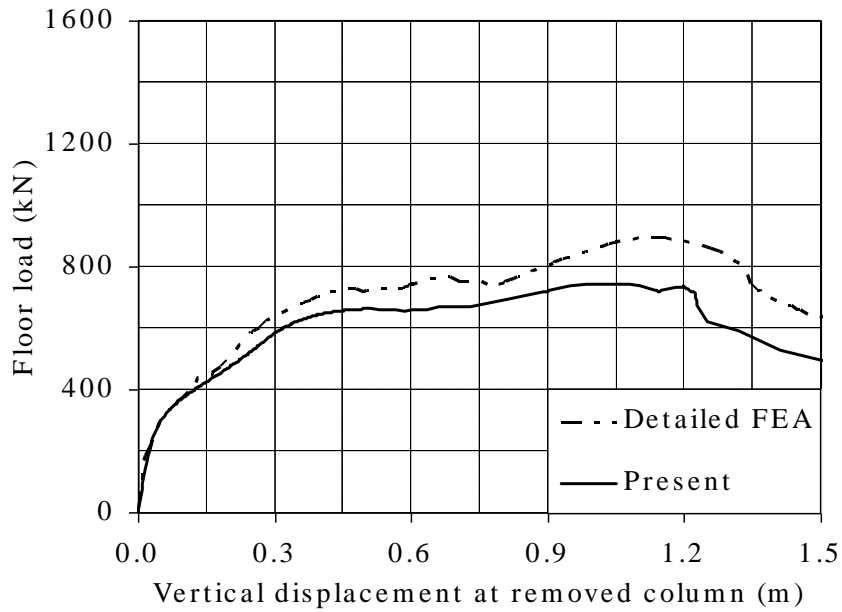
(a) Deck thickness = 0.45 mm (bolt-group = 3x1, slab reinforcement = 60mm^2/m)
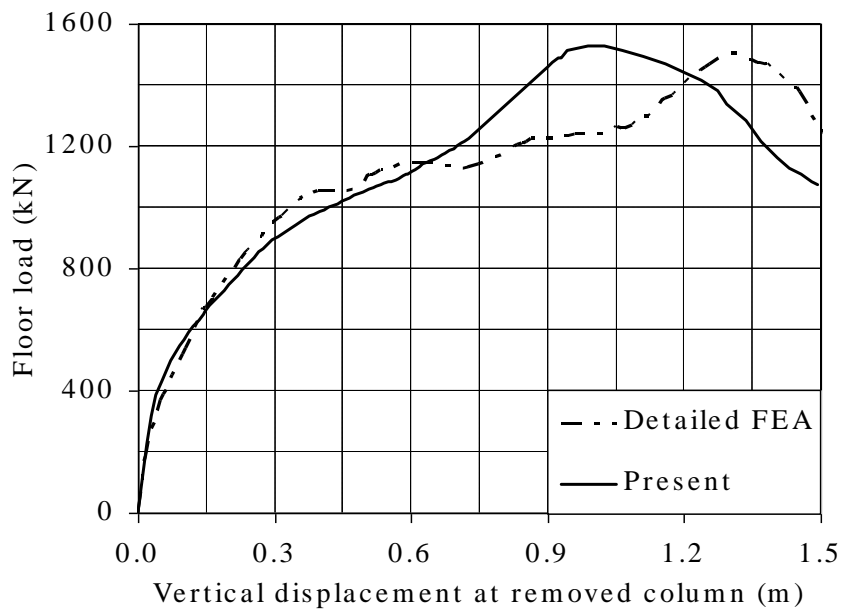
(b) Deck thickness = 1.8 mm (bolt-group = 3x1, slab reinforcement = 60mm^2/m)

Figure 4.5: Collapse resistance of NIST floor due to internal column removal for various deck thicknesses: Comparison between the presented method and detailed FEA by Alashker et al. (2010)
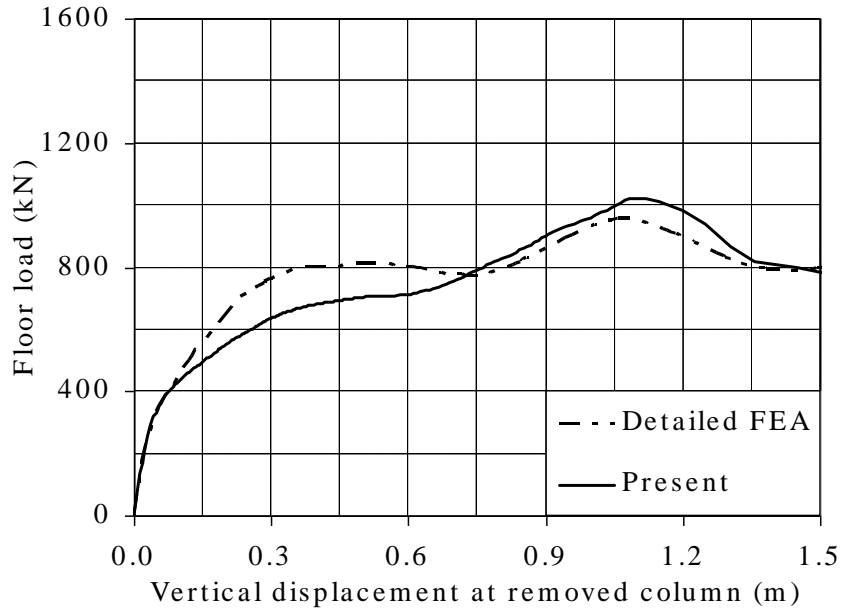
(a) No slab reinforcement (bolt-group = 3x1, deck thickness = 0.9mm)
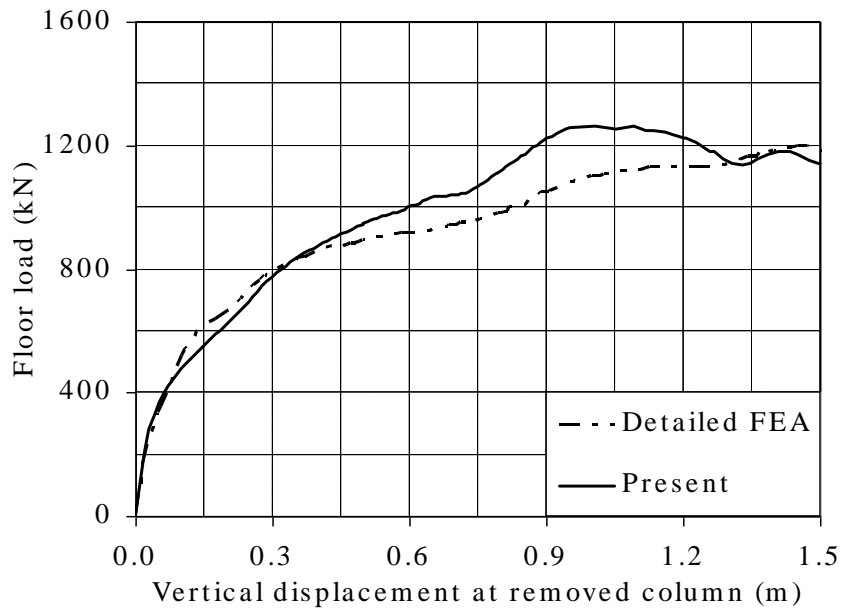
(b) Slab reinforcement density = 120 mm^2/m (bolt-group = 3x1, deck thickness = 0.9mm)

Figure 4.6: Collapse resistance of NIST floor due to internal column removal for various slab reinforcement densities: Comparison between the presented method and detailed FEA by Alashker et al. (2010)

137
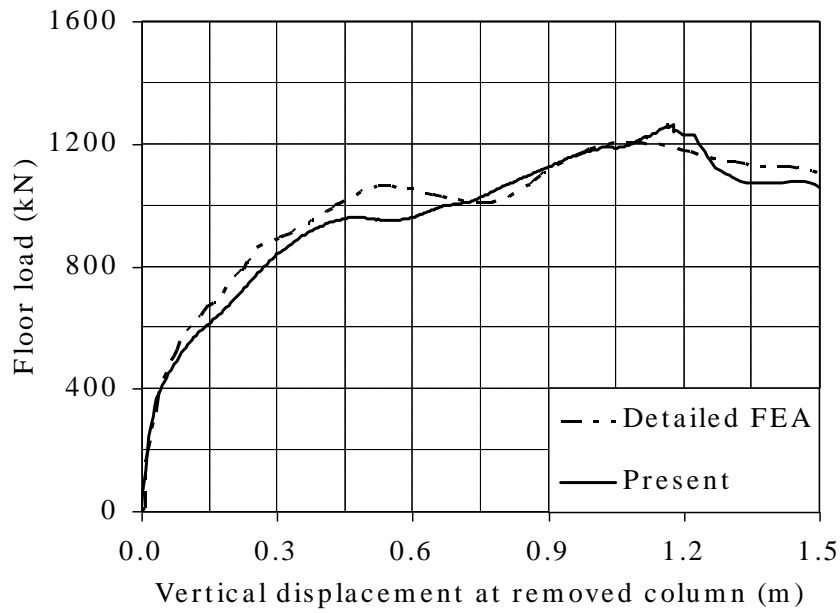
(a) fin plate with 4x1 bolt-group (deck thickness = 0.9mm, slab reinforcement = 60mm^2/m)
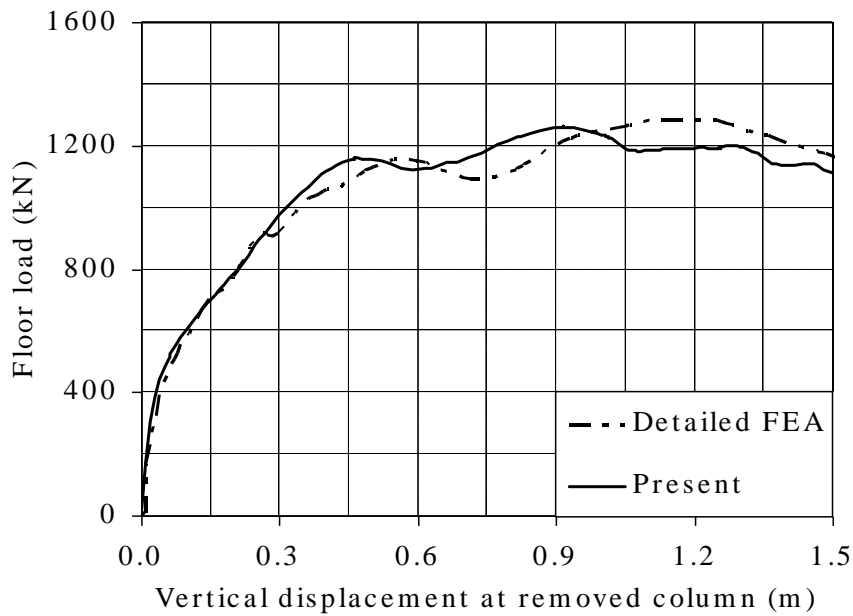
(b) fin plate with 5x1 bolt-group (deck thickness = 0.9mm, slab reinforcement = 60mm^2/m)

Figure 4.7: Collapse resistance of NIST floor due to internal column removal for various connection designs: Comparison between the presented method and detailed FEA by Alashker et al. (2010)
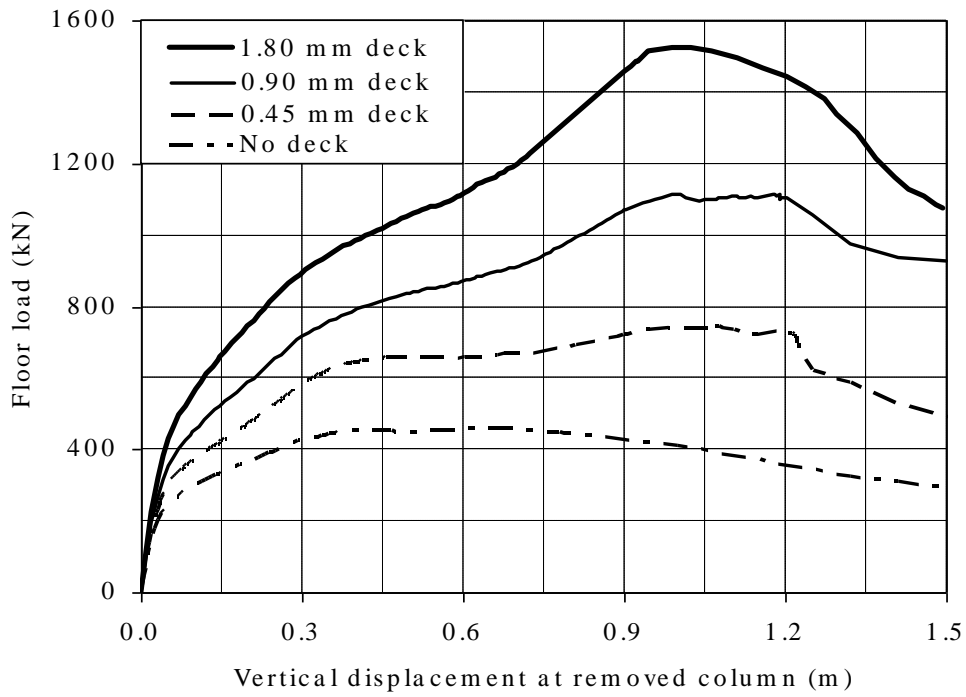
Figure 4.8: Influence of deck thickness on collapse resistance of NIST floor
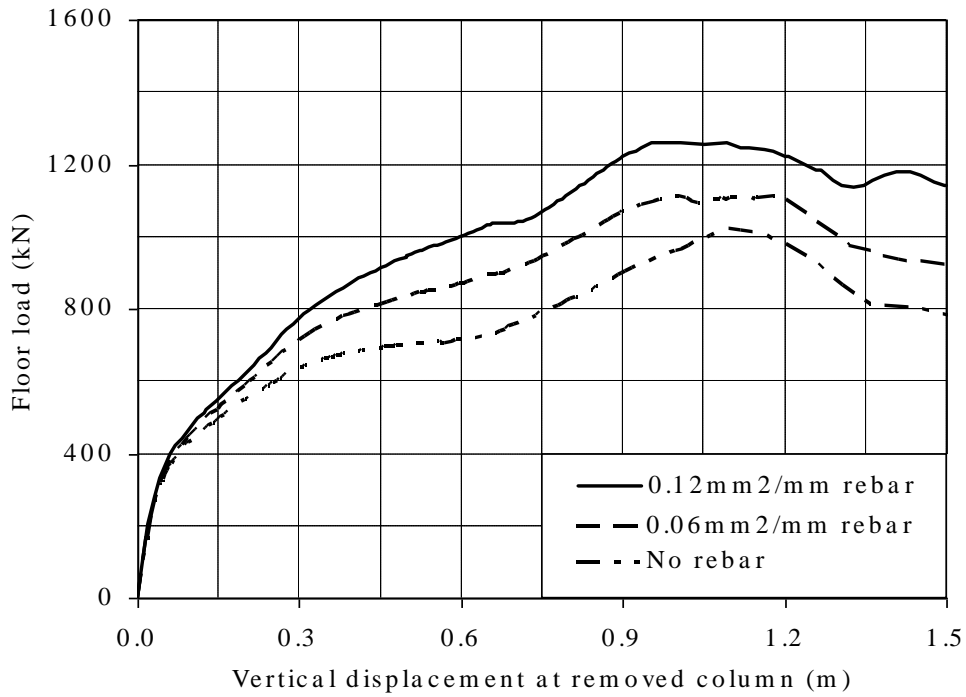
Figure 4.9: Influence of reinforcement density on collapse resistance of NIST floor
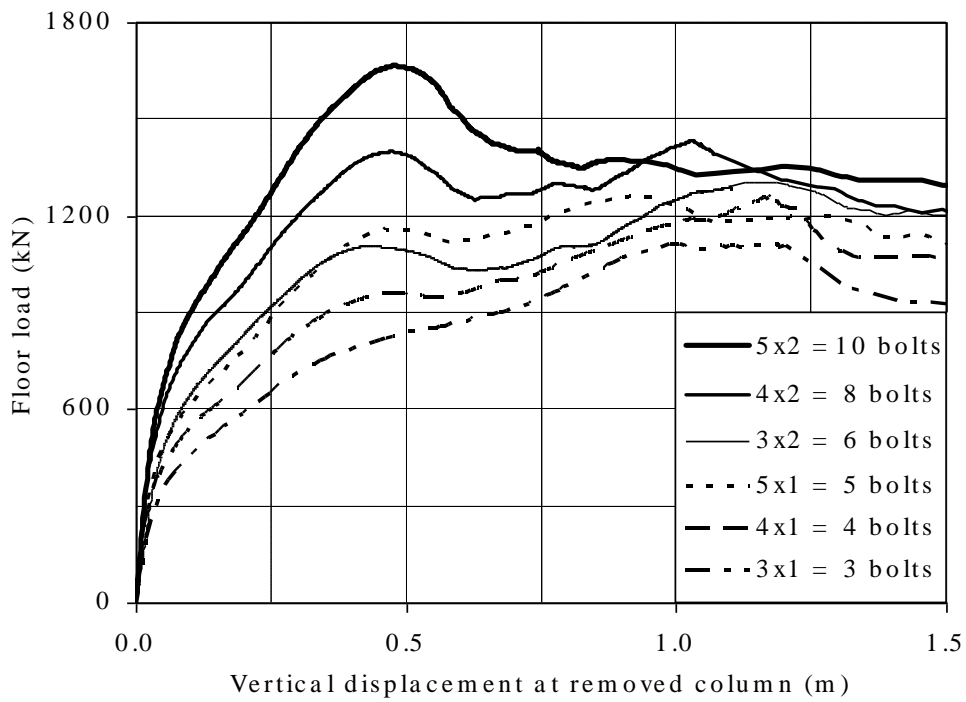
(a) single line and double line bolt-groups
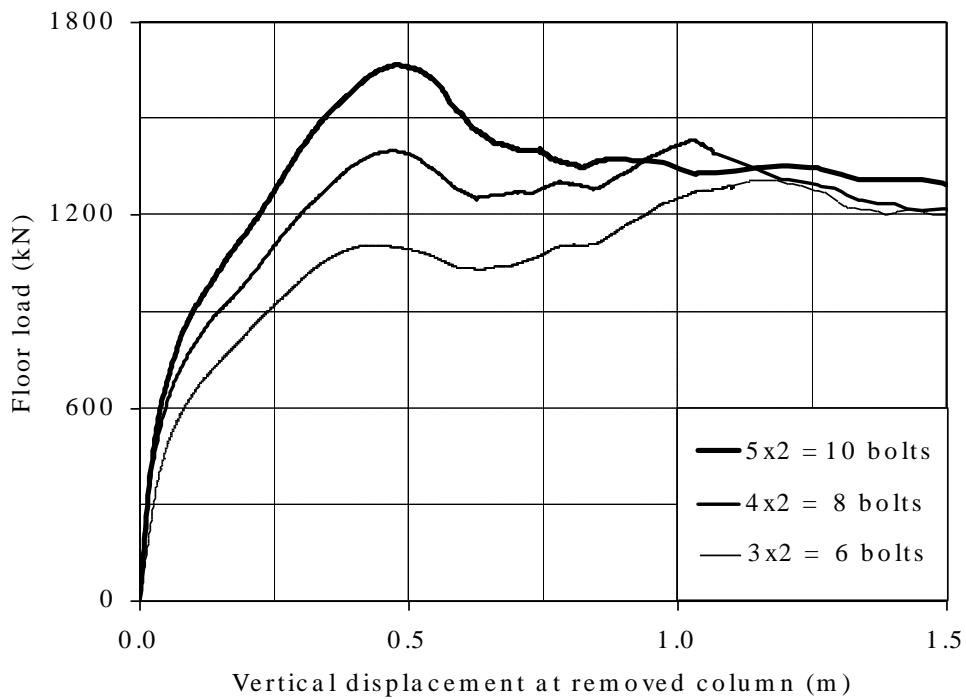
(b) double line bolt-groups

Figure 4.10: Influence of connection design on collapse resistance of NIST floor

140
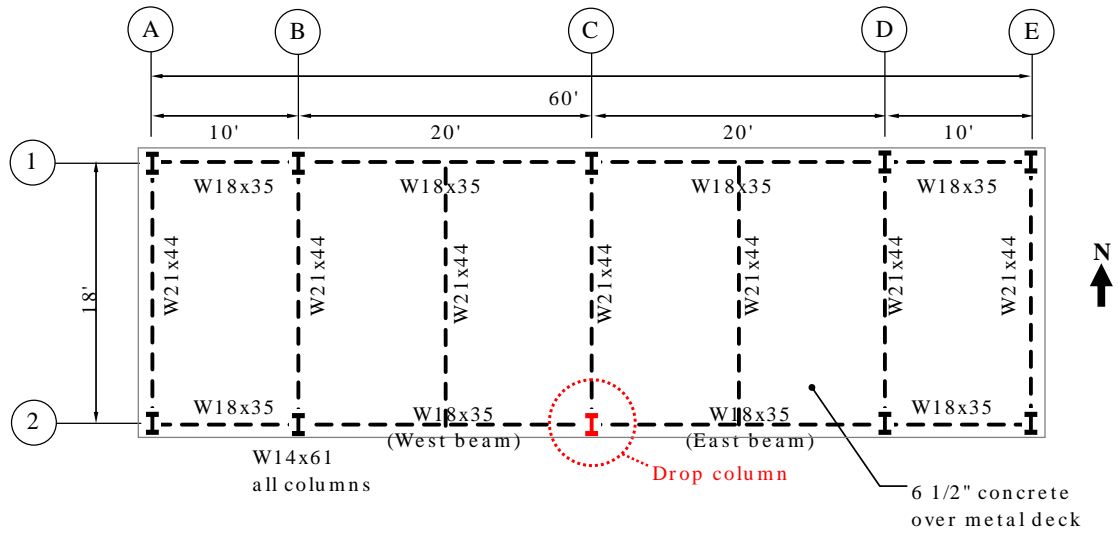
Figure 4.11: Layout of the UCB floor and location of perimeter column removal
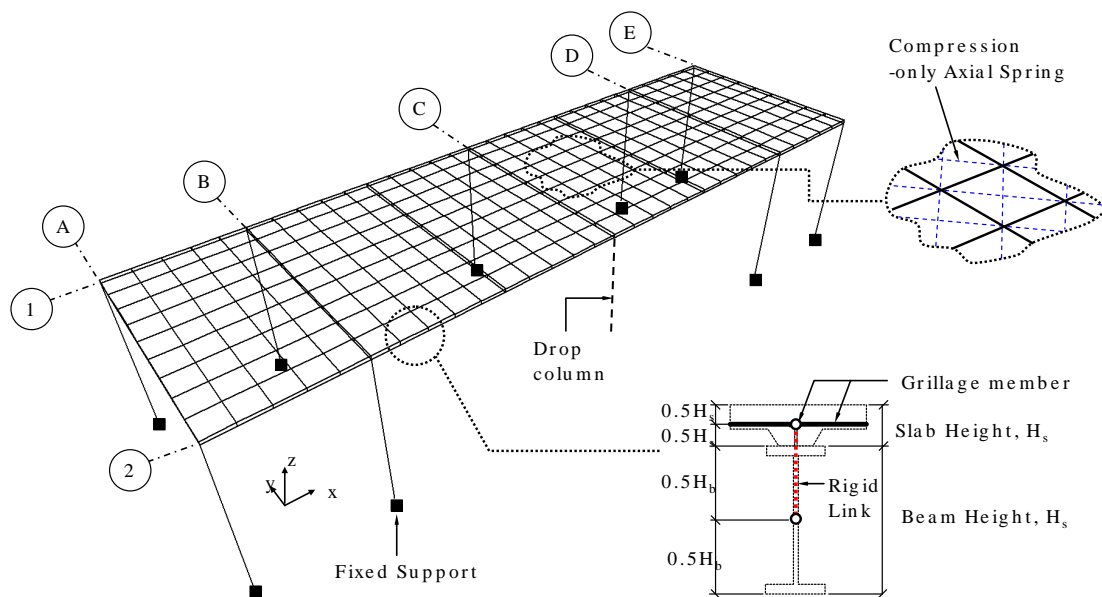
Figure 4.12: Numerical model of UCB test floor system used in the study
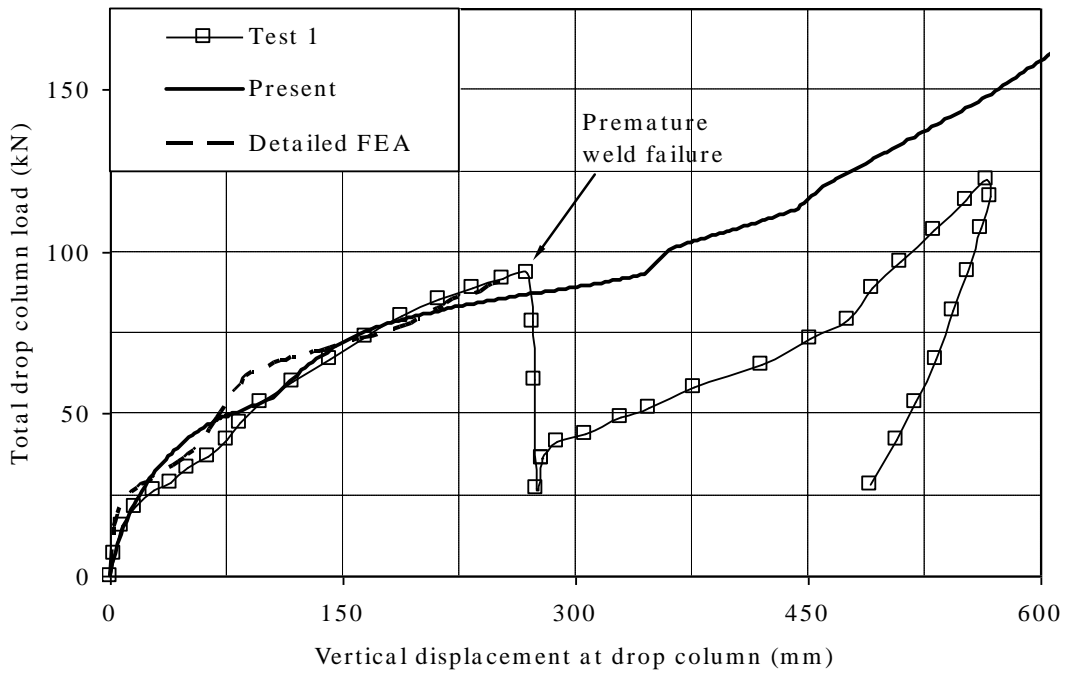
(a) Column drop load verses vertical displacement for Test 1 (without cable)
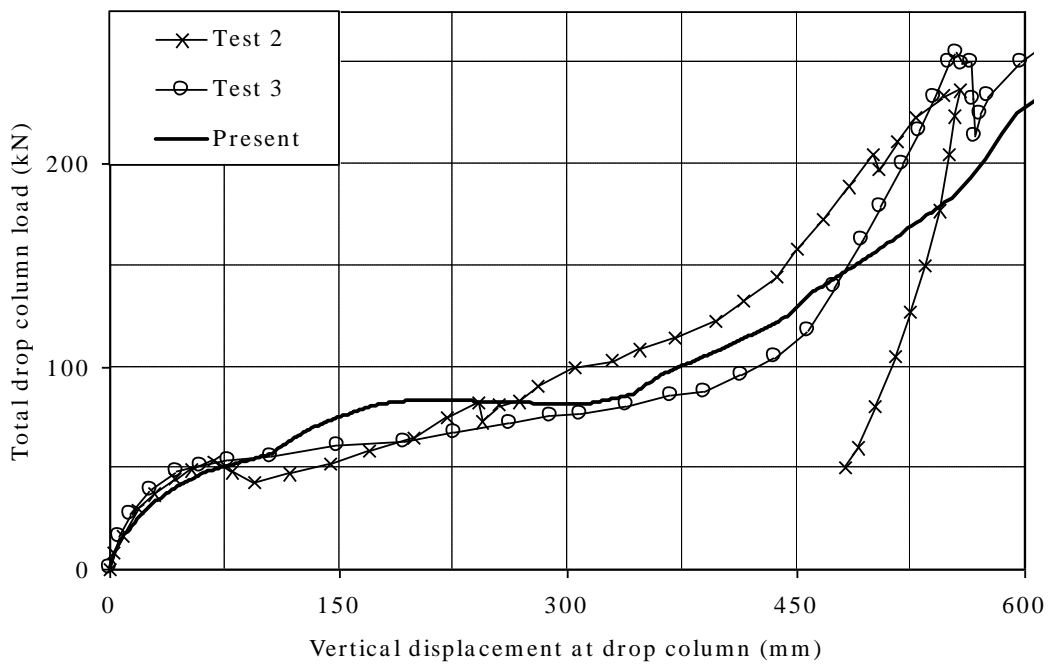
(b) Column drop load verses vertical displacement for Test 2 and 3 (with cable)

Figure 4.13: Collapse resistance of UCB test floor due to perimeter column removal: Comparison between the presented method, detailed FEA by Yu et al. (2010) and experiment by Tan and Astaneh-asl (2003)

142
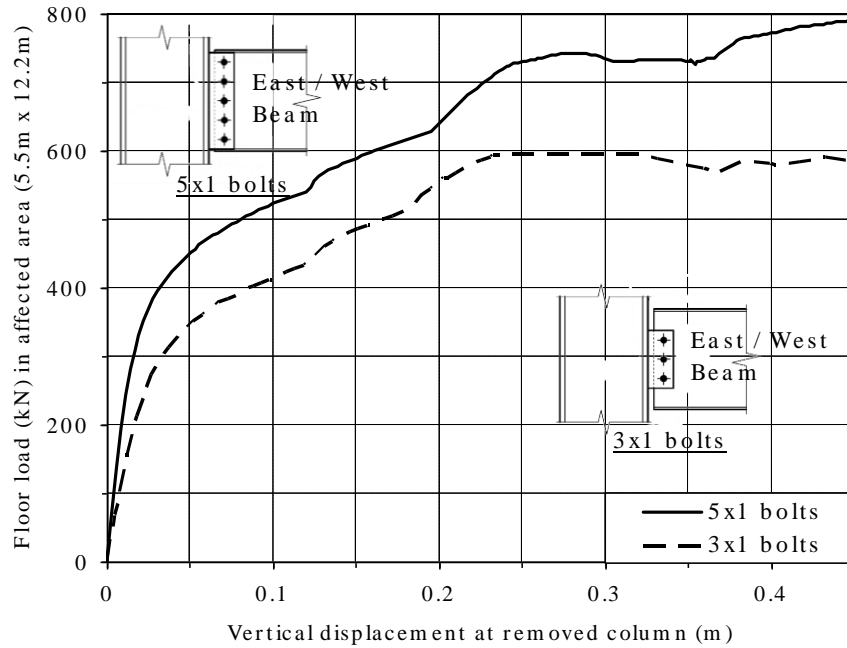
(a) total floor load (affected area of 5.5 m x 12.2 m) applied statically versus column drop displacement
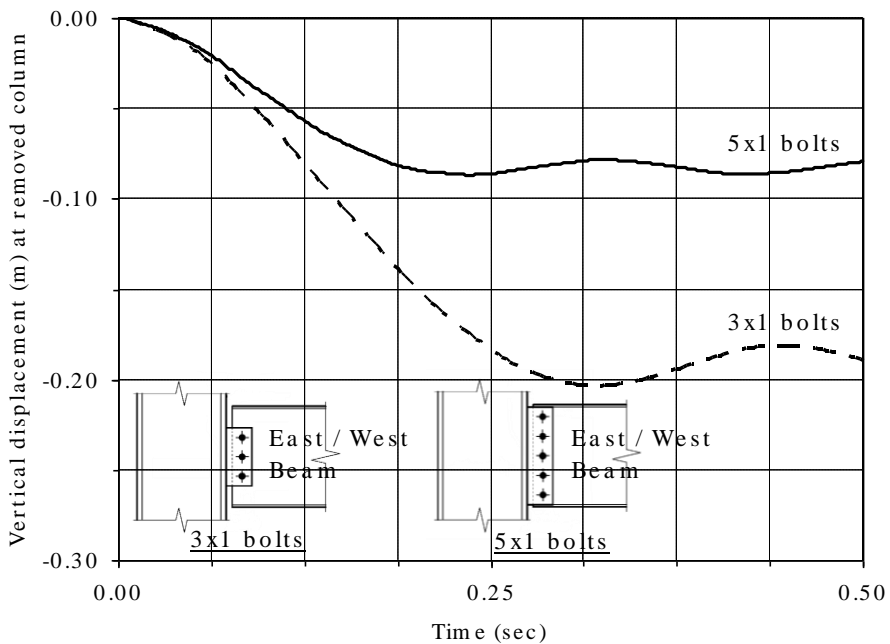
(b) displacement time-history at removed column due to sudden removal (floor mass assumed to be 6 kN/m^2)

Figure 4.14: Influence of the connection design on static and dynamic collapse resistances of UCB test floor

143

Chapter 5: Robustness Enhancement of Composite Building with Belt-Truss System

5.1 Introduction

The tragic collapse of WTC towers on September 11, 2001 initiated a new wave of discussion on robustness of building structures to unforeseen hazards not explicitly considered in design codes, such as terrorist attacks. Many regarded the collapse as proportionate to the cause, and total collapse was unavoidable by any sensible engineering practice given the severity of damage caused by plane collision. Post-collapse investigation conducted by the NIST (2005) suggested that the exceptional robustness is largely contributed by the "hat trusses", the name given to truss system positioned at roof top. If not for the multi-storey fire arising from impact of commercial planes, the towers could have survived or stood longer than the actual one hour after the plane collision. The superior redundancy provided by the hat trusses were believed to facilitate redistribution of forces away from the damaged area, and provide alternative load path to the severely damaged towers. Other than these studies, research on structural robustness and collapse characteristics of buildings incorporating truss systems still remains limited in the open literature. Therefore, there is a pressing need to investigate the potential of truss system as robustness enhancement of multi-storey buildings.

This chapter investigates the effectiveness of belt truss system for robustness enhancement of multi-storey buildings. The 8-storey steel-concrete composite building located in Cardington, UK is used as an example for illustration. The building was designed and constructed according to BS5950 (BSI, 2000). Therefore the study presented in this chapter can provide an insight into the robustness performance of local buildings (in Singapore˙ which comply with the same code of practice. The study focuses on the influence of (1) truss configuration, (2) brace strength, (3) brace slenderness, and (4) truss position on the dynamic force and displacement demands during sudden column removal event. This information is critical for effective and safe application of belt truss system as robustness enhancement of multi-storey composite building.

5.2 Numerical modeling of Cardington building

The 8-storey composite building shown in Figure 5.1 is an actual building constructed in Cardington facility in the UK for fire experiment. This building shares many similarities in design concept with local buildings due to the adoption of British Standards (BSI, 2000) in Singapore. All typical beams and columns are 9.0 m and 4.125 m in length. The beams comprise UB 356x171x51, while the columns comprise UC 305x305x118 for the four lowest storeys and UC 254x254x89 for the remaining storeys. Shear connections based on UK practice are adopted throughout the building (BCSA, 2002). These connections consist of fin-plate type for beam-to-beam connection and flexible-end-plate type for beam-to-column connection. The floor structure consists of composite slab of trapezoidal profile reinforced with anti-crack wire mesh A146 (T6 bars at 200 mm spacing), placed 6 mm above the steel deck. Shear studs are welded to the beam flange to allow for shear transfer between the slab and beam. Permanent load of each floor is estimated to be about 3.86 kN/m^2, whereas the design imposed load is 2.50 kN/m^2. Detailed information of Cardington building is available from the official test report (British Steel, 1998).

5.2.1 Two-dimensional frame

A two-dimensional frame (grids 1/B to 1/F) shown in Figure 5.2 is selected for parametric study in section 5.3 and 5.4. Based on the recommendation by DoD (2009), full intensity of permanent load and 50% of imposed load are considered for robustness evaluation. For a tributary width of 3 m, an equivalent frame loading of $w = 15.33$ kN/m is imposed on the beams. Actual material properties from laboratory test are not used because the emphasis is on behavioral study rather than quantitative assessment of the collapse vulnerability. Concrete and steel materials have stress-strain relationships according to standards material models discussed in chapter 2. For concrete material, the compressive strength f_c is taken as 30 N/mm^2, whereas tensile strength is ignored. For steel material, the yield strength f_y and elastic modulus E_s are taken as 275 N/mm^2 and 210 kN/mm^2 respectively.

The ribs of composite slab are oriented in the direction perpendicular to the beams. Therefore concrete within and steel deck can be ignored when modeling composite beam action. Full composite action between the concrete flange (70 mm solid slab in Figure 5.3) and steel beam is assumed by using rigid link constraint. Analysis according to Eurocode 4 (BSI, 2004b) suggests an effective width of 1575 mm for center portion of the double-span beam (4 m length from location of column removal) and 844 mm for the remaining portion. As shown in chapter 4, floor slab can provide significant restraining force for development of catenary action in beam and slab. To resemble this behavior, translational restraints are provided at the boundaries of the frame as shown as "▷" in Figure 5.2.

To model the buckling and post-buckling behavior of brace member of belt truss, maximum geometry imperfection of $e_0 = L/1000$ is introduced at mid-span of the brace member according to principal buckling mode shown in Figure 5.4. This imperfection magnitude corresponds to average value measured in the laboratory (Bjorhovde, 1972), and is therefore appropriate for performance evaluation. Modeling of the brace follows the recommendation discussed in Chapter 2, in which the plastic zone length and mesh size in the plastic zone are taken as $L/2$ and $L/24$, respectively. All braces are rigidly

connected to the steel frame. Therefore full-strength connections are considered at the member ends.

Fin-plate is the most commonly used shear connection in Singapore. Therefore fin-plate connection instead of flexible-end-plate is adopted for all beam-beam and beam-column connections in the numerical study. The geometry of the connection considered here is similar to the 3x1 connection shown in Figure 4.2a of previous chapter. In the present study, 10 mm gap and 50 mm edge distance instead of 25.4 mm and 38.1 mm are adopted to resemble local construction practice. The fin-plate connection is modeled using equivalent plastic zone element as discussed in section 2.4 of chapter 2. The critical failure mode of the bolt-row is governed by ductile tear-out of the beam web (thickness = 7.4 mm). Therefore, the yield and ultimate resistance of each bolt-row can be determined from AISC360-05 with resistance factor of 1.0. The ultimate resistance of each bolt-row is about 191 kN. Therefore, the ultimate tensile capacity of the 3x1 fin-plate connection is about 573 kN. The objective of present study is to compare the displacement and force demands of building for various designs of belt truss systems. Therefore, rotational capacities of connections are not considered in the present study. In the modeling, tensile behavior of each bolt-row is assumed to be the same as compressive behavior.

5.2.2 Three-dimensional building

For the three-dimensional building studied in section 5.5, the same approach adopted in two-dimensional frame is used to model the connection, belt truss and steel frames. Instead of using EC4 effective width concept, the composite slab is modeled directly using the slab model proposed in chapter 2. The spacing of grillage is 1 m in both orthogonal directions. The equivalent T-section grillage in deck direction is determined from equations (2.11) to (2.14) based on deck geometry of $s = 300$ mm, $b_1 = 188$ mm and $b_2 = 136$ mm. The stiffness of compression-only spring is calculated as $k_s = 1.5$ x 10^6 N/mm by taking h_c equal to concrete topping, i.e. 60 mm in equation (2.19).

The beams, columns and slabs are modeled using frame elements at their respective centroids. Due to the difference in depth, rigid link constraint is used to enforce full

147

composite action between the beam and slab. Verification study is carried out with focus on the dynamic characteristics of the floor structure to ascertain the accuracy of the proposed numerical model. The results from detailed FEA by El-Dardiry and Ji (2006) and in-situ testing by Ellis and Ji (1996) are used as the reference of comparison. The natural frequencies are compared in Table 5.4. It can be seen that the natural frequencies predicted by the proposed numerical model compare well with detailed FEA by El-Dardiry and Ji (2006) and in-situ testing by Ellis and Ji (1996). In addition, reasonable prediction of the first three model shapes is also evident from Figure 5.16.

5.3 Influence of belt truss on building robustness

Structural systems of local medium-rise and high-rise buildings commonly consist of perimeter columns and central reinforced concrete core. For robustness design, removal of concrete core is not required because the strong core is likely to survive accidental loadings like explosion and vehicular impact. For most buildings with internal columns, the probability of internal column failure is significantly lower than perimeter columns as the internal columns are protected by building envelope against external threats. Therefore, DoD (2009) allows omission of internal column removal in robustness design for building without underground parking. In view of these factors, robustness design of medium-rise and high-rise building requires avoidance of disproportionate collapse due to sudden removal of a perimeter column. This chapter investigates the potential of belt truss system as robustness enhancement of medium-rise and high-rise building. The belt truss system is installed around the building perimeter to provide alternate load path in the event of failure of any perimeter column.

The robustness performance of building is governed by two dynamic demands, namely displacement demand and force demand. Displacement demand is the key indicator of vertical progressive collapse. It refers to the deformation of a structure under extreme loading, and must be controlled to avoid fracture failure of the weakest link in a structure (typically the beam-column connection). Meanwhile, force demand is the key indicator of horizontal progressive collapse. Little attention has been given to horizontal progressive collapse as most studies focus on idealized sub-structure, rather than global

response. To explore the potential of using belt truss as robustness enhancement, factors influencing both dynamic demands need to be identified.

In the presented study, column force demand during accidental limit state (ALS) is compared to the demand under ultimate limit state (ULS) design requirement. The first limit state corresponds to column removal event, whereas the latter corresponds to the minimum requirement of column design. The ULS design forces are derived from current design code, BS5950 (BSI, 2000), hence represents the lower bound capacity of the column. Therefore, when force demand under ALS is greater than ULS, the column is deemed as vulnerable to failure. Column failure should be avoided as it can trigger horizontal progressive collapse.

5.3.1 Robustness evaluation using "alternate load path" approach

Robustness evaluation is performed according to alternate load path approach recommended by DoD (2009). According to alternate load path approach, sudden removal of column needs to be considered for robustness design of building. Then, the structure need to be checked for ability to resist both vertical and horizontal progressive collapse. Vertical progressive collapse is triggered by excessive deformation at the weakest link, e.g. beam-to-column connection. Meanwhile, horizontal progressive collapse is triggered by excessive force demand in the supporting column. The two-phase approach for simulation of sudden column removal as discussed in section 3.3.3 of chapter 3 is adopted here. In the nonlinear time-history analysis, removal of column is carried over a short period of 0.01 seconds. No damping effect is considered ($\xi = 0.001\%$ to avoid numerical instability) in the analysis as most energy-absorbing capacity is likely dominated by material yielding (Powell, 2009). A convergence study shows that time step of 0.0025 seconds can be used to analyze the structure with sufficient accuracy.

Current codes of practice for robustness design allow two types of analysis to determine the displacement and force demands for robustness evaluation, i.e. the nonlinear static and nonlinear time-history analysis (GSA, 2003; DoD, 2009). In nonlinear static analysis, loading on floor area originally supported by the removed column needs to be amplified

by a Dynamic Increase Factor (DIF). This is to consider for dynamic effects due to sudden removal of column. Although DIF can vary according to properties of structure and loading, the codes conservatively recommend a constant DIF = 2.0 for static analysis. The equivalent static loading based on amplified loading for 8-storey Cardington building frame is shown in Figure 5.5.

The present study is based on nonlinear time-history analysis which directly considers the dynamic nature of structural response when subjected to sudden column removal. This type of analysis is more accurate in evaluation of displacement and force demands compared to nonlinear static analysis, but interpretation of analysis results can be less straight forward. In the present study, DIF is used as an indication of the global force demand of the structure when subjected to column removal. DIF is back-calculated from the maximum value of total reaction force obtained from nonlinear-time history analysis using equation (5.1), assuming only mass supported by damaged bay is excited during sudden column removal, and maximum forces in all columns occur concurrently. The denominator and second term of the numerator of equation (5.1) represents static weight of the damaged bay. It is equal to half of total building static weight (which is same as total static reaction, W_S) as the loading tributary area of damaged bay is half of that of the overall building as shown in Figure 5.5.

$$DIF = \frac{W_D - 0.5W_S}{0.5W_S} \qquad (5.1)$$

where,

$W_S = $ Total static reaction in z-axis (from static analysis)

$W_D = $ Total dynamic reaction in z-axis (from nonlinear time-history analysis)

5.3.2 Factors influencing dynamic displacement and force demands

As mentioned previously, the displacement demand is the key indicator of vertical progressive collapse whereas the force demand is the key indicator of horizontal progressive collapse. Both types of progressive collapse need to be avoided in the context of robustness design. Therefore, to explore the potential of belt truss in robustness enhancement, factors influencing both of the dynamic demands need to be identified. To do this, 54 analyses involving sudden removal of perimeter column have been carried out on the two-dimensional frame as shown in Figure 5.2. These analyses consist of varying truss configurations, brace strengths and slenderness ratios, as tabulated in Table 5.1. These specimens are designed to have similar weight so that consistent comparison can be made regarding the efficiency of each specimen. The original perimeter frame weighs about 31.768 tons over an elevation area of 36 m x 33 m = 1,188 m^2, which is equivalent to 26.74 kg/m^2 of the elevation area. The brace members of belt truss system add less than 5% to the original weight.

The response histories of K-brace, X-brace and N-brace belt truss with slenderness ratio $L/r = 170$ are shown in Figure 5.6. Maximum vertical displacement occurs at the location of column removal. According to GSA (2003), the rotational capacity of partially-restrained steel joint is 2.5% radians, which corresponds to maximum displacement of 225 mm at the location of column removal. Connection will fracture beyond this rotation and trigger vertical progressive collapse. For the specimen without belt truss, maximum vertical displacement is found to be about 1414 mm, which is significantly greater than the criteria set by GSA (2003). Therefore, the building frame is at high risk of vertical progressive collapse when subjected to column removal. Installation of belt truss at the top of the building reduces the maximum displacement by -44%, -80% and -83% respectively when K-brace, X-brace and N-brace belt trusses are used. Among all, X-brace and N-brace belt trusses satisfy the 2.5% radian rotational criteria recommended by GSA (2003).

Before the column is removed, the 9 m span composite beam systems behave primarily in flexural mode. Under gravity load, steel beams are stressed in compression due to hogging

moment near to both ends. After the column removal, the beams are forced to span twice longer. Almost immediately, the compression force increases marginally in the hogging region (beam end next to supporting column) as shown in Figure 5.6b. On the other hand, the force reversed into tension in the sagging region (beam end next to the removed column) as shown in Figure 5.6c. As displacement increases, the beam switches from flexural to catenary mode as evident in time history of K-brace belt truss and non-BT specimens. Catenary action serves as the last line of defense to arrest progression of collapse. However its effect is only obvious when deformation is relatively large compared to the criteria set by GSA (2003). Both time-history plots show that the axial response is capped at the connection strength, which is about 573 kN.

Although all belt truss specimens have similar weight, the specimens perform differently due to the difference in energy-absorbing capacity and failure mode. The static load-displacement relationship for each of the specimens is shown in Figure 5.7 It is clearly shown that incorporating belt truss can significantly improve the energy-absorbing capacity (i.e. area under the load-displacement curve) of a structure. System with high energy-absorbing capacity exhibits lower deformation when subjected to column removal event.

In general, X-brace and N-brace belt trusses perform much better than K-brace belt truss as the energy-absorbing capacity is greater. The better performance is attributed by the presence of tension load path after initial buckling of compression braces. It can be seen from the deformed shapes shown in Figure 5.12a and Figure 5.12b that half of the braces buckle while the remaining yield in tension. The tension load path allows truss action of belt truss system to remain effective in the inelastic response. For K-brace belt truss however, the buckling of compression braces causes loss of truss action as shown in Figure 5.12c. As a result, the energy-absorbing capacity of K-brace belt truss is much lower compared with X-brace and N-brace belt trusses.

5.3.2.1   Strength of brace member

The flexural and axial strengths of a brace member are directly related to the yield strength f_y. Therefore the influence of brace strength can be studied by varying the

material yield strength from $0.5f_0$ to $3.0f_0$, where f_0 is the reference strength of 275 MPa. As shown in Figure 5.8, inclusion of belt truss can reduce the displacement demand significantly. Generally the displacement reduces with increase of brace strength. As a result, the risk of vertical progressive collapse can be reduced. However, it is shown that the effectiveness of belt truss reduces when yield strength greater than f_0 is used, in which similar displacement is observed although yield strength is increased from f_0 to $3.0f_0$.

Not only does increasing brace strength incur additional construction cost, but it also induces higher force demand in columns in the proximity of damaged area. By normalizing the dynamic force to static weight of the structure using equation (5.1), the intensity of dynamic force demand within the damaged bay can be represented by the dynamic increase factor shown in Figure 5.9. A nonlinear relationship between the force demand and brace strength is observed, where the maximum force demand occurs when very large or very small brace strength is used. For an inelastic system, total force transferred to supporting columns is limited by ultimate capacity of belt truss. Therefore stronger belt truss absorbs larger force, and transfers higher force to the supporting columns. Nonetheless, large DIF up to 1.80 is also observed in building without belt truss. The large DIF is caused by tension stiffening effect of catenary action of the floor beams. The effect of catenary action is influential only in large deformation. Therefore, effect of tension stiffening on stronger structural systems (i.e. buildings with belt truss system) is insignificant. Out of the 54 dynamic analyses, DIF is found to range from 1.1 to 1.8. On local member level, the column force demand is found to behave similarly to DIF on global system level, i.e. column force increases with brace strength.

Nonetheless, there is a change of force distribution with inclusion of belt truss, i.e. larger force demand on upper storey columns, as shown in Figure 5.10. at the 7th storey, the design force under ULS requirement is 508 kN, inclusion of belt truss increases the column force by 54%, 95% and 112% for 1.0, 2.0 and $3.0f_0$ brace strength respectively. The findings show that sufficient (but not excessive) brace strength should be used for a good compromise between displacement demand and force demand. It is also evident that codified DIF of 2.0 recommended by DoD (2009) and GSA (2003) is only reasonable for

very strong system, which is rare in practice. For most building structures, the codified DIF can lead to overly conservative evaluation of the robustness performance.

5.3.2.2   Belt truss configuration

Although all belt truss systems are capable of reducing the displacement demand, their effectiveness depends on the truss configuration. From the findings, N-brace and X-brace belt truss exhibit similar performance in reducing displacement demand. However, significantly lower performance is observed in K-brace belt truss with high slenderness ratio. The poor performance of K-brace is attributed by the loss of truss action after buckling of the compression brace, and therefore less ductile inelastic response. The energy absorbing capacity of each system can be represented by the area under respective load-displacement relationship shown in Figure 5.7.

From global perspective, truss configuration may have insignificant influence on the force demand. However, uneven column force demand is found in left column (LC) and right column (RC) of N-brace belt truss. In both belt truss systems, load shedding to tension brace occurs when compression brace buckles. Unlike X-brace which has tension load path to both LC and RC columns, N-brace has only tension load path to RC. This phenomenon leads to asymmetrical load transfer mechanism in the inelastic N-brace belt truss system. As shown in Figure 5.11, the force difference between LC and RC at the 7th storey is about 32%, and can be greater when stronger brace is used. N-brace and X-brace belt trusses are more superior over K-brace belt truss in reducing displacement demand, and therefore should be prioritized for design or retrofitting practice. Due to the uneven force demand distribution of N-brace belt truss, X-brace belt truss is considered as the best configuration for robustness enhancement of new and existing buildings.

5.3.2.3   Slenderness of brace member

Unlike X-brace and N-brace belt trusses, performance of K-brace belt truss can be improved by using less slender brace member. For comparison between high ($L/r = 170$) and intermediate slenderness ratio ($L/r = 90$) in Figure 5.8, significant improvement is observed in the latter when strength is increased beyond f_y. Reducing its slenderness

means greater buckling capacity and energy-absorbing capacity. Due to the less ductile inelastic response, performance of K-brace belt truss is rather sensitive to the brace strength. Because of this, drastic change in the displacement demand is observed.

Opting for less slender brace maybe beneficial in reducing displacement demand, but it also means greater buckling capacity and force demand. As shown in Figure 5.9, specimens with higher slenderness ratio tend to induce lesser force demand. The effect is most obvious when high brace strength is used, i.e. for yield strength of $2f_y$, the force demand of $L/r = 90$ specimens is about 20% greater than $L/r = 170$ specimens. X-brace and N-brace belt trusses with high slenderness ratio should be used to achieve optimum effectiveness in mitigating displacement demand, while minimizing the force demand. On the contrary, brace with low slenderness ratio is necessary when K-brace belt truss is used. In this case, higher force demand is anticipated and needs to be controlled by reducing the member strength.

5.3.2.4   Position of belt truss along building height

Influences of the brace strength, slenderness ratio and belt truss configuration have studied in previous sections. In this section, influence of the position of belt truss on displacement and force demands is studied. Three positions of X-brace belt truss as shown in Figure 5.13a are considered in the numerical study. It is found that position of belt truss has only marginal contribution in reducing displacement demand. Considering the 3 positions of X-brace belt truss as shown in Figure 5.13a, the maximum vertical displacement is found to be 251, 229 and 208 mm for case (i), (ii) and (iii), respectively. The smaller demand can be attributed by the shorter load path when belt truss is placed nearer to the column removal position.

Unlike the displacement demand, force demand in the column is significantly influenced by the position of belt truss. As shown in Figure 5.13, the column force demand for Accidental Limit State (ALS) and Ultimate Limit State (ULS) is compared. As discussed previously, inclusion of belt truss can induce greater force demand in supporting column (LC and RC shown in Figure 5.13a), especially on the upper storeys. Although reducing brace strength can limit the force increase, it is not as effective as lowering the belt truss

position. By lowering the belt truss position, the column force demand under ALS can be controlled within the ULS design forces. When belt truss is placed at 4th storey, the ALS force demands are marginally higher than ULS design forces at these storeys only. Meanwhile, when belt truss is placed at 1st storey, all ALS force demands are within the ULS design forces. In other words, the risk of overstressing supporting columns is lower when belt truss is placed at lower storeys.

Nonetheless, significant tension force is also observed in the middle column (MC as shown in Figure 5.13a) when a belt truss is provided at the 7th storey. In normal design situation, the column splice connection is designed to transfer mainly compressive force, and not tension force. The column splice connection can fail in a brittle manner when tension force exceeds the connection capacity. As a result, the effectiveness of belt truss for robustness enhancement can be compromised. To address this problem, lowering the position of belt truss can also help in reducing the tension force demand in middle column. As shown in Figure 5.13c, the maximum tension force is found to be about 833 kN when a belt truss is provided at the 7th storey. By lowering the belt truss to 4th storey, the tension force demand can be reduced by about 34%. The risk of splice failure has been considerably reduced in view of the reduced demand as well as increased capacity (relative to the upper storey). Almost no tension force is anticipated when a belt truss is placed at the 1st storey.

When retrofitting an existing building against consequence of column removal at 1st storey, the position of belt truss should be placed on lower storeys such that strengthening of column and column splice can be minimized, if not avoided. In addition, significant saving in construction time and cost can be achieved by avoiding high-elevation construction work. For new building incorporating belt truss system, placing belt truss at lower storeys lead to saving in material cost of the column and splice connections. However, belt truss system can only be effective for robustness enhancement when column damage occurs below the belt truss storeys, i.e. column damage occurring on upper floors will not benefit from belt truss. To retrofit existing building against the threat of malicious activities, the use of belt truss on lower storey is deemed sufficient as

the risk of damaging 1st storey column is significantly higher than upper storeys. However, to design for column removal on every storey, multiple belt truss system will be necessary.

5.4 Strategies for robustness enhancement of high-rise building

As discussed in the previous section, belt truss can influence the robustness performance of building depending on brace strength, truss configuration, brace slenderness and position of the belt truss. To deal with extreme loading with low probability of occurrence such as terrorist attack, extensive retrofit of existing building or over-designing new building may not be economically feasible. Therefore, strategies for effective application of belt truss for robustness enhancement of high-rise building are proposed here.

5.4.1 Strategy 1: Robustness enhancement of new buildings

1st storey columns are generally more exposed to accidental loadings (e.g. bomb explosion, vehicular impact etc.) compared to upper storey columns, and therefore deserve special consideration in robustness design of building. However, a strategy for robustness design should not be only effective for removal of 1st storey columns, but also removal of any other columns on upper storeys. The strategy needs to be in line with the philosophy of robustness design as recommended by Eurocode 1 (BSI, 2006) which conceptually requires a robust structure to be insensitive to all kinds of accidental events. Based on this concept, a strategy for robustness design of new high-rise building is proposed here.

Strategy 1 provides protection against column failure occurring in any storey of a building. For belt truss to be effective, it should be provided above the location of column removal. Therefore, belt truss should be provided at the highest storey to prevent disproportionate collapse in case of damage (or complete removal) of any column in lower storeys. This strategy can increase force demand in supporting column in proximity of column removal as discussed in section 5.3.2.4. For low-rise building, column force

demand is normally contained within the requirement under normal design condition (i.e. Ultimate Limit State), and no increase of material cost is anticipated for the column. However, adopting the same strategy for medium-rise and high-rise building can lead to excessive column force demand at upper storeys of a building. In this case, multiple belt trusses as shown in Figure 5.14a will be required to control the force demand.

To illustrate effectiveness of the proposals, the 20-storey building frames as shown in Figure 5.14a are considered in the numerical study. The frames have similar geometry, structural configurations and loadings as the 8-storey two-dimensional frame discussed in section 5.3, except heavier columns i.e. UC305x305x240 are used for 1st to 12th storey. Properties of the belt trusses considered in the study are summarized in Table 5.2. It can be seen that belt trusses considered in the study also have weight per elevation area similar to the 8-storey frame.

As shown in Table 5.3, inclusion of single belt truss at 19th storey of the 20-storey building frame reduces the displacement demand by about 67%. However, it induces significant force demand in the supporting columns at upper storeys. As shown in Figure 5.14b, force demand in 10 upper storeys has exceeded the ULS design force when single belt truss system is installed on the roof. When double belt truss system is used, the force demand on the upper columns has been reduced and only 4 upper storeys has marginally exceeded the ULS design force. Incorporating triple and quadruple belt truss system can further reduce the force demand on upper storeys, but the contribution of belt truss to reduction of displacement and force demands is marginal compared to double belt truss system. Similarly, using multiple belt truss system can also reduce the tension force demand in MC substantially. As shown in Figure 5.14c, the tension force in MC can be reduced by almost 50% when switching from single to double belt truss system. Further reduction of the force demand can also be achieved by incorporating triple and quadruple belt truss, but the contribution is marginal compared to double belt truss system.

For design of high rise building, providing more number of belt trusses leads to smaller column force demands but also increases the construction cost. The study based on 20-storey building shows that providing more than two belt trusses is not cost effective as

the reduction in displacement and force demands are marginal. Therefore, provision of belt truss for every 10 storeys can be used as a general rule of thumb for preliminary design of new high rise buildings.

5.4.2 Strategy 2: Robustness enhancement of existing buildings

The strategy recommended for design of new building may not be practical for retrofitting existing building. This is because retrofitting existing building at high elevation can be risky and costly compared to construction of new building. Therefore belt truss should be installed at one of the lowest storeys. This strategy is only effective to prevent disproportionate collapse caused by failure of 1st storey column, which can be triggered by accidental events e.g. bomb explosion, vehicular impact etc.

As discussed previously, inclusion of single belt truss in the 20-storey building frame can reduce the displacement demand by more than 70%, and the effectiveness is dependant on position of the single belt truss. The study shows that smaller displacement demand is observed when lowering the position of belt truss. On the other hand, greater force demand is also observed in supporting columns at upper storeys. Instead of using multiple belt trusses, lowering the position of single belt truss can also significantly reduce the force demand in supporting columns as shown in Figure 5.15b. The maximum tension force in middle column (i.e. MC as shown in Figure 5.15a) is reduced by almost 70% when lowering the single belt truss from 19th storey to 6th storey. In order to prevent disproportionate collapse in existing building caused by failure of 1st storey column, the single belt truss should be installed at one of the lowest storeys, but at a sufficient distance away from ground level to avoid being directly damaged by bomb explosion or vehicular impact.

5.5 Robustness enhancement of Cardington building using belt truss system: A case study

So far, the previous sections have focused only on the robustness behavior of two-dimensional frames. In this section, robustness evaluation involving sudden column removal of Cardington building will be carried out in the three-dimensional context. The purpose of the study is to investigate the effectiveness of belt truss system in enhancing robustness of large and complex three-dimensional building. 13 cases of sudden column removal using nonlinear time-history analysis are performed using the numerical model discussed in section 5.2.2. In addition to the perimeter column removal event, the study considers corner column and upper-storey column removal events.

Case 1: Removal of 1st storey perimeter column D1

Case 2: Removal of 1st storey corner column A1

Case 3: Removal of 4th storey corner column A1

For each column removal event, 2 types of brace strength are used to illustrate the influence of strength to the robustness performance. For easy reference, smaller brace member is identified as "S", whereas larger brace member as "L". The "(M)" and "(T)" shown in Table 5.5 refer to the positions of belt truss, i.e. (M) denotes Mid-height while (T) denotes Top of the building.

5.5.1 Effectiveness of belt truss as robustness enhancement

Similar to previous findings on the 2D frame, i.e. sections 5.3 and 5.4, significant reduction of displacement demand can be achieved by incorporating belt truss in the building system. Table 5.5 shows displacement demands of the building with different belt truss positions and brace strengths when subjected to different cases of column removal. The findings show that belt truss is not only effective in the case of perimeter column removal (i.e. case 1), but also removal of corner column (i.e. case 2) and upper

storey column (i.e. case 3). Generally, 80% to 90% reduction in displacement is observed from the study involving three-dimensional building system. Similar to previous findings on the 2D frame, the effectiveness of belt truss is also dependent on the strength of brace member. The study shows that greater reduction of displacement demand is observed for corner column removal (case 2) in comparison with perimeter column removal (case 1). When belt truss with SHS 80x5 brace member is installed on the top of the building, the displacement demand of case 1 is about 3.8 times greater than case 2. Therefore, smaller brace member can be used in the last bay to save cost and to control force demand in the supporting columns. Generally, the position of the belt truss shows insignificant influence on the displacement demand of the building. The displacement demands are consistent with the findings of previous analysis involving 2D frame.

In this study involving three-dimensional building, the DIF back-calculated from global base reaction of nonlinear time-history analysis cannot be used as an indication of global force demand. This is because the assumption that maximum forces in all columns occur concurrently is no longer valid for large and complex systems. Therefore, column force demand in each column needs to be investigated directly. As shown in Figure 5.17 and Figure 5.18, column force demand is indeed amplified by the use of strong brace member. Therefore, the conclusion regarding the relationship between brace strength and force demand is still valid for large building systems, i.e. the force demand increases with brace strength; therefore excessive brace strength should be avoided.

Lowering the position of belt truss to lower storeys is an effective way to control column force demands when removal of 1st storey column is considered. For all cases of column removal considered in the present study, huge column force demand is observed on upper storeys (4th to 8th storey) when belt truss is installed at the top of the building. As shown in Figure 5.17 and Figure 5.18, the compression force in supporting column (parts a and b of the figures) and tension force in the damaged column (part c of the figures) can be greatly reduced by moving the belt truss to mid-height of the building. For case 1 involving removal of 1st storey perimeter column D1, column force demand can be kept within the ULS design forces when belt truss is installed at mid-height. That reduces the risk of overstressing supporting column C1 and D2 in the event of column removal. The

tension force in the damage column D1 is also negligibly small. For case 2 involving removal of 1st storey perimeter column A1, force demand greater than ULS is still observed in column A2 although it has been significantly reduced by installing belt truss at mid-height. The capacity of column A2 is significantly larger than the ULS design force (due to the presence of large opening in the proximity, see Figure 5.1). Therefore, ALS force greater than ULS does not necessarily indicate high risk of column failure for this case.

Installing belt truss near the 1st storey is favorable only for removal of 1st storey column. This is because the belt truss needs to be located above the removed column in order to provide effective alternate load path. For case 3 involving the removal of 4th storey corner column, installing belt truss below the 4th storey has almost no effect on the displacement demand. For design of high-risk buildings, at least a belt truss should be placed at top storey of the building such that alternate load path is available in case any columns at lower storeys is damaged or completely removed. Multiple belt trusses should be considered for tall buildings to control force demand in the supporting columns as discussed in section 5.4.

5.6 Concluding remarks

1. This chapter discusses the potential of belt truss system as robustness enhancement of multi-storey composite building. Any form of progressive collapse, i.e. vertical or horizontal progressive collapse will be as destructible as a disproportionate collapse and therefore must be prevented in the design of a robust structure. The first type of progressive collapse is governed by displacement demand, while the second type is governed by force demand in the structure.

2. Behavioral study on two-dimensional composite frame shows key influences of belt truss on building robustness:

   a) Increasing brace strength reduces displacement demand but increases force demand. Study covering a wide range of brace strengths shows that the dynamic increase factor (DIF) for belt truss building ranges from 1.1 to 1.8, in

which dynamic increase factor of 1.8 corresponds to strongest brace member used in the study. It also shows that DIF = 2.0 recommended by current codes of practice (GSA, 2003; DoD, 2009) is conservative for designing building incorporating truss system.

b) N-brace and X-brace belt trusses have higher inelastic capacity and energy-absorbing capacity compared to K-brace belt truss. Therefore, these systems perform significantly better than K-brace belt truss in reducing displacement demand during column removal event.

c) Position of belt truss has insignificant influence on the displacement demand. However, installing belt truss on lower storeys can greatly reduce the column force demand on the upper storeys.

3. Robustness enhancement strategies have been conceptualized based on findings of the behavioral study.

a) For design of new building, X-brace belt truss with high slenderness ratio is preferred. Belt truss needs to be provided above the location of column removal to be effective. For low-rise building, belt truss should be provided at the highest storey to prevent disproportionate collapse in case of damage (or complete removal) of any column in lower storeys. For medium-rise and high-rise buildings however, adopting the same strategy can lead to excessive column force demand at upper storeys of the building. Therefore, multiple belt trusses will be required to control force demand. Providing more belt trusses leads to smaller column force demands but increases construction cost. Based on the present study, provision of belt truss for every 10 storeys can be adopted as rule of thumb for preliminary design of high-rise building.

b) Retrofitting existing building at high-elevation can be risky and costly as compared to construction of new building. Therefore belt truss should be installed at one of the lowest storeys, but at a sufficient distance away from ground level to avoid being directly damaged by bomb explosion or vehicular

impact. This strategy is only effective to prevent disproportionate collapse caused by failure of 1st storey column, which can be triggered by accidental events e.g. bomb explosion, vehicular impact etc.

4. A case study of three-dimensional building system shows consistent findings with the behavioral study on two-dimensional frame. Both studies show that belt truss system is effective in reducing the displacement demand in the event of column removal. The effectiveness of belt truss in reducing displacement demand is governed by the brace strength, i.e. stronger brace member reduces the displacement demand. Nevertheless, both studies discourage the use of excessive strength for the brace member in order to control force demand in the supporting columns. In addition, both studies also show that the position of belt truss is influential on the magnitude and distribution of column force demands.

Table 5.1: Properties of belt truss used in the study of 8-storey Cardington 2D frame

Truss configuration	Brace section (mm x mm)	Slenderness, L/r ratio	Weight per area (kg/m^2)	Yield strength (N/mm^2)
K	SHS 100x10	165	1.161	275
X	SHS 80x8	167	1.206	275
N	SHS 150x8	170	1.188	275
K	SHS 170x5.5	91	1.192	275
X	SHS 140x4.3	89	1.221	275
N	SHS 250x7	100	1.780	185

Note: SHS 100x10 denotes square hollow section of 100 mm width and 10 mm thickness

Table 5.2: Properties of belt truss used in the study of 20-storey Cardington 2D frame

Number of belt truss (X-brace)	Brace section (mm x mm)	Slenderness, L/r ratio	Weight per area (kg/m^2)	Yield strength (N/mm^2)
1	SHS 130x12	102	1.186	275
2	SHS 130x6	98	1.246	275
3	SHS 130x4	96	1.266	275
4	SHS 115x3.5	109	1.307	275

Note: SHS 130x12 denotes square hollow section of 130 mm width and 12 mm thickness

Table 5.3: Displacement demands of 20-storey Cardington 2D frame when subjected to sudden column removal: Influence of number and position of belt truss

Number of belt truss	Position (at storey)	Max. displ. (mm)	Ratio
-	-	1689	1.00
1	19th	553	0.33
	13rd	473	0.28
	6th	343	0.20
2	9th, 19th	297	0.18
3	6th, 13rd, 19th	256	0.15
4	4th, 9th, 14th, 19th	168	0.10

Table 5.4: Natural frequencies of Cardington floor: Comparison between the presented method, detailed FEA by El-Dardiry et al. (2006) and Insitu test by Ellis et al. (1996)

Mode	Present method [a]	Detailed FEA (El-Dardiry et al., 2006) [b]	Insitu test (Ellis et al., 1996) [c]	Ratio	
				[a]/[b]	[a]/[c]
1	7.116	6.890	-	1.03	-
2	7.271	7.160	-	1.02	-
3	7.456	7.240	-	1.03	-
4	7.832	7.560	7.580	1.04	1.03
5	7.956	7.570	-	1.05	-
6	8.244	8.010	8.490	1.03	0.97

Table 5.5: Displacement and global force demands of Cardington 3D building when subjected to different cases of sudden column removal

Case	Column removal	Brace section (SHS)	Belt truss position	Max. vertical displacement (mm)
1	1D1	None	None	860
1S(T)	1D1	80x5	Top	134
1S(M)	1D1	80x5	Mid	131
1L(T)	1D1	150x8	Top	44
1L(M)	1D1	150x8	Mid	31
2	1A1	None	None	675
2S(T)	1A1	60x4	Top	53
2S(M)	1A1	60x4	Mid	44
2L(T)	1A1	80x5	Top	35
2L(M)	1A1	80x5	Mid	26
3	4A1	None	None	698
3S(T)	4A1	60x4	Top	27
3S(M)	4A1	60x4	Mid	696

Note: 80x5 denotes square hollow section of 80 mm width and 5 mm thickness

150x8 denotes square hollow section of 150 mm width and 8 mm thickness

60x4 denotes square hollow section of 60 mm width and 4 mm thickness
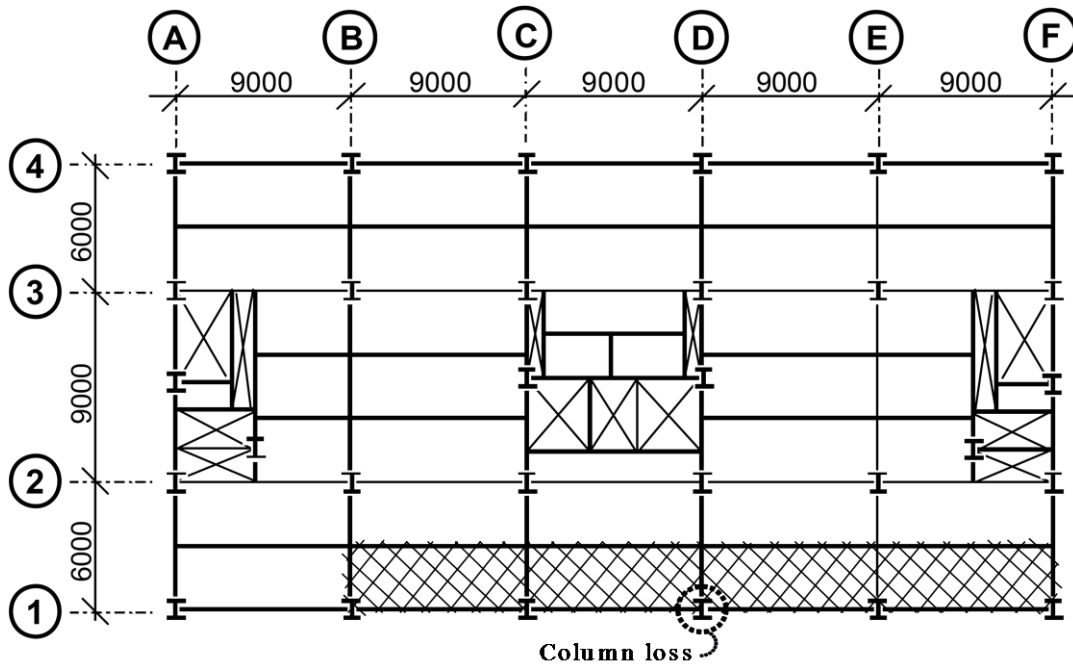
Figure 5.1: Floor layout of Cardington building and 2D frame studied (hatched region)
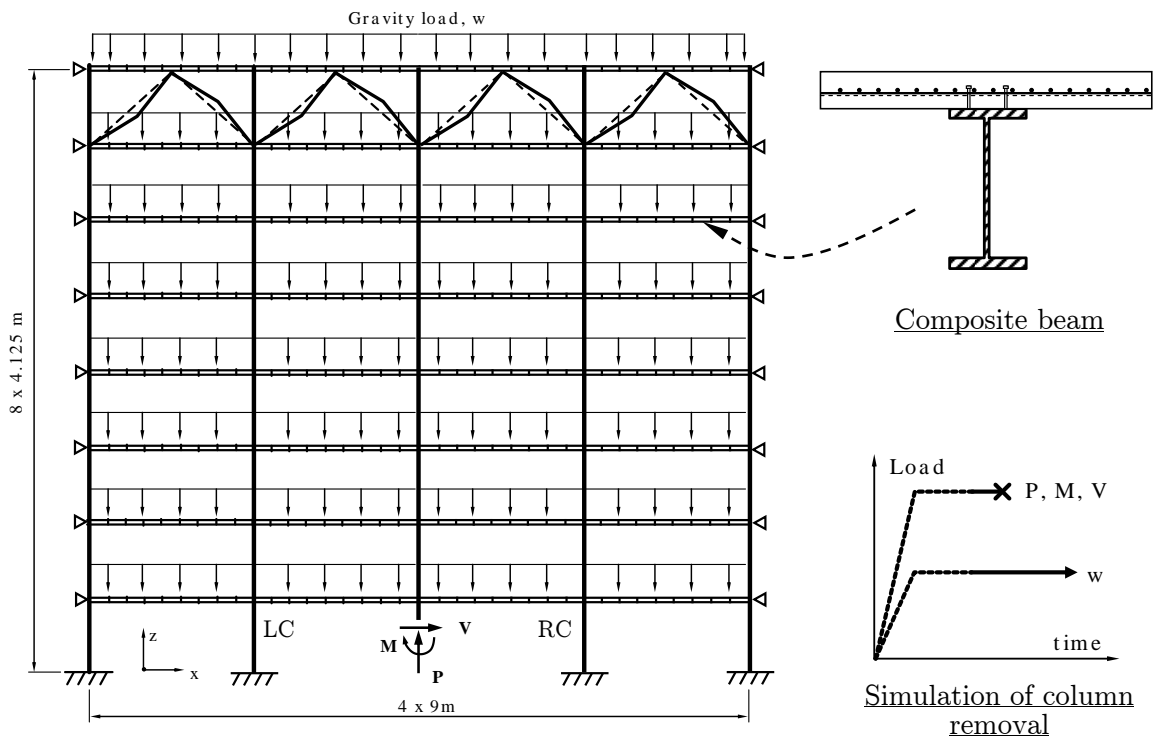
Figure 5.2: Numerical model of 8-storey Cardington 2D frame
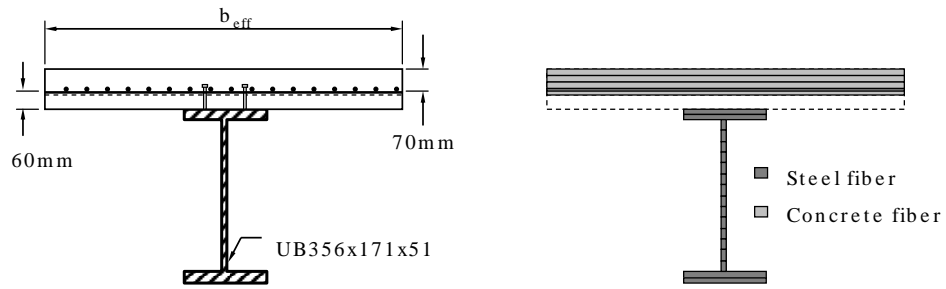
(a) physical geometry   (b) fiber section

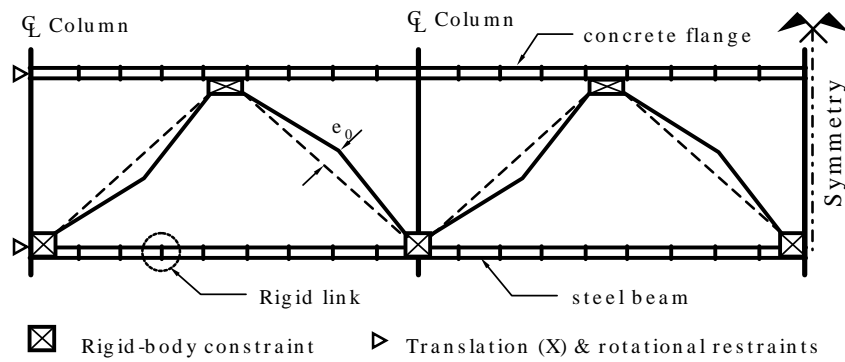Figure 5.3: Fiber sections of steel beam and composite slab

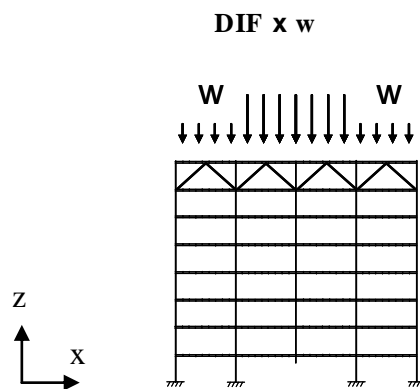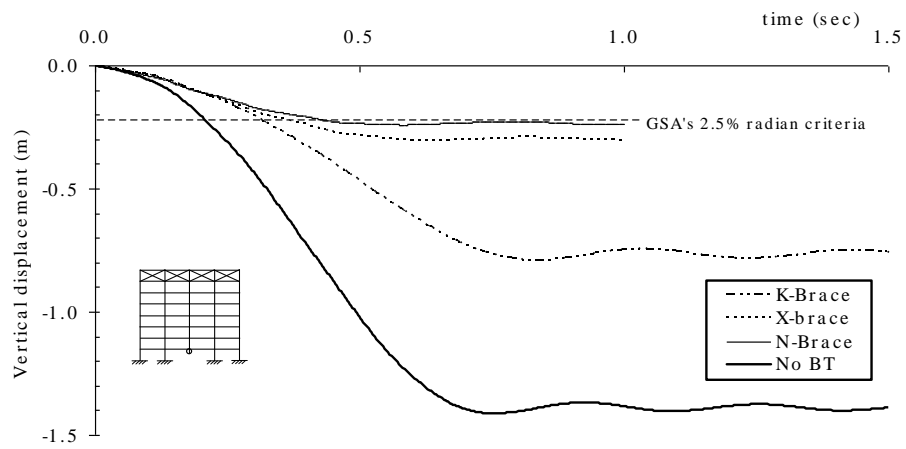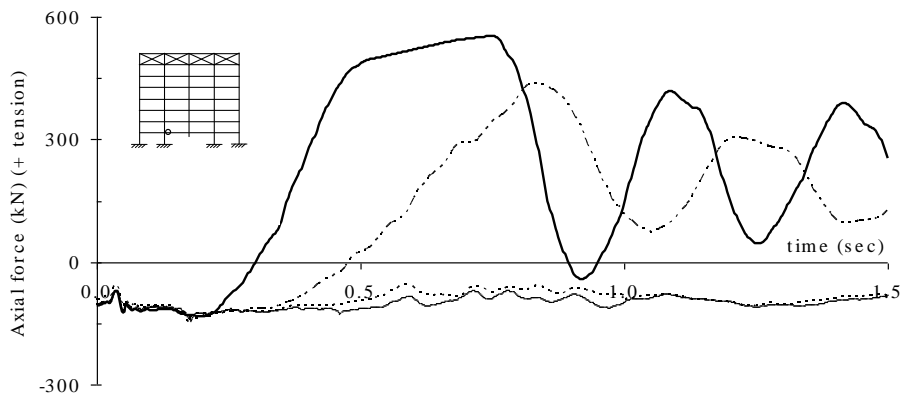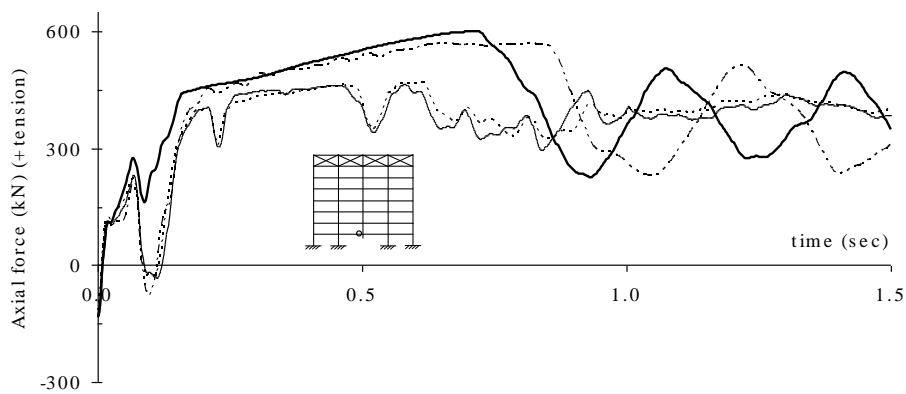Figure 5.4: Modeling of belt truss system (imperfection exaggerated)

Figure 5.5: Equivalent static load due to sudden column removal

169

(a) vertical displacement at location of column removal

(b) axial force of beam in the hogging region

(c) axial force of beam in the sagging region

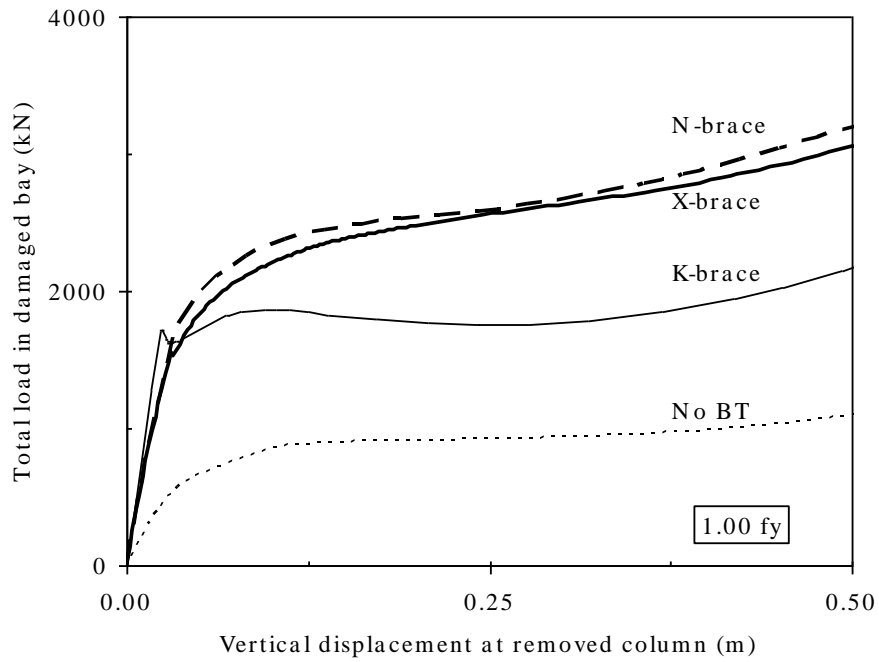Figure 5.6: Displacement time-history due to sudden removal of column D1 of 2D frame

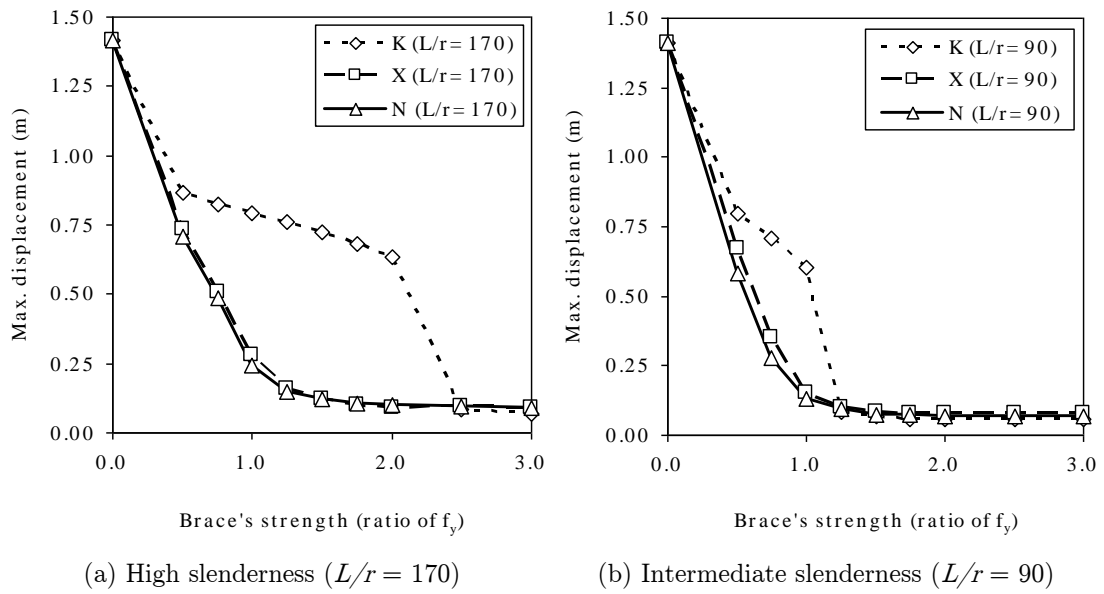Figure 5.7: Load-displacement relationships of 2D frame with different types of belt truss (BT) system

(a) High slenderness ($L/r = 170$)   (b) Intermediate slenderness ($L/r = 90$)

Figure 5.8: Influence of the brace strength on displacement demand of 2D frame

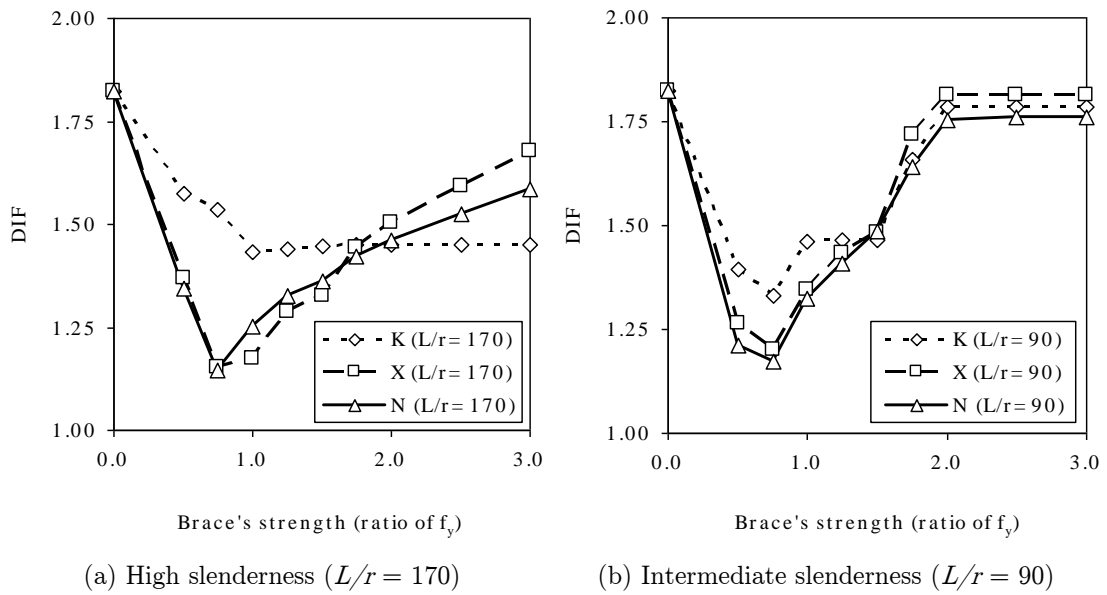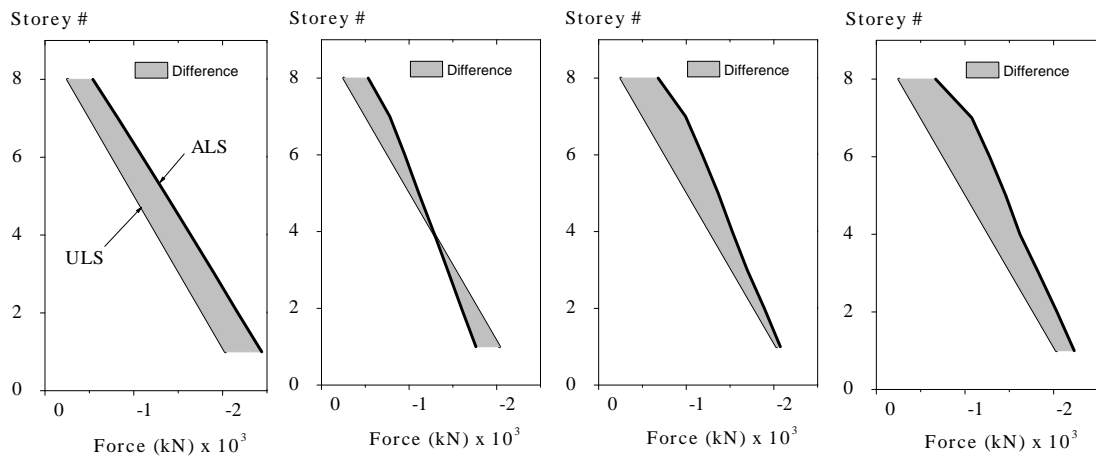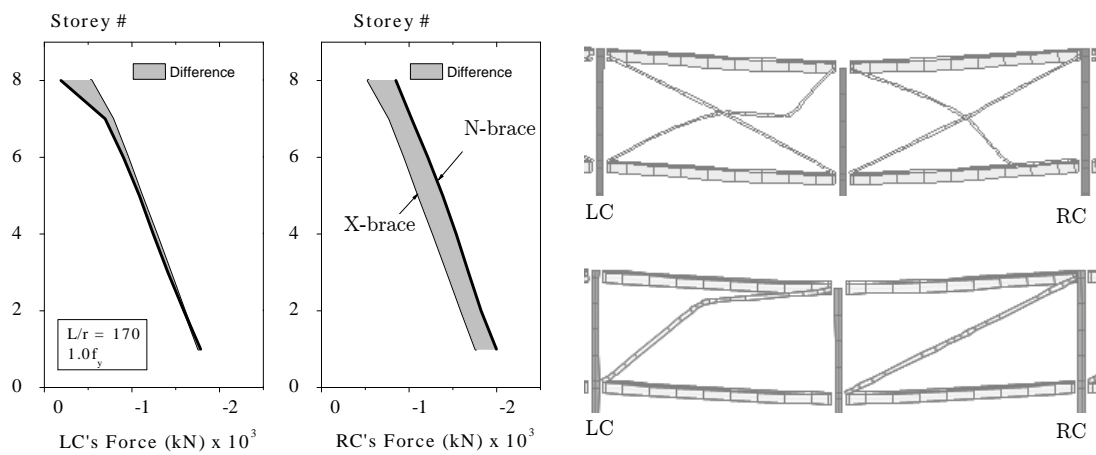(a) High slenderness ($L/r = 170$)   (b) Intermediate slenderness ($L/r = 90$)

Figure 5.9: Influence of the brace strength on global force demand of 2D frame
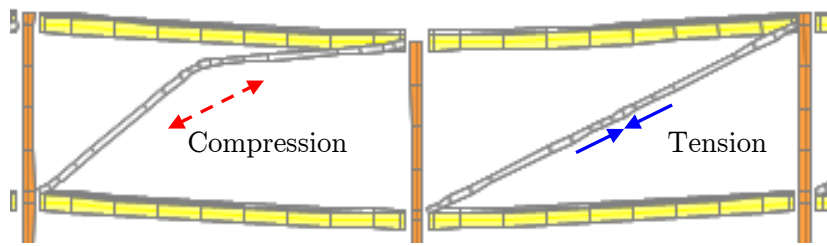
172

(a) no belt truss   (b) X-brace with $1.0f_y$ (c) X-brace with $2.0f_y$ (d) X-brace with $3.0f_y$

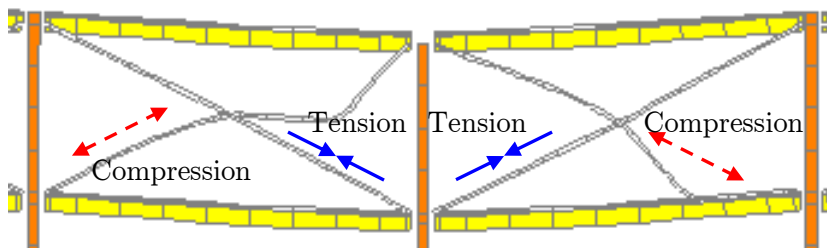Figure 5.10: Influence of the brace strength on column (LC) force of 2D frame

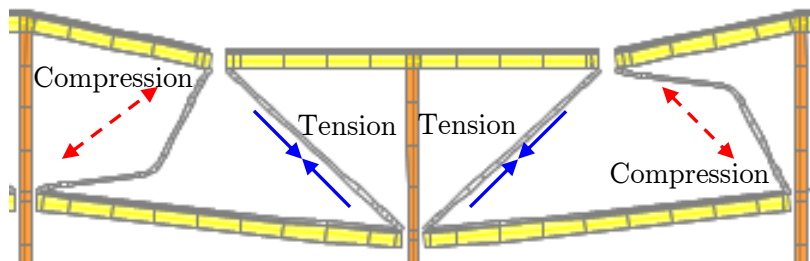(a) Uneven force demand in LC and RC   (b) failure mode of X and N-brace belt truss

Figure 5.11: Uneven column force in 2D frame caused by N-brace belt truss

(a) N-brace belt truss

(b) X-brace belt truss

(c) K-brace belt truss

Figure 5.12: Deformed shapes and truss actions of various belt truss systems

(i) BT at 7th storey   (ii) BT at 4th storey   (iii) BT at 1st storey   (iv) no BT

(a) Various belt truss (BT) positions considered in study

(i) BT at 7th storey   (ii) BT at 4th storey   (iii) BT at 1st storey   (iv) no BT

(b) Compression force envelope in column LC for various positions of X-brace belt truss (BT)

(i) BT at 7th storey   (ii) BT at 4th storey   (iii) BT at 1st storey   (iv) no BT

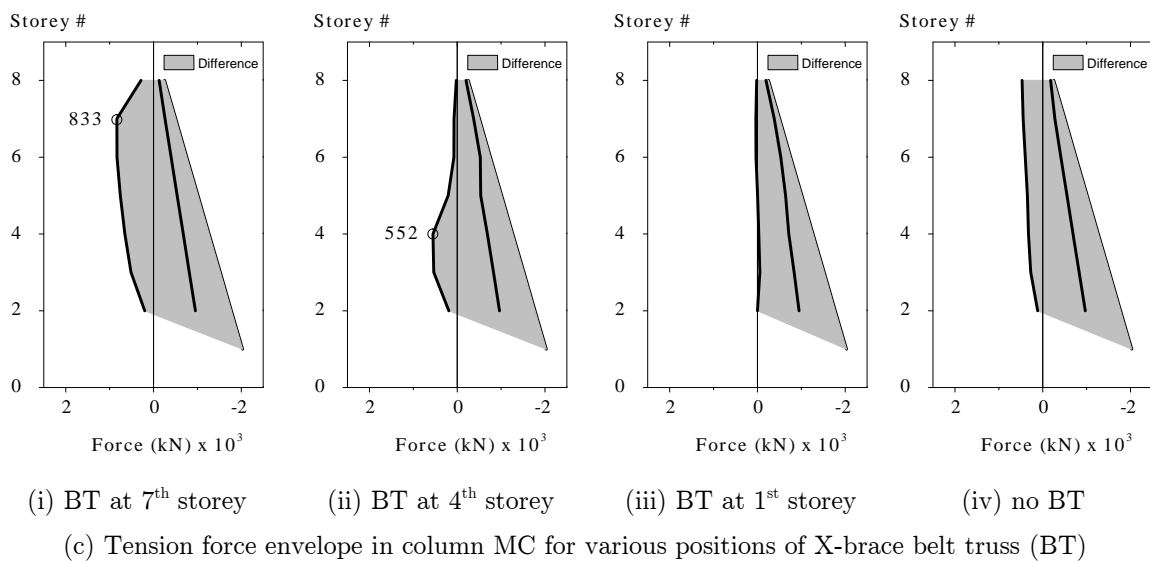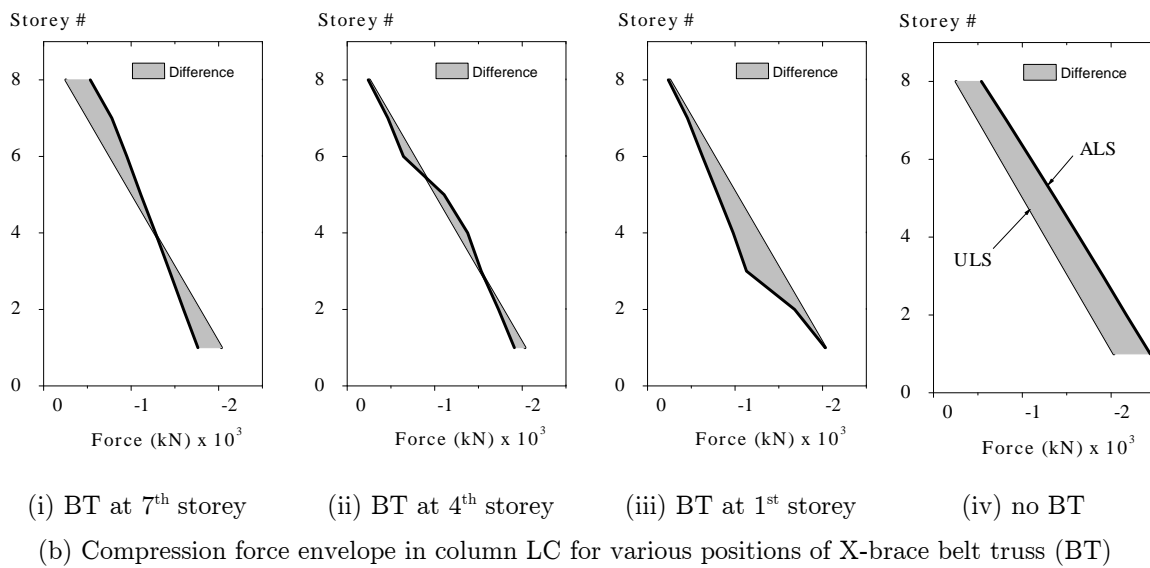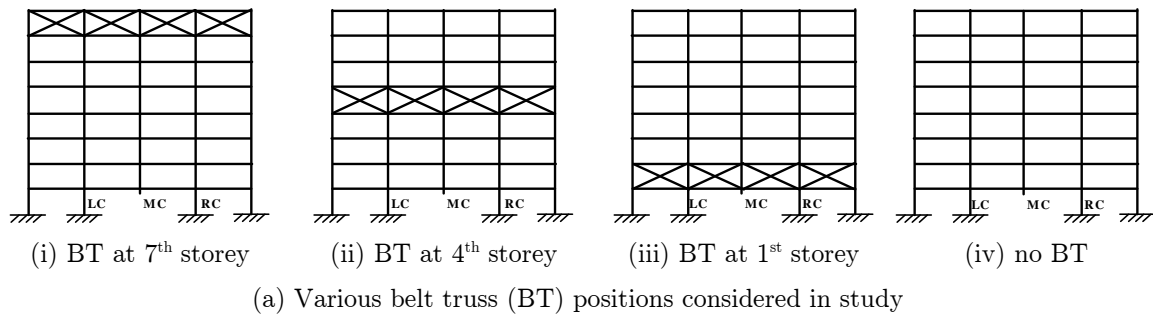(c) Tension force envelope in column MC for various positions of X-brace belt truss (BT)

Figure 5.13: Influence of the belt truss (BT) position on column force demand of 8-storey Cardington 2D frame

(i) single BT   (ii) double BT   (iii) triple BT   (iv) quadruple BT

(a) various belt truss (BT) arrangements considered in study

(i) single BT   (ii) double BT   (iii) triple BT   (iv) quadruple BT

(b) compression force envelope in column LC for various positions of X-brace belt truss (BT)

(i) single BT   (ii) double BT   (iii) triple BT   (iv) quadruple BT

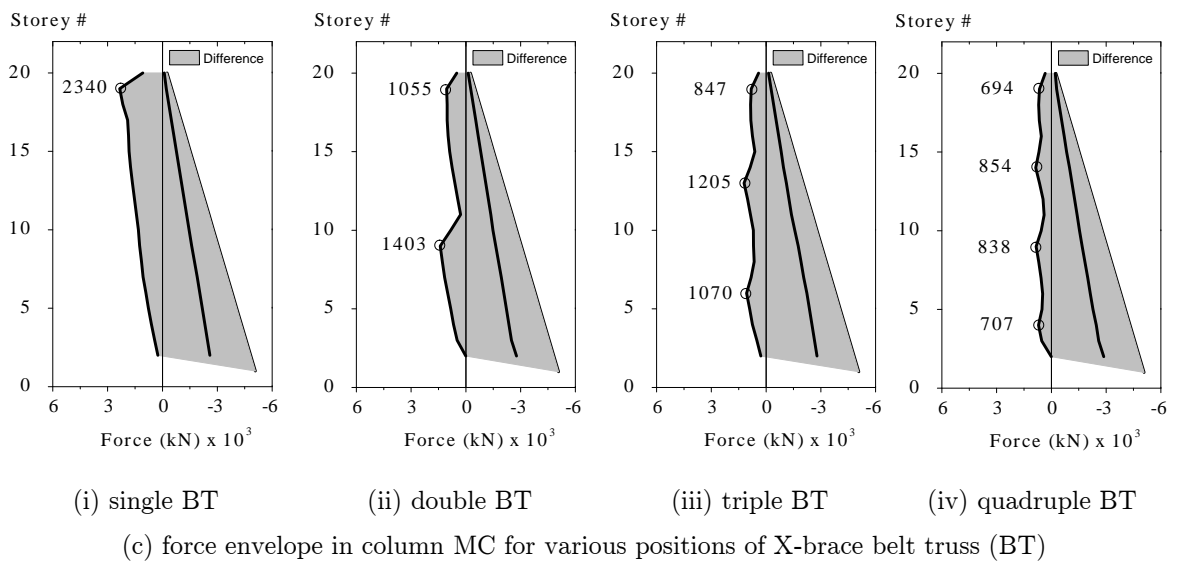(c) force envelope in column MC for various positions of X-brace belt truss (BT)
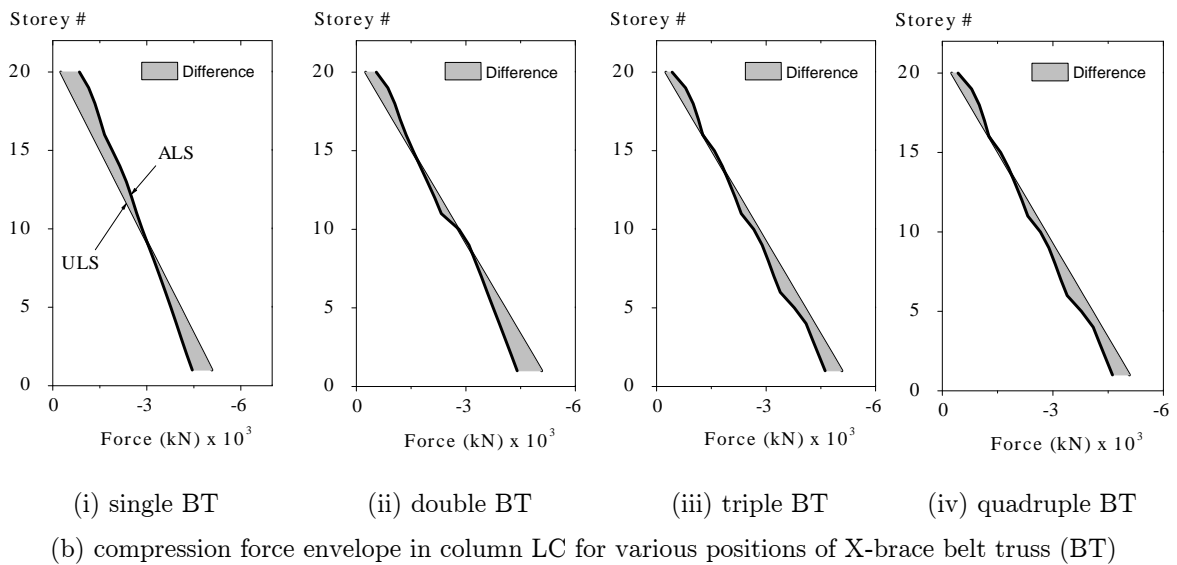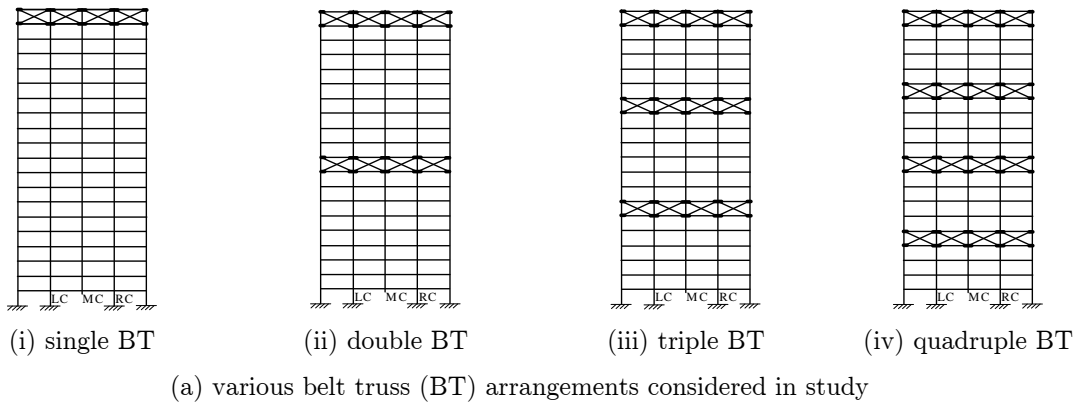
Figure 5.14: Influence of the number and position of belt truss on column force demand of 20-storey Cardington 2D frame

(i) BT at 19th storey   (ii) BT at 13rd storey   (iii) BT at 6th storey   (iv) no BT

(a) Various belt truss (BT) positions considered in study

(i) BT at 19th storey   (ii) BT at 13rd storey   (iii) BT at 6th storey   (iv) no BT

(b) compression force envelope in column LC for various positions of X-brace belt truss (BT)

(i) BT at 19th storey   (ii) BT at 13rd storey   (iii) BT at 6th storey   (iv) no BT

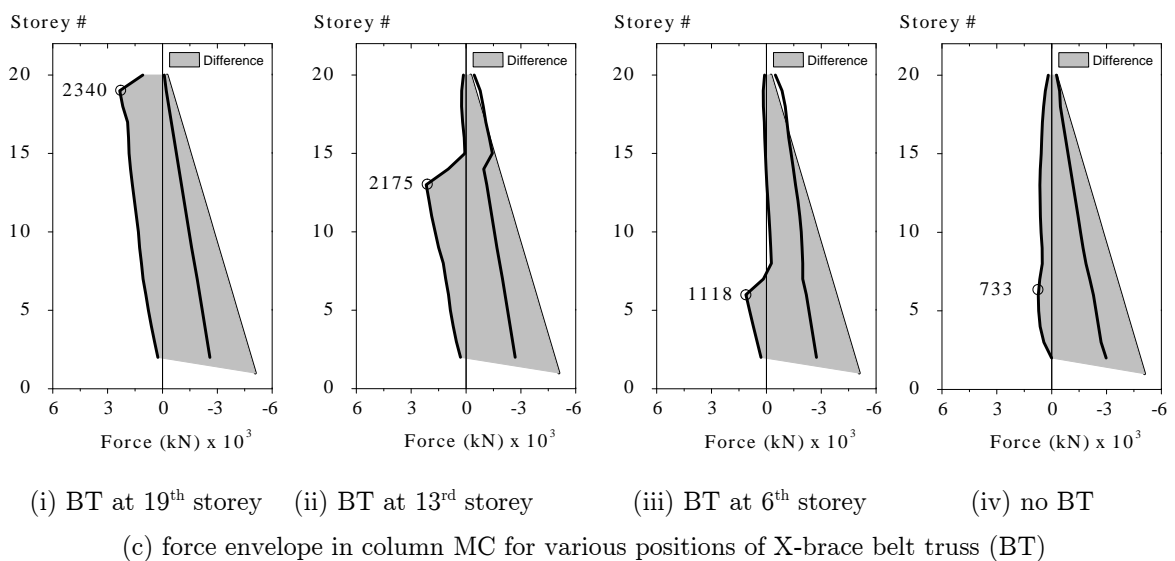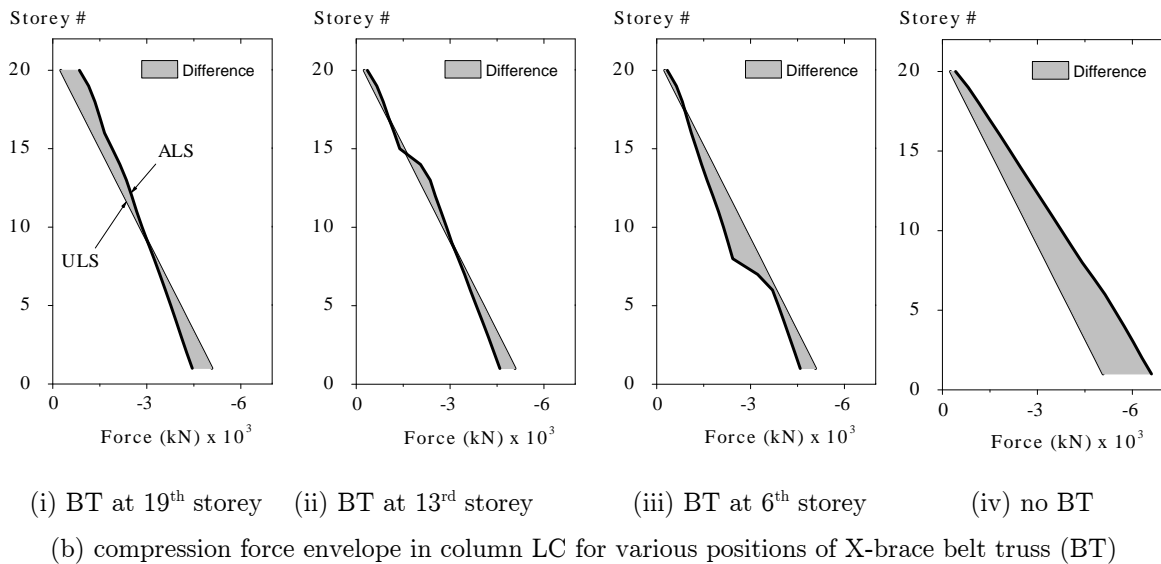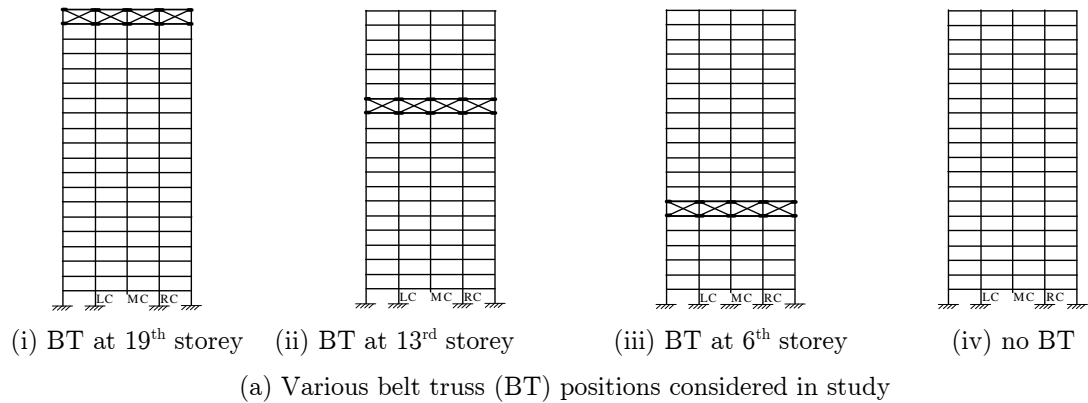(c) force envelope in column MC for various positions of X-brace belt truss (BT)

Figure 5.15: Influence of the belt truss position on column force demand of 20-storey Cardington 2D frame

177
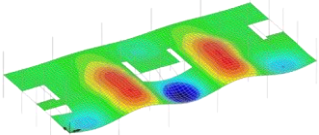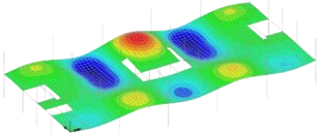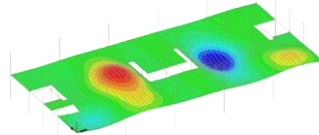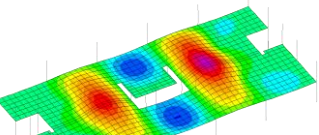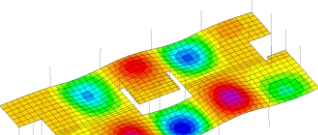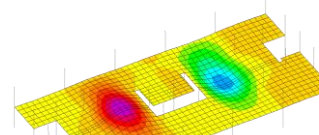
Method	Mode 1	Mode 2	Mode 3
Detailed FEA			
	Frequency = 6.890 Hz	Frequency = 7.160 Hz	Frequency = 7.240 Hz
Present			
	Frequency = 7.116 Hz	Frequency = 7.271 Hz	Frequency = 7.456 Hz

Figure 5.16: Natural frequencies and corresponding vibration modes of Cardington floor structure: Comparison between the presented method and detailed FEA by El-Dardiry and Ji (2006)
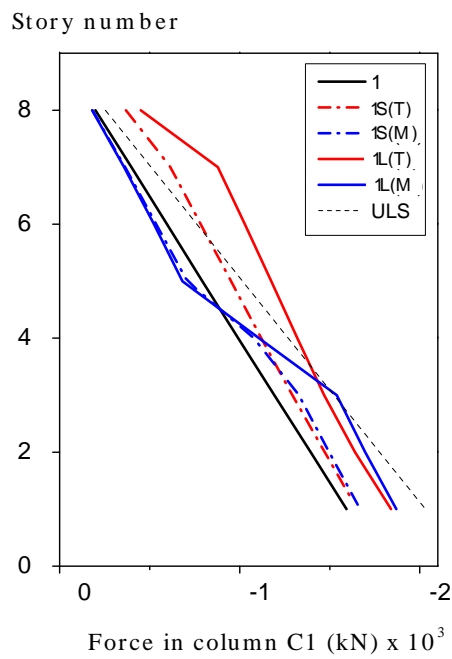
(a) column C1
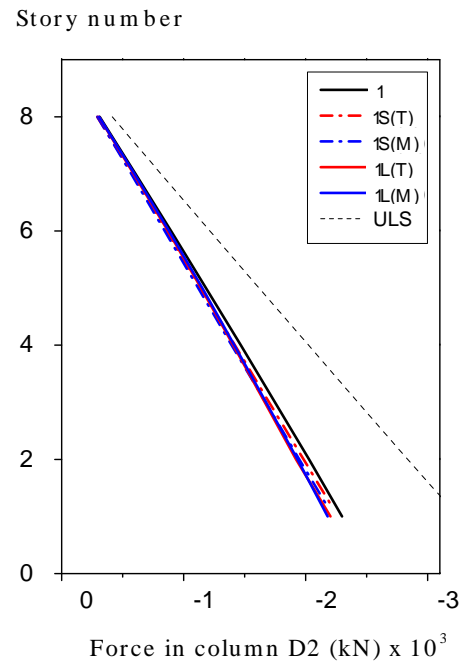
(b) column D2
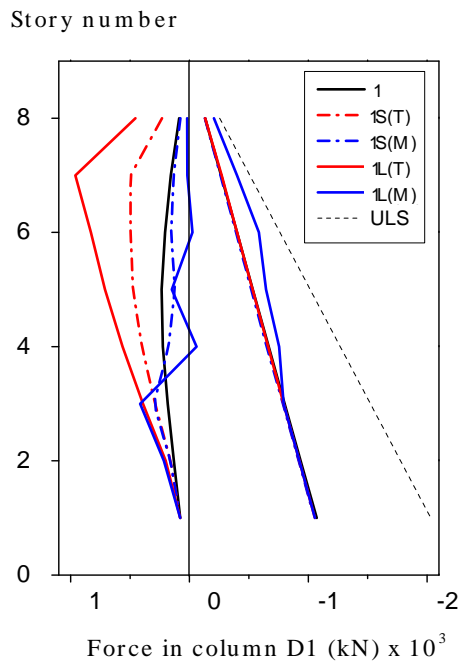
(c) column D1
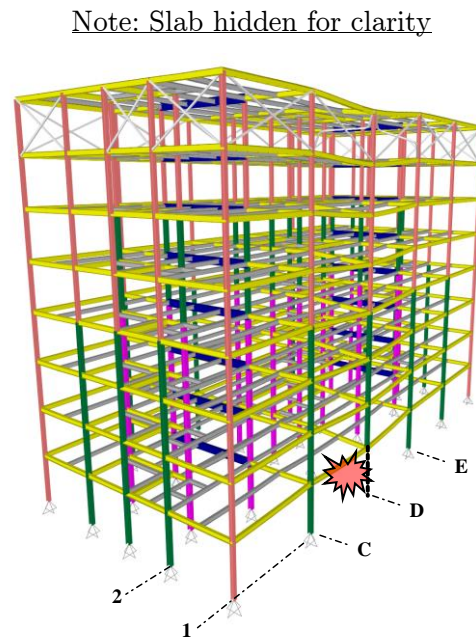
(d) deformed shape

Figure 5.17: Column forces of 3D Cardington building: sudden removal of storey 1 perimeter column D1 (Case 1)

Story number

Force in column A2 (kN) x 10^3

(a) column A2

Story number

Force in column B1 (kN) x 10^3

(b) column B1

Story number

Force in column A1 (kN) x 10^3

(c) column A1

Note: Slab hidden for clarity

(d) deformed shape

Figure 5.18: Column forces of 3D Cardington building: sudden removal of storey 1 corner column A1 (Case 2)
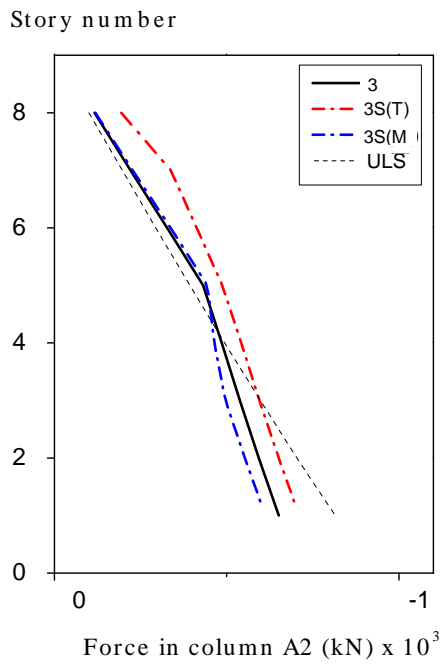
(a) column A2

(b) column B1
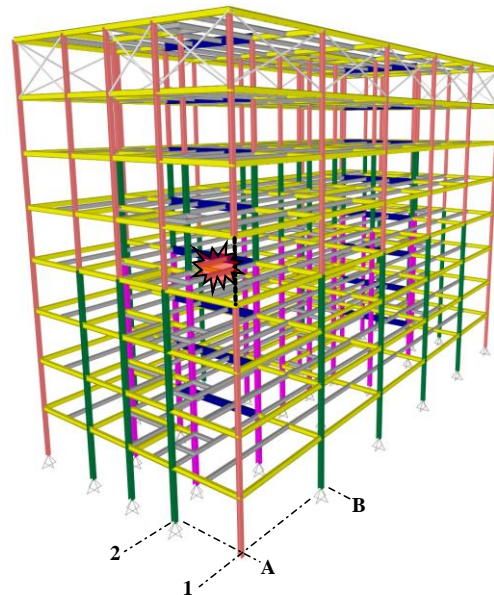
(c) column A1

(d) deformed shape

Figure 5.19: Column forces of 3D Cardington building: sudden removal of storey 4 corner column A1 (Case 3)

Chapter 6: Equivalent Static Analysis for Robustness Design

6.1 Introduction

Robustness study presented in the previous chapter is performed using nonlinear time-history analysis, a method commonly considered as the most accurate for robustness evaluation. In spite of the good accuracy, nonlinear time-history analysis is less appropriate for application in design practice due to the higher computation requirement. On the other hand, nonlinear static analysis with dynamic increase factor (DIF) to account for dynamic effects can be convenient for repetitive analysis in the design practice. Current robustness codes recommends the use of DIF = 2.0 for both linear and nonlinear static analyses to a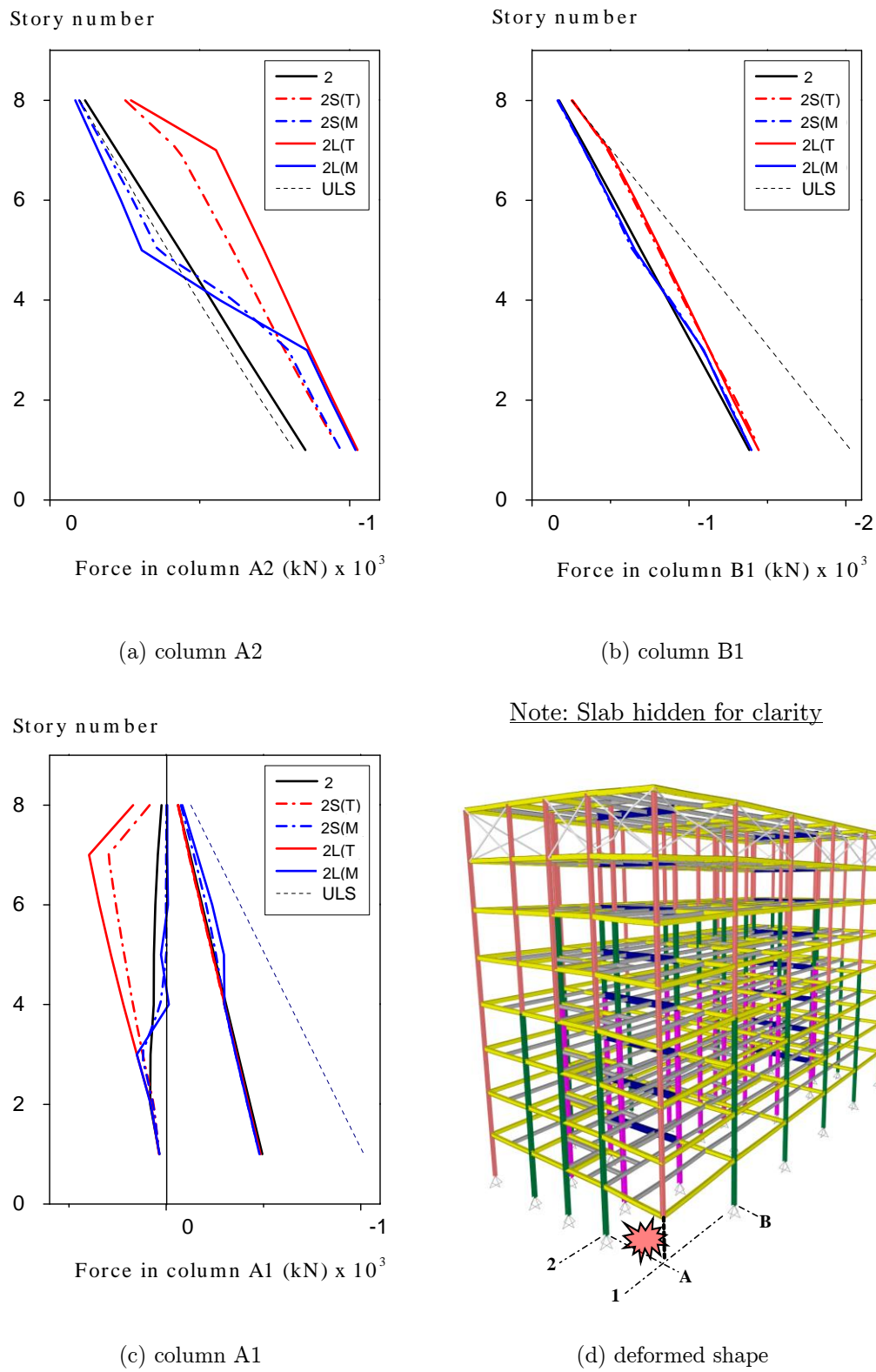ccount for dynamic effects during sudden column removal event (GSA, 2003; DoD, 2009). The codified approach is easy to apply but can also lead to very conservative prediction as shown in the following sections.

In this chapter, an equivalent static analysis (ESA) based on energy-balance concept is studied. The method is first proposed by Izzuddin et al. (2008) and then by Powell (2009) for robustness evaluation of conventional framed structures utilizing only the nonlinear static response. Dynamic demands due to sudden column removal can be approximated by using energy-balance concept without the need of actual dynamic analysis. Therefore, significant saving in computational demand is expected. Currently the accuracy of ESA on realistic and large building system is not well studied. In view of the potential benefits

of ESA, verification studies are carried out in this chapter by comparing the dynamic demands predicted by ESA and nonlinear time-history analysis.

6.2 Energy-balance concept

Dynamic response of structure when subjected to sudden column removal is similar in effect to sudden application of gravity load on the affected sub-structure (Izzuddin et al. 2008; Powel, 2009). Consider a simple frame structure with gravity load of P_n as shown in Figure 6.1a. The frame moves downward almost immediately after the central column is removed as the gravity load exceeds the static structural resistance of the damaged frame. The change of potential energy due to deformation of the structure is converted to strain energy and kinetic energy which leads to increasing velocity. The velocity starts to decrease beyond the static displacement (i.e. displacement due to the same gravity loading applied statically instead of suddenly) as the static resistance of the structure is now greater than the gravity load. The frame reaches the maximum displacement $D_{max,n}$ when velocity of the motion reduces to zero, and subsequently rebounds into free vibration mode. For robustness design, maximum deformation and internal force in structural members need to be limited to structural capacities to prevent disproportionate collapse.

Considering a single degree-of-freedom system, the change of potential energy in structure is equal to the external work done W_e by gravity load P_n from initial position to maximum displacement of $D_{max,n}$,

$$W_e = P_n \cdot D_{max,n} \tag{6.1}$$

and the corresponding strain energy is equal to internal work done W_i by the structure,

$$W_i = \int_0^{D_{max,n}} P \ \mathrm{d}D \tag{6.2}$$

Maximum displacement occurs at a state of energy balance, i.e. $W_e = W_i$ (Izzuddin et al., 2008). Therefore the relationship between gravity loading P_n and the corresponding maximum displacement $D_{max,n}$ can be expressed as,

$$P_n = \frac{\int_0^{D_{max,n}} P \, dD}{D_{max,n}} \tag{6.3}$$

Equation (6.3) can be used to approximate maximum displacement and force demands of a structure when static load-displacement relationship of the damaged structural system (i.e. the frame with removed column shown in Figure 6.1b) is known. The integral component of Equation (6.3) is the area under the load-displacement curve, and is representative of the strain energy of a structure.

Consider two scenarios, i.e. when $P_n = P_1$ and $P_n = P_2$, the corresponding states of energy balance are shown in Figure 6.2a and Figure 6.2b. The two depicted hatched areas are identical when state of energy balance is achieved. The first scenario represents elastic response of lightly loaded structure. As shown in Figure 6.1a, area under the load-displacement curve which represents the internal work done of linear system is always equal to $0.5 \cdot DIF_1 \cdot P_1 \cdot D_{max,1}$. Substituting the numerator of Equation (6.3) with $0.5 \cdot DIF_1 \cdot P_1 \cdot D_{max,1}$, DIF_1 can be derived as 2.0. This serves as the basis of DIF = 2.0 as recommended by current codified approaches (DoD, 2009; GSA, 2003). For nonlinear system however, the maximum gravity load resisted by the system is limited by the system capacity. At a state of energy balance when $D = D_{max,2}$, the gravity load resisted by the system is $P = DIF_2 \cdot P_2$ as shown in Figure 6.1b. For most practical structures which are likely to undergo nonlinear response when subjected to extreme loading, the use of DIF = 2.0 can be overly conservative as will be shown in the following section. For any static load-displacement curve generated from nonlinear static analysis, the corresponding capacity curve which relates the gravity load to the maximum displacement can be generated as shown in Figure 6.2c. This capacity curve can be used

to estimate the displacement and force demands in a structure for robustness design without the need of a computationally demanding nonlinear time-history analysis.

6.3 Comparison between equivalent static analysis and nonlinear time-history analysis

In this section, dynamic displacement and force demands predicted by equivalent static analysis (ESA) will be compared to the demands predicted by nonlinear time-history analysis. The verification study presented here focused on the robustness performance of a realistic composite floor system, an eight-storey two-dimensional frame with belt truss system, and an eight-storey three-dimensional building with belt truss system.

6.3.1 Realistic modeling of composite floor system

The UCB floor system discussed in section 4.3 of chapter 4 is studied here using equivalent static analysis (ESA). The robustness performance of the floor system under sudden removal of the perimeter column is studied using nonlinear time history analysis in chapter 4. Two types of fin plate connection are considered in the study. Here, the same nonlinear time-history analysis is repeated many times for various magnitudes of floor loading. The displacement time-history for each case with different floor weight (W) is plotted in Figure 6.3a and Figure 6.4a for systems adopting 3x1 connection and 5x1 connection respectively. Capacity curves of the floor system for both types of connections are generated based on equation (6.3). These capacity curves are shown in Figure 6.3b and Figure 6.4b for systems adopting 3x1 and 5x1 fin plate connections respectively. As shown in the same figures, the capacity curves derived from both ESA and nonlinear time-history analysis agree very well from small loading to high loading condition. The maximum difference between ESA and nonlinear time-history analysis is found to be about 7% only. The ESA can thus be utilized to perform quick and realistic robustness design in the practice. For example, the contribution of connection design to robustness performance of the floor system can be easily evaluated using ESA. As shown in Figure 6.5, adoption of stronger connection can reduce dynamic displacement by almost 50% for

most of the loading intensities. The static analysis used to generate the load-displacement curve requires only 15-25 minutes of computation, whereas each data point of the nonlinear time-history analysis requires about 90 minutes of computation. In nonlinear time-history analysis, a total of 16 data points are used to approximate the capacity curves for both floor systems. Therefore, application of ESA for the numerical study results in saving of computational time by approximately 70 times compared to nonlinear time-history analysis.

6.3.2 Two-dimensional frame with belt truss system

The two-dimensional frame discussed in section 5.3 of the previous chapter is studied here using ESA. The load-displacement curves of the frame with varying truss configurations and brace strengths are shown in Figure 6.6 to Figure 6.8. The curves are generated by using displacement-control nonlinear static analysis. Then, capacity curves for each of the system can be generated based on equation (6.3). The maximum displacements predicted by ESA and nonlinear time-history analysis are compared in Figure 6.9 for specimens with brace slenderness of $L/r = 170$ and different brace strength and truss configuration. It is evident that ESA is very accurate in prediction of displacement demand. Not only does ESA show reduction of displacement demand as brace strength increases, but also it can estimate the magnitude of displacement demands to reasonably good accuracy.

Based on the predicted displacement demand, the force demand can be determined directly from the load-displacement curves. The force demand is determined as the maximum capacity up to the estimated maximum displacement. Therefore, for hardening response like X-brace and N-brace belt trusses, the force demand corresponds to the maximum displacement predicted by ESA. However, for softening response like K-brace belt truss, the force demand can also be the ultimate load which may not occur at the maximum displacement predicted by ESA. In general, reasonably accurate prediction of force demand is observed by using ESA. From the comparison shown in Figure 6.10, it is evident that ESA is able to capture the general behaviors correctly. ESA is able to show

the magnitude of dynamic excitation (in term of DIF) is influenced by the brace strength and truss configuration. Similar to the findings of nonlinear time-history analysis, greater force demand is anticipated when too strong or too weak brace strength is used. Generally, ESA overestimates the DIF in most cases as compared to the results of nonlinear time-history analysis. For K-brace belt truss, maximum overestimation of DIF is found to be about 19%. For X-brace and N-brace belt trusses, the overestimation of DIF is found to be about 13%. As an approximate method (static analysis instead of dynamic analysis), the overestimation of ESA is acceptable when compared to the overestimation of current codified DIF of 2.0, which is found to be about 40%, 75% and 74% for K-brace, N-brace and X-brace belt trusses, respectively.

For member design, the column force can be obtained by assuming the equivalent static load pattern shown in Figure 5.5 of the previous chapter. The equivalent load pattern assumes that only the mass in the damaged bay is excited during column removal. This assumption is reasonable as the column force estimated by ESA compares well with nonlinear time-history analysis as shown in Figure 6.11. For belt truss specimens ($L/r =$ 170) with varying brace strength and truss configurations, the compression force in left column (LC) is shown to be marginally over-estimated. Similar to the trend of DIF, higher over-estimation of force demand is found in K-brace belt truss compared to N-brace and X-brace belt trusses. Maximum over-estimation of force demand in column LC is 28%, 15% and 12% for K-brace, N-brace and X-brace belt trusses, respectively. The overestimation of ESA is considered insignificant when compared to the overestimation of current codified DIF of 2.0, which is found to be about 56%, 40% and 39% for K-brace, N-brace and X-brace belt trusses, respectively.

6.3.3 Three-dimensional frame with belt truss system

The three-dimensional building discussed in section 5.5 of the previous chapter is studied here using ESA. The dynamic demands estimated by ESA and nonlinear time-history analysis are compared in Table 6.1. Static load-displacement curves for the 13 cases of column removal events are generated by using displacement-control nonlinear static

analysis. Then, capacity curve for each case is generated based on equation (6.3). The relationship between static weight of the damaged bay and maximum dynamic displacement can be obtained directly from the capacity curves. For illustration, the capacity curves for perimeter and corner column removal with belt truss installed at the top of building are shown in Figure 6.12. The unit area weight of the floor is 5.11 kN/m^2 for every floor of the building. Therefore the static weight of the damaged bay for Case 1 is 8 x 5.11 kN/m^2 x 6m x 18 m = 4415 kN, while the static weight for the damaged bay for Case 2 is half of the magnitude for case 1. From the capacity curve, maximum displacement is approximately 200 and 72 mm for case 1S(T) and 2L(T), respectively. The notation "(T)" denotes for belt truss positioned at top storey the building. The predicted demands are significantly lower than codified approach which uses DIF = 2.0. For all other cases, displacement demand predicted by ESA is tabulated in Table 5.5. As evident from the table, the prediction of ESA is only 23% to 50% higher than the prediction of nonlinear time-history analysis, compared to the prediction of codified approach which can differ by up to 727%! It should be noted that the improved accuracy offered by ESA requires almost the same computational demand and pre/post-processing effort as the codified approach.

The force absorbed by the structure in the damaged bay can be determined from the load-displacement curves as shown in Figure 6.12. For Case 1 and 2, the dynamic forces corresponding to dynamic displacement of 200 and 72 mm are about 5613 kN and 3233 kN respectively. The total force resisted by the supporting columns consists of dynamic component (from damaged bay) and static component (from adjacent undamaged bay). Therefore, the total column force envelope can be plotted as the sum of both components in Figure 6.13. For small brace section i.e. case 1S(T) and 1S(M), force envelope in supporting column C1 compares very well with nonlinear time-history analysis. "(T)" denotes for belt truss positioned at top storey the building, whereas "(M)" denotes for belt truss positioned at mid-height of the building. However, for larger brace, i.e. Cases 1L(T) and 1L(M), over-estimation of column force in the supporting column C1 is observed. The main reason for this inconsistency is attributed to the difference in estimation of displacement demand. For a structural system that undergoes severe

inelasticity, e.g. Cases 1S(T) and 1S(M), the slope of capacity curve is smaller than one that behaves elastically. Therefore over-estimation of force demand as a result of over-estimated displacement demand is significantly higher for a stronger system. By using displacement from nonlinear time-history analysis instead of ESA to estimate the column force demand, significantly better estimation can be achieved as shown as curve (*–*–*) in Figure 6.13. For most practical structures that undergo considerable inelasticity, estimation of column force demand using ESA should be reasonably accurate. On the other hand, marginal underestimation of the tension force in the damage column D1 is observed. This can be caused by fundamental difference between dynamic analysis and static analysis, i.e. inertia forces are ignored in the latter. The difference is less critical as the magnitude is negligible compared to ULS force.

6.4 Concluding remarks

1. This chapter discusses methodology and validation of Equivalent Static Analysis (ESA) for robustness evaluation of building. ESA adopts energy balance concept to estimate dynamic displacement and force demands of a building from its static response. As a result, significant saving in computational resource can be achieved with the use of nonlinear static analysis instead of nonlinear time-history analysis.

2. Until now, study on accuracy of ESA has been limited to simplified frame structures with small degree of freedom. To the best knowledge of the candidate, no study on application of ESA on large and realistic building system has been reported in the literature. In view of the potential benefits of ESA, verification studies are carried out in this chapter by comparing the dynamic demands predicted by ESA and nonlinear time-history analysis for large and realistic building systems. The findings presented in this chapter provide new evidence that ESA can also be reasonably accurate in estimation of displacement and force demands of large and realistic building systems when subjected to sudden column removal.

3. The verification study presented in this chapter focuses on the robustness performance of a realistic composite floor system, an eight-storey two-dimensional

frame with belt truss system, and an eight-storey three-dimensional building with belt truss system. By taking nonlinear time-history analysis as the reference, the comparison study shows that the results of ESA are always more consistent and accurate than the results of current codified method although both methods require practically the same computation effort. Therefore, it is recommended that the current codified method be replaced by ESA as a design tool in the practice. Hence, ESA can be useful in the preliminary stage of building design, in which fast and reasonably accurate analysis (instead of time-consuming nonlinear time-history analysis) is required.

Table 6.1: Displacement and global force demands of Cardington 3D building when subjected to different cases of "sudden" column removal: Comparison between nonlinear time-history analysis (NLTH) and ESA prediction

Case	Column loss	Brace section	BT position	Max. vertical displacement (mm)		
				NLTH	ESA	Codified
1	1D1	-	-	860	1061(1.23)	1156(1.34)
1S(T)		80x5	Top	134	200 (1.49)	784 (5.85)
1S(M)			Mid	131	189 (1.44)	792 (6.05)
1L(T)		150x8	Top	44	57 (1.25)	116 (2.64)
1L(M)			Mid	31	43 (1.39)	99 (3.19)
2	1A1	-	-	675	920 (1.36)	-
2S(T)		60x4	Top	53	72 (1.36)	341 (6.43)
2S(M)			Mid	44	62 (1.48)	320 (7.27)
2L(T)		80x5	Top	35	48 (1.37)	105 (3.00)
2L(M)			Mid	26	39 (1.50)	91 (3.50)
3	4A1	-	-	698	926 (1.33)	-
3a(T)		60x4	Top	27	37 (1.37)	57 (2.11)
3a(M)			Mid	696	918 (1.32)	-

Note: 80x5 denotes square hollow section of 80 mm width and 5 mm thickness

value in parentheses ( ) denotes the ratio of predicted response to NLTH response

(a) before column removal

(b) displacement after column removal
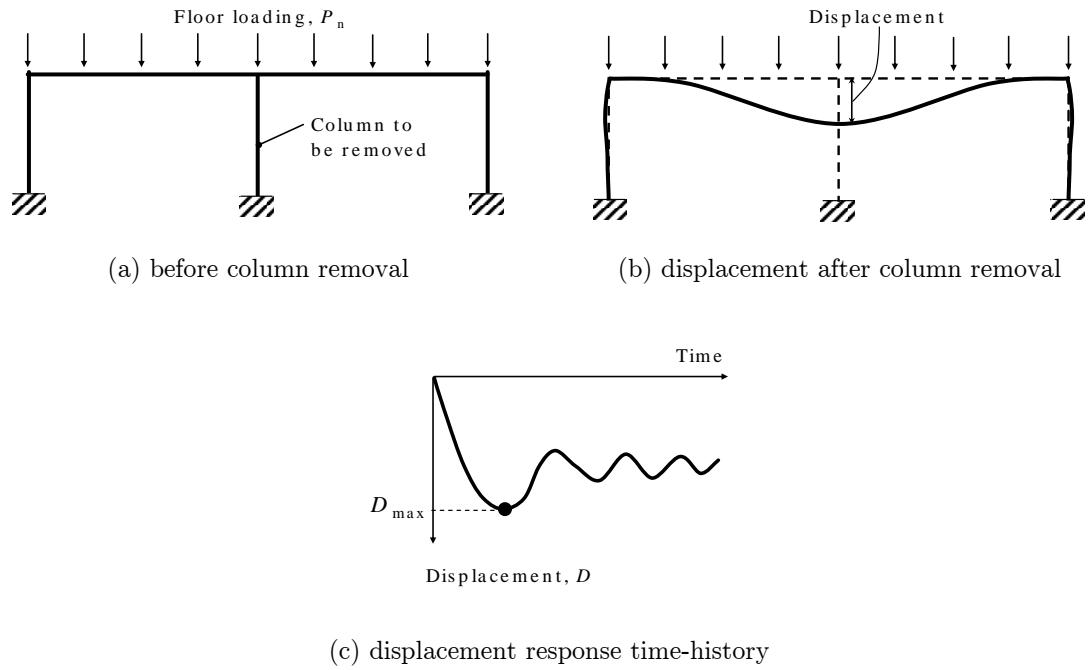

(c) displacement response time-history

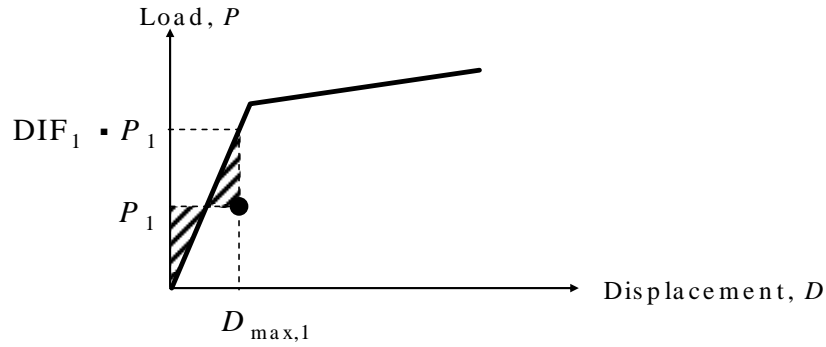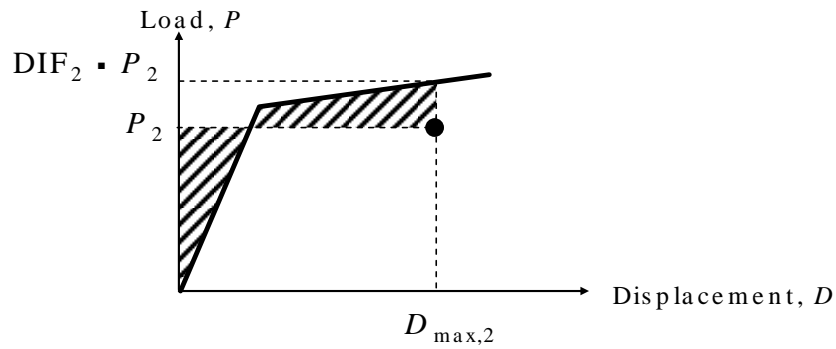Figure 6.1: Dynamic response of simple frame due to sudden column removal

(a) state of energy balance when $P = P_1$ and $D = D_{max,1}$ (elastic response)

(b) state of energy balance when $P = P_2$ and $D = D_{max,2}$ (inelastic response)
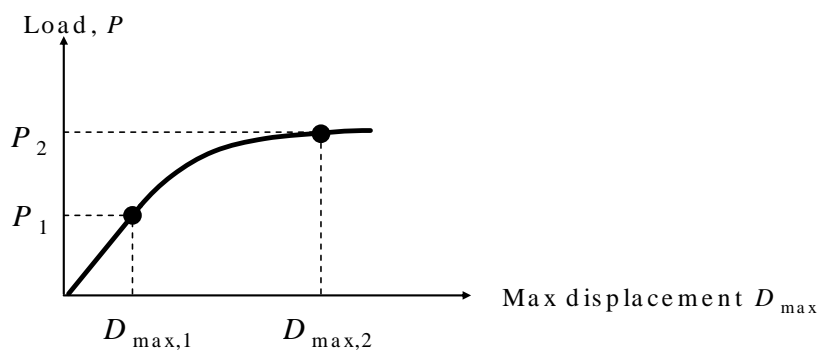
(c) capacity curve: relationship between gravity load and maximum displacement

Figure 6.2: States of energy balance for simple frame and corresponding capacity curve
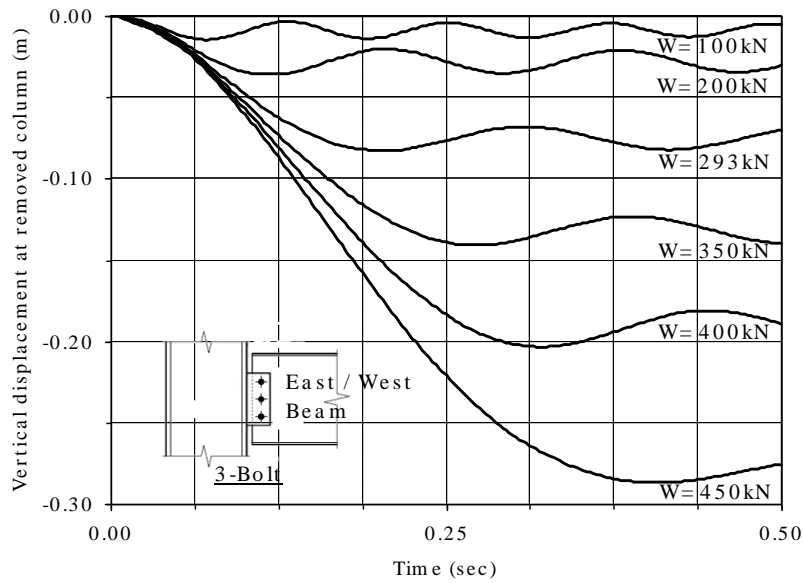
(a) displacement time-history due to sudden column removal from NLTH analysis
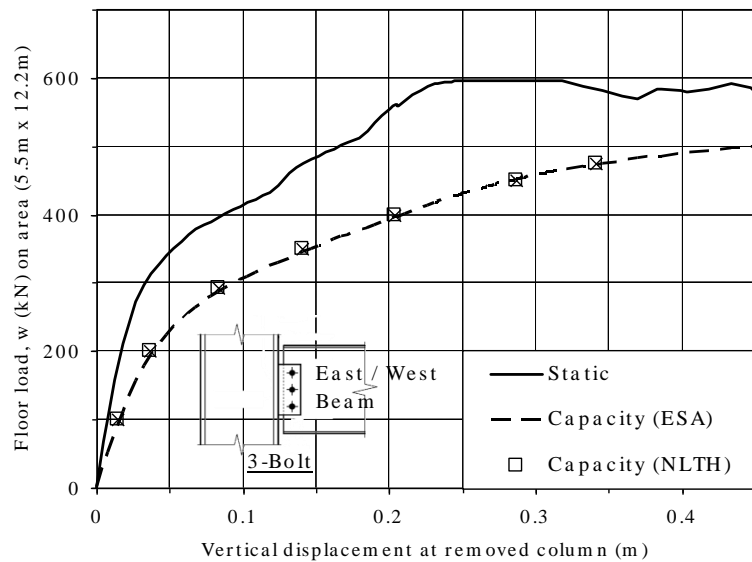
(b) capacity curve of UCB floor due to sudden column removal

Figure 6.3: Displacement time-history and capacity curve of UCB floor (3x1 fin plate connection) due to sudden column removal: Comparison between equivalent static analysis (ESA) and nonlinear time-history (NLTH) methods

194
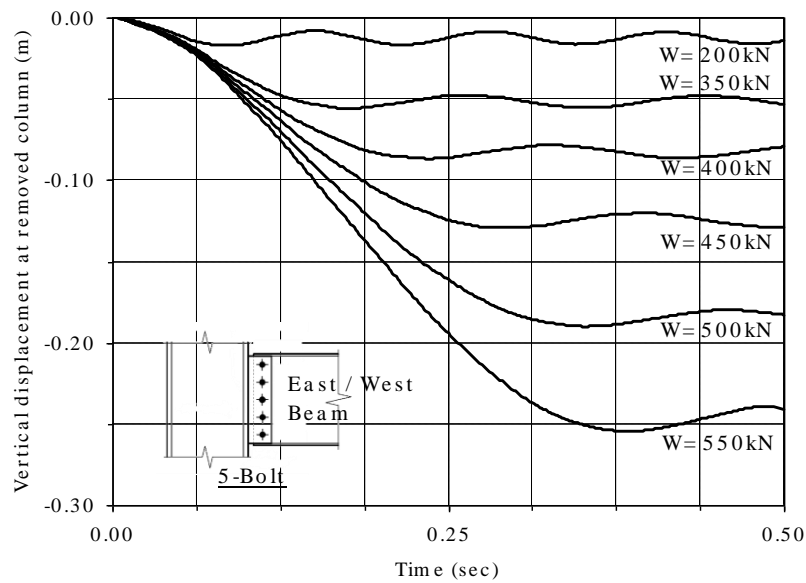
(a) displacement time-history due to "sudden" column removal from NLTH analysis
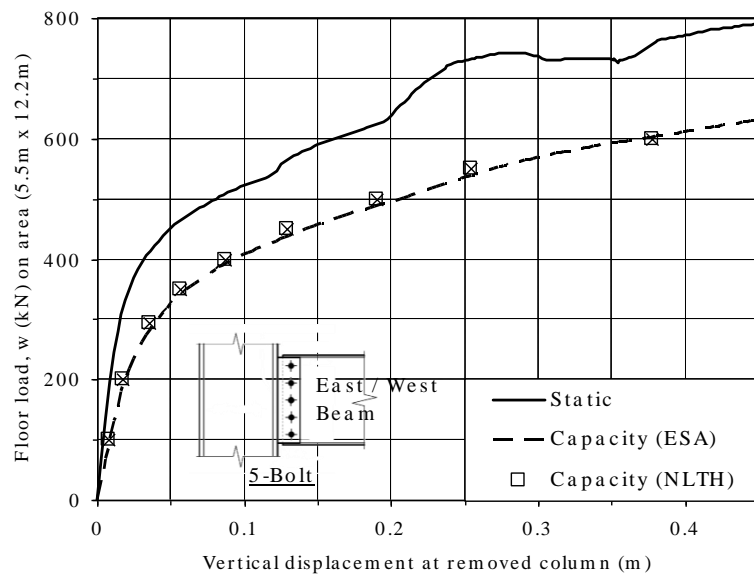
(b) capacity curve of UCB floor due to "sudden" column removal

Figure 6.4: Displacement time-history and capacity curve of UCB floor (5x1 fin plate connection) due to "sudden" column removal: Comparison between equivalent static analysis (ESA) and nonlinear time-history (NLTH) methods

195
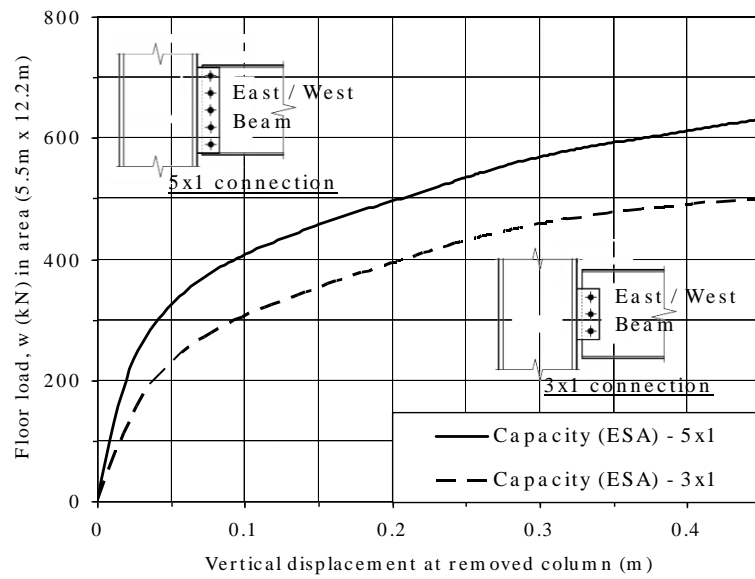
Figure 6.5: Influence of connection design on capacity of UCB floor under sudden column removal
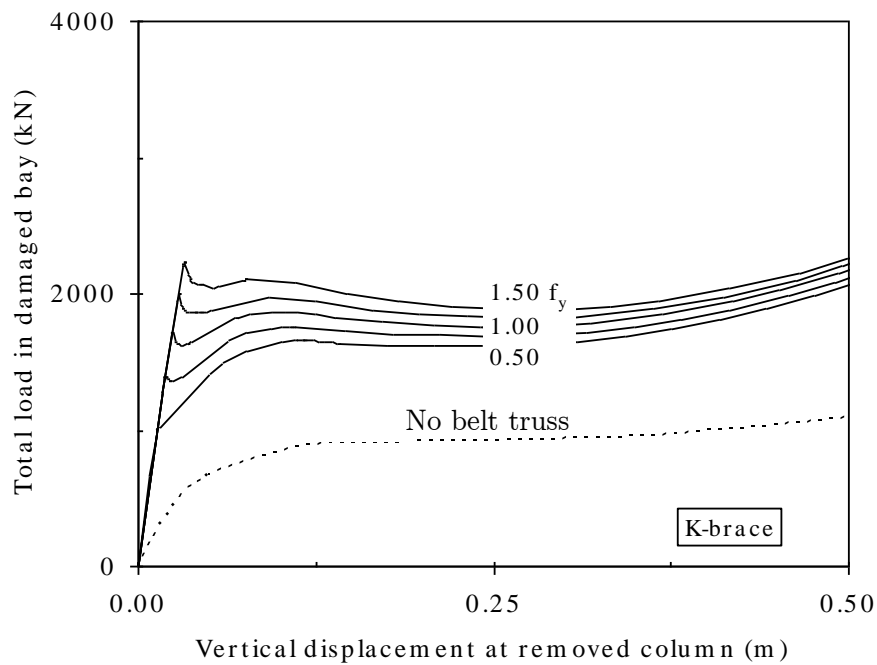
Figure 6.6: Load-displacement relationships of 2D frame with K-brace belt truss of varying strength
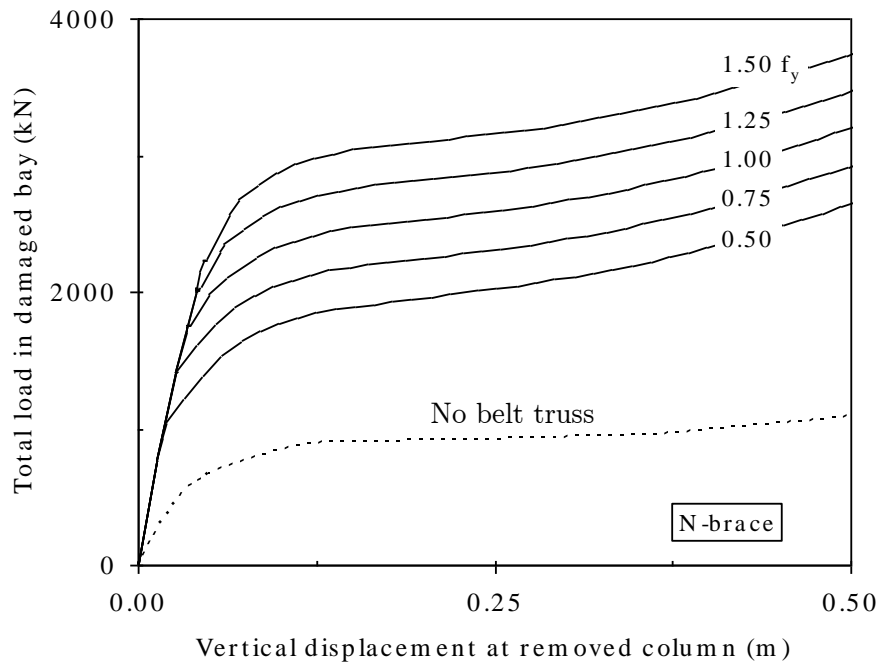
Figure 6.7: Load-displacement relationships of 2D frame with N-brace belt truss of varying strength
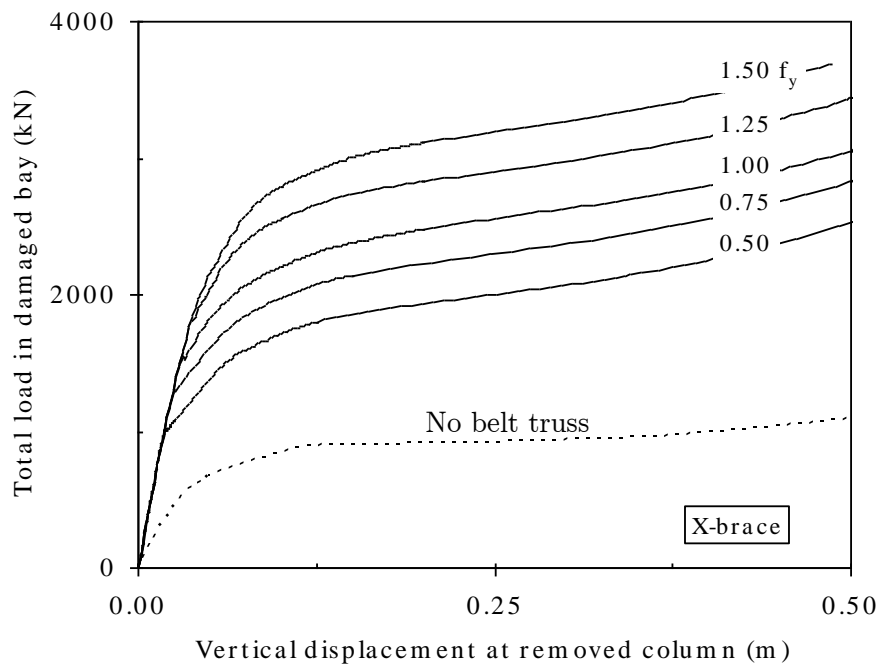
Figure 6.8: Load-displacement relationships of 2D frame with X-brace belt truss of varying strength

(a) K, N and X brace belt truss

(b) K-brace belt truss

(c) N-brace belt truss

(d) X-brace belt truss
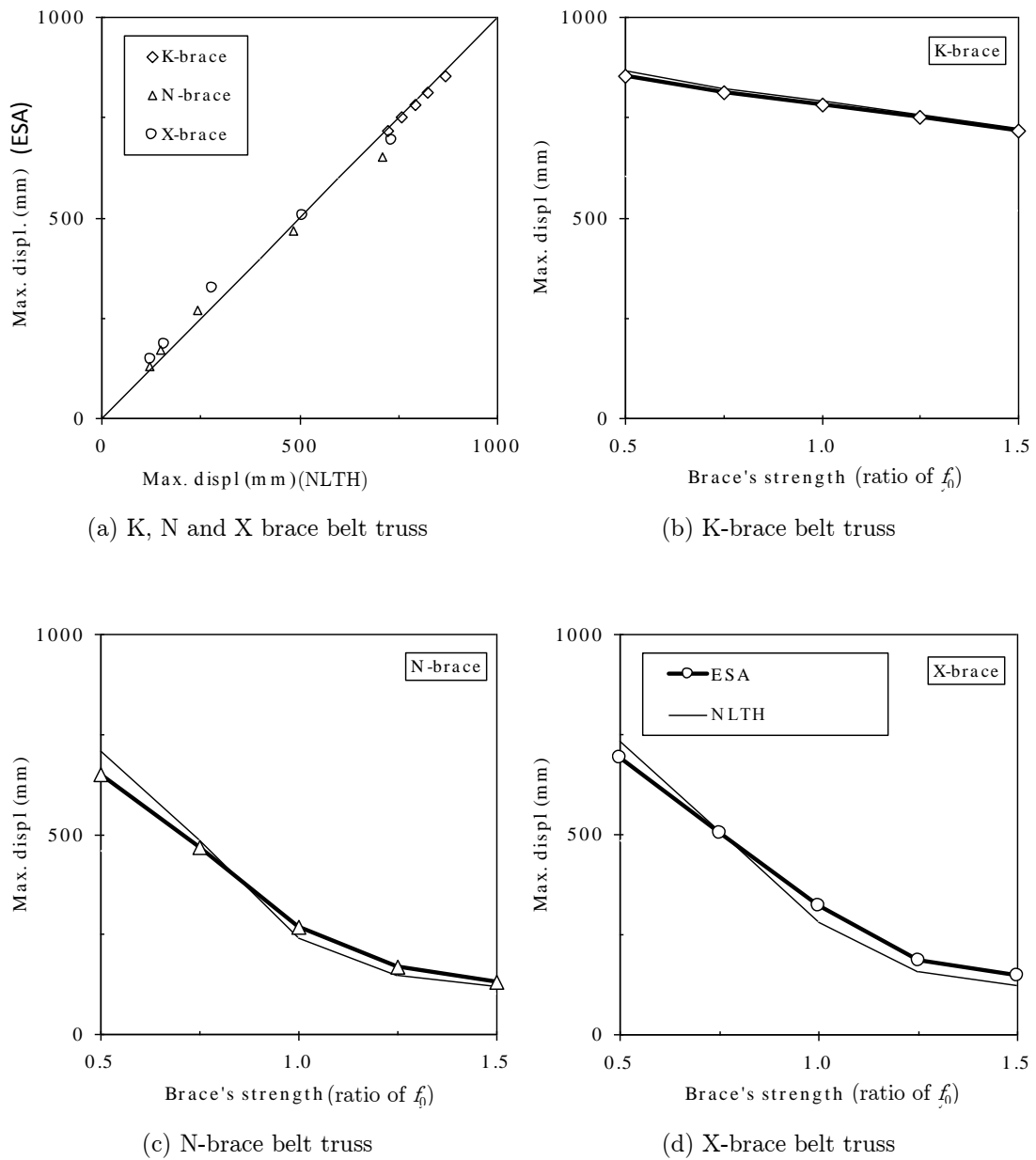
Figure 6.9: Accuracy of equivalent static analysis (ESA) in estimation of global displacement demand

(a) K, N and X brace belt truss

(b) K-brace belt truss

(c) N-brace belt truss

(d) X-brace belt truss
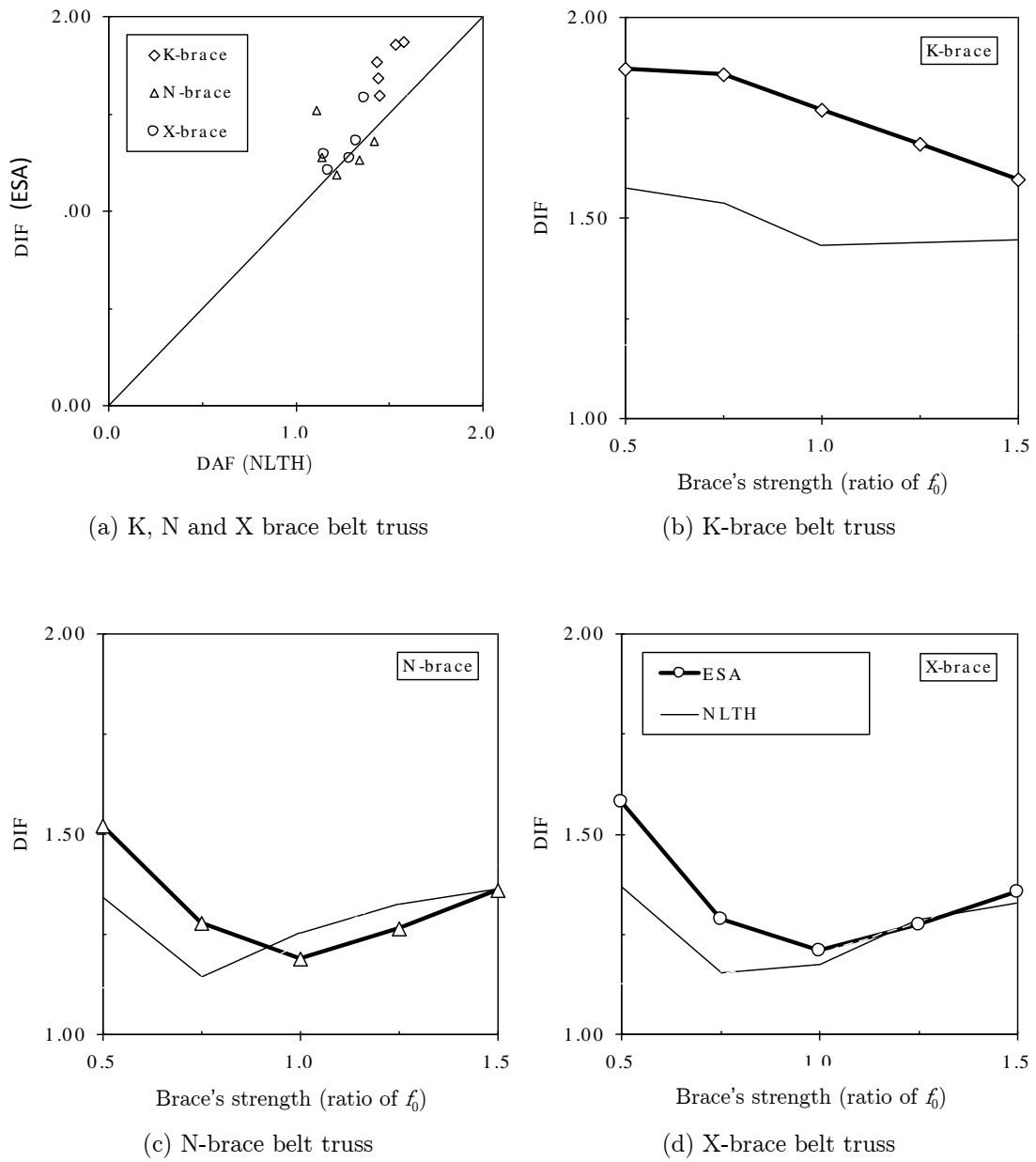
Figure 6.10: Accuracy of equivalent static analysis (ESA) in estimation of global force demand

(i) 0.75 f_0 (ii) 1.00 f_0 (iii) 1.25 f_0 (iv) 1.50 f_0

(a) Column LC or RC of K-brace belt truss

(i) 0.75 f_0 (ii) 1.00 f_0 (iii) 1.25 f_0 (iv) 1.50 f_0

(b) Column LR or RC of X-brace belt truss

(i) 0.75 f_0 (ii) 1.00 f_0 (iii) 1.25 f_0 (iv) 1.50 f_0

(c) Column RC of N-brace belt truss
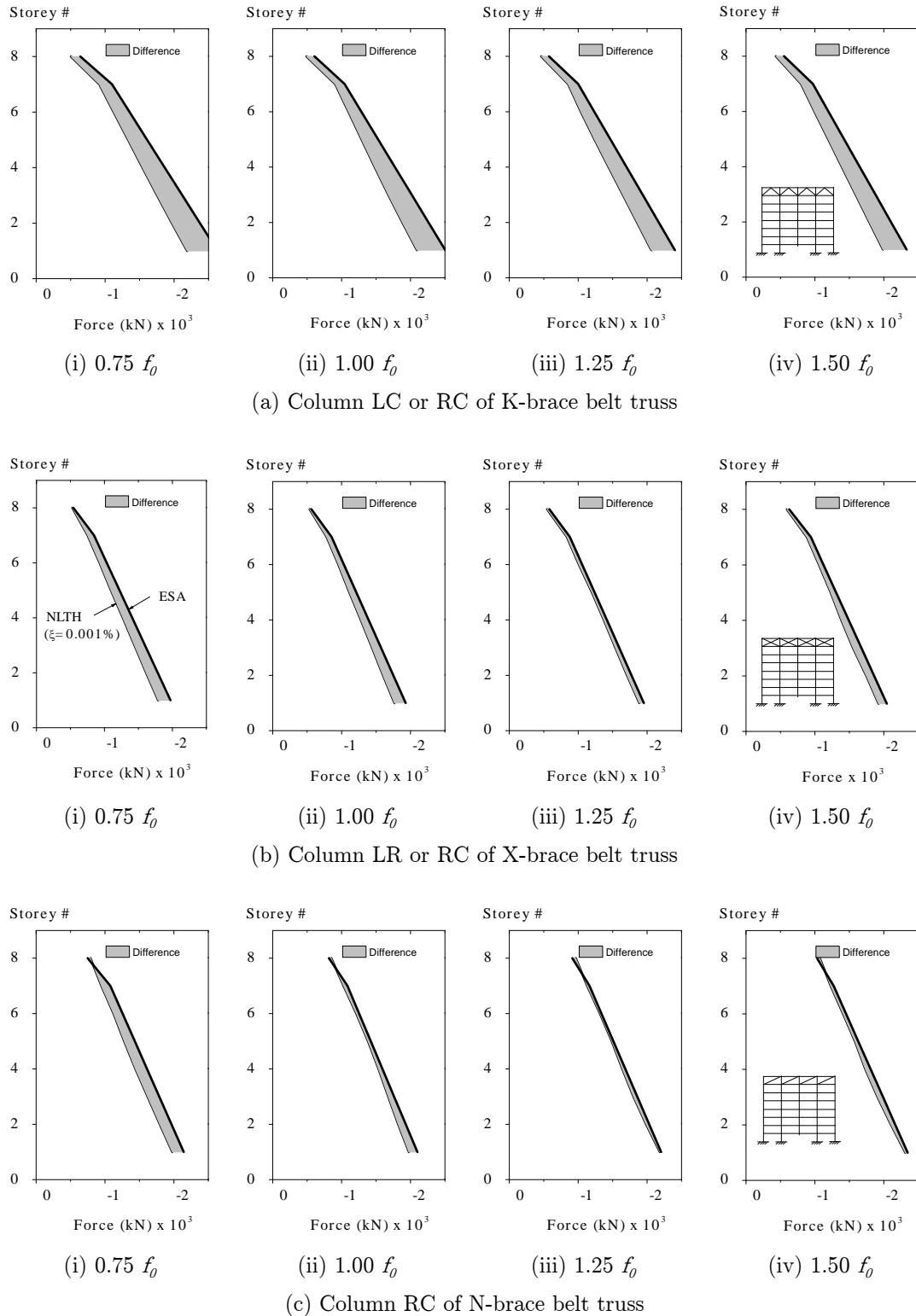
Figure 6.11: Accuracy of equivalent static analysis (ESA) in estimation of column force demand
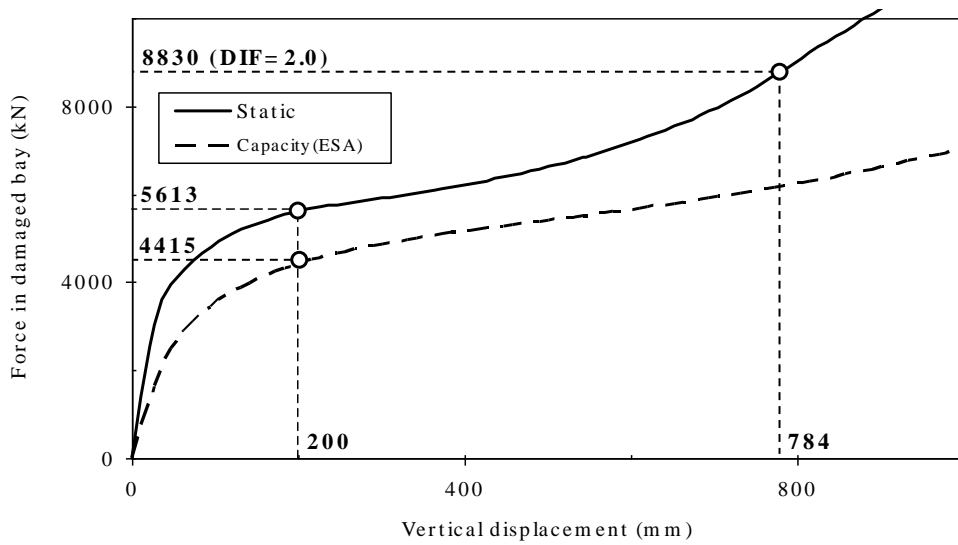
(a) Case 1S(T): Removal of 1st storey perimeter column D1
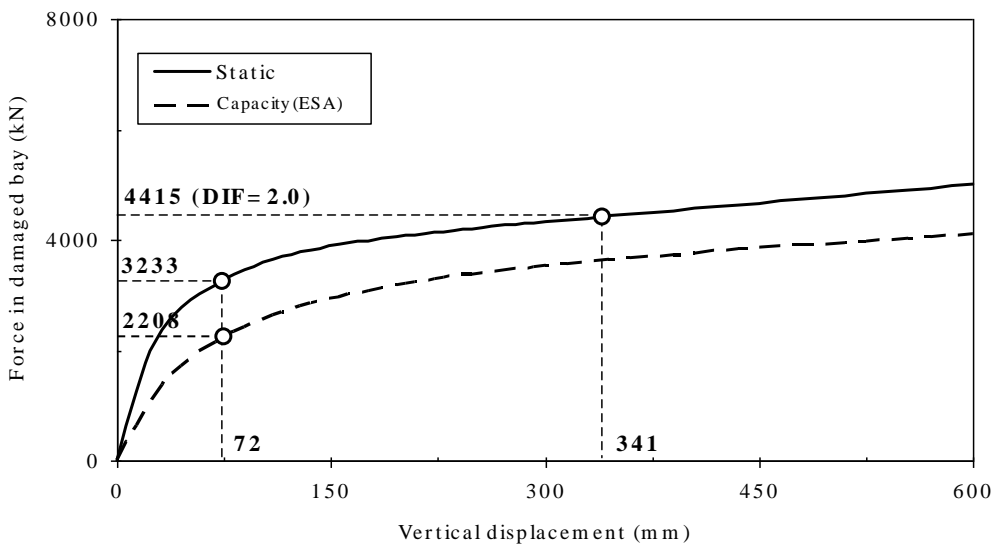
(b) Case 2S(T): Removal of 1st storey corner column A1

Figure 6.12: Static response of Cardington building due to perimeter and corner column removal

(a) Belt truss at top (1.0H)

(b) Belt truss at mid-height (0.5H)
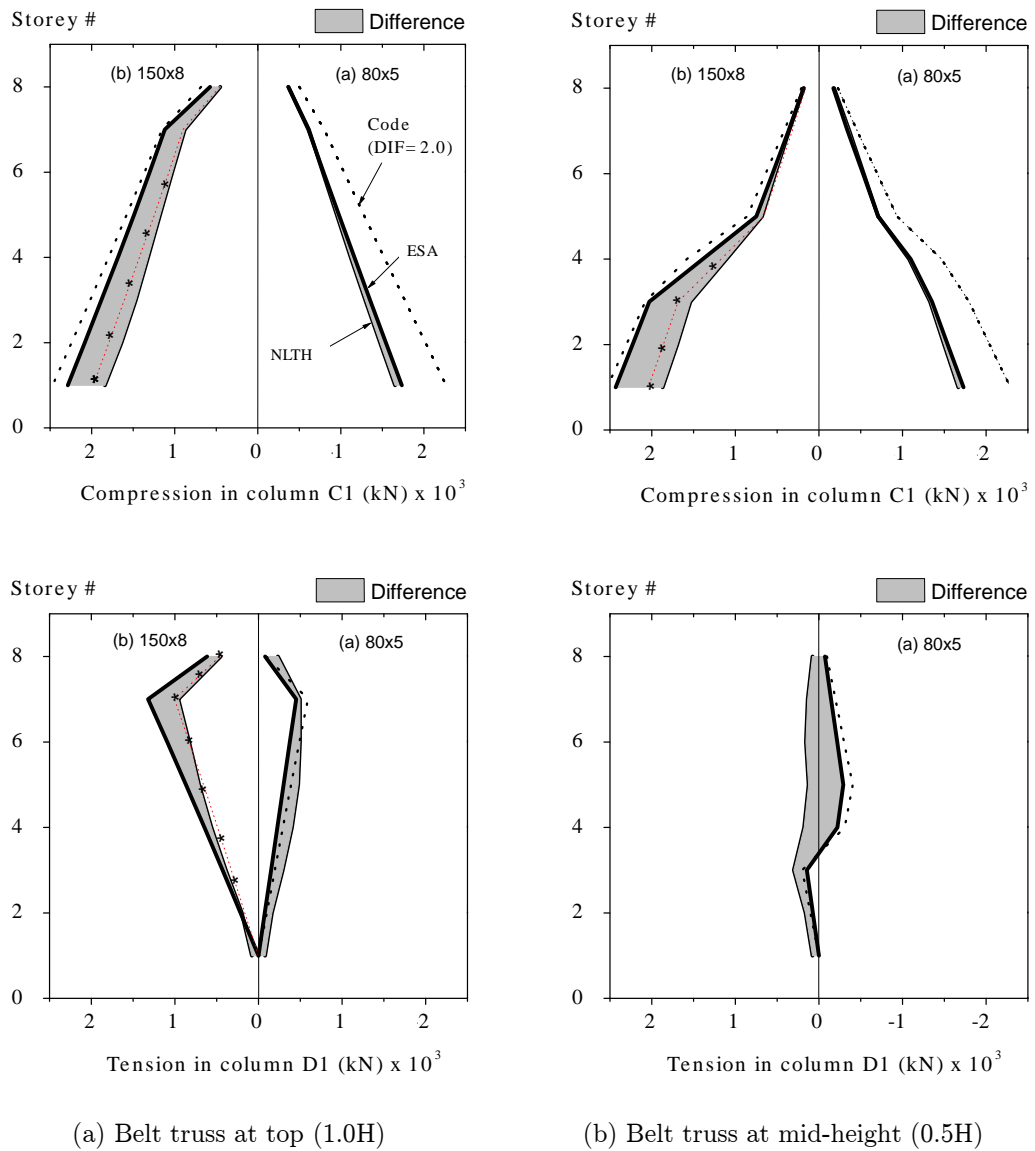
Figure 6.13: Accuracy of equivalent static analysis (ESA) in estimation of column force (Case 1)

This page intentionally left blank

Chapter 7: Conclusions and Recommendations

7.1 Conclusions

Literature review shows that current progressive collapse analysis tends to be either too sophisticated (hence computationally inefficient) or too simplified (hence inaccurate) for evaluation of building robustness in the design practice. To overcome this, an efficient progressive collapse analysis (ePCA) method is proposed in this thesis. ePCA is essentially a novel modeling approach to maintain the efficiency of simplified finite element analysis yet of producing reasonably accurate results for realistic robustness evaluation. In addition, ePCA allows distinct damage behaviors of main structural components to be modeled consistently using the same plastic zone method. This consistent nature not only makes it easier for users to use only a single damage model, but also avoids the use of sophisticated constitutive model (2D or 3D) for material damage.

7.1.1 Efficient progressive collapse analysis

The strength of ePCA lies in the efficient and consistent manner in which the main structural components of a composite building, i.e. steel frames, composite floor slabs and steel connections, are modeled. The proposed beam-column model for analysis of steel frame is based on the plastic zone method. It captures the influences of material and

geometry imperfections, and the spread-of-plasticity behaviors across-section and along-member of the steel frames. The proposed slab model is based on the modified-grillage method, capturing the flexural response of slab using a grillage method, and the membrane response of slab using a truss analogy. Material damage of the grillage member is also modeled consistently using the same plastic zone method. For fin plate shear connections, spring model proposed by Sadek et al. (2008) is adapted with minor modification to replace the original spring model by an equivalent plastic zone element. This modification is important to simplify modeling of large building systems. All of the proposed numerical models have shown good agreement with numerical and experimental findings from the literature. In addition to computational efficiency and reasonably accurate results, ePCA also retains the simplicity of conventional frame analysis commonly used in the design practice. These features are keys to effective implementation of robustness design in the practice.

7.1.2 Robustness design of composite floor system

In chapter 4, the ePCA method is used to study progressive collapse resistance of large and realistic composite floor systems. Two critical cases, i.e. internal and perimeter column removal are studied. Comparison with experimental and numerical results from the literature shows reasonable accuracy of ePCA for performance evaluation of large and realistic floor system. The study shows that it is crucial to include the membrane action of floor slab in the modeling, as it plays an important role in collapse resistance in two ways, i.e. (a) it enhances load-carrying capacity of floor system by catenary action, and (b) it resists the out-of-balance force of catenary action in slab and restrains the column from being pulled inward. By using the proposed ePCA, these important behaviors can be simulated with sufficient accuracy for robustness evaluation in the practice without the need of computationally demanding detailed finite element analysis.

The use of ePCA instead of detailed finite element analysis can significantly reduce the computational time and pre/post-processing effort. For the study of NIST floor system, the model based on ePCA method consists of only 996 frame elements compared to

295,000 solid and shell elements used in detailed finite element analysis by Sadek et al. (2008) and Alashker et al. (2010). Based on a conservative estimate, the use of ePCA instead of detailed FEA can save computational time by as much as 22,000 times. Unlike simplified FEA which normally leads to poor prediction of the progressive collapse resistance, prediction of ePCA however has shown to compare reasonably well with detailed FEA. Out of 7 cases considered in the study, the absolute differences between the results of ePCA and detailed FEA average only about 5%.

The collapse resistance can be efficiently improved by thicker steel deck, more slab reinforcement and stronger connection. When a floor system is subjected to column removal, the study shows that stronger connection improves initial stiffness and inelastic capacity in small-deformation response, while the slab reinforcement and steel deck improves the inelastic capacity in large-deformation response. Therefore, strong and ductile shear connection together with sufficient slab reinforcement and effective deck continuity can be a cost effective strategy for enhancing the robustness of composite floor system. When designing shear connection, brittle failure modes e.g. shear failure of bolts, should be avoided to ensure sufficient ductility and post-ultimate resistance in the inelastic response.

7.1.3 Robustness enhancement of composite building using belt truss system

Another robustness enhancement strategy studied in the thesis is the use of belt truss system for multi-storey building. The study shows that belt truss system is very effective in reducing the displacement demand of building when subjected to sudden column removal. It also reveals a counter-intuitive finding, i.e. an excessively strong belt truss is not necessarily beneficial as it tends to induce large force demand in the supporting columns. Therefore adequate (but not excessive) brace member should be used for designing new building and retrofitting existing building. The position of belt truss has negligible influence of displacement demand, but can greatly influence the distribution of force demand in supporting columns. The study shows that providing belt truss at upper

storey can lead to high column force demand at upper storey column. On the other hand, the truss configuration and slenderness of brace member can also influence the robustness performance of building although their effects are less significant as compared to the two factors mentioned above.

Robustness enhancement strategies have been conceptualized based on findings of the behavioral study. For design of new building, X-brace belt truss with high slenderness ratio is preferred. The position of belt truss is dependent on building height. For belt truss to be effective, it should be provided above the level where column removal is most likely to occur. Therefore, belt truss should be provided at the highest storey to prevent disproportionate collapse in case of damage (or complete removal) of any column in lower storeys. This robustness enhancement strategy can increase the force demand in supporting column in proximity of column removal. For low-rise building, column force demand is normally contained within the requirement under normal design condition (i.e. Ultimate Limit State), and no increase of material cost is anticipated for the column. On the other hand, adopting the same strategy for medium-rise and high-rise buildings may lead to excessive column force demand at upper storeys of the building. In this case, multiple belt trusses will be required to control the force demand. Providing more belt trusses leads to smaller column force demands but increases construction cost. The study based on 20-storey building shows that provision of belt truss for every 10 storeys is effective for robustness enhancement of high-rise buildings. This rule of thumb may be adopted in the preliminary design of new buildings.

The strategy recommended for design of new buildings may not be practical for retrofit of existing building. This is because retrofit of existing building at high-elevation may be more difficult and costly as compared to construction of new buildings. Therefore belt truss should be installed at one of the lowest storeys, but at a sufficient distance away from ground level to avoid being directly damaged by bomb explosion at ground level or vehicular impact. This strategy is only effective to prevent disproportionate collapse caused by failure of column on or near the ground level, which can be triggered by accidental events at the ground level e.g. bomb explosion, vehicular impact etc. Therefore, this strategy is recommended for retrofitting existing buildings against terrorist attack.

7.1.4 Equivalent static analysis for practical robustness design

Engineers prefer static analysis to dynamic analysis due to its simplicity and computational efficiency in design. Nevertheless, the solution accuracy may be seriously in doubt unless a rational static approach takes into account the key features of the response. In the context of structural robustness, previous works have shown that codified static method with dynamic increase factor of 2.0 can lead to very conservative estimate of the dynamic demands in terms of force and displacement. As an alternative, the equivalent static analysis (ESA) based on energy balance has been shown to produce good estimate of the dynamic demands, but the study has been mainly limited to simple frame structures. In this thesis, the validity of ESA for robustness evaluation of large and realistic composite floor systems and composite building is examined. The numerical examples consists of a steel-concrete composite floor system and a 8-storey composite building incorporating belt truss system subjected to sudden removal of column. Based on comparison with the results obtained by a detailed dynamic analysis, the findings show that ESA is capable of producing reasonably good estimate of the maximum force and displacement demands, for both elastic and inelastic responses. In contrast, the codified static method can only estimate the demands well for the elastic response but significantly overestimate the demands for the inelastic response. Since the computational efforts are about the same, the ESA approach is recommended instead of the codified static method for robustness check.

Until now, study on accuracy of ESA has been limited to simplified frame structures. To the best knowledge of the candidate, no study on application of ESA on large and realistic building system has been reported in the literature. Therefore, the findings presented in chapter 6 provide new evidence that ESA can be reasonably accurate in estimation of displacement and force demands of large and realistic building systems when subjected to sudden column removal.

7.2 Recommendations for future research

1. The proposed ePCA should be extended to model progressive collapse behavior of main structural components of reinforced concrete building with minor modification. The same plastic zone method can also be used to model nonlinear behaviors of reinforced concrete members (i.e. beam and column) with proper fiber section to represent the nonlinear cross-sectional response.

2. Verification study shows that the prediction of ePCA compares reasonably well with the findings of experimental and numerical study. The examples used in verification study consist of composite floor systems with regular layout. For future study, experimental study involving composite floor systems with irregular layout should be carried out to validate the accuracy of ePCA.

3. In addition to belt truss system studied in chapter 5, future research can utilize the computational efficiency of ePCA to study other innovative structural systems that excel in robustness performance. Some possible structural systems that have good robustness performance are knee-brace truss, eccentrically-braced truss, viereendeel truss etc.

4. It is common to use concrete infill tubular section for brace member of outrigger and belt trusses for tall buildings. The beam-column model proposed in chapter 2 should be improved to model nonlinear response of the composite member, so that robustness performance of such system can be evaluated with reasonable accuracy.

References

ABAQUS (2005). *ABAQUS/Standard user's manual.* Version 6.5. ABAQUS Inc., Providence, Rhode Island.

Abdullah, R., and Samuel Easterling, W. (2009). "New evaluation and modeling procedure for horizontal shear bond in composite slabs." *Journal of Constructional Steel Research*, 65(4), pp. 891-899.

AISC (2005). *AISC 360-05: Specification for structural steel buildings*, American Insititute of Steel Construction, Chicago, Illinois.

Alashker, Y., El-Tawil, S., and Sadek, F. (2010). "Progressive collapse resistance of steel-concrete composite floors." *Journal of Structural Engineering*, 136(10), pp. 1187-1196.

Allen, D. E., and Schriever, W. R. (1972). "Progressive collapse, abnormal loads, and building codes." *Structural Failures: Modes, Causes, Responsibilities*, ASCE, New York, 21-47.

Al-Jabri, K. S., Burgess, I. W., and Plank, R. J. (2005). "Spring-stiffness model for flexible end-plate bare-steel joints in fire." *Journal of Constructional Steel Research*, 61(12), pp. 1672-1691.

Bailey, C. G., White, D. S., and Moore, D. B. (2000). "The tensile membrane action of unrestrained composite slabs simulated under fire conditions." *Engineering Structures*, 22(12), pp. 1583-1595.

BCSA (2002). *Joints in steel construction: Simple connections*, London, UK.

Beedle, L. S., and Tall, L. (1960). "Basic column strength." *Journal of Structural Engineering*, 86(5), pp. 139-173.

Beer, H., and Schultz, G. (1970). "Theoretical basis for the European column curves." *Construction Metallique* (3), pp. 58.

Bignell, V., Peters, G., Pym, C. and Hunter-Brown, C. (1977). *Catastrophic failures*, Open University Press, Milton Keynes.

Bjorhovde, R. (1972). "Deterministic and probabilistic approaches to the strength of steel Columns." Ph.D. dissertation, Lehigh University, Bethlehem, Pa.

Bjorhovde, R., and Birkemoe, P. O. (1979). "Limit states design of H.S.S. columns." *Canada Journal of Civil Engineering*, 8(2), pp. 276-291.

Bjorhovde, R., and Tall, L. (1971). "Maximum column strength and the multiple column curve concept." Lehigh University, Bethlehem, Pa.

Black, R. G., Wenger, W. A., and Popov, E. P. (1980). "EERC-80/40: Inelastic buckling of steel struts under cyclic load reversal." Berkeley: Earthquake Engineering Research Centre. University of California.

Blandford, G. E. (1996). "Progressive failure analysis of inelastic space truss structures." *Computer and Structures*, 58(5), pp. 981-990.

British Steel (1998). "The behaviour of a multi-storey steel framed building subjected to fire attack." British Steel Plc, UK.

BSI (1997). *Structural use of concrete - Part 1. Code of practice for design and construction*, British Standard Institute.

BSI (2000). *BS 5950: Structural use of steelwork in building. Part 1: Code of practice for design - Rolled and welded sections*, British Standard Institute.

BSI (2004a). *BS EN 1992-1-1:2004 Design of concrete structures. Part 1: General rules and rules for buildings*, British Standard Institute.

BSI (2004b). *BS EN1994-1-1:2004 Design of composite steel and concrete structures. Part 1.1: General rules and rules for buildings*, British Standards Institute.

BSI (2005a). *Eurocode 3: Design of steel structures. Part 1-1: General rules and rules for buildings*, British Standard Institute.

BSI (2005b). *Eurocode 3: Design of steel structures. Part 1-8: Design of joints*, British Standard Institute.

BSI (2006). *BS EN 1991-1-7:2006 Eurocode 1 Actions on structures. Part 1-7: General actions: Accidental loads*, British Standard Institute.

Chan, S. L. (2001). "Review: Non-linear behaviour and design of steel structures." *Journal of Constructional Steel Research*, 57, pp. 1217-1231.

Chen, W. F. (2008). "Advanced analysis for structural steel building design." *Frontiers of Architecture and Civil Engineering in China*, 2(3), pp. 189-196.

CSA (1984). "CAN3-S16.1-M84: Steel structures for buildings - Limit states Design." Canadian Standards Association.

CSI (2009). *CSI analysis reference manual for SAP2000, ETABS, and SAFE*, Computer & Structures INC, Berkeley, California.

Corley, W. G., Mlakar, P. F., Sozen, M. A., and Thornton, C. H. (1998). "The Oklahoma City bombing: Summary and recommendations for multihazard mitigation." *Journal of Performance of Constructed Facilities*, 12(3), pp. 100-112.

Davison, B., and Owens, G. W. (2003). *Steel designers' manual*, Blackwell Publishing.

Delatte, N. J. (2009). *Beyond failure : forensic case studies for civil engineers*, American Society of Civil Engineers, Reston, Va.

DoD (2009). "UFC 4-023-03 : Design of buildings to resist progressive collapse." US Department of Defense.

ECCS (1983). "Ultimate limit state calculation of sway frames with rigid joints." European Convention for Constructional Steelwork.

Elghazouli, A. Y., and Izzuddin, B. A. (2001). "Analytical assessment of the structural performance of composite floors subject to compartment fires." *Fire Safety Journal*, 36(8), 769-793.

Elghazouli, A. Y., and Izzuddin, B. A. (2004). "Realistic modeling of composite and reinforced concrete floor slabs under extreme loading. II: Verification and application." *Journal of Structural Engineering*, 130(12), pp. 1985-1996.

Ellingwood, B. R. (2006). "Mitigating risk from abnormal loads and progressive collapse." *Journal of Performance of Constructed Facilities*, 20(4), pp. 315-323.

Ellis, B. R., and Ji, T. (1996). "Dynamic testing and numerical modeling of the Cardington steel framed building from construction to completion." *The Structural Engineer*, 74(11), pp. 186-192.

El-Dardiry, E., and Ji, T. (2006). "Modelling of the dynamic behaviour of profiled composite floors." Engineering Structures, 28, p.p 567-579.

Jain, A. K., Goel, S. C., and Hanson, R. D. (1978). "UMEE 78R3: Hysteresis behaviour of bracing members and seismic response of braced frames with different proportions." *Rep.*, submitted to the University of Michigan, Ann Arbor.

Jiang, X. M., Chen, H., and Liew, J. Y. R. (2002). "Spread-of-plasticity analysis of three-dimensional steel frames." *Journal of Constructional Steel Research*, 58, pp. 193-212.

Jofriet, J. C., and McNeice, G. M. (1971). "Finite element analysis of reinforced concrete slabs." *J. Struct. Div.*, 97(3), pp. 785-806.

FEMA (1996). *The Oklahoma City Bombing: Improving building performace through multi-hazard mitigation*, Federal Emergency Management Agency, Washington, DC.

FEMA (2000). "FEMA 355D: State of the art report on connection performance." Federal Emergency Management Agency, New York.

FEMA (2002). "FEMA 403: World Trade Center building performance study: Data collection, preliminary observations, and recommendations." Federal Emergency Management Agency, New York.

Fu, F. (2009). "Progressive collapse analysis of high-rise building with 3-D finite element modeling method." *Journal of Constructional Steel Research*, 65(6), pp. 1269-1278.

Griffiths, H., Pugsley, A., and Saunders, O. A. (1968). *Report of the inquiry into the collapse of flats at Ronan Point, Canning Town ; presented to the Minister of Housing and Local Government*, , H.M.S.O., London.

GSA (2003). "Progressive collapse analysis and design guidelines for new federal office buildings and major modernization projects." US General Services Administration.

Hallquist, J. (2006). *LS-DYNA keyword user's manual*. Version 971, Livermore Software Technology Corporation, Livermore, California.

Hayes, J. R., Woodson, S. C., Pekelnicky, R. G., Poland, C. D., Corley, W. G., and Sozen, M. (2005). "Can strengthening for earthquake improve blast and progressive collapse resistance?" *Journal of Structural Engineering*, 131(8), pp. 1157-1177.

Hill, C. D., Blandford, G. E., and Wang, C. T. (1989). "Post-buckling analysis of steel space trusses." *Journal of Structural Engineering*, 115(4), pp. 900-919.

Hinman, E. E., and Hammond, D. J. (1997). *Lessons from the Oklahoma City bombing : defensive design techniques*, ASCE Press, New York, N.Y.

Izzuddin, B. A., Elghazouli, A. Y., and Tao, X. (2002). "Realistic modelling of composite floor slabs under fire conditions." *15th ASCE Engineering Mechanics Conference*, Columbia University, New York.

Izzuddin, B. A., Vlassis, A. G., Elghazouli, A. Y., and Nethercot, D. A. (2008). "Progressive collapse of multi-storey buildings due to sudden column loss − Part I: Simplified assessment framework." *Engineering Structures*, 30(5), pp. 1308-1318.

Kaewkulchai, G., and Williamson, E. B. (2004). "Beam element formulation and solution procedure for dynamic progressive collapse analysis." *Computer and Structures*, 82, pp. 639-651.

Kaewkulchai, G., and Williamson, E. B. (2006). "Modeling the impact of failed members for progressive collapse analysis of frame structures." *Journal of Performance of Constructed Facilities*, 20(4), pp. 375-383.

Khandelwal, K., and El-Tawil, S. (2005). "Macromodel-based simulation of progressive colapse: Steel frame structures." *Journal of Structural Engineering*, 134(7), pp. 1070-1078.

Kwasniewski, L. (2010). "Nonlinear dynamic simulations of progressive collapse for a multistory building." *Engineering Structures*, 32(5), pp. 1223-1235.

Kim, J., and Kim, T. (2009a). "Assessment of progressive collapse-resisting capacity of steel moment frames." *Journal of Constructional Steel Research*, 65(1), pp. 169-179.

Kim, T., and Kim, J. (2009b). "Collapse analysis of steel moment frames with various seismic connections." *Journal of Constructional Steel Research*, 65, pp. 1316-1322.

Kim, T., Kim, J., and Park, J. (2009c). "Investigation of Progressive Collapse-Resisting Capability of Steel Moment Frames Using Push-Down Analysis." *Journal of Performance of Constructed Facilities*, 23(5), pp. 327-335.

Kwasniewski, L. (2010). "Nonlinear dynamic simulations of progressive collapse for a multistory building." *Engineering Structures*, 32(5), pp. 1223-1235.

Lee, C. H., Kim, S., and Lee, K. (2010). "Parallel axial-flexural hinge Model for nonlinear dynamic progressive collapse analysis of welded steel moment frames." *Journal of Structural Engineering*, 136(2), pp. 165-173.

Levy, M., and Salvadori, M. (1992). *Why buildings fall down : how structures fail*, W.W. Norton, New York.

Liang, X., Shen, Q., and Gosh, S. K. (2008). "Assessing ability of seismic structural systems to withstand progressive collapse: Design of steel frame buildings." Building and Fire Research Laboratory, National Institute of Standards and Technology, Gaithersburg, MD.

Liew, J. Y. R., Punniyakotty, N. M., and Shanmugam, N. E. (1997). "Advanced analysis and design of spatial structures." *Journal of Constructional Steel Research*, 42(1), pp. 21-48.

Liew, J. Y. R., Chen, H., and Shanmugam, N. E. (2001). "Inelastic Analysis of Steel Frames with Composite Beams." *Journal of Structural Engineering*, 127(2), pp. 194-202.

Liu, J. L. (2010a). "Preventing progressive collapse through strengthening beam-to-column connection, Part 1: Theoretical analysis." *Journal of Constructional Steel Research*, 66(2), pp. 229-237.

Liu, J. L. (2010b). "Preventing progressive collapse through strengthening beam-to-column connection, Part 2: Finite element analysis." *Journal of Constructional Steel Research*, 66(2), pp. 238-247.

Marjanishvili, S. M., and Agnew, E. (2006). "Comparison of various procedures for progressive collapse analysis." *Journal of Performance of Constructed Facilities*, 20(4), pp. 365-374.

Marjanishvili, S. M. (2004). "Progressive analysis procedure for progressive collapse." *Journal of Performance of Constructed Facilities*, 18(2), pp. 79-85.

McKenna, F., Fenves, G. L., Filippou, F. C., and Mazzoni, S. (2006). "Open system for earthquake engineering simulation (OPENSEES) v2.2.0." Pacific Earthquake Engineering Research Center, University of California, Berkeley.

MHA (2010). "Guidelines for enhancing building security in Singapore." Ministry of Home Affair, Singapore.

NIST (2005). "Final report on the collapse of World Trade Center towers." NCSTAR 1. Federal building and fire safety investigation of the World Trade Center disaster, US Department of Commerce Gaithersburg, MD, USA.

NIST (2006). "Best practice for reducing potential for progressive collapse in buildings." National Institute of Standards and Technology.

ODPM (2004). *The building regulations 2000: Approved Document A3: Disproportionate collapse*, Office of Deputy Prime Minister, London.

Orbison, J. G., McGuire, W., and Abel, J. F. (1982). "Yield surface applications in nonlinear steel frame analysis." *Comput Methods Appl Mech Eng*, 33(1), pp. 557-573.

Pinto, P. E., and Giuffre, A. (1970). "Comportamento del cemento armato per sollecitazioni cicliche di forte intensita." *Giornale del Genio Civile*, No. 5.

Powell, G. "Disproportionate collapse: The futility of using nonlinear analysis." *Proc., Structures 2009: Don't mess with structural engineers*, ASCE, pp. 1908-1917.

Ramesh, G., and Krishnamoorthy, C. S. (1994). "Inelastic post-buckling analysis of truss structures by dynamic relaxation method." *International Journal of Numerical Methods in Engineering*, 37, pp. 3633-3657.

Ramli-Sulong, N. H., Elghazouli, A. Y., and Izzuddin, B. A. (2007). "Behaviour and design of beam-to-column connections under fire conditions." *Fire Safety Journal*, 42(6–7), pp. 437-451.

Ross, S. S. (1984). *Construction disasters : design failures, causes, and prevention*, : McGraw-Hill, New York.

Sadek, F., El-Tawil, S., and Lew, H. S. (2008). "Robustness of composite floor systems with shear connections: Modeling, simulation, and evaluation." *Journal of Structural Engineering*, 134(11), pp. 1717-1725.

Spacone, E., Filippou, F. C., and Taucer, F. F. (1996). "Fiber beam-column model for nonlinear analysis of RC frames. I: Formulation." *Earthquake Engineering and Structural Dynamics*, 25(7), pp. 711-725.

Tan, S., and Astaneh-Asl, A. (2003). "Final Report: Cable-based retrofit of steel building floors to prevent progressive collapse." *Rep.*, submitted to University of California Berkeley.

Thai, H.-T., and Kim, S.-E. (2009). "Large deflection inelastic analysis of space trusses using generalized displacement control method." *Journal of Constructional Steel Research*, 65, pp. 1987-1994.

Uriz, P., Filippou, F. C., and Mahin, S. A. (2008). "Model for cyclic inelastic buckling of steel braces." *Journal of Structural Engineering*, 134(4), pp. 619-628.

Vlassis, A. G., Izzuddin, B. A., Elghazouli, A. Y., and Nethercot, D. A. (2008). "Progressive collapse of multi-storey buildings due to sudden column loss – Part II: Application." *Engineering Structures*, 30(5), pp. 1424-1438.

Vlassis, A. G., Izzuddin, B. A., Elghazouli, A. Y., and Nethercot, D. A. (2009). "Progressive collapse of multi-storey buildings due to failed floor impact." *Engineering Structures*, 31(7), pp. 1522-1534.

Vogel, U. (1985). "Calibrating frames." *Stahlbau*, pp. 295-301.

Yang, Y. B., Yang, Y. T., and Chang, P. K. (1997). "Effects of member buckling and yielding on ultimate strengths of space trusses." *Engineering Structures*, 19(2), pp. 179-191.

Yu, H., Burgess, I. W., Davison, J. B., and Plank, R. J. (2009). "Experimental investigation of the behaviour of fin plate connections in fire." *Journal of Constructional Steel Research*, 65(3), pp. 723-736.

Yu, M., Zha, X., and Ye, J. (2010). "The influence of joints and composite floor slabs on effective tying of steel structures in preventing progressive collapse." *Journal of Constructional Steel Research*, 66(3), pp. 442-451.